



Universität Hamburg

DER FORSCHUNG | DER LEHRE | DER BILDUNG

BNITM

Bernhard-Nocht-Institut für Tropenmedizin



Sex-specific factors affecting intracellular infection of human primary macrophages by visceral *Leishmania* spp.

Dissertation

For the award of the degree

“doctor rerum naturalium “

(Dr. rer. nat)

at the Faculty of
Mathematics, Informatics and Natural Science
- Department Biology-

University of Hamburg

submitted by

Annika Bea

from Groß-Bieberau, Germany

Hamburg, February 2024

This work has been conducted in the research groups and under the guidance of Prof. Dr.med.vet. Hannelore Lotter and PD Dr. rer. nat. Joachim Clos at the Bernhard-Nocht-Institute for Tropical Medicine

1. Examiner: **Prof. Dr. rer. nat. Tim-Wolf Gilberger**
Deutsches Elektronen-Synchrotron (DESY)
CSSB Centre for Structural Systems Biology
Notkestraße 85, Gebäude 15, 22607 Hamburg
2. Examiner: **PD Dr. rer. nat. Joachim Clos**
Leishmania genetics group
Bernhard-Nocht-Institute for Tropical Medicine (BNITM)
Bernhard Nocht Straße 74, 20359 Hamburg

Date of oral defence: 19.04.2024

Chairman of committee: Prof. Dr. rer. nat. Tim Gilberger

Deputy chairman of committee: Prof. Dr. rer. nat. Minka Breloer

Members of committee: PD Dr. rer. nat. Joachim Clos

Prof. Dr. med. vet. Hannelore Lotter

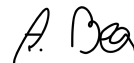
Prof. Dr. rer. nat. Iris Bruchhaus

Eidesstattliche Erklärung / Declaration on oath

Hiermit erkläre ich an Eides statt, dass ich die vorliegende Dissertationsschrift selbst verfasst und keine anderen als die angegebenen Quellen und Hilfsmittel genutzt habe.

I hereby declare, under oath, that I have written the present dissertation on my own and have not used other than the acknowledged resources and aids.

Hamburg, 22.02.2024



Annika Bea

Table of content

Eidesstattliche Erklärung / Declaration on oath	III
Table of content	IV
Summary	VII
Zusammenfassung	IX
List of figures	XI
List of tables	XIII
Abbreviations and symbols	XV
1 Introduction	1
1.1 Leishmaniasis - the infectious disease	1
1.1.1 Disease manifestation and epidemiology	1
1.1.2 Life cycle of Leishmania spp.	3
1.1.3 Leishmania infantum	5
1.1.4 Diagnosis and treatment of leishmaniasis	6
1.2 The innate immune system	7
1.2.1 Cells of the innate immune system	7
1.2.1.1 Human primary macrophages - functions und subsets	8
1.2.2 Immune response to Leishmania infection	9
1.2.2.1 Macrophages as host cell for Leishmania parasites	9
1.3 Sex-specific differences in the immune system	10
1.3.1 Genetic determinants	10
1.3.2 Influence of sex hormones on the immune response	11
1.3.3 Sex-specific differences in leishmaniasis	12
1.4 Aim of thesis	13
2 Material and Methods	14
2.1 Material	14
2.1.1 Laboratory equipment	14
2.1.2 Consumables	15
2.1.3 Chemicals and solutions	16
2.1.4 Kits	16
2.1.5 Antibodies	16
2.1.6 Culture media and buffers	18
2.1.6.1 Preparation of fetal calf serum (FCS)	18
2.1.7 Stimulants for in vitro treatment	19
2.1.8 Parasite strains	20
2.1.9 Human samples	20

2.1.10 Software and Databases	20
2.2 Methods	21
2.2.1 Cell culture methods	21
2.2.1.1 Culture of Leishmania promastigotes	21
2.2.1.2 Cell counting of parasites	21
2.2.1.3 Cryopreservation of parasites	21
2.2.1.4 Isolation of leukocytes from human blood samples	22
2.2.1.5 Isolation of human CD14+ monocytes from PBMCs	22
2.2.1.6 Cell count determination	23
2.2.1.7 Differentiation of human monocytes into monocyte-derived macrophages	23
2.2.1.8 In vitro polarisation of macrophages	24
2.2.1.9 Cryopreservation of PBMCs	24
2.2.1.10 In vitro treatment of macrophages with steroid hormones	24
2.2.1.11 In vitro infection of macrophages	24
2.2.1.12 Incubation of macrophages with phagocytosis beads	25
2.2.1.13 Labelling of parasitophorous vacuoles	26
2.2.1.14 Cell fixation	26
2.2.1.15 Flow cytometry	26
2.2.1.15.1 Staining of cells for flow cytometry analysis	26
2.2.1.15.2 Spectral unmixing for flow cytometry	27
2.2.2 Molecular methods	27
2.2.2.1 RNA isolation from macrophages	27
2.2.2.2 Control of RNA integrity using Bioanalyser Aiglent 2100	28
2.2.2.3 RNA Sequencing	29
2.2.3 Biochemical methods	29
2.2.3.1 Cytometric bead assay (LEGENDplex™)	29
2.2.4 High content screening (HCS) by automated confocal microscopy	30
2.2.4.1 Immunofluorescent staining for HCS	30
2.2.4.2 Image acquisition	30
2.2.4.3 Image analysis	30
2.2.5 In silico methods	32
2.2.5.1 Analysis of RNA Sequencing	32
2.2.5.2 Statistical analysis	33
3 Results	34
3.1 Adaptation of high content screening (HCS) system for Leishmania spp. infected primary human monocyte-derived macrophages (hMdMs)	34
3.1.1 Implementation of an in vitro infection model of hMdMs with Leishmania spp.	34
3.1.1.1 Localisation study of Leishmania parasites in macrophages	36

3.1.1.2 Quantification of infection parameters using confocal high content screening (HCS)	39
3.1.2 Delineation of macrophages exhibiting distinct polarisation states	41
3.1.2.1 Morphology-based characterisation of polarised macrophages	41
3.1.2.2 Phenotypic characterisation of polarised macrophages	44
3.2 Sex-specific differences during infection with viscerotropic <i>L. infantum</i>	46
3.2.1 Course of <i>L. infantum</i> infection in macrophages from male and female donors	46
3.2.2 Characterisation of <i>L. infantum</i> infected human macrophages	48
3.2.3 Cytokine profiling of <i>L. infantum</i> -infected human macrophages	50
3.2.4 Sex-specific transcriptional change in <i>L. infantum</i> infected human macrophages	54
3.3 Influence of steroid hormones on <i>L. infantum</i> infection	71
3.3.1 Influence of androgens on the infection with <i>L. infantum</i>	71
3.3.2 Influence of estrogens on the infection with <i>L. infantum</i>	73
3.3.2.1 Cytokine profiling of E2-treated macrophages after <i>L. infantum</i> infection	75
3.3.3 Influence of steroid hormones on macrophage polarisation	81
4. Discussion	83
4.1 In vitro infection model and HCS assay for human primary macrophages	83
4.2 Sex-specific differences during in vitro infection of macrophages with <i>L. infantum</i>	84
4.2.1 <i>L. infantum</i> infection increases viability of human primary macrophages	85
4.2.2 <i>L. infantum</i> infection affects macrophage polarisation	85
4.2.3 <i>L. infantum</i> infection triggers distinct cytokine release in the supernatant of female and male primary human macrophages	86
4.3 Transcriptome profiling of <i>L. infantum</i> -infected macrophages	87
4.3.1 Transcriptional changes in response to <i>L. infantum</i> infection	88
4.3.2 Sex-specific transcriptional changes in response to <i>L. infantum</i> infection	90
4.3.3 Gene-specific RNA abundance of <i>L. infantum</i> during infection	91
4.4 Influence of sex hormones on infection with <i>L. infantum</i>	92
Supplementary data	94
Publications	116
Bibliography	117
Acknowledgments	129

Summary

Leishmaniasis is one of the most important neglected tropical diseases and is caused by protozoan parasites of the genus *Leishmania*. Depending on infecting parasite species and host immune status, the disease can manifest itself as self-healing skin ulcers, severe mucosal necrosis, or disseminated, often lethal, visceral infections of haematopoietic organs. To date, there are no licensed vaccines available and treatment options are limited and often accompanied by severe adverse effects.

Many parasitic diseases occur with a sex bias in terms of incidence, morbidity and mortality towards male individuals. Leishmaniasis is such an example as it presents with higher numbers of clinical cases in male patients in various endemic areas. The reasons for this observed sex-specific difference are highly multifactorial and can include biological differences such as variances in chromosomes and hormones, as well as sociocultural disparities that can alter the susceptibility towards an infection and influence the outcome of the disease.

Within the mammalian host, *Leishmania* parasites proliferate mainly in macrophages, while suppressing effective elimination by the host. In order to better understand the biological sex differences in leishmaniasis, the present project aimed to analyse the influence of donor sex on the infection of macrophages with *Leishmania* species at the cellular and transcriptional level. For the first time, using an *in vitro* infection model based on primary human macrophages with *L. infantum* and a high-throughput analysis, higher infection rates and parasite loads were detected in male macrophages than in female macrophages. These differences were most pronounced in later phases of infection (from 28 hours post infection).

Due to their high plasticity in response to external stimuli, macrophages can polarise into pro-inflammatory M1 and anti-inflammatory M2 macrophages, which are distinguished by their different morphological and phenotypic characteristics. In this study, the polarisation during infection with *L. infantum* was investigated using microscopy- and flow cytometry-based methods. *L. infantum*-infected macrophages showed increased M1 polarisation and decreases in M2-like macrophages in both sexes, especially at early stages of infection, with a higher tendency towards M1 polarisation observed in female cells.

Quantitative RNA sequencing of infected macrophages and corresponding controls of both sexes showed the most pronounced changes in mRNA levels at early time points of infection, but also more differentially expressed genes (DEGs) in female than in male macrophages. Over time (6, 28 and 52 hours after infection), the number of DEGs decreased in infected cells of both sexes. Genes that were similarly upregulated in both sexes were genes associated with important immunological signalling pathways, including TNF signalling, NF- κ B signalling, HIF-1 α signalling, IL-17 signalling and FoxO signalling, mineral absorption, macrophage cytoskeletal remodelling and cytokine response. Specifically upregulated genes in female macrophages were associated with a more strongly induced interferon signalling pathway and proteasomal activities, while genes associated with interleukin response and *Leishmania* survival were preferentially upregulated in male macrophages. These results suggest that female macrophages exhibit increased transcriptomic

activation and an enhanced anti-parasitic immune response, possibly leading to more effective elimination of the parasites in female-derived macrophages.

The influence of sex hormones on *L. infantum* infection was investigated by pre-treating macrophages with androgens or estrogens prior to infection. While the administration of testosterone demonstrated no impact on infection rate or parasite burden, estradiol treatment correlated weakly with reduced parasite burden in infected female macrophages.

Taken together, this project identified several biological factors that may contribute to the divergent susceptibilities of sexes towards *Leishmania* infections. These factors include variances in macrophage polarisation, disparities in the expression of immunity-related genes, and the influence of sex hormones. These findings serve as a foundational framework for subsequent experiments which may identify therapeutic targets.

Zusammenfassung

Die Leishmaniose ist eine der wichtigsten vernachlässigten, Vektor-übertragenen Tropenkrankheiten und wird durch einzellige Parasiten der Gattung *Leishmania* verursacht. Je nach infizierender Parasiten-Art und Immunstatus des Wirts kann sich die Krankheit in Form spontan abheilender Hautläsionen, schwerer Schleimhautnekrosen, oder einer disseminierten, oft tödlichen, viszeralen Infektion hämatopoetischer Organe manifestieren. Bis heute gibt es keine zugelassenen Impfstoffe und die Behandlungsmöglichkeiten sind begrenzt und oft mit schwerwiegenden Nebenwirkungen verbunden.

Viele parasitäre Krankheiten treten mit einer erhöhten Inzidenz, Morbidität und Mortalität in männlichen Individuen auf. Die Leishmaniose ist ebenfalls ein solches Beispiel, da sie in vielen endemischen Gebieten eine höhere Fallzahl in männlichen Patienten aufweist. Die Gründe für diesen beobachteten geschlechtsspezifischen Unterschied sind multifaktoriell und schließen biologische Unterschiede, chromosomal und hormonell, aber auch soziokulturelle Unterschiede, ein, die die Anfälligkeit für eine Infektion verändern und den Ausgang der Krankheit beeinflussen können.

Innerhalb des Säugewirts vermehren sich *Leishmania*-Parasiten hauptsächlich in Makrophagen und unterdrücken dabei effektive Eliminierung durch den Wirt. Um die biologischen Geschlechtsunterschiede in der Leishmaniose besser zu verstehen, hatte das vorliegende Projekt zum Ziel, den Einfluss des Wirtsgeschlechts auf die Infektion von Makrophagen mit *Leishmania*-Arten. auf zellulärer und transkriptionaler Ebene zu analysieren. Erstmals konnten mithilfe eines *in vitro* Infektionsmodells basierend auf primären humanen Makrophagen mit *L. infantum* und einer Hochdurchsatzanalyse höhere Infektionsraten und Parasitenlasten in männlichen Makrophagen im Vergleich zu weiblichen Makrophagen nachgewiesen werden. Diese Unterschiede waren in späteren Phasen der Infektion (ab 28 Stunden nach der Infektion) am stärksten ausgeprägt.

Aufgrund ihrer hohen Plastizität können Makrophagen als Reaktion auf äußere Reize in pro-inflammatorische M1- und anti-inflammatorische M2-Makrophagen polarisieren, die sich durch ihre unterschiedlichen morphologischen und phänotypischen Eigenschaften unterscheiden lassen. In dieser Studie wurde diese Polarisierung während der Infektion mit *L. infantum* durch die Anwendung von Mikroskopie- und Durchflusszytometrie-basierter Methoden untersucht. *L. infantum*-infizierte Makrophagen zeigten eine Zunahme der M1-Polarisation und eine Abnahme der M2-ähnlichen Makrophagen in beiden Geschlechtern, insbesondere in frühen Stadien der Infektion, wobei in weiblichen Zellen eine höhere Tendenz zu M1-Polarisation beobachtet werden konnte.

Die quantitative RNA-Sequenzierung infizierter Makrophagen und entsprechender Kontrollen beider Geschlechter zeigte die auffälligsten Veränderungen der RNA-Level zu frühen Zeitpunkten der Infektion sowie mehr differentiell exprimierte Gene (DEGs) in weiblichen als in männlichen Makrophagen. Über die Zeit (6, 28 und 52 Stunden nach der Infektion) reduzierte sich die Zahl der DEGs in infizierten Zellen beider Geschlechter. Bei Genen, die in beiden Geschlechtern in ähnlicher Weise hochreguliert waren, handelte es sich um Gene, die mit wichtigen immunologischen Signalwegen in Verbindung stehen, darunter TNF-Signalweg, NF- κ B-Signalweg, HIF-1 α -Signalweg, IL-17-Signalweg und FoxO-Signalweg, Mineralabsorption, Umbau des

Makrophagen-Zytoskeletts und Zytokinantwort. Spezifisch hochregulierte Gene in weiblichen Makrophagen konnten beispielsweise einem stärker induzierten Interferon-Signalweg und proteasomalen Aktivitäten zugeordnet werden, während in männlichen Makrophagen Gene hochreguliert waren, die mit der Interleukin-Antwort und dem Überleben von *Leishmanien* in Verbindung stehen. Diese Ergebnisse deuten darauf hin, dass weibliche Makrophagen eine erhöhte transkriptionelle Aktivierung und eine verstärkte, gegen den Parasiten gerichtete Immunantwort aufweisen, was möglicherweise zu einer effektiveren Eliminierung der Infektion in weiblichen Makrophagen führt.

Der Einfluss von Geschlechtshormonen auf die Infektion mit *L. infantum* wurde untersucht, indem Makrophagen vor der Infektion mit Androgenen oder Östrogenen behandelt wurden. Während die Verabreichung von Testosteron keine Auswirkungen auf die Infektionsrate oder die Parasitenlast zeigte, deutete die Behandlung mit Östradiol auf eine tendenziell geringere Parasitenbelastung bei nachfolgenden Infektionen von weiblichen Makrophagen hin.

Insgesamt wurden im Rahmen dieses Projekts mehrere potenzielle biologische Faktoren ermittelt, die zu den unterschiedlichen Anfälligkeiten der Geschlechter beitragen könnten. Zu diesen Faktoren gehören Unterschiede in der Makrophagenpolarisierung, Unterschiede in der Expression von immunitätsbezogenen Genen und der Einfluss von Sexualhormonen. Diese Erkenntnisse dienen als Grundlage für nachfolgende Experimente, die potenzielle therapeutische Ziele identifizieren können.

List of figures

Figure 1: Status of endemicity of leishmaniasis.	3
Figure 2. The life cycle of Leishmania parasites.	5
Figure 3: Age distribution of blood donors.	20
Figure 4: RNA integrity control using Agilent 2100 Bioanalyser	28
Figure 5: Schematic depiction of customised image analysis algorithm established in Harmony® software.	32
Figure 6: Schematic depiction of the workflow for in vitro infection of primary monocyte derived macrophages with Leishmania spp. parasites.	35
Figure 7: Comparison of monocyte subset frequencies in female and male blood donors and control of monocyte isolation.	36
Figure 8: Determination of intracellular localisation of Leishmania spp. amastigotes within human monocyte derived macrophages by labelling of parasitophorous vacuoles.	38
Figure 9: Quantification of Leishmania spp. parasite infection in human monocyte-derived macrophages using confocal (HCS).	40
Figure 10: Morphology-based distinction of M1- and M2-like polarised macrophages using confocal HCS.	43
Figure 11: Phenotypic characterisation of M1- and M2-like polarised macrophages using flow cytometry and tSNE analysis.	46
Figure 12: Quantification of infection parameters in female and male L. infantum-infected macrophages over time using confocal high content screening.	48
Figure 13: Phenotypical and morphological M1/M2 characterisation of female and male macrophages following L. infantum infection.	49
Figure 14: Secretion of cytokines related to parasite elimination by female and male L. infantum-infected macrophages using cytometric bead assay.	52
Figure 15: Secretion of cytokines related to parasite survival by female and male L. infantum-infected macrophages using cytometric bead assay.	53
Figure 16: Phagocytosis of carboxylated latex beads by female and male monocyte-derived macrophages.	55
Figure 17: Analysis of differentially expressed genes between naïve female and male macrophages.	57
Figure 18: Analysis of differentially expressed genes between uninfected and infected macrophages from female and male donors.	58
Figure 19: Analysis of differentially expressed genes between uninfected and infected macrophages from female donors.	60
Figure 20: Analysis of differentially expressed genes between uninfected and infected macrophages from male donors.	62
Figure 21: Analysis of differentially upregulated genes between female and male macrophages upon L. infantum infection.	65
Figure 22: Analysis of differentially downregulated genes between female and male macrophages upon L. infantum infection.	67
Figure 23: Comparison of the magnitude of gene expression control within similarly regulated genes in female and male macrophages.	69
Figure 24: Analysis of differentially expressed genes in L. infantum parasites during infection.	70

Figure 25: Schematic depiction of the workflow for the treatment of monocyte derived macrophages with steroid hormones before infection with <i>L. infantum</i> .	71
Figure 26: Influence of testosterone treatment on the infection of macrophages with <i>L. infantum</i> .	73
Figure 27: Influence of estradiol treatment on the infection of macrophages with <i>L. infantum</i> .	74
Figure 28: Correlation analysis between estradiol treatment and <i>L. infantum</i> infection in female macrophages .	75
Figure 29: Measurement of cytokines related to parasite elimination in culture supernatants of estradiol-treated female and male macrophages after <i>L. infantum</i> infection using cytometric bead assay.	77
Figure 30: Measurement of cytokines related to parasite survival in culture supernatants of estradiol-treated female and male macrophages after <i>L. infantum</i> infection using cytometric bead assay.	80
Figure 31: Morphology-based M1/M2 characterisation of steroid hormone-treated female and male macrophages after <i>L. infantum</i> infection.	82
Figure S1: Determination of intracellular localisation of <i>Leishmania</i> spp. amastigotes within human monocyte derived macrophages by labelling of parasitophorous vacuoles.	98
Figure S2: Morphology-based M1/M2 characterisation of female and male macrophages after phagocytosis and <i>L. infantum</i> infection.	98
Figure S3: Analysis of differentially expressed genes between naïve and bead-containing macrophages from female donors.	101
Figure S4: Analysis of differentially expressed genes between naïve and bead-containing macrophages from male donors.	103
Figure S5: Analysis of differentially expressed genes between naïve and <i>L. infantum</i> -infected macrophages at 52 hpi.	113
Figure S6: Analysis of differentially expressed genes between naïve and <i>L. infantum</i> -infected macrophages at 52 hpi.	115
Figure S7: Correlation analysis between testosterone treatment and <i>L. infantum</i> infection in female macrophages.	115

List of tables

Table 1: List of utilised laboratory equipment	14
Table 2: List of utilised consumables	15
Table 3: List of utilised chemicals and solutions	16
Table 4: List of utilised kits	16
Table 5: List of utilised antibodies	16
Table 6: List of utilised culture media	18
Table 7: List of utilised buffers	19
Table 8: List of utilised stimulants	19
Table 9: List of utilised parasite strains	20
Table 10: List of utilised softwares and databases	20
Table 11: List of utilised well plates, seeding strategy and application	23
Table 12: List of volume for infection and washing for different plates	25
Table S1: Parameters for customised automated image analysis sequence established in Harmony software®	94
Table S2: Summary of donor dataset used for transcriptomical analysis and sequencing parameters.	98
Table S3: Differentially expressed genes between female and male naïve macrophages at 6 hpi, sorted by log ₂ (fold change).	99
Table S4: Differentially expressed genes between female and male naïve macrophages at 16 hpi, sorted by log ₂ (fold change).	100
Table S5: Differentially expressed genes between female and male naïve macrophages at 52 hpi, sorted by log ₂ (fold change),	100
Table S6: Top 100 differentially expressed genes between female naïve and bead-containing macrophages at 6 hpi, sorted by log ₂ (fold change).	103
Table S7: Top 100 differentially expressed genes between female naïve and bead-containing macrophages at 16 hpi, sorted by log ₂ (fold change).	104
Table S8: Top 100 differentially expressed genes between male naïve and bead-containing macrophages at 6 hpi, sorted by log ₂ (fold change).	106
Table S9: Top differentially expressed genes between male naïve and bead-containing macrophages at 16 hpi, sorted by log ₂ (fold change).	107
Table S10: Top differentially expressed genes between male naïve and bead-containing macrophages at 52 hpi, sorted by log ₂ (fold change).	108
Table S11: Top 100 differentially expressed genes between female uninfected and <i>L. infantum</i> -infected macrophages at 6 hpi, sorted by log ₂ (fold change).	108
Table S12: Top 100 differentially expressed genes between female uninfected and <i>L. infantum</i> -infected macrophages at 16 hpi, sorted by log ₂ (fold change).	109
Table S13: Top differentially expressed genes between female naïve and <i>L. infantum</i> -infected macrophages at 52 hpi, sorted by log ₂ (fold change).	110
Table S14: Top 100 differentially expressed genes between male uninfected and <i>L. infantum</i> -infected macrophages at 6 hpi, sorted by log ₂ (fold change).	110

Table S15: Top 100 differentially expressed genes between male uninfected and <i>L. infantum</i> -infected macrophages at 16 hpi, sorted by log ₂ (fold change).	112
Table S16: Top differentially expressed genes between male naïve and <i>L. infantum</i> -infected macrophages at 52 hpi, sorted by log ₂ (fold change).	113
Table S17: Top 50 differentially expressed genes in infected samples over time pooled from female and male donors.	114
Table S18: Differentially expressed genes between infected female and male samples at 6 hpi.	114

Abbreviations and symbols

°C	degree Celsius
AF	Alexa Fluor
APC	Antigen presenting cells
APC	Allophycocyanine
AR	Androgen receptor
ARE	Androgen responsive element
AUC	Area under the curve
BNITM	Bernhard-Nocht Institute for Tropical Medicine
BSA	Bovine serum albumin
BUV	Brilliant Ultraviolet
BV	Brilliant violet
<i>CASP</i>	<i>Caspase</i>
CCL	CC-Chemokine ligand
CCR	CC-Chemokine receptor
CD	Cluster of differentiation
CL	Cutaneous leishmaniasis
<i>CLEC4A</i>	<i>C-type lectin domain family 4 member E</i>
CX ₃ CR1	CX ₃ C-chemokine receptor 1
CXCL	CXC Motif Chemokine Ligand
CXCR	CXC motif chemokine receptor
<i>CYBB</i>	<i>Cytochrome b-245 heavy chain</i>
DAPI	4,6-Diamidin-2-phenylindol
DC	Dendritic cell
DCL	Diffuse dermal leishmaniasis
ddH ₂ O	Double-distilled water
DEG	Differentially expressed genes
DHT	5- α -Dihydrotestosterone
DIC	Different interference contrast
DMSO	Dimethyl sulfoxide
DNA	Desoxyribonucleic acid

<i>DNA2</i>	<i>ATP-dependent helicase/nuclease DNA2</i>
e.g.	Exempli gratia (lat.: for example)
E2	17- β -Estradiol
<i>ENO1</i>	<i>α-enolase</i>
<i>ENO2</i>	<i>γ-enolase</i>
ERE	Estrogen responsive element
ER α /ER β	Estrogen receptor
FACS	Fluorescence activated cell sorting
FC	Fold change
FCS	Fetal calf serum
Fig	Figure
FITC	Fluorescein isothiocyanate
FoxO	forkhead box O
FSC	Forward scatter
g	gram
<i>GFPT2</i>	<i>Glutamine-fructose-6-phosphatase transaminase 2</i>
GM-CSF	Granulocyte-Macrophage colony-stimulating factor
GO	Gene orthology
h/hrs	hour/hours
HCS	High content screening
HIF-1 α	Hypoxia-inducible factor 1 α
HIV	Human immunodeficiency virus
HLA-DR	Human leucocyte antigen - HL subtype
hMdM	human monocyte-derived macrophages
hpi	hours post infection
HSP90	Heat Shock Protein 90
IDO1	indoleamine 2,3-dioxygenase
IFIT	Interferon induced protein with tetratricopeptide repeats
IFN	Interferon
IL	Interleukin
IL4I1	L-amino-acid oxidase

<i>INHBA</i>	<i>Inhibin β-A</i>
iNOS	Inducible nitric oxide synthetase
<i>IRAK-1</i>	<i>interleukin 1 receptor associated kinase 1</i>
IRF	Interferon regulatory factor
ISG	Interferon stimulated gene
KEAP1	Kelch-like ECH-associated protein 1
KEGG	Kyoto Encyclopedia of Genes and Genomes
L.	Leishmania
LCF	Leishmania chemotactic factor
<i>LHSP90</i>	pan- <i>Leishmania</i> Heat Shock Protein 90
LPG	Lipophosphoglycan
m	Milli
M	Molar
M-CSF	Macrophage colony-stimulating factor
MACS	Magnetic activated cell sorting
MCL	Mucocutaneous leishmaniasis
MFI	Median fluorescence intensity
min	minute(s)
MIP	Macrophage inflammatory protein
<i>MMP10</i>	<i>Matrix metalloproteinase 10</i>
MOI	Multiplicity of infection
MRC1	Macrophage mannose receptor 1
<i>MRS</i>	<i>Macrophage scavenger receptor</i>
ms	millisecond
MT1	metallothionein family 1
n	Sample size
NCF2	Neutrophil cytosolic factor
NET	Neutrophil extracellular trap
NGS	Next Generation Sequencing
NLRP3	<i>NACHT, LRR and PYD domains-containing protein 3</i>
NO	Nitrogen oxide
NOD	Nucleotide-binding oligomerization domain

<i>NOTCH1</i>	<i>Neurogenic locus notch homolog protein 1</i>
NTD	Neglected tropical disease
OAS	2'-5' oligoadenylate synthetase
OASL	2'-5' oligoadenylate synthetase-like
ON	Overnight
PAMPS	Pathogen-associated molecular patterns
PBMCs	Peripheral blood mononuclear cells
PBS	Phosphate buffers saline
PC	Principal Component
PCA	Principal Component Analysis
PDKL	Post kala-azar dermal leishmaniasis
PE	Phycoerythrin
Per-CP	Peridinin-Chlorophyll-protein
PFA	Paraformaldehyde
POC	Percentage of control
PPAR	Peroxisome proliferator-activated receptor
PRR	Pattern recognition receptor
PSG	Promastigotes secretory gel
<i>PSMA7</i>	<i>Proteasomal subunit α type</i>
<i>PSMD11</i>	<i>26S proteasome non-ATPase regulatory subunit 11</i>
PTGER4	Prostaglandin E2 receptor EP4 subtype
PV	Parasitophorous vacuole
RAC2	Ras-related C3 botulinum toxin substrate 2
RNA	Ribonucleic acid
RNS	Reactive nitrogen species
ROS	Reactive oxygen species
rpm	rounds per minute
RPMI	Roswell Park Memorial Institute
RSAD2	radical SAM domain-containing 2
RT	Room temperature
SOCS3	Suppressor of cytokine signaling 3
SOD2	Superoxid dismutase 2

spp.	Species
SSC	Sideward scatter
Tab.	Table
TGF	Transforming growth factor
T _H	T Helper cell
TLRs	Toll-like receptors
TNF	Tumor necrosis factor
<i>TNFAIP6</i>	<i>TNF-α induced protein 6</i>
<i>TNIP3</i>	<i>TNFAIP3-interactin protein 3</i>
Tregs	Regulatory T-cells
tSNE	T-distributed stochastic neighbour embedding
U	Units
UKE	University Medical Center Hamburg-Eppendorf
VL	Visceral leishmaniasis
WHO	World Health Organisation
XCI	X-linked inactivation
XIST	X-inactive specific transcript
α	Anti / alpha
μ	Micro

1 Introduction

1.1 Leishmaniasis - the infectious disease

1.1.1 Disease manifestation and epidemiology

Leishmaniasis is one of the most important neglected tropical diseases (NTDs), according to the World Health Organisation (WHO). Leishmaniasis is endemic in 99 mostly tropical and subtropical countries with 12 million infected people worldwide. It is estimated that 0.7-1.5 million new cases and 20,000-40,000 leishmaniasis-related deaths occur annually (1-3). In general, globally rising temperatures and the resulting spread of the vectors are likely to expand the endemic regions and increase the number of leishmaniasis cases (4, 5). The most important risk factors for leishmaniasis are poverty, malnutrition and immunosuppression, as well as poor housing conditions and lack of access to medical assistance. Causative agents of leishmaniasis are protozoan parasites of the genus *Leishmania* (*L.*) (taxon: *Euglenozoa*, class: *Kinetoplastea*, order: *Trypanosomatida*). *L. donovani* was first discovered at the beginning of the 20th century, and described independently by William B. Leishman and Charles Donovan, while Pjotr Borovski identified *L. major* in 1898 (6). To date, approximately 53 *Leishmania* species are known, of which 31 are pathogenic to mammals and 20 *Leishmania* species are pathogenic to humans. Due to the high diversity in this genus, human pathogenic species are further divided into two subgenera, *Leishmania* and *Viannia* (*L. V.*), according to their development in the vector. Additionally, countries endemic for leishmaniasis have been divided into Old World, referring to the eastern hemisphere (Asia, Middle East, Africa and Europe) and New World, referring to the western hemisphere (Mexico, Central and South America and the USA) (7).

Depending on the *Leishmania* species, the host immune-status and regional factors, three main clinical manifestations of varying severity can be observed: cutaneous leishmaniasis (CL), mucocutaneous leishmaniasis (MCL) and visceral leishmaniasis (VL). Additionally, post kala-azar dermal leishmaniasis (PKDL) is a complication following VL (8).

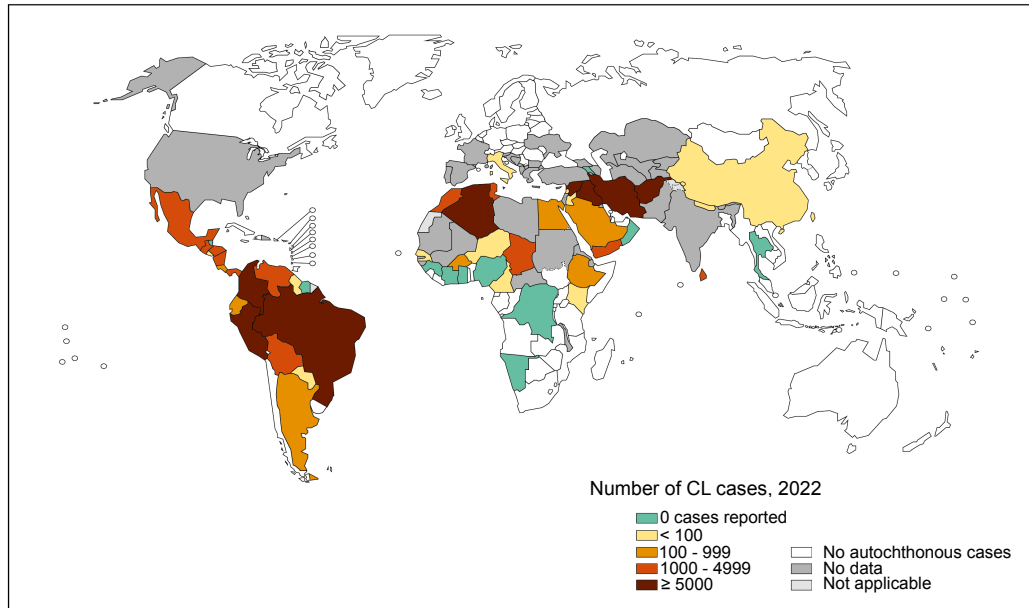
The most common form of leishmaniasis is CL (colloquially: oriental sore) with an estimated incidence of 0.6-1.2 million annually. In 2022, 8 countries accounted for 85% of global CL cases (Afghanistan, Algeria, Brazil, Columbia, Iran, Iraq, Peru and Syrian Arab Republic) with more than 5000 cases each (Fig. 1A) (9). CL is most commonly caused by *L. tropica*, *L. aethiopica* and *L. major* in the Old World and *L. mexicana*, *L. amazonensis* and *L.V. braziliensis* in the New World. These species are more sensitive to temperature and adapted to lower temperatures of approximately 34°C with their dermatropism (10). Symptoms of CL can range from slow-healing but self-limiting ulcers or nodules around the site of inoculation to a dissemination along the lymphatics. The latter manifestation is referred to as diffuse cutaneous leishmaniasis (DCL) and is mainly caused by an insufficient immune response and/or high parasite loads. In both cases, involved body parts are marked with life-long scars often leading to social stigmatisation (11).

In ML (Espundia), the dissemination of ulcers also includes the mucosal membranes of nose, pharynx and the entire oral cavity which can ultimately lead to destruction of infested areas and severe disfigurement. This manifestation occurs in 1-10% of CL cases caused by *L.V. braziliensis*

complex and may not appear until years after the initial ulcers have healed. ML can have a fatal outcome due to secondary infections through necrotic respiratory tract tissue (12).

VL, also known as kala-azar (Hindi for “black fever”), is mostly caused by *L. donovani* or *L. infantum* in the Old World and *L. chagasi* (synonym of *L. infantum*) in the New World. These species are characterised by a higher temperature tolerance of up to 37°C (10). In 2022, about 85% of VL cases were reported from 7 countries (Brazil, Ethiopia, India, Kenya, Somalia, South Sudan and Sudan) (Fig. 1B) (9). VL is the most severe form of leishmaniasis with very high mortality if left untreated or in cases of treatment failure. Infected host cells enter the lymphatics and spread throughout the body, resulting in the dissemination of parasites to inner organs such as spleen, liver and bone marrow. Consequences are irregular fever bouts, weight loss, anaemia, the enlargement of liver and/or spleen (hepato-splenomegaly) and occasional discolouration of the skin. Immune suppression, reactivation of dormant infections or secondary infections may contribute to a fatal outcome. Even after successful treatment of acute VL, PKDL may develop. This form is characterised by a skin rash, which can appear nodular, macular, or maculo-papular. People with active VL or PKDL are considered a natural reservoir for transmission (6, 12).

A Cases of cutaneous leishmaniasis



B Cases of visceral leishmaniasis

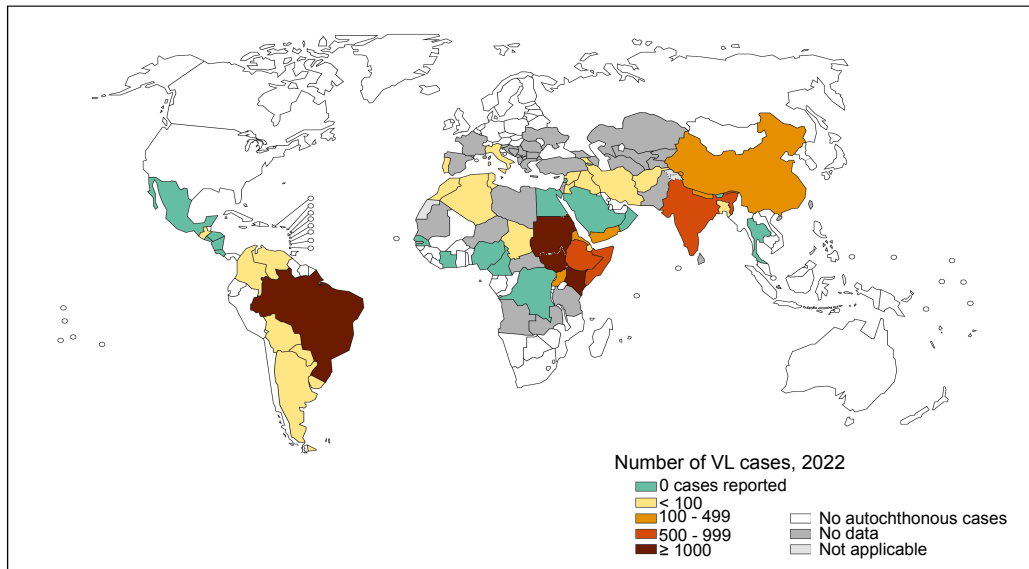


Figure 1: Status of endemicity of leishmaniasis.

Endemicity of countries for the year 2022 based on the reported new cases of (A) cutaneous leishmaniasis and (B) visceral leishmaniasis as reported by 11.2023. Number of cases are indicated in displayed colour code. Non-endemic countries are depicted in white and countries without available data in dark grey. Graphic modified and adapted from (<https://www.who.int/data/gho/map-gallery-search-results?&maptopic=910b5dfc-ce2e-4440-8b43-8d83f4a85485&term=leishmaniasis>)

1.1.2 Life cycle of *Leishmania* spp.

Leishmania parasites are transmitted to the mammalian hosts by the bites of female phlebotomine sandflies. Approximately 70 species, mostly belonging to the genera *Phlebotomus* or *Lutzomyia*, are known to transmit *Leishmania* parasites during their blood feeding (8). This means that *Leishmania* spp. parasites are characterised by a biphasic life cycle. One part occurs in sandflies and the other in mammalian host cells. The ability to adapt to the changing environmental parameters, e.g. pH and temperature, is critical for the parasite and causes it to alternate between two morphologically distinct stages: a non-flagellated amastigote form inside mammalian host cells

and motile, flagellated promastigotes inside the digestive tract of the sandfly vector (13). The transmission cycle starts when non-motile amastigotes are taken up by a female sandfly during a blood meal on an infected mammalian host. The otherwise intracellular amastigotes are released from skin macrophages due to tissue damage caused by the sandfly bite and get ingested or infected cells are ingested (14). Inside the abdominal midgut of the sandfly, the amastigotes differentiate into procyclic promastigotes, the replicative, weakly motile form of promastigotes. Further development into nectomonad promastigotes, the migratory form of promastigotes, allows them to migrate towards the foregut until they reach the stomodeal valve, which separates the midgut from the foregut. Attachment of the parasites to the gut wall is essential for the parasites persistence in the sandfly and is mediated by the parasitic surface molecule lipophosphoglycan (LPG) binding to galactose in the gut lining. Upon reaching the midgut-foregut junction, the parasites differentiate into leptomonad promastigotes, which eventually transform into the mammal-infective metacyclic promastigotes. (14). Depending on the vector and *Leishmania* species, the conversion from amastigotes to metacyclic promastigotes takes 7-14 days. Successful transmission from the vector into the mammalian host is supported by the production of promastigote secretory gel (PSG) by leptomonad promastigotes, which obstructs the midgut and forces the sandfly to regurgitate before the meal and thus transfer the metacyclic promastigotes (15).

After the injection of the parasites into the skin, a local inflammatory response causes the recruitment of mononuclear phagocytes such as macrophages, dendritic cells or neutrophil granulocytes. *Leishmania* parasites additionally release *Leishmania* chemotactic factor (LCF) to induce recruitment and phagocytosis by neutrophils (16). Within macrophages, which are considered the main host cell, parasites differentiate into the clinically relevant amastigote form. This takes place in the phagolysosome of cells and is triggered by the increase in temperature (37°C) and decrease in pH-value (pH=5,5) encountered during transmission from insect vector (25°C, pH=7,4). Amastigotes multiply slowly by binary fission until infected macrophages are phagocytised by other cells or the host cell ruptures and parasites are released. This way, amastigotes can reinfect other host cells and proliferate further until they are ingested by a sandfly during a subsequent blood meal, leading to a new start of the cycle (17). The rupture of cells and dissemination of amastigotes are associated with the onset of symptoms (Fig. 2).

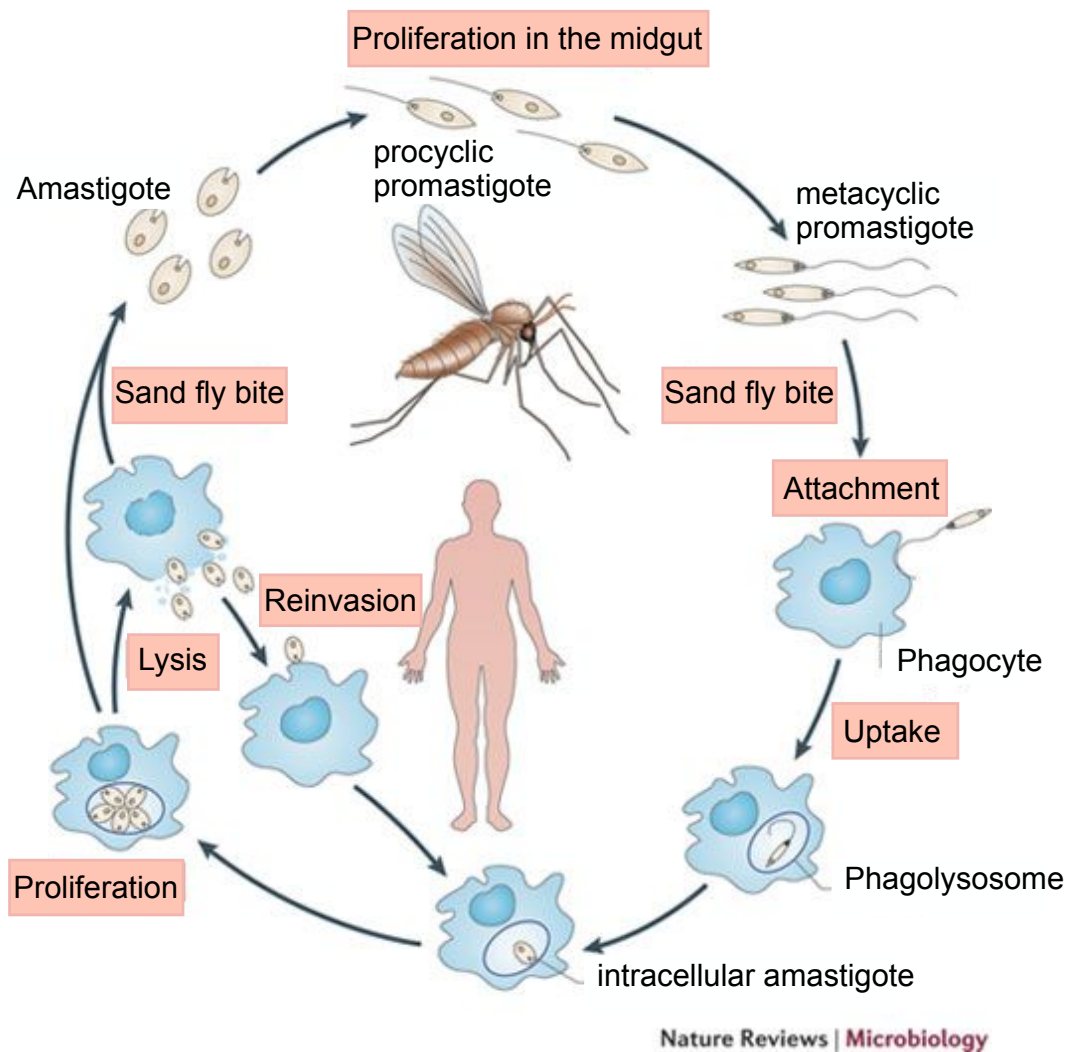


Figure 2. The life cycle of *Leishmania* parasites.

Non-motile amastigotes are ingested by a phlebotomine sandfly during a blood meal on an infected host. The parasites differentiate into procyclic promastigotes in the midgut of the sandfly, before they develop into infective metacyclic promastigotes. During a second blood feed, the sandfly regurgitates metacyclic promastigotes into the host's skin. The parasites can be engulfed by several different phagocytes, in which they differentiate into amastigotes and proliferate within the phagolysosome. After rupture of the host cell, the released parasite can invade new host cells or they are taken up by another sandfly during a blood feed. Illustration based on (17)

1.1.3 *Leishmania infantum*

L. infantum belongs to the *L. donovani* complex and causes VL around the Mediterranean Basin, the Middle East and, increasingly, South and Central America. In endemic regions, immunocompromised patients and infants are mainly affected by the disease. In contrast, *L. donovani* causes VL mainly in India, Bangladesh, Nepal, Sudan, Ethiopia, Eritrea and other parts of East Africa. The genetic similarity between *L. infantum* and *L. donovani* is about 99%, but there are clear differences in geographical distribution of the species, transmitting sandfly species and disease etiology. Two transmission cycles are known for VL, the anthroponotic and zoonotic transmission. The former describes the transmission of parasites from human to human through sandfly bites, and thus humans with active VL or PKDL can act as mammalian reservoir. For the latter, mammalian reservoirs comprise domestic animals, e.g. dogs, but also in peridomestic rodents, e.g. hares (18). Although mammalian reservoirs are observed, e.g. in Sudan or Nepal, a

solely anthroponotic transmission is proposed for *L. donovani*, whereas zoonotic transmission is observed for *L. infantum*, even with evidence for direct transmission through blood transfusions or perinatal transmission from mother to child (19, 20). Differences in the availability and abundance of primary hosts or preferences for specific blood meal sources of different sandfly species are possible explanations for the observed differences in transmission (21).

Another characteristic of *L. infantum* is its clinical pleomorphism as it can cause both VL and CL in endemic regions. Host immune status is certainly a determinant of disease manifestation, as visceralisation is more often observed in human immunodeficiency virus (HIV) positive patients (22), but genetic polymorphism, such as variability in genotype, chromosome size and among the isoenzymatic profile (classification by zymodeme expression) of *L. infantum* parasites has also been discussed as a possible explanation for the variation in the clinical outcome (23, 24). The study of clinical isolates revealed that VL was almost exclusively caused by *L. infantum* zymodeme MON-1 in immunocompetent patients, whereas a large number of different *L. infantum* strains were found in CL. However, the distinction is not as simple, since MON-1 zymodeme was also found in cutaneous cases (23, 25, 26). Additionally, differences in the gene copy number of important antigens or genes encoding metabolic functions were found but would need to be correlated to different clinical outcomes more precisely (23).

1.1.4 Diagnosis and treatment of leishmaniasis

Diagnosis of leishmaniasis can be done directly by the detection of parasites in aspirates, biopsies or smears of skin lesions using microscopic examination or polymerase chain reaction (PCR), or indirectly by serological testing for anti-leishmanial antibodies or delayed-type hypersensitivity/interferon- γ release assay response. Chosen diagnostic method depends on the suspected disease manifestation and availability of resources. In general, it is recommended that results are confirmed by multiple diagnostic methods, as there is no universal test to detect all forms of leishmaniasis and immunosuppression may alter the results of some tests. In addition, not all tests can differentiate between *Leishmania* spp. or active leishmaniasis and previous infection (27, 28).

At present, there are no licensed vaccines available and treatment options for leishmaniasis are limited and without universal recommendation. Commonly used drugs for systemic treatment of leishmaniasis are **pentavalent antimonials**, such as sodium stibogluconate or meglumine antimoniate, which can be used against all forms of leishmaniasis. These drugs are readily available and relatively easy to administer intramuscularly or intravenously, but often accompanied by severe, even fatal, adverse effects, such as myalgia, nausea, cytopenia and even cardiac dysfunction. Additionally, the emergence and spread of *Leishmania* strains resistant to treatment with pentavalent antimonials has been observed especially in parts of India, Nepal and Bangladesh. **Amphotericin-deoxycholate** and the less toxic **liposomal Amphotericin B** are considered the most effective antileishmanial drugs, even in immunosuppressed patients. However, their high cost, need for intravenously administration and cold storage conditions make it inaccessible to affected patients in many endemic countries. Additionally, severe side effects, such as hypokalaemia, renal impairment or anaemia are observed upon administration. The first oral

drug against leishmaniasis is **Miltefosine**. The side effects are minor compared to other treatments, but its teratogenic properties and concerns for resistance limit the benefits and therefore the usage (27, 29, 30). Lastly, treatment of leishmaniasis using **immunomodulatory compounds**, such as Imiquimode, has been tested for cutaneous leishmaniasis by topical application. These compounds are able to potentiate the immune response through the interaction with Toll-like receptors (TLRs) on antigen presenting cells (APCs), such as macrophages. This increases the leishmanicidal activity of cells by the induction of pro-inflammatory cytokine release and increased nitric oxide production as well as augmented T-cell activation (30, 31). To minimise drug dosages, treatment duration and the risk of resistance, a combination of treatment strategies is recommended and often already applied.

1.2 The innate immune system

1.2.1 Cells of the innate immune system

As we are constantly challenged by pathogens in our environment, it is critical to have both a rapid immune response to fight initial infections and a long-term protection against reoccurring pathogens. The vertebrate immune system can therefore be generally subdivided into two parts: the innate immune system, which is responsible for the immediate and pathogen-unspecific response to infections, and the pathogen-specific response and immune memory that are later elicited by the adaptive immune system. The adaptive immune system is composed of B- and T-lymphocytes and is characterised by the production of antigen-specific antibodies and T-cell clones. The innate immune system contains various elements for the protection from invading pathogens such as physical barriers, cellular and humoral components (32, 33).

The first line of defence in the innate immune system are epithelial cell layers that act as physical barriers to prevent infiltration of infectious agents. Mucosal lining of epithelial cells can confer additional microbicidal properties and prevent pathogen spreading.

Penetration of the physical borders by pathogens leads to the activation of innate immune cells within hours. Haematopoietic cells of the innate immune system include monocytes and macrophages, dendritic cells (DCs), natural killer cells, mast cells and natural killer T-cells as well as neutrophilic, basophilic and eosinophilic granulocytes. The cellular response has a broad specificity and is characterised by the recognition of pathogens via common molecules on their surface, the so-called pathogen-associated molecular patterns (PAMPs). These molecules bind to pattern recognition receptors (PRRs), such as membrane-bound TLRs, nucleotide-binding oligomerisation domain (NOD) like receptors and scavenger receptors or to soluble PRRs of the complement system. Binding to PRRs initiates the immune response characterised by phagocytosis of microbes, secretion of cytokines or opsonisation of pathogens (33, 34). Amongst others, macrophages, neutrophils and DCs are important phagocytic cells of the innate immune system. Internalisation of microbes mostly leads to the elimination via multiple microbicidal pathways, and some of the phagocytic cells are able to present phagocytised antigens to lymphocytes, building a bridge between the innate and adaptive immune system. Subsequent secretion of cytokines and other immune modulators, such as reactive oxygen species (ROS)

contribute to the recruitment and activation of further immune cells and aid with efficient clearance of the pathogen (33, 34).

1.2.1.1 Human primary macrophages - functions und subsets

Macrophages are a heterogeneous cell population with a high degree of plasticity. With the exception of some tissue-resident macrophage populations that derive from early yolk sac precursors, such as microglia in the brain or Kupffer cells in the liver, macrophages are haematopoietic cells originating from the terminal differentiation of bone-marrow monocytes (35, 36). Under steady state conditions, intermediate monocytes, characterised by the expression of Cluster of Differentiation (CD) 14, CD16 and high amounts of CX₃C-chemokine receptor 1 (CX₃CR1), can infiltrate the tissue and replace or replenish tissue-resident macrophages. Following an activating stimulus, e.g. infection, damaged tissue or tumour growth, inflammatory monocytes (CD14⁺, CD16⁻) egress the bone marrow due to the interaction of the CC-Chemokine receptor 2 (CCR2) expressed on monocytes with its ligands, and circulate in the blood stream towards the affected tissue, where they transmigrate to the site of stimulus (37, 38). Macrophages are prominent leukocytes at the site of the inflammation where they execute their effector functions, such as phagocytosis, secretion of immune mediators and antigen presentation. However, two main macrophage subpopulations have been recognised depending on the type of stimulus but also on the microenvironment at the site of infiltration: the classically activated pro-inflammatory macrophages (M1) and the alternatively activated, anti-inflammatory macrophages (M2), which can be differentiated by surface molecule expression patterns, profiling of secreted proteins and functional properties, and can influence the outcome of infectious or autoimmune diseases (39-42). The main extracellular stimuli associated with M1 polarisation are Interferon (IFN)- γ and TLR4 signaling by LPS. This subset is characterised by high secretion of IL-12, IL-23 and Tumor Necrosis Factor (TNF)- α , the usage of inducible nitric oxide synthase (iNOS) for the production of reactive nitrogen species (RNS) and higher levels of glutathione compared to M2 macrophages (43). IFN- γ -polarised macrophages are characterised by the expression of activation markers CD80 and CD68 and immunoglobulin receptor CD64 (44).

M2 stimuli include IL-4 and IL-10 (M2a), immune complexes (M2b) and glucocorticoids (M2c). Elevated levels of arginase and polyamines are features of the M2-macrophage subset. Additional characterisation is done by the increased secretion of IL-10 and CCL17 as well as the expression of CD163, CD200R and CD206 (43, 45, 46).

Functional differences include increased phagocytosis rates and tissue-remodelling functions in M2-macrophages, whereas M1-macrophages are associated with microbicidal and anti-tumoral functions (43).

No general prediction can be made for the influence of macrophage polarisation on disease progression or outcome. In infectious diseases, such as leishmaniasis, M1 macrophage polarisation is crucial for the host defence against microbicidal pathogens by the production of ROS and pro-inflammatory cytokines, whereas the exacerbation of the immune response can lead to immunopathology. Conversely, M2 polarisation would promote tissue repair and control the

excessive immune response but M2-macrophages are unable to control proliferation of the infectious agent (43). Additionally it was shown, that general dysregulation of macrophage polarisation, either skewed towards M1 macrophages or M2 macrophages can lead to the manifestation of autoimmune diseases, such as asthma systemic lupus erythematosus or insulin sensitivity (47-49).

1.2.2 Immune response to *Leishmania* infection

1.2.2.1 Macrophages as host cell for *Leishmania* parasites

The immune response elicited by the infection with *Leishmania* parasites is highly dependent on the host species and immune status, as well as on the infecting *Leishmania* spp.. Most of the findings concerning the immune response to *Leishmania* infection were obtained from murine *in vivo* experiments and although many mechanisms identified are applicable to human immune responses, the situation is much more diverse and complicated in human leishmaniasis and remains elusive for large parts (50).

After the transmission of the parasites into the mammalian host, ~ 90% of parasites are lysed by the host complement system, depending on the infecting species and parasite differentiation stage (51). Neutrophils are the first immune cells at the site of parasite inoculation. This massive recruitment may be attributed to the tissue damage caused by the vector bite, immunomodulatory components in the sand fly saliva or parasite-induced secretion of chemoattractants, but the exact stimuli are not fully understood (50). In addition to phagocytosis of the parasites, neutrophils also react to the infection with the formation of neutrophil extracellular traps (NETs) and the secretion of Interleukin (IL)-8, IL-1 β , TNF- α and Macrophage Inflammatory Protein (MIP)-1 β , causing further recruitment of neutrophils and other immune cells. Besides active elimination of parasites by NETosis or ROS production against some *Leishmania* spp., neutrophils can also function as a intermediate host cell or “Trojan Horses”, ensuring parasite survival at early time points after infection. Thus, viable parasites can be transferred to the primary host cells, macrophages, by phagocytosis of apoptotic neutrophils when macrophages reach the site of infection. The second route of macrophage infection is the direct phagocytosis of promastigotes or amastigotes. This is facilitated through various receptors, such as TLRs, fibronectin receptor (FnR), C1 and C3 (Mac-1) or C-type lectin receptors (CLRs) (50, 52).

Successful elimination of the parasites and generation of a protective immune response is dependent on macrophage polarisation and the interaction of innate and adaptive immune cells. A pro-inflammatory immune response is correlated with the secretion of pro-inflammatory cytokines by infected macrophages, such as IL-18 or IL-12. High levels of pro-inflammatory cytokines can also be secreted by infected DCs or by pro-inflammatory macrophages in the environment. This leads to the differentiation of CD4⁺ T-cells into pro-inflammatory T helper type (T_H) 1 cells upon antigen recognition. Characteristic for T_H1 cells is the release of IFN- γ , which is also observed upon activation of NK cells. IFN- γ signaling, in turn, triggers the polarisation of macrophages into M1 macrophages, inducing increased production of highly leishmanicidal ROS, higher levels of iNOS

and thus an elevated RNS concentration in infected macrophages, enabling parasite elimination (50, 51, 53).

The anti-inflammatory response, on the other hand, is closely correlated with high IL-4 levels released by a variety of cells, supporting the differentiation of CD4⁺ T-cells into anti-inflammatory T_H2 cells. In contrast to T_H1 cells, T_H2 cells secrete anti-inflammatory cytokines, such as IL-10, IL-13 and Transforming Growth Factor (TGF)- β , which favours polarisation of macrophages towards anti-inflammatory M2 macrophages, leading to increased survival of parasites by arginase expression and polyamine biosynthesis in infected macrophages (50, 51, 53).

This paradigm observed in standardised mouse models was utilised for many years but in human infections, a mix of T_H1 and T_H2 response was observed more commonly. Additionally, more recent studies also indicate involvement of further T-cell subsets, for example regulatory T-cells (Tregs) and T_H17 cells that are currently investigated more closely (54, 55).

Direct modulation of the immune response by *Leishmania* parasites is observed at various levels. Inside the macrophages, as parasites can modulate the secretion of cytokines, e.g. by boosting IL-10 release and inhibiting the secretion of IL-12, inhibit antigen-presentation and increase macrophage survival (56).

1.3 Sex-specific differences in the immune system

Interestingly, many infectious diseases, autoimmune diseases and cancers occur with a sex-bias in terms of incidence, morbidity and mortality. Whereas the frequency of autoimmune diseases is higher in females, infectious diseases and malignant cancers are more often observed in male patients. This is generally due to females mounting stronger immune responses than males, which is beneficial when fighting infectious agents, albeit making them more susceptible to autoimmune diseases (57-59).

On the biological level, this dimorphism is largely due to differences in the sex-chromosomes and steroid hormones.

1.3.1 Genetic determinants

The described differences can be partly attributed to the differences in the composition of the sex chromosomes, as female individuals have two X chromosomes, and males have one X and one Y chromosome. While the Y chromosome contains very few protein-coding genes, only a few of which have an epigenetic influence on immunology, the X chromosome contains up to 800 protein-coding genes, many of which are associated with immune regulation (60). To prevent double gene dosage in females, one of the X-chromosomes is inactivated during development. This is achieved by the expression of X-inactive specific transcript (XIST), that inactivates the expressing chromosome by chromatin-silencing. However, this silencing is not complete and low expression of various genes is detected after X-linked inactivation (XCI), called XCI escape. Immune-relevant escapee genes include *TLR7*, *CD40L* and *interleukin 1 receptor associated kinase 1 (IRAK-1)*, possibly contribute to the observed sex-bias. In addition, due to the mosaicism in females, the

expression originates from two presumably slightly different alleles, which may result in a broader reactivity (61, 62).

1.3.2 Influence of sex hormones on the immune response

Sex hormones are lipophilic steroid hormones and can be broadly divided into three groups: androgens (testosterone, dihydrotestosterone (DHT), androstenedione, androstenediol, and dehydroepiandrosterone (DHEA)), estrogens (estrone, estradiol, estriol and estrerol) and progesterones. The latter two are associated with biologically female characteristics. All of them have been described to interact with immune cells and thus influence the subsequent immune response. While androgens and progesterones tend to have immunosuppressive effects, estrogens can lead to a stronger immune response. Estrogen receptors are expressed on all immune cells and androgen receptors are expressed on monocytes, macrophages, neutrophilic granulocytes and partly on B- and T-lymphocytes (63, 64).

Signaling of steroid hormones is executed by binding to their respective receptor. For both androgens and estrogens, direct and indirect genomic signaling is described. There are classical and non-classical androgen receptors (AR) and estrogen receptors (ER α /ER β). Classical receptors are localised in the cytoplasm bound to the heat shock protein 90 (HSP90) complex. Upon binding of respective steroid hormone, a conformational change leads to the dissociation from HSP90 and the dimerisation of two receptor monomers. As a dimer, steroid hormone receptors translocate into the nucleus, where they bind to androgen responsive elements (ARE) or estrogen responsive elements (ERE), respectively, in the promotor region of target genes and regulate transcription. Non-classical receptors are localised in the cytoplasm or in the plasma membrane, where they are coupled to G-protein-coupled receptors. Non-classical receptors can regulate their gene expression through DNA-binding-dependent and -independent mechanisms, e.g. via second messengers (64-66).

Sex hormones can alter the activity of innate and adaptive immune cells and the subsequent immune response in various ways, as summarised in the review of Klein and Flanagan (57). In innate immune cells, androgens have been shown to suppress iNOS, NO and TNF- α expression in macrophages as well as a general down regulation of TLR4. Additionally, the number of neutrophils was increased upon androgen treatment (59, 67). For cells of the adaptive immune system, influence of androgens has been described for T_H17 cells, in which they increase the release of IL-17, and increase the number of T_{regs}. On the other hand, the number and activity of CD8⁺ T-cells was reduced, the same as the antibody response. Cytokine expression was skewed towards increased IL-10, TGF- β , IL-1 β and IL-2 secretion and lower levels of CCL-3 and IFN- γ (57, 58, 68-70).

In contrast to androgens, estrogens are found to induce the global expression of TLR-4, TLR7 and TLR9 on innate immune cells, such as macrophages and DCs, and induce DC activation and their increased CCL-2 secretion. In neutrophils, estrogens enhance degranulation and elastase release, whereas eosinophils decrease in numbers and mobilisation. From innate immune cells, increased secretion of pro-inflammatory cytokines, such as TNF- α and IL-6 was measured upon estrogen

treatment. A concentration-dependent difference was observed for the influence on T-cells: low levels of estrogens induce T_H1 cell differentiation and enhance antigen-specific $CD4^+$ T-cell response, whereas high levels of estrogens promote T_H2 cell differentiation. Lastly, higher $CD8^+$ T-cells and antibody response was observed under the influence of estradiol (57, 71, 72).

1.3.3 Sex-specific differences in leishmaniasis

Leishmaniasis presents with notably higher number of clinical cases and higher mortality in male patients for CL and VL in various endemic areas (73, 74). In addition to the influence of the infecting *Leishmania* species (75) this phenomenon is probably linked to two factors, societal and biological differences between sexes (76).

Sociocultural determinants leading to higher incidences of leishmaniasis in male patients include differences in vector exposure, for example, due to different working environments of men and women (77), as well as an overrepresentation in healthcare centres and clinical trials compared to female patients, who often experience lower treatment prioritisation and limited access to healthcare in endemic countries. Additionally, lower compliance with preventive measures against leishmaniasis and higher rates of discontinued treatment in male patients can also cause this discrepancy (75, 76, 78).

However, results of many epidemiological studies with minimal influence of gender-specific determinants, still demonstrate sex-specific differences, emphasising that this phenomenon cannot be explained by cultural or behavioural determinants only, and biological factors can alter the susceptibility towards an infection and influence the outcome of the disease. Male predominance was observed in VL caused by species from both New and Old World (79-81), as well as in CL caused by infection with, for example, *L. panamensis*, *L. braziliensis* or *L. mexicana* in the New World. The discrepancy in the latter infection was associated with elevated serum levels of GM-CSF and $IFN-\gamma$ in females (82-84). Moreover, differences in tropism and disease manifestation between sexes were observed in *L. tropicana* infection, that manifested more commonly as CL in females and as VL in males. Similarly, in *L. mexicana* infection, higher cases of anergic diffuse cutaneous leishmaniasis (ADCL) were observed in males, whereas localised CL was more prominent in females, potentially caused by an increased number and activity of NK cells resulting in increased levels of $TNF-\alpha$ and $IFN-\gamma$. Interestingly, age-dependent differences in sex-specific incidences were observed, with the strongest sex differences occurring in infants under one year of age and adults between 20 and 59 years, hinting to an influence of sex hormones on infection (74, 75, 78, 85, 86).

In addition, animal models for leishmaniasis present a sex dichotomy as well and can therefore be used to study distinct sex-specific immune responses (87). In rodent models of cutaneous leishmaniasis, a clear correlation was found between T_H2 -associated cytokine levels and susceptibility to leishmaniasis and lesion formation, as males presented increased mRNA expression for cytokines such as IL-4, IL-10 and $TGF-\beta$, whereas female animals showed increased levels of pro-inflammatory mediators, including nitric oxide (NO), IL-12, IL-6, IL- 1β and $IFN-\gamma$ (75, 88, 89). Mice lacking the IL-4 receptor α were resistant to infection with *L. mexicana*

(90). Other mouse models observed differences in the immune cell populations infiltrating at the site of infection, with increased eosinophil recruitment in males (91). Additionally, experiments conducted *in vivo* and *in vitro* emphasised, that sex hormones contribute significantly to the outcome of both CL and VL. Mock and Nancy showed that gonadectomised male mice exhibited slightly lower parasite burdens in the liver, whereas the supplementation of female mice with testosterone resulted in a significant increase in detected *L. donovani* units (92). Similar effects were observed upon castration and hormone supplementation in hamsters (88, 93). *In vitro*, estradiol-treated macrophages exhibit enhanced parasite killing (89, 94), whereas testosterone promoted lower antimicrobial activities and increased parasite uptake (95, 96).

1.4 Aim of thesis

Leishmaniasis is a neglected tropical disease transmitted by sandfly vectors. Leishmaniasis occurs with a sex bias towards males in its two most prevalent human manifestations, cutaneous and visceral leishmaniasis, mirroring the sex disparity seen in many other infectious diseases. This is observed in epidemiological studies, as well as in rodent animal models for leishmaniasis (75, 87).

The aim of this thesis is to investigate the underlying biological factors contributing to the sex bias in leishmaniasis. Specifically, the research will focus on elucidating differences using infected primary human macrophages, as the main host cells for proliferation and persistence of *Leishmania* parasites, on immunological, cellular and transcriptomical levels.

In order to investigate the putative determinants for the distinct susceptibility of female and male macrophages to *L. infantum* infection, an analysis of infected macrophages was conducted, focusing on the following parameters:

1. Investigation of sex-difference in *in vitro* infection assay by
 - Quantification of viability, infection rate and parasite load of female- and male-derived primary human macrophages over time using confocal high content screening and automated customised image analysis
 - Determination of the polarisation states of macrophages during infection using morphology- and phenotype-based distinction methods
 - Measurement of secreted cytokines using cytometric bead assay (LEGENDplex™)
 - Comparative transcriptome analysis of infected female and male macrophages and respective controls as determined by RNA sequencing
2. Influence of sex hormones on *L. infantum* infection by pre-treatment of macrophages prior to infection and analyses with aforementioned methods

2 Material and Methods

2.1 Material

2.1.1 Laboratory equipment

Table 1: List of utilised laboratory equipment

Laboratory equipment	Provider
2100 Bioanalyser	Agilent Technologies, Inc., Waldbronn, Germany
Centrifuge benchtop 2-16KL	Sigma Laborzentrifugen GmbH, Osterode am Harz, Germany
Centrifuge Eppendorf® 5415 D	Eppendorf, Hamburg, Germany
Centrifuge Eppendorf®5415 R	Eppendorf, Hamburg, Germany
Centrifuge J2-HS	Beckmann Coulter, Brea, US
Cytek® Aurora 5-Laser spectral Flow Cytometer	Cytek® Biosciences, Amsterdam, Netherlands
EVOS® FL Auto Cell Imaging System	Thermo Fisher Scientific, Inc., Waltham, US
Fume Hood	Werner Hassa GmbH, Lübeck, Germany
Horizontal role shaker KS250 basic	IKA-Werke GmbH, Staufen, Germany
Incubator HERA Cell 150i CO ₂	Thermo Fisher Scientific, Inc., Waltham, US
Incubator New Brunswick TM Galaxy® 170S	Eppendorf, Hamburg, Germany
Laminar flow cabinet LaminAir® HB2448	Hareus instruments by Thermo Fisher Scientific, Inc., Waltham, US
Laminar flow cabinet MSC Advantage	Thermo Fisher Scientific, Inc., Waltham, US
LSR Fortessa™ Flow Cytometer	BD® Biosciences, Heidelberg, Germany
LSR II™ Flow Cytometer	BD® Biosciences, Heidelberg, Germany
Multichannel pipet	Mettler Toledo®, Gießen, Germany
Multisizer™3 Coulter counter	Beckmann Coulter, Brea, US
NanoDrop 2000 Spectrophotometer	Thermo Fisher Scientific, Inc., Waltham, US
MrFrosty™ Freezing Container	Thermo Fisher Scientific, Inc., Waltham, US
Neubauer chamber	Carl Roth®, Karlsruhe, Germany
NextSeq™1000/2000-System	Illumina, San Diego, US
NextSeq™550-System	Illumina, San Diego, US
Opera Phenix High content screening system	revivvty, Hamburg, Germany
Pipet-Lite XLS electric pipette	Mettler Toledo®, Gießen, Germany
Plate shaker	IKA-Werke GmbH, Staufen, Germany
Vortexer VF2	IKA-Werke GmbH, Staufen, Germany

Laboratory equipment	Provider
Waterbath 1002	Lauda GmbH&Co, Lauda-Königshofen, Germany
Pipets (0.1-2 µL, 1-10 µL, 2-20 µL, 10-100 µL, 50-200 µL, 100-1000 µL)	Mettler Toledo®, Gießen, Germany

2.1.2 Consumables

Table 2: List of utilised consumables

Consumable	Provider
Well plates flat bottom Standard (6-well, 12-well)	Sarstedt, Nümbrecht, Germany
Well plates round bottom (96-well)	Sarstedt, Nümbrecht, Germany
Well plates V-bottom (96-well)	Greiner Bio-One, Frickenhausen, Germany
Cell scraper	Sarstedt, Nümbrecht, Germany
Cryopreservation tube 2ml	Sarstedt, Nümbrecht, Germany
Culture flask without filtered cap (T25 cm ² , T75 cm ²)	Sarstedt, Nümbrecht, Germany
Eppendorf tubes (1.5 mL, 2 mL)	Sarstedt, Nümbrecht, Germany
Falcons (15 mL, 50 mL)	Sarstedt, Nümbrecht, Germany
5 mL polystyrene tube	Sarstedt, Nümbrecht, Germany
Phenoplates ultra+Lid (96 well)	revivvy, Hamburg, Germany
Parafilm M	Sigma-Aldrich, St.Louis, US
α-CD14 magnetic beads	BD® Biosciences, Heidelberg, Germany
Carboxylate-modified red fluorescent latex beads (0.2 µm)	Sigma-Aldrich, St.Louis, US
Pipette Tips glass (5 mL, 10 mL, 25 mL)	Costar, New York, US
Pipette Tips surthob (filtered) (10 µL, 200 µL, 1000µL)	Biozym Scientific GmbH, Hessisch Oldendorf, Germany
Pipette Tips (10 µL, 200 µL, 1000µL)	Eppendorf, Hamburg, Germany
Pipette Tips for multichannel pipettes (300 µL)	Mettler Toledo®, Gießen, Germany
Pipette Tips for electric pipette (1200 µL)	Mettler Toledo®, Gießen, Germany
SepMate® tubes (50 mL)	StemCell, Cologne, Germany
Bottle top filter (0.22 µm)	MerckMilipore, Darmstadt, Germany

2.1.3 Chemicals and solutions

Table 3: List of utilised chemicals and solutions

Solution or chemical	Provider
0.04% trypan blue	Gibco Life Technologies by Thermo Fisher Scientific, Inc., Waltham, US
4% PFA	Thermo Fisher Scientific, Inc., Waltham, US
Biocoll®	Bio&Sell, Feucht/Nürnberg, Germany
DPBS	PAN Biotech™, Aidenbach, Germany
TRIzol® Reagent	Invitrogen™ by Thermo Fisher Scientific, Inc.
Ethanol	Carl Roth®, Karlsruhe, Germany
2-Propanol (Isopropanol)	Carl Roth®, Karlsruhe, Germany
CASYton	Beckmann Coulter, Brea, US
Charcoal, Dextran coated	Sigma-Aldrich, St.Louis, US

2.1.4 Kits

Table 4: List of utilised kits

Kit	Provider
eBioscience™ Foxp3/ Transcription Factor Staining Buffer kit	Invitrogen™ by Thermo Fisher Scientific, Inc.
LEGENDplex™ Customised human 12-Plex panel	Biolegend, San Diego, US
NextSeq1000/2000 P2 Reagents (200 Cycles) Kit v3	QIAGEN, Hilden, Germany
NextSeq500/550 Mid Output Kit v2.5 (150 Cycles)	QIAGEN, Hilden, Germany
NucleoSpin RNA clean up kit	Machery-Nagel, Düren, Germany
QIAseq Stranded mRNA Lib Kit UDI-A	QIAGEN, Hilden, Germany
Red Blood Cell (RBC) lysis kit	Biolegend, San Diego, US
RNA 6000 Pico Kit	Agilent Technologies, Inc., Waldbronn, Germany
UltraComp eBeads™ Plus Compensation Beads	Invitrogen™ by Thermo Fisher Scientific, Inc.

2.1.5 Antibodies

Table 5: List of utilised antibodies

Antibody	Clone	Host	Fluorochrome	Provider	Dilution	Application
α-human CD163	GHI/61	Mouse	PerCP-Cy5.5	Biolegend, San Diego, US	1:12,5	
α-human CD16	3G8	Mouse	FITC	Biolegend, San Diego, US	1:15	
α-human CD86	IT2.2	Mouse	PE-Cy7	Biolegend, San Diego, US	1:15	

Antibody	Clone	Host	Fluorochrome	Provider	Dilution	Application
α -human CD200R	OX-108	Mouse	PE	Biolegend, San Diego, US	1:12,5	Flow cytometry
α -human CD64	10.1	Mouse	APC-Fire	Biolegend, San Diego, US	1:12,5	
α -human CD206	15-2	Mouse	APC	Biolegend, San Diego, US	1:12,5	
α -human CD14	MSE2	Mouse	BV-510	Biolegend, San Diego, US	1:15	
α -human CD68	Y1/82A	Mouse	BV-421	Biolegend, San Diego, US	1:11	
α -human HLA-DR	G46-6	Mouse	BUV-395	BD Bioscience®, Heidelberg, Germany	1:11	
DAPI				Sigma-Aldrich, Munich, Germany Reconstituted in DPBS Stock = 1mg/mL	1:100	Immuno-fluorescence microscopy
α -LHSP90		Mouse	Uncoupled	Produced at BNTIM	1:4000	
α -mouse/human secondary antibody		Goat	AF-647	Invitrogen by Thermo Fisher Scientific, Inc.	1:8000	
α -mouse/human secondary antibody		Goat	AF-488	Invitrogen by Thermo Fisher Scientific, Inc.	1:8000	
LysoBrite™ red DND-99				Sigma-Aldrich, Munich, Germany	1:250	

2.1.6 Culture media and buffers

2.1.6.1 Preparation of fetal calf serum (FCS)

All FCS was heat-inactivated before usage. This was done by placing it in a water bath at 56°C for 30 min. Afterwards it was aliquoted and stored at -20°C until further usage.

To supplement the medium used for macrophage culture, FCS was additionally stripped with activated charcoal to remove non-polar and lipophilic components, particularly steroid hormones. For this purpose, 25 mL of heat-inactivated FCS was incubated with 0.5 g activated charcoal and incubated overnight (ON) at 4°C on a laboratory roller mixer. The following day, the charcoal-stripped FCS was centrifuged (15 min, 800 g, 4°C) and sterile filtered through a 0.22 µm filter before storing it at -20°C.

Table 6: List of utilised culture media

Medium	Provider and/or Composition	Application
M199 medium with Earl's balanced salt solution	Sigma-Aldrich, Munich, Germany	Cultivation and freezing of <i>Leishmania</i> parasites
Supplemented M199 medium (pH 7,4) (M199+)	1x M199 20% FCS (heat-inactivated) (Sigma-Aldrich, Munich, Germany) 40 mM HEPES (Biomol, Hamburg, Germany) 10 mg/L Haemin (Sigma-Aldrich, Munich) 0.1 mM Adenine (Carl Roth, Karlsruhe, Germany) 6 µM 6-Biopterin (Biomol, Hamburg, Germany) 2 mM L-Glutamine (Sigma-Aldrich, Munich, Germany) 100 U Penicillin (Sigma-Aldrich, Munich, Germany) 100 µg/mL Streptomycin (Sigma-Aldrich, Munich, Germany) Storage at 4°C	
Freezing medium for parasites	30% M199+ 50% FCS (heat-inactivated) (Sigma-Aldrich, Munich, Germany) 20% DMSO (Carl Roth, Karlsruhe, Germany) Storage -20°C	
RPMI 1640 With or without phenol red	PAN Biotech, Aidenbach, Germany	Cultivation and freezing of cells
Supplemented RPMI (cRPMI)	88% cRPMI 10% FCS (heat-inactivated, charcoal-stripped) (Capricorn, Ebsdorfergrund, Germany) 1% L-Glutamine (PAN Biotech, Aidenbach, Germany) 1% Penicilline-Streptomycin (PanReac AppliChem,) 10 ng/mL M-CSF / GM-CSF Storage 4°C	
Freezing medium for cells	90% FCS (heat-inactivated, charcoal-stripped) (Capricorn, Ebsdorfergrund, Germany) 10% DMSO (Carl Roth, Karlsruhe, Germany) Storage -20°C	

Table 7: List of utilised buffers

Buffer	Composition
1x PBS (pH 7.4)	2.7 mM KCl (Merck, Darmstadt, Germany) 1.5 mM KH ₂ HPO ₄ (Merck, Darmstadt, Germany) 8.1 mM Na ₂ HPO ₄ 137 mM NaCl (Merck, Darmstadt, Germany) In ddH ₂ O
MACS buffer (10X)	20 mM EDTA (Merck, Darmstadt, Germany) 5% protease-free BSA (Serva, Heidelberg, Germany) in 1xPBS (pH 7.4)
FACS buffer	0.1 % FCS (heat-inactivated) in DPBS
Washing buffer (Immunofluorescence staining)	0.1% Triton X-100 (Carl Roth, Karlsruhe, Germany) in 1xPBS (pH 7.4)
Permeabilisation buffer (Immunofluorescence staining)	50 mM NH ₄ Cl (Carl Roth, Karlsruhe, Germany) 0.1% Triton X-100 (Carl Roth, Karlsruhe, Germany) in 1xPBS (pH 7.4)
Blocking buffer (Immunofluorescence staining)	2% protease-free BSA (Serva, Heidelberg, Germany) 0.1% Triton X-100 (Carl Roth, Karlsruhe, Germany) in 1xPBS (pH 7.4)

2.1.7 Stimulants for *in vitro* treatment

Table 8: List of utilised stimulants

Stimulant	Provider and reconstitution
Recombinant IFN- γ (lyophilised)	Sigma-Aldrich, Munich, Germany Reconstituted in ddH ₂ O Stock concentration = 1 μ g/ μ L
Recombinant IL-4 (lyophilised)	Sigma-Aldrich, Munich, Germany Reconstituted in ddH ₂ O Stock concentration = 0.1 μ g/ μ L
17- β -Estradiol (lyophilised)	Sigma-Aldrich, Munich, Germany Reconstituted in Ethanol Stock concentration = 0.937 mg/mL \triangleq 3.443 μ M
5- α -Dihydrotestosterone solution	Merck, Darmstadt, Germany Reconstituted in Methanol Stock concentration 1 mg/mL \triangleq 3.443 μ M
Recombinant M-CSF solution (25 μ g)	Biologend, San Diego, US Reconstituted in PBS Stock concentration = 0.2 mg/mL
Recombinant GM-CSF solution (10 μ g)	Biologend, San Diego, US Reconstituted in PBS Stock concentration = 0.2 mg/mL

2.1.8 Parasite strains

Table 9: List of utilised parasite strains

Strain	Identification number	Origin	Provider
<i>Leishmania major</i> 5ASKH	MHOM/TM/1973/5ASKH	Turkmenistan	David Evans, London School of Hygiene and Tropical Medicine, United Kingdom
<i>Leishmania braziliensis</i>	MHOM/PE/01/LH2182 (PER005) clone 2	Peru	Jean-Claude Dujardin, Institute of Tropical Medicine, Antwerp
<i>Leishmania donovani</i>	BPK190/0 clone 3	Nepal	Jean-Claude Dujardin, Institute of Tropical Medicine, Antwerp
<i>Leishmania infantum</i> belonging to MON-1 zymondeme	MHOM/FR/91/LEM2259 clone 3511	France	Annie Sulahian, Centre National de Référence des Leishmanioses, Montpellier

2.1.9 Human samples

Ethical approval for all experiments using fresh human blood samples was obtained from the Ethics Committee of the University of Hamburg (202-10067-BO). Blood donations (500 mL) of healthy donors were collected and further processed into to separate blood components (erythrocyte concentrate, buffy coat and blood plasma) by centrifugation at Transfusionsmedizin und Blutspendezentrum, University clinic Eppendorf (UKE). This resulted in 50 mL-65 mL buffy coat per donor. Samples were stored ON at room temperature (RT) and provided the following day free of charge with details of donor's sex, year of birth and cytomegalovirus serological status.

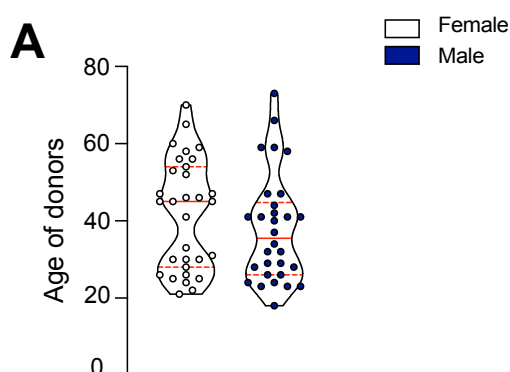


Figure 3: Age distribution of blood donors.

(A) Age distribution of female and male blood donors used in the thesis. Data is shown as violin blot with indicated median (red solid line) and quartiles (red dotted line). $n_{F/M}=30/29$

2.1.10 Software and Databases

Table 10: List of utilised softwares and databases

Software / Databases	Application
Harmony software (v 4.6, Perkin Elmer)	Automated image analysis of confocal, immunofluorescent pictures

Software / Databases	Application
legendplex.qognit.com	Evaluation of LEGENDplex™ data
SpectroFlo®	Cytek® Aurora 5L flow cytometer operation software
EndNote X9.3.3	Literature library and citation manager
LibreOffice, version 7.3.5.2	Data processing and analysis
GraphPad Prism10, version 10.0.1	Graphical illustration and statistical analysis of data
FlowJo v10.10.0	Analysis of flow cytometry data
ImageJ, version 1.53a	Microscope image processing
Intaglio™, version 3.9.5	Figure composition and assembly
interactivenn.net	Generation of Venn diagrams
BioRender.com	Figure composition
heatmapper.ca online tool	Generation of expression heatmaps
ShinyGO v0.80	Gene ontology enrichment analysis
TritypDB	Database for trypanosomatidae
Pubmed-NCBI	Literature research

2.2 Methods

2.2.1 Cell culture methods

2.2.1.1 Culture of *Leishmania* promastigotes

Leishmania parasites were routinely maintained in their flagellated and elongated promastigote stage which normally occurs in the midgut of female sandflies. To mimic these conditions, parasites were cultured in T25² flasks without filtered cap at 25°C in 10 mL M199+ (pH 7,4) medium and restricted air supply. Cell densities were microscopically monitored and cultures were diluted every three to four days to 1*10⁵-1*10⁶ parasites/mL.

2.2.1.2 Cell counting of parasites

Parasites were diluted 1:1000 in CASYton and counted using Beckmann Coulter cell counter. This cell counter measures the size and conductivity of the cells in a suspension to receive the specific number of viable parasites. All measurements were done in duplicates.

2.2.1.3 Cryopreservation of parasites

For long-term storage, parasites were stored in liquid nitrogen at -196°C. For this, late logarithmic phase promastigote cultures were counted (2.2.1.2) and 1*10⁸ parasites were pelleted by centrifugation for 10 minutes (min) at 2500 rounds per minute (rpm) and 4°C. The supernatant was discarded and parasites were resuspended in 500 µL of cold M199+ (pH 7,4) medium and

transferred into 2 mL cryopreservation tubes containing 500 μ L parasite freezing medium. Cell suspension was mixed thoroughly and tubes were immediately placed at -80°C in a styrofoam box. Cryovials were transferred into liquid nitrogen tank the next day.

For thawing of parasites, T25² flasks were prepared with 10 mL M199+ (pH 7.4) medium. Parasite suspensions from liquid nitrogen tank were rapidly thawed by shortly placing them in a 37°C water bath and immediately transferred into the culture flasks once defrosted. To remove residues of DMSO, parasites were diluted 1:10 the next day and 1:100 two days after thawing.

2.2.1.4 Isolation of leukocytes from human blood samples

All reagents were brought to RT and 50 mL SepMate™ tubes were filled with 15 mL Biocoll density gradient solution through the insert. Blood samples were diluted with Dubelcco's Phosphate-buffered Saline (DPBS) in a ratio of 1:2 and distributed to SepMate™ tubes by carefully pipetting the solution onto the insert. Samples were centrifuged for 10 min at 200 g and RT. Cells were thereby separated according to their density which resulted in a erythrocytes and granulocytes being retained under the insert of the SepMate™ tube ,while other peripheral blood mononuclear cells (PBMCs) were enriched in the plasma above the insert. To recover the PBMCs, the top layer was carefully poured into a new 50 mL falcon which was then filled up to 50 mL with DPBS. To remove platelets from the cell solution, samples were then washed by centrifugation without break (10 min, 120 g, RT). Supernatant was carefully removed and cells from one donor were pooled. The cells were wash again by adding 10 mL DPBS and centrifugation for 8 min at 300 g and RT. After removing the supernatant completely, cells were resuspended in 5 mL 1x RBC lysis buffer by brief vortexing and incubated on ice for 5 min with occasional shaking. After 5 min, the lysis was stopped by adding 20 mL cold DPBS and centrifugation for 5 min at 350 g and 4°C . Supernatant was removed and cells were washed with 10 mL cold DPBS with same centrifuge settings as before. The isolated cells were resuspended in 10 mL cold DPBS for counting (2.2.1.6). For the isolation efficacy control, 1×10^6 cells were retained from each donor and stored at 4°C until flow cytometry staining (2.2.1.15.1). The rest of cells was used for the for purification of CD14⁺ monocytes (2.2.1.5) or prepared for cryopreservation (2.2.1.9)

2.2.1.5 Isolation of human CD14⁺ monocytes from PBMCs

CD14⁺ monocytes make up about 10% of PBMCs in human peripheral blood and were purified from PBMCs in order to differentiate them into monocyte-derived macrophages (hMdMs). The amount of PBMCs required was calculated based on the required amount of CD14⁺ monocytes and pelleted by centrifugation (5 min, 350 g, 4°C). Supernatant was discarded and cells were washed with 2 mL 1x MACS buffer (5 min, 350 g, 4°C). Supernatant was discarded completely and cells were resuspended in 50 μ L vortexed α -CD14 magnetic particle per 1×10^7 PBMCs and mixed thoroughly. After incubation for 30 min at RT, cells were diluted to $1-8 \times 10^7$ cells/mL with 1x MACS buffer and transferred to a 5 mL polystyrene tube. The tube was placed at the magnet for 10 min and labelled CD14⁺ monocytes pelleted at the side of the magnet. The supernatant was carefully removed completely with a pipette without disturbing the pellet before the tube was detached from the magnet. For washing, the cell pellet was resuspended in 1 mL 1x MACS buffer and placed at

the magnet again for 4 min. The supernatant was removed carefully again after incubation. The washing step was repeated but the cells were resuspended in 5 mL cold DPBS afterwards and transferred to a new 50 mL tube. The cells were counted (2.2.1.) and 1×10^6 cells were retained from each donor and stored at 4°C until flow cytometry staining (2.2.1.). The rest of cells were pelleted (5 min, 350 g, 4°C) and resuspended in the suitable volume of pre-warmed cRPMI and used for the differentiation into macrophages (2.2.1.7) or for *in vitro* polarisation into different subtypes of macrophages (2.2.1.8)

2.2.1.6 Cell count determination

Cell count of isolated cells was determined using the Neubauer counting chamber (depth=0.1 mm, area=0.0025 m²). Cells were diluted 1:100 (PBMCs) or 1:10 (purified CD14⁺ monocytes) in 0.04% trypan blue and 10 µl of the solution was pipetted into the chamber. Trypan blue is used as an indicator of the intactness of cells, as it passes through the perforated membrane of apoptotic cells and stains them blue. Viable cells were counted in all four large squares. The concentration of the cells was subsequently calculated using following equation:

$$C = n * D * 10000$$

C = concentration of cells [cells/mL]

n = mean number of viable cells per square

D = dilution factor of cell solution

10000 = correction factor depending on depth and area of chamber

2.2.1.7 Differentiation of human monocytes into monocyte-derived macrophages

For the differentiation of human monocytes into hMdMs, isolated CD14⁺ monocytes (2.2.1.6) were cultured in suitable well plates with respective volume of pre-warmed cRPMI medium with 10 ng/mL macrophage colony stimulating factor (M-CSF) at 37°C and 5% CO₂ (Tab. 11). Half of the medium was carefully removed with a pipette on day four and six after isolation and replaced with new medium, whereby the concentration of M-CSF was always calculated for the final medium volume again. Complete medium change was done at day 8 after isolation. Cells were used for *in vitro* infection on day eleven post isolation (2.2.1.11). If not stated differently, macrophages differentiated with M-CSF were used in the following thesis.

Table 11: List of utilised well plates, seeding strategy and application

Plate type	Amount of cells and medium per well	Application
6-well plate	1×10^6 cells in 5 mL	Staining for flow cytometry
12-well plate	5×10^5 cells in 2 mL	RNA isolation
96-well Phenoplates	1×10^5 cells in 200 µL	Confocal high content screening

2.2.1.8 *In vitro* polarisation of macrophages

For characterisation of different macrophage subpopulations, *in vitro* polarisation of macrophages was performed. For generation of M1-like macrophages, isolated CD14⁺ monocytes (2.2.1.6) were cultured and differentiated into macrophages as previously mentioned (2.2.1.7) with cRPMI but under the addition of 10 ng/mL granulocyte-macrophage colony stimulating factor (GM-CSF) instead of M-CSF with respective medium changes. On day eight, the complete medium was removed from wells and cRPMI with 10 ng/mL GM-CSF and 20 ng/mL Interferon (IFN)- γ was added. Cells were analysed on day eleven using confocal high content screening (2.2.4) or stained for flow cytometry (2.2.1.15.1). For generation of M2-like macrophages, cells were cultured in cRPMI + 10 ng/mL M-CSF until day eight. On day eight, the medium was additionally supplemented with 20 ng/mL Interleukin (IL)-4 until day eleven.

2.2.1.9 Cryopreservation of PBMCs

Up to 1×10^8 cells were frozen per cryovial. Therefore, isolated cells were pelleted by centrifugation (1200 rpm, 4°C for 5 min). Supernatant was discarded and cells were resuspended 1 mL cold freezing medium per 1×10^8 cells. 1 mL of the cell suspension was transferred into each 1 mL cryopreservation tube and placed in a pre-cooled Mr. Frosty™ freezing container for gentle freezing of the cells. The freezing container was placed at -80°C ON. Cryovials were transferred into liquid nitrogen tank the next day.

For thawing of the cells, cryovials from liquid nitrogen tank were removed and rapidly thawed by brief immersion in a 37°C water bath. Cells were transferred into 10 mL pre-warmed culture medium and washed by centrifugation (1200 rpm, 4°C for 5 min). The washing step was repeated with 1 mL pre-warmed culture medium and cells were subsequently placed in suitable culture flasks or plates with required culture medium and placed at 37°C and 5% CO₂.

2.2.1.10 *In vitro* treatment of macrophages with steroid hormones

Mature macrophages were treated with steroid hormones in order to investigate the influence on the infection with *Leishmania* parasites. Therefore, CD14⁺ monocytes were differentiated into hMdMs in 96-well or 6-well plates using supplemented RPMI without phenol red with 10 ng/mL M-CSF (2.2.1.7). The medium was completely removed from cells on day eleven and replaced by pre-warmed supplemented RPMI w/o phenol red with 10 ng/mL M-CSF and corresponding steroid hormone (5- α -Dihydrotestosterone or 17- β -Estradiol) in required concentration (0.01-5 μ M) in a volume of 50 μ L per well. Cells were placed at 37°C and 5% CO₂ for 30 min before *Leishmania* parasites were directly added according to chapter 2.2.1.11 without change of medium.

2.2.1.11 *In vitro* infection of macrophages

Four days before infection, late logarithmic promastigote parasite cultures were diluted 1:10 in M199⁺ medium in order to generate stationary phase cultures with metacyclic promastigotes for the infection.

For the *in vitro* infection of hMdMs, the parasites were counted (2.2.1.2) and the corresponding number of stationary parasites for the required multiplicity of infection (MOI) were sedimented by centrifugation for 10 min at 2.500 rpm and 4°C. The pelleted parasites were resuspended in the volume of pre-warmed cRPMI+10 ng/mL M-CSF required for the number and size of wells. Cell culture medium was discarded with a suction pump, and the appropriate volume of parasite suspension was added per well (Tab. 12). Cells were incubated for 4 hours (hrs) at 5% CO₂ and 37°C for viscerotropic species (*L. donovani* and *L. infantum*) and 34°C for dermatropic species (*L. major* and *L. braziliensis*).

After the incubation, extracellular parasites were removed by washing with DPBS twice. Cells were then either directly fixed with 4% paraformaldehyd (PFA) for 4 hours post infection (hpi) time point (2.2.1.14) or covered with adequate volume of supplemented RPMI+10 ng/mL M-CSF and incubated further at 34 °C / 37°C and 5% CO₂. At desired time point, cells were used for labelling of parasitophorous vacuoles (2.2.1.13), fixed with 4% PFA for confocal microscopy, (2.2.1.14) or harvested for flow cytometry staining (2.2.1.15.1), or RNA isolation (2.2.2.1). Supernatant was collected and stored at -20°C for cytokine profiling (2.2.3.1).

Table 12: List of volume for infection and washing for different plates

Plate type	Volume of parasite suspension per well	Volume for washing steps per well
6-well plate	1 mL	2 mL
12-well plate	500 µL	1 mL
96-well Phenoplates	100 µL	150 µL

2.2.1.12 Incubation of macrophages with phagocytosis beads

To generate samples as phagocytosis control for RNA sequencing, hMdMs were incubated with carboxylate-modified polystyrene latex beads. The appropriate volume of bead suspension was diluted in the volume of cRPMI+10 ng/mL M-CSF required for the number and size of wells. Medium from macrophages was discarded with a suction pump, and appropriate volume of bead suspension was added per well (Tab. 12). Cells were incubated for 4 hrs at 5% CO₂ and 37°C.

The number of particles per milliliter in the stock solution was calculated using following equation:

$$N = \frac{(6 \cdot 10^{10}) \cdot S \cdot P_L}{\pi \cdot P_S \cdot d^3}$$

N=Number of particles per milliliter

S= %solids (w/w)

P_L=density of latex (g/mL)

P_S=density of bulk polymer (g/mL)

d=diameter of particles (µm)

With the specific parameters for the beads used in this study, a concentration of 5.712*10⁹ particles/mL was calculated and used for calculations for dilution.

2.2.1.13 Labelling of parasitophorous vacuoles

Labelling of *Leishmania* spp.- induced parasitophorous vacuoles (PVs) was done using LysoBrite™ Red DND-99, which specifically labels acidic compartments within cells, according to manufacturer's instructions. Briefly, the medium of infected cells and respective controls was replaced by 100 μ L cRPMI supplemented with LysoBrite™ Red DND-99 at 28 hpi. Cells were further incubated for 2 hrs before fixation (2.2.1.14) and LysoBrite signal was detected using high content screening (2.2.4).

2.2.1.14 Cell fixation

Cells for confocal microscopy were cultured in 96-well plates. At desired time point, cells were washed twice with 150 μ L DPBS and incubated with 100 μ L 4% PFA for 20 min at RT for fixation. The cells were washed with 150 μ L DPBS again after incubation. For storage, the cells were covered with 200 μ L DPBS and placed at 4°C sealed with parafilm until immunofluorescent staining (2.2.4.1).

2.2.1.15 Flow cytometry

2.2.1.15.1 Staining of cells for flow cytometry analysis

Cells set aside for the isolation efficacy control were transferred into a 5 mL polystyrene tube and pelleted (5 min, 1500 rpm, 4°C), followed by washing with 1 mL FACS buffer with same centrifuge settings. The supernatant was removed completely and cells were stained with anti (α)-CD14, α -CD16 and α -HLA-DR in the mentioned dilution (Tab. 5) in a total volume of 50 μ L FACS buffer for 30 min at 4°C protected from light. 1 mL FACS buffer was added to tube and cells were washed (5 min, 1200 rpm, 4°C). Cells were subsequently fixed using eBioscience Foxp3/Transcription Factor buffer Kit according to manufacturer's instructions. Briefly, solutions and buffers were diluted following specifications and cells were resuspended in 100 μ L diluted fixation/permeabilisation solution and incubated for 30 min at 4°C in the dark. 1 mL diluted permeabilisation buffer was added to tube and cells were washed (5 min, 1200 rpm, 4°C). The washing step was repeated and cells were resuspended in 100-150 μ L diluted permeabilisation buffer in a final step for measurement at the Cytex® Aurora flow cytometer (2.2.1.15). Unstained samples were included with every staining and served as control for autofluorescence and background staining.

For the staining of mature macrophages after *in vitro* polarisation or *L. infantum*-infection, cells were cultured in 6-well plates and at least 3 wells were pooled per condition. The medium was discarded at required infection time point or after polarisation and cells were covered with 5 mL ice-cold DPBS and incubated for 20 min on ice to detach the adherent macrophages. DPBS was collected after incubation and replaced by 2 mL ice-cold DPBS followed by careful scraping of the cells. Cell solution was collected and macrophages were pelleted (5 min, 1200 rpm, 4°C) and resuspended in 1 mL DPBS for transfer into 5 mL polystyrene tube. Cells were pelleted once again (5 min, 1500 rpm, 4°C) and washed with 1 mL FACS buffer with similar centrifuge settings. Supernatant was removed completely and cells were stained in with all antibodies used for flow

cytometry in specified dilution (Tab. 5) in 50 μL total volume for 30 min at 4°C protected from light. Further handling of cells was done as mentioned above, except fixation was performed using 200 μL diluted fixation/permeabilisation solution.

2.2.1.15.2 Spectral unmixing for flow cytometry

In order to reliably distinguish between different fluorophores, spectral unmixing was performed following instructions of SpectroFlo® software enclosed with Cytex® Aurora flow cytometer. Single stained samples of UltraComp eBeads™ Plus composition beads were prepared for the definition of emission spectra for every applied fluorophore. Therefore, beads were thoroughly vortexed and 10 μL suspension were distributed to each 5 mL polystyrene tube. 1 μL of respective antibody was added for 10 min and beads were fixed afterwards similar to cells.

2.2.2 Molecular methods

2.2.2.1 RNA isolation from macrophages

All steps of the RNA isolation were carried out under the fume hood and under RNase-free conditions. Human primary macrophages were differentiated (2.2.1.7.) and infected with *Leishmania* parasites (2.2.1.11) or incubated with phagocytosis beads (2.2.1.12). After the desired incubation time, supernatant was removed carefully and cells were washed twice with 1 mL pre-warmed PBS. The supernatant was removed completely after the second washing step, and cells from one condition and sex were pooled by pipetting up and down with 500 μL TRIzol® several times in succession in all corresponding wells. The cell solution was then transferred into a 1.5 mL Safe-Lock tube and immediately stored at -70°C until further processing. The sample was thawed on ice and 500 μL pre-warmed TRIzol® were added, followed by centrifugation for 10 min at 13000 rpm and 4°C. The supernatant was transferred to a new 1.5 mL Safe-Lock tube and 200 μL cold chloroform were added and mixed with the sample by thoroughly inverting the tube for 15 to 20 sec. After an incubation for 3 min at RT, the sample was centrifuged for 30 min at 13000 rpm and 4°C, whereupon a clear separation of the phases should be visible. The upper, aqueous, RNA-containing phase was transferred into a new 1.5 mL tube and 500 μL Isopropanol were added. After thoroughly inverting the tube, the sample was incubated for 10 min at RT and centrifuged for 15 min at 12000 rpm and 4°C. The supernatant was discarded and the pellet was resuspended in 1 mL undenatured 70% ethanol and centrifuged for 5 min at 13000 rpm and 4°C. The ethanol was carefully removed and the pellet was dried at 56°C until no residues of ethanol could be detected. The pellet was then resuspended in 100 μL of RNase-free water and further purification of the sample was performed using the NucleoSpin RNA clean-up Kit according to the manufacturer's instructions. Briefly, the lysis buffer was premixed with undenatured 100% ethanol at a ratio of 1:1. To adjust the binding conditions, six times the volume of the premix was added to each sample (600 μL) and vortexed. The mixture was added to the column and centrifuges for 30 sec at 8000 *g and RT. The flow-through was discarded and 700 μL of wash buffer RA3 were added, following the same centrifugation as before. After discarding the flow-through, the second washing step included 350 μL RA3 and centrifugation for 2 min at 8000 *g and RT. The column was placed in a new 1.5

mL tube and the silica membrane was dried for 3 min with open lid. Elution of the RNA was done by pipetting 50 μ L of RNase-free water onto the center of the membrane and incubation for 5 min at RT. Collection of RNA was done by centrifugation for 1 min at 8000 *g and RT. If required, the elution was repeated. Sample concentration was measured at NanoDrop™ and samples were immediately stored at -80°C.

2.2.2.2 Control of RNA integrity using Bioanalyser Agilent 2100

On-chip automated electrophoresis was conducted to quantify RNA concentration more precisely and to investigate RNA integrity. This was performed using Agilent 2100 Bioanalyser with Agilent RNA 6000 Pico Kit and 2100 Expert Software. Preparation of required solutions and loading of the chip was done according to manufacturer's instructions. As recommended, all samples were diluted to a concentration between 0.2 ng/ μ L and 5 ng/ μ L with RNase free water based on the concentrations obtained with NanoDrop™. Furthermore, diluted samples were heat denatured for 2 min at 70°C and 1 μ L per sample was used for analysis. RNA intactness was evaluated based on the RNA integrity number (RIN), a feature of the software that rates the integrity of a sample on a scale of 1 to 10, taking in account various properties of the generated gel and electropherogram. A RIN of 1 is equal to total degradation of the sample, whereas 10 is equal to intact RNA. In general, samples with a RIN of 5 were considered sufficient for further processing with additional control of the electropherogram. Since RIN calculation could not always be done for infected samples due to additional peaks for *Leishmania* 16S and 23S RNA (Fig. 4B), the electropherogram was evaluated for signs of degradation and loss of integrity. All samples that passed the quality measurements were further processes by the NGS facility as described in 2.2.2.3.

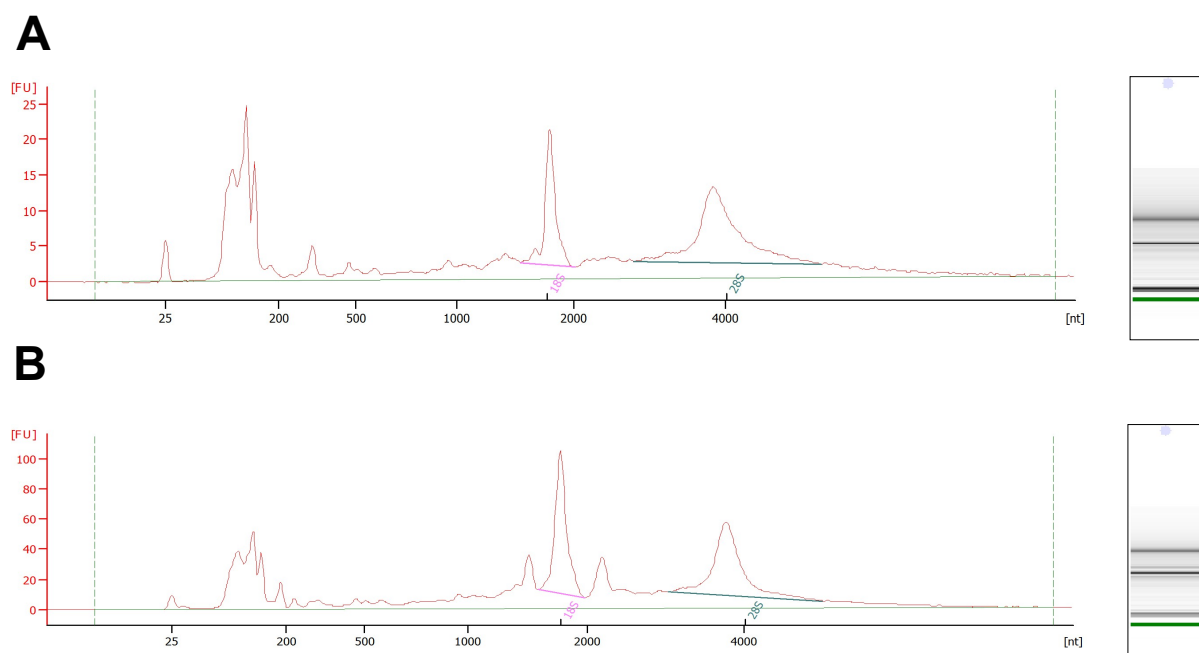


Figure 4: RNA integrity control using Agilent 2100 Bioanalyser

1 μ L of diluted RNA samples were analysed with Agilent 2100 Bioanalyser using Agilent RNA 6000 Pico Kit and 2100 Expert Software. Electropherogram and gel picture obtained from exemplary (A) uninfected sample and (B) sample infected with *L. infantum*. Human 18S and 28S RNA are indicated.

2.2.2.3 RNA Sequencing

After integrity control, further processing of the samples was carried out at the NGS core facility of BNITM under the lead of Dániel Cadar. Library preparation was performed using QIAseq Stranded mRNA Lib Kit UDI-A according to manufacturer's instructions. Libraries were divided onto two cartridges to gain a higher sequencing depth and were sequenced using NextSeq 1000/2000 P2 Reagents (200 Cycles) Kit v3 on the Illumina NextSeq1000/2000 system. This run generated 100 bp paired-end reads with a sequencing depth of around 5 million reads per sample from one cartridge, whereas the other cartridge didn't pass the internal quality check of the sequencer due to high variations and generally lower sequencing depth (around 2.5 million reads per sample). The libraries were therefore sequenced again on the Illumina NextSeq500/550 system using a NextSeq500/550 Mid Output Kit v2.5 (150 Cycles), generating 75 bp paired-end reads with a sequencing depth of 2.5 million per sample. Raw data processing is described in 2.2.5.1.

2.2.3 Biochemical methods

2.2.3.1 Cytometric bead assay (LEGENDplex™)

LEGENDplex™ is a cytometric bead assay, that allows the detection of multiple analytes simultaneously in samples and was used for measurement of cytokines in the cell culture supernatant of infected macrophages. Cytokines in the samples are captured by analyte-specific antibody-covered beads and are distinguished during the analysis using differentiation of size and fluorescence intensities of beads.

The assay was performed in 96-well V-bottom-plates. Samples were used undiluted and all standards and samples were measured in duplicates. All reagents were used at RT and reconstituted or diluted according to manufacturer's instructions if required. Standard solution was diluted 1:4 for six dilution steps. Pre-mixed beads were vortexed for 1 min before usage and regularly for 30 sec during usage. 10 µL Assay buffer was pipetted into all wells followed by 10 µL of either supernatant or standard according to plate layout. Finally, 10 µL of pre-mixed and vortexed beads were added before sealing the plate with aluminium foil and incubating it at 4°C ON on a plate shaker (800 rpm). The next day, 200 µL 1x washing buffer were added per well and the samples were washed (5 min, 1050 rpm, RT). The supernatant was discarded and 10 µL detection antibody were added followed by 1 h incubation on plate shaker at RT. 10 µL SA+PE were added directly and incubated for further 30 min on plate shaker. 200 µL 1x washing buffer were added per well and the samples were washed (5 min, 1050 rpm, RT). After discarding the supernatant, cells were resuspended in 150 µL 1x washing buffer for measurement at the LSRII™ or LSR Fortessa™ flow cytometer. Samples were measured in PE and APC channel and 300 events were recorded per analyte. Data Analysis was performed using LEGENDplex™ Cloud-based analysis software (legendplex.qognit.com).

2.2.4 High content screening (HCS) by automated confocal microscopy

2.2.4.1 Immunofluorescent staining for HCS

All incubation steps were carried out at RT on a plate shaker with 300 rpm. Pipetting and discarding of solutions was done carefully with multichannel pipettes without scratching the bottom of the wells. Fixed cells were washed twice with 150-200 μ L washing buffer by incubation for 5 min. Cells were then permeabilised by incubation with 150-200 μ L permeabilisation buffer for 15 min. After discarding the permeabilisation buffer, cells were incubated with 150 μ L blocking buffer for 30 min. The primary antibody, parasite-specific anti- pan-*Leishmania* heat shock protein (LHSP90) antibody, was diluted according to Tab. 5 in blocking buffer and cells were stained by incubation with 60 μ L of dilution for 1-1.5 hrs. After incubation, cells were washed three times with 200 μ L washing buffer for 5 min each. For staining with the secondary antibody, α -mouse-IgG coupled to Alexa Fluor (AF) 647 or AF488 was diluted (Tab. 5) in blocking buffer together with 4,6-Diamidin-2-phenylindol (DAPI) for nuclear staining and cells were incubated in 60 μ L of dilution for 0.5-1 h. Afterwards, cells were washed twice with 200 μ L washing buffer for 5 min followed by a washing step with 200 μ L 1XPBS. Cells were covered with exactly 200 μ L 1XPBS and stored at 4°C until measurement (2.2.4.2.).

2.2.4.2 Image acquisition

Two-dimensional microscopy images were created with confocal high-content microscope Opera Phenix® after defining settings in associated Harmony software® (version 4.6). Pictures for determination infection parameters, e.g total macrophages, %infected macrophages and parasite number per infected macrophage, were taken in confocal setting with 20X magnification water objective, which resulted in a numerical aperture (NA) of 1. Required fluorescence channels were added and measured as followed: DAPI signal was measured for detection of nuclear staining in DAPI channel (excitation: 405 nm emission: 435-480 nm) with an exposure time of 350-400 ms and 100% laser power. Detection of total parasites stained with α -LHSP90-AF647 or α -LHSP90-AF488 was detected in AF647 (excitation: 640 nm, emission, 650-760 nm) or AF488 channel (excitation: 488 nm, emission, 500-550 nm), respectively, with an exposure time of 300 ms and 100% laser power. Labelled PVs were detected in the AF568 channel (excitation: 561 nm, emission, 570-630 nm) with 500 ms exposure time and 100% laser power. 15-32 fields were detected per well at seven different planes on the z-axis (first plane=-11 μ m, last plane=1 μ m, distance between planes = 2 μ m) to increase resolution.

To create pictures with higher magnification, the 40X magnification water objective was used. In this case, the stack was adjusted to -3 μ m to 2 μ m with 1 μ m distance between planes.

2.2.4.3 Image analysis

Analysis of acquired microscopy pictures was done using image analysis sequence set up in the Harmony software® with exact parameters described in Tab. S1. This analysis was originally implemented by Dr. Hanno Niss in the cause of his doctoral project for the detection of intracellular *Leishmania* parasites within host cells (97). Briefly, the image analysis sequence is divided into

different steps that are based on each other and consist of different processing modules, called *building blocks* (Fig. 3). In a first step, the input image was defined by merging all confocal images from fluorescent channels followed by the image segmentation, during which different objects of the cells are defined. To calculate the viability of macrophages, determination the total number of cells was done by the detection of cell nuclei according to their DAPI signal and size using the *find nuclei* building block. Additionally, the cytoplasm of cells was defined by the detection of LHSP90-staining in the AF fluorescent channel (LHSP90-AF647 or AF488) using the *find cytoplasm* building block. For the detection of *Leishmania* parasites to calculate, for example, total parasite number or the proportion of infected macrophages, intracellular spots, defined by fluorescence signals in the DAPI and AF channels within previously defined cell bodies, were detected using the *find spots* building block. Afterwards, the properties of detected objects were calculated by selecting *Calculate Intensity Properties* and *Calculate Morphology Properties* for all segments separately. The previously calculated properties were then used to differentiate between false-positive spots and parasites, as well as uninfected and infected cells within the *Select Population* building block. The final step was to use the *Define Results* building block to calculate and display the desired readout values and parameters, such as total number of macrophages and *Leishmania* parasites, %infected macrophages and mean number of parasites per infected macrophage. Some data sets were normalised to the respective control to calculate viability, infection rate and parasite burden. The normalised data was represented as percentage of control (POC) and calculated according to the following formula:

$$\text{POC} = \frac{X_d}{X_c}$$

POC=Percentage of data point in comparison to control

Xd=value for data point

Xc=respective mean value of control at data point

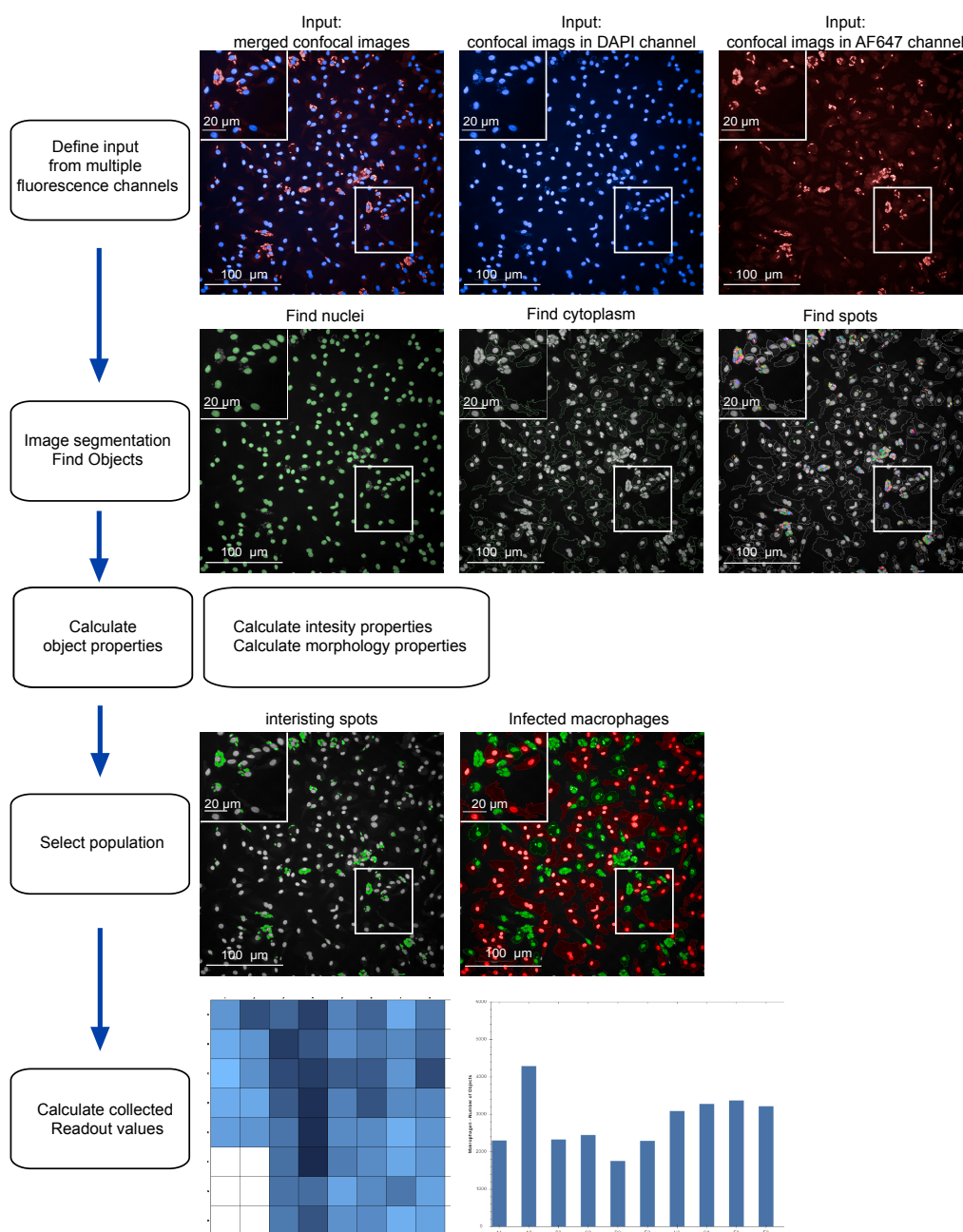


Figure 5: Schematic depiction of customised image analysis algorithm established in Harmony® software.

Consecutive steps of customised algorithm in Harmony® software for analysis of confocal microscopy pictures are depicted with associated building blocks. Exemplary microscopy images were acquired with Opera Phenix® confocal microscope using a water-immersion objective with 20X magnification, scale bar=100 µm and scale bar=20 µm in close-up images.

2.2.5 *In silico* methods

2.2.5.1 Analysis of RNA Sequencing

Raw data from the two runs of the second cartridge were merged before further analysis. All raw data was processed using the Nextflow RNAseq (v.3.8) pipeline. Quality control of raw data was done with FastQC and quality reports were generated using MultiQC (v1.11). The trimmed reads were aligned to human genome GRCh38 obtained from iGenomes ([s3://ngi-igenomes/igenomes/Homo_sapiens/NCBI/GRCh38](https://ngi-igenomes/igenomes/Homo_sapiens/NCBI/GRCh38)) as provided by the Nextflow RNAseq pipeline and infected samples

were additionally aligned to the genome of *L. infantum* obtained from Tritryp (<https://tritrypdb.org/tritrypdb/app/record/genomic-sequence/LinJ.36>). Expression data was normalised using variance stabilizing transformation (VST) in R package DESeq2 (v1.34). Relation between samples of different conditions (sex, infection state and time points) were evaluated using principal component analysis (PCA). This was computed on VST data using the scikit-learn (v1.2) Python package. Differential expression analyses between different conditions within time points or across time were conducted with DESeq2 (v1.34) package and multiple testing correction was done using Benjamini-Hochberg method. A comparison was defined as significant with an adjusted p-value > 0.05. The sequencing batch was used as a covariant in the statistical model to account for batch effects. When accounting for phagocytosis, infected samples were compared to uninfected as well as to phagocytosis control samples and for the genes that were significantly regulated in both comparisons, the maximal p-value of the two comparisons was selected for Benjamini-Hochberg correction (98)

Further visualisations were performed on VST normalised data. Volcano plots were created with R package EnhancedVolcano (v1.12). Heatmaps were created with freely available tool Heatmapper (<http://heatmapper.ca/>). Venn diagrams were created using online tool InteractiVenn (<http://www.interactivenn.net/>). Kyoto Encyclopedia of Genes and Genomes (KEGG) pathways analysis and GO-term enrichment analysis of all significantly different expressed genes or genes that passed the log₂fold change threshold indicated in the figure legend were conducted using shinyGO (v0.8) (<http://bioinformatics.sdstate.edu/go/>) with default settings. All genes that were detected in the transcriptome were set as background. Obtained results were additionally verified with Enricher (<https://maayanlab.cloud/Enrichr/>) as recommended.

2.2.5.2 Statistical analysis

Statistical analysis was done in GraphPad Prism 10.0.1. All data were tested for Gaussian distribution using Shapiro-Wilk test and then further analysed with parametric or non-parametric version of statistical test indicated in figure legends. Significances are shown in graphics as follows:

*	= p < 0.05
**	= p < 0.01
***	= p < 0.001
****	= p < 0.0001

Numerical depiction of p-values for comparisons with p < 0.1 to indicated potential trends.

3 Results

In order to better understand the biological causes underlying the sex bias in *Leishmania* infections, this work focuses on the extended characterisation of infected female- and male-derived macrophages, as they present the main host cell for *Leishmania* parasites. Characterisation was performed at the cellular, immunological, and transcriptional level. The results are divided into three main parts: the adaptation and further development of the high content screening system for *Leishmania spp.*-infected human primary macrophages, the sex-specific differences observed during infection with *L. infantum* and the investigation of the influence of steroid hormones on *L. infantum* infection.

Part of the result acquisition and figure compilation in the first section was done by Fahten Habib during her master's thesis (99) supervised as part of this doctoral thesis and are marked in the figure legends accordingly.

3.1 Adaptation of high content screening (HCS) system for *Leishmania spp.* infected primary human monocyte-derived macrophages (hMdMs)

3.1.1 Implementation of an *in vitro* infection model of hMdMs with *Leishmania spp.*

The use of the automated confocal HCS system enables the multiparametric measurement and readout quantification of infected macrophages, such as % infected macrophages and *Leishmania* parasites per infected macrophage, at various time points after infection by analysing fluorescence microscopy pictures with a customised image analysis sequence (Tab. S1). These parameters allow to determine infectivity and persistence of different *Leishmania spp.*, as well as differences in susceptibility between donor-derived host cells. To this end, the *in vitro* infection model was adapted to primary human macrophages. Human CD14⁺ monocytes were acquired from buffy coats of female and male blood donors by positive immunomagnetic sorting. Differentiation into macrophages was performed by culturing sorted cells under the addition of M-CSF for ten days. Eleven days after seeding, the mature macrophages were infected with *Leishmania* metacyclic promastigotes at the required MOI. Extracellular parasites were removed by washing after 4 hrs, and cells were further incubated for the desired time period (Fig. 6A). Characterisation of infected macrophages and respective controls was done by immunofluorescent staining in order to quantify infection parameters such as percent infected macrophages and *Leishmania* per infected cell using confocal high content microscopy (Opera Phenix®) and a customised image analysis sequence (Harmony software®) (3.2.1) or for phenotypical characterisation by flow cytometry (3.2.2). Cells were also used for RNA isolation and further processing in order to carry out a transcriptome analysis (3.2.4). The supernatant was used for cytokine profiling using a cytometric beads assay (LEGENDplex™) (3.2.3)(Fig. 6B).

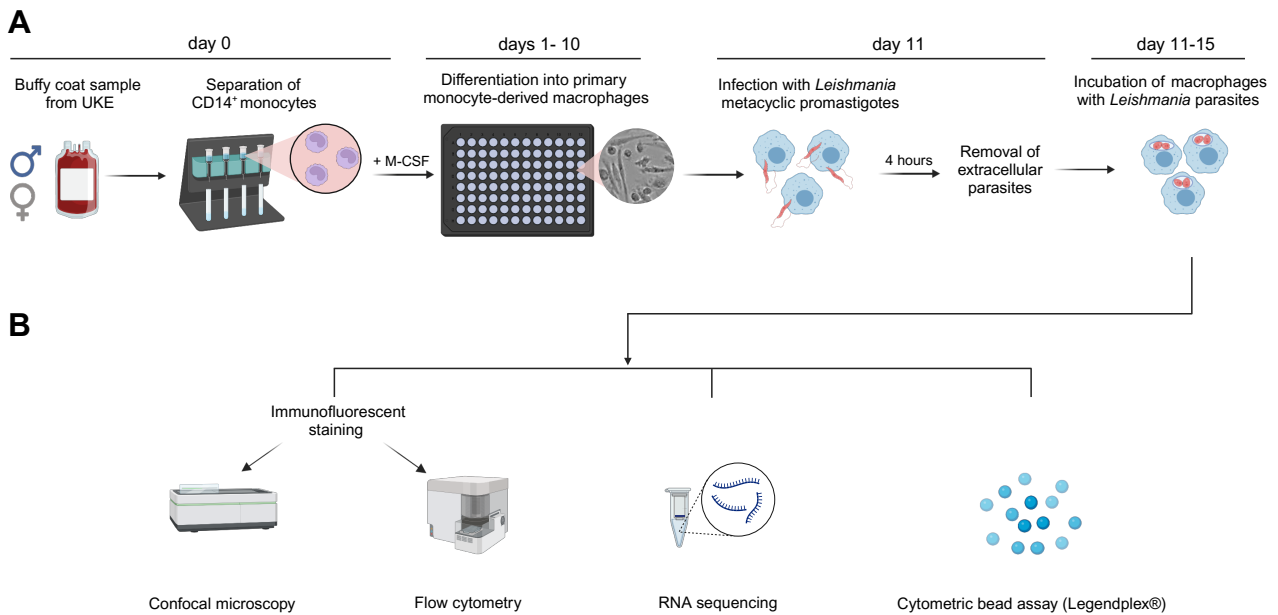


Figure 6: Schematic depiction of the workflow for *in vitro* infection of primary monocyte derived macrophages with *Leishmania spp.* parasites.

(A) CD14⁺ monocytes were isolated with immunomagnetic positive selection from buffy coat samples of female and male blood donors. Monocytes were differentiated into primary monocyte derived macrophages (hMdMs) under the addition of M-CSF over 10 days. On day 11, mature macrophages were infected with *Leishmania spp.* parasites for four hours. After removal of extracellular parasites, cells were incubated for the required time period. (B) Subsequently, the infected cells were immunofluorescently stained for characterisation by confocal microscopy and flow cytometry or processed for RNA sequencing. The supernatant was used for cytokine profiling. Figure created with BioRender.com

Immunofluorescent staining of isolated PBMCs and CD14⁺ monocytes and subsequent analysis by flow cytometry was used to investigate the frequency of monocytes and different monocyte subsets in both sexes as well as the isolation efficiency of monocytes from PBMCs. To analyse the abundance of monocytes within the isolated PBMCs, the expression of CD14 and CD16 within HLA-DR⁺ PBMCs was analysed (Figure 7A). This analysis showed, that ~50% of HLA-DR⁺ cells isolated from buffy coats of healthy female and male donors were characterised as monocytes by their sole or simultaneous expression of CD14 and CD16 (Fig. 7B). Monocytes were further subdivided and the abundance of classical (CD14⁺CD16⁻), intermediate (CD14⁺CD16⁺) and non-classical monocytes (CD14⁻CD16⁺) of total monocytes was analysed. The proportion of classical monocytes was found to be the most prominent subset, accounting for ~60% of the monocytes, which was significantly higher than the proportion of intermediate or non-classical monocytes (both ~20%) (****=p<0.0001). This was true for both sexes, and no significant difference in the abundance of monocytes or monocyte subsets between male and female donors was found (Figure 7C). The isolation efficacy was assessed by comparing the percentage of HLA-DR⁺CD14⁺ cells in samples before (Figure 7D) and after the isolation of CD14⁺ monocytes by magnetic activated cell sorting (MACS) (Fig. 7E), according to the gating scheme. This showed a high purity of samples after sorting, however only samples with an isolation efficiency of >80% (%HLA-DR⁺ cells * CD14⁺ cells) were used for further experiments.

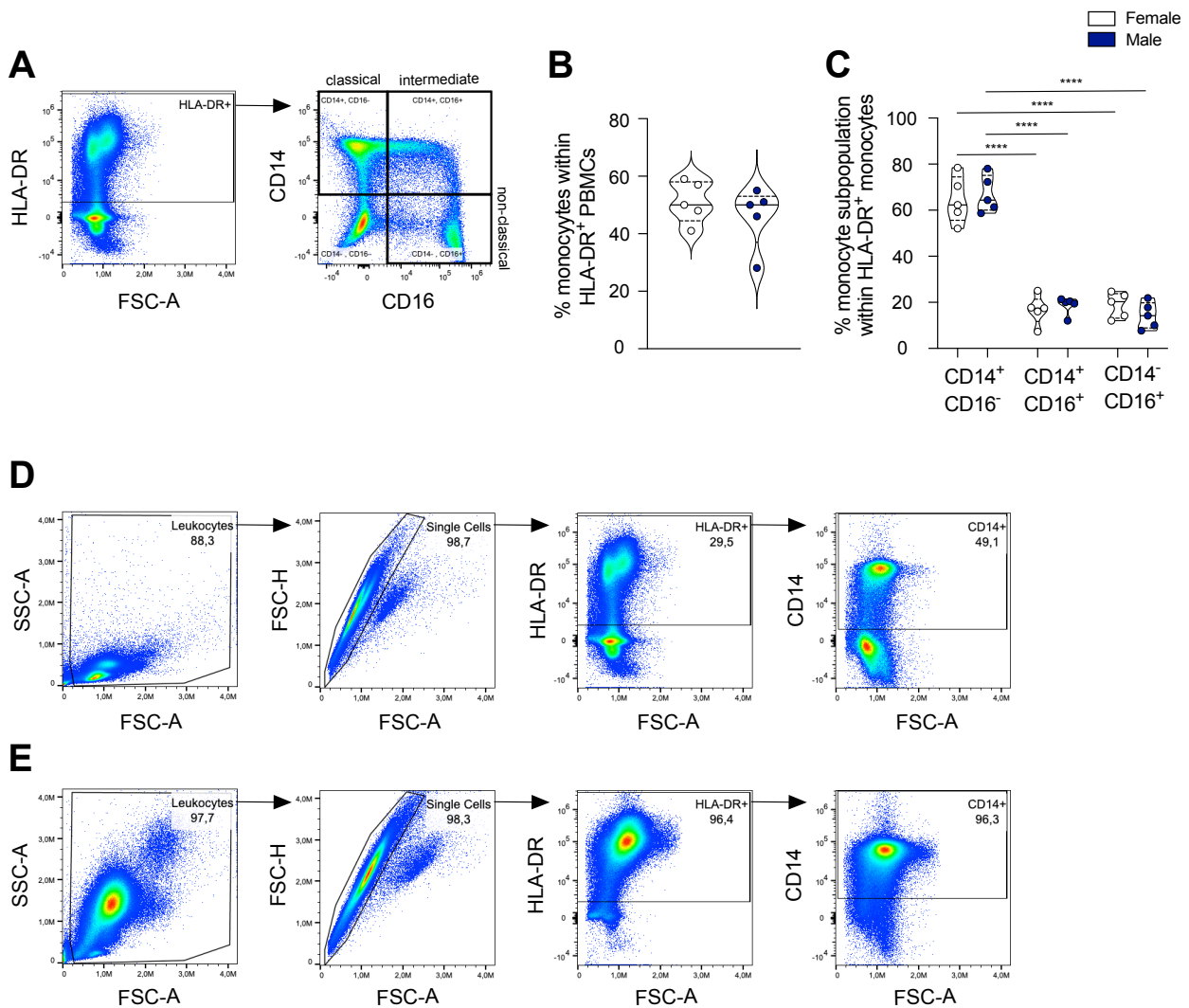


Figure 7: Comparison of monocyte subset frequencies in female and male blood donors and control of monocyte isolation.

PPBMCs were isolated from buffy coat of female and male blood donors, immunofluorescently stained with α -CD14-BV510, α -CD16-FITC, α -HLA-DR-BUV395 and analysed by flow cytometry (Cytek® Aurora). (A) Gating strategy to identify monocytes and their subsets out of human HLA-DR⁺ PBMCs. (B) Percentage of monocytes out of HLA-DR⁺ PBMCs. (C) Percentage of classical monocytes (CD14⁺CD16⁻), intermediate monocytes (CD14⁺CD16⁺) and non-classical monocytes (CD14⁻CD16⁺) within HLA-DR⁺ monocytes of female and male blood donors. Data is shown as violin plot with indicated median (solid line) and quartiles (dotted lines), $n_{F/M} = 5/5$. P-values were calculated using ordinary one-way ANOVA with Holm-šídák Correction. Gating strategy to determine the percentage of primary HLA-DR⁺CD14⁺ monocytes (D) before MACS in PBMCs and (E) after MACS purification to assess the isolation efficacy. One exemplary experiment is shown. (****= $p < 0.0001$)

3.1.1.1 Localisation study of *Leishmania* parasites in macrophages

After the injection into the mammalian host, *Leishmania* parasites are phagocytosed by many different phagocytic cells, mostly macrophages. Within a macrophage, parasites establish a niche, called phagosome or PV, where they differentiate into the amastigote stage and replicate, partially sheltered from the host immune response. PVs partly consist of endolysosomal components of the host and therefore exhibit an acidic pH (100). This fact can be used to determine the intracellular localisation of the parasites following a *in vitro* infection. Macrophages were infected with *L. major*, *L. braziliensis*, *L. donovani* or *L. infantum* for 28 hrs before the cells were incubated with LysoBrite™

Red DND-99, a lysosomotropic fluorescent dye, that specifically accumulates in acidic organelles and labels them. Infected cells were imaged by confocal microscopy with uninfected and infected cells without LysoBrite™ Red DND-99 treatment used as controls. Host cell and parasite nuclei were stained with DAPI and parasite cytoplasm with parasite.-specific α -LHSP90-AF488. LysoBrite™ Red DND-99 signal was detected in AF568 channel. Upon infection with any *Leishmania* spp., a clear induction of a LysoBrite™ signal was observed compared to the respective controls (Figure 8A). The signals are seen in clear circular structures of 3-5 μ m diameter around the early amastigotes, for both *L. infantum* (Figure 8B) and *L. donovani* (Figure S1A) infection. Whereas an infection with *L. major* triggers similar signals with a diameter of only 2-3 μ m (Figure S1B), infection with *L. braziliensis* causes a weaker and more diffuse signal (Figure S1C). When quantifying the fluorescence intensity of the LysoBrite™ Red DND-99 signal within macrophages, significantly higher intensities were observed in infected macrophages compared to uninfected cells (**=p<0.001, ****=p<0.0001) and cells without LysoBrite™ Red DND-99 treatment (**=p<0.01, ***=p<0.001, ****=p<0.0001), allowing differentiation between macrophage-derived lysosomes and PVs. The highest fluorescent intensity was detected in *L. infantum*- (****=p<0.0001) and *L. donovani*-infected cells (****=p<0.0001), while the faintest signal was observed in *L. braziliensis*-infected cells. (Fig. 8C).

In summary, the intracellular localisation of *Leishmania* parasites following *in vitro* infection could be demonstrated by the formation of PVs for all *Leishmania* spp..In addition, differences in the phenotypic occurrence of PVs between the different parasite species was observed.

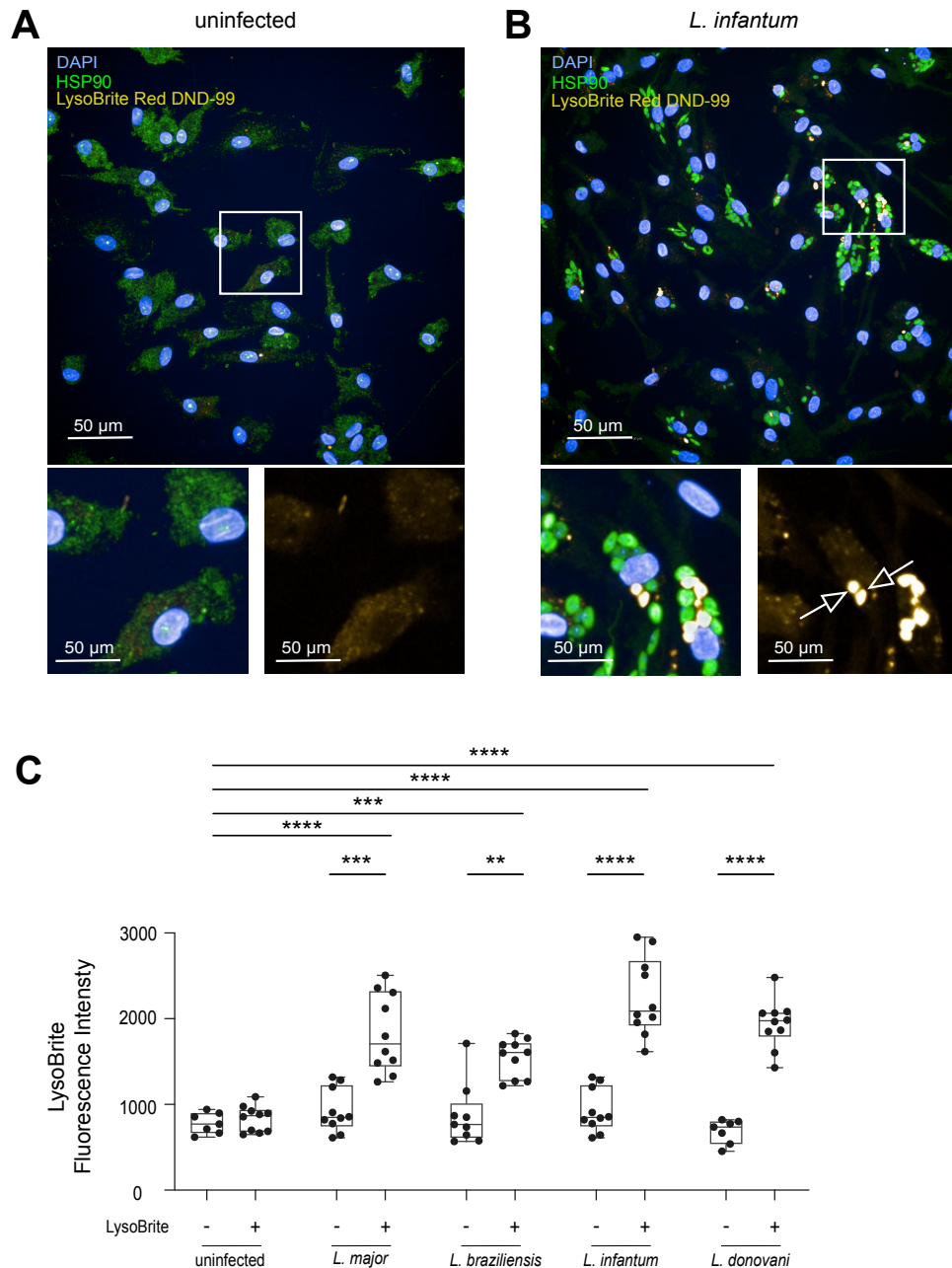


Figure 8: Determination of intracellular localisation of *Leishmania* spp. amastigotes within human monocyte derived macrophages by labelling of parasitophorous vacuoles.

Mature macrophages were infected with *Leishmania* metacyclic promastigotes (*L. major*, *L. braziliensis*, *L. infantum* and *L. donovani*) at 20:1 and incubated for 28 hpi. Before fixation, the cells were incubated with LysoBrite™ Red DND-99 for 2 h at 37°C and 5% CO₂. Images were acquired using Opera Phenix® confocal microscope. Nuclei stained with DAPI (blue), *Leishmania* parasites stained with α-LHSP90-AF488 (green) and PVs labelled with LysoBrite® detected in AF568 channel (yellow) for (A) uninfected macrophages and (B) *L. infantum* infected macrophages. Arrows point to intracellular PVs. Scale bar = 50 μM. (C) The fluorescent intensity of intracellular PVs was quantified using the Harmony® image analysis software. The data are expressed as boxplot, n=10 independent PV measurements within the infected cell. P-values were calculated using One-way ANOVA with Dunnett's correction for comparison to uninfected control and two-way paired Student's t-tests for comparisons to controls without LysoBrite™. (**=p<0.01, ***=p<0.001, ****=p<0.0001). Parts adapted from (99).

3.1.1.2 Quantification of infection parameters using confocal high content screening (HCS)

To validate the automated image analysis and to ensure the reliable and unbiased detection of cells and parasites, mature macrophages were infected with four different *Leishmania* species, of which two were dermatropic (*L. major* and *L. braziliensis*) and two viscerotropic species (*L. infantum* and *L. donovani*). Cells were infected at different MOI (8:1, 10:1, 15:1 or 20:1) for either 28, 52 or 76 hpi. At 28 hpi, representative fluorescence images were taken of *Leishmania* spp.-infected macrophages (Fig A). Slight morphological differences could be observed between species. Whereas *L. braziliensis* displayed a rounder morphology, the other three species showed a mixture of elongated, spindle-shaped and more ovoid phenotypes. For *L. braziliensis*, this was in accordance with its morphology observed in promastigote cultures, in which it already exhibited a much rounder cell shape compared to other species, suggesting that culture conditions were sub-optimal for *L. braziliensis* which is normally grown in biphasic medium (101). Although this makes it difficult to make a statement about stage differentiation for *L. braziliensis*, signs of stage transformation from promastigote to amastigote, such as shortening of flagellum and rounding of the cell bodies, could be observed in all other species.

When looking at % infected macrophages, a titration could be seen in relation to the used MOI at investigated time points and for all species. The initial infection rate at 28 hpi was similar between *L. major* (Fig 9B), *L. braziliensis* (Fig 9C) and *L. donovani* (Fig 9E) with 40-60% infected macrophages at the lowest MOI and 90-95% infected macrophages at the highest MOI. In contrast, infection with *L. infantum* (Fig 9D) triggered a lower percentage of infected macrophages, ranging from 7% to 45% infected macrophages, depending on the MOI. During the observation time, a reduction of the infection rate became apparent at varying degrees in all *Leishmania* species. Until 72 hpi, infection rate decreased by 10-25% (*L. major*), 20-40% (*L. braziliensis*), 50-60% (*L. infantum*) and 15-35% (*L. donovani*) for each MOI.

Similar observations were made when analysing *Leishmania* amastigotes per infected cell, where the number of parasites detected within infected macrophages was seen proportional to the used MOI. The number of parasites per infected macrophage at 28 hpi varied between the species, ranging from a mean of one parasite to six parasites at the lowest MOI and two to twelve parasites for the highest MOI. The lowest number was observed for *L. infantum* for all timepoints and MOIs. For *L. braziliensis* and *L. donovani*, a reduction of 30-50% could be observed from 28 hpi to 72 hpi for each MOI. For *L. major* and *L. infantum* slightly increased parasite numbers were observed.

Based on the obtained results, a reliable detection of parasites and calculation of the infection rate of hMdMs was observed using the customised, automated image analysis sequence (Harmony software®). Thereby, variations in the infection patterns of different *Leishmania* species became visible in the infection rate and parasite load. Additionally, an early clearance of the parasite was observed over time.

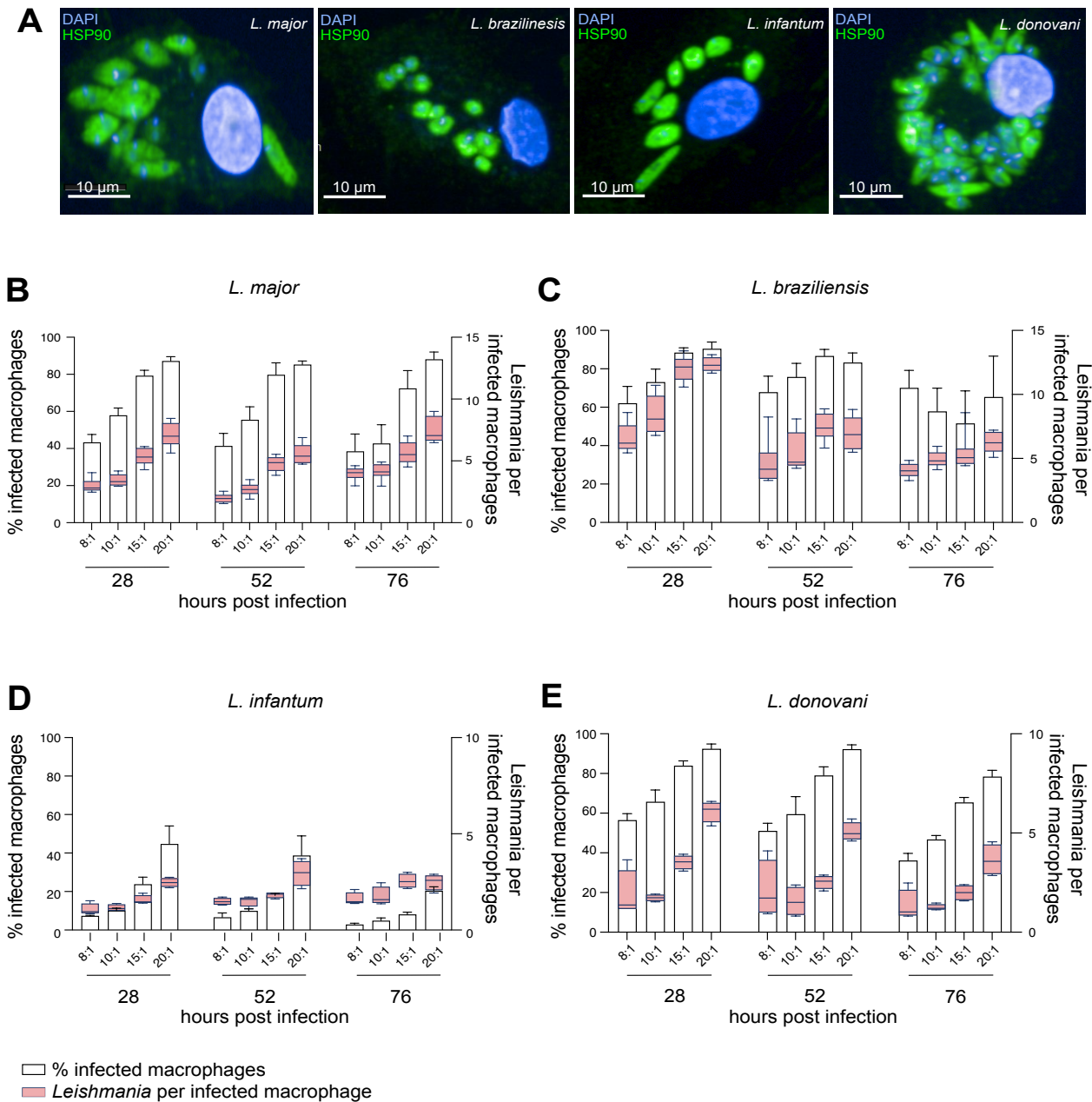


Figure 9: Quantification of *Leishmania* spp. parasite infection in human monocyte-derived macrophages using confocal (HCS).

Mature macrophages were infected with *Leishmania* metacyclic promastigotes at different MOI (8:1, 10:1, 15:1 and 20:1) and incubated for 28, 52 and 76 hours post infection. hMdMs were fixed at required time point and stained with DAPI (Nucleus, blue) and α-LHSP90-AF 488 (*Leishmania* parasites, green). (A) Representative confocal images of *Leishmania* spp.-infected macrophages at 28 hpi. Images were acquired with Opera Phenix® confocal microscope, scale bar=10µm. Quantification of % infected macrophages (represented in white bar as mean + SD) and *Leishmania* per infected macrophage (represented in magenta boxplot) using customised image analysis sequence (Harmony® software) for (B) *L. major* (C) *L. braziliensis* (D) *L. infantum* and (E) *L. donovani* infected macrophages. The data represents values for one exemplary experiment per *Leishmania* spp. (technical replicates=4). Parts adapted from (99).

3.1.2 Delineation of macrophages exhibiting distinct polarisation states

Two distinct polarisation states are described for macrophages. Classically activated M1 macrophages are associated with pro-inflammatory properties, while alternatively activated M2 macrophages are thought to have anti-inflammatory and tissue-healing properties, indicating that the outcome of an infection may be influenced by the polarisation of macrophages. The two polarisation states of macrophages can be divided by their distinct features in morphology and phenotypical differences (102).

3.1.2.1 Morphology-based characterisation of polarised macrophages

Since M1 and M2 macrophages can be distinguished by differences in their morphologies, the aim was to establish a new building block within the image analysis software to detect the macrophage subpopulations based on their distinct morphology. M1 macrophages appear with a smaller and round cell shape, whereas M2 macrophages have more elongated and extended cell bodies (103). To define parameters for the detection, positive controls were created by differentiating monocytes into M1-like (GM-CSF+IFN- γ) and M2-like (M-CSF+IL-4) macrophages. Unpolarised macrophages (M0=M-CSF) were used as a sample with mixed macrophage populations. Observation of the differently differentiated macrophages with differential interference contrast microscopy (DIC) (Fig. 10A (a, e, i)) revealed distinct morphology variations between the samples. M1-like macrophages displayed a homogenous, roundish cell morphology, while M2-like macrophages correlated with heterogeneous cell shapes. In general, M2-like macrophages were more spindle-shaped and exhibited cytoplasmic extensions at the apical ends of the cells. In the M0 sample, both cell types could be found.

When conducting immunofluorescent staining with DAPI for nuclear staining and α -LHSP90-AF647 staining of the cytoplasm for confocal imaging of the cells (Fig. 10A (b,f,j)), the same variations in morphology were observed as previously discussed. The immunofluorescent images of the positive controls were used to characterise the morphological properties of M1-, and M2-like macrophages and to implement markers to distinguish between the subgroups. Therefore, the automated image analysis sequence in the Harmony software® (Tab. S1) was extended to quantify the cytoplasmic properties of the cells defined in *Find Cytoplasm* building block. This was done by adding a *Calculate Morphology properties* section, in which the cells were characterised by four different parameters. By using a *Select Population* building block, these parameters could subsequently be utilised to assign macrophages to the two different polarisation states by defining a range that is specific for either one of the states. Results for the specification as M1 macrophage (Fig 10A (c,g,k)) and M2 macrophage (Fig 10A (d,h,l)) were generated and cells which were allocated to respective subpopulations were highlighted in green (positive) and cells not assigned in red (negative). The first parameter used for characterisation was cell roundness, which was expressed as a value that indicates the roundness of the cytoplasm (0.5 is considered a perfect spherical shape). Further parameters were cell width and cell length as well as the ratio of cell width to cell length. The specific ranges were set as depicted in Fig. 10B. Due to the higher heterogeneity of M2 macrophages, finding suitable parameters for this polarisation state was more difficult and some

cells could not be classified to either group and were excluded from analysis. When quantifying the percentage of different subpopulations within the differently polarised macrophages, a significantly higher proportion of M1-like macrophages was found in macrophages polarised towards M1 macrophages (****= $p < 0.0001$) in comparison to M2-like macrophages. The outcome was reversed when looking at macrophages polarised towards M2 macrophages, where significantly more cells were found to be positive for M2 macrophages than M1 macrophages (*= $p < 0.05$). Additionally, the analysis showed significantly more cells assigned to M1 analysis outcome in macrophages polarised with IFN- γ compared to polarisation with IL-4 (**= $p < 0.001$) and vice versa for the detection of M2-like macrophages (****= $p < 0.0001$). Within unpolarised M0 macrophages, the percentage of cells positive for M1 analysis outcome was significantly higher than the percentage allocated to M2-like macrophages (****= $p < 0.0001$), although the biological replicates were highly dispersed (Fig. 10C).

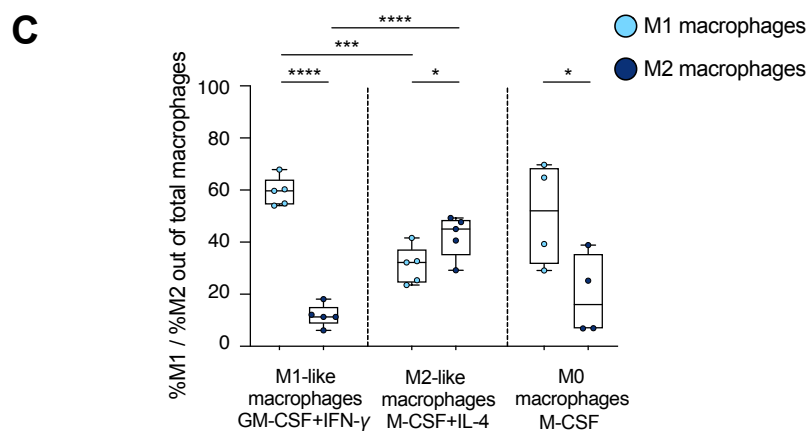
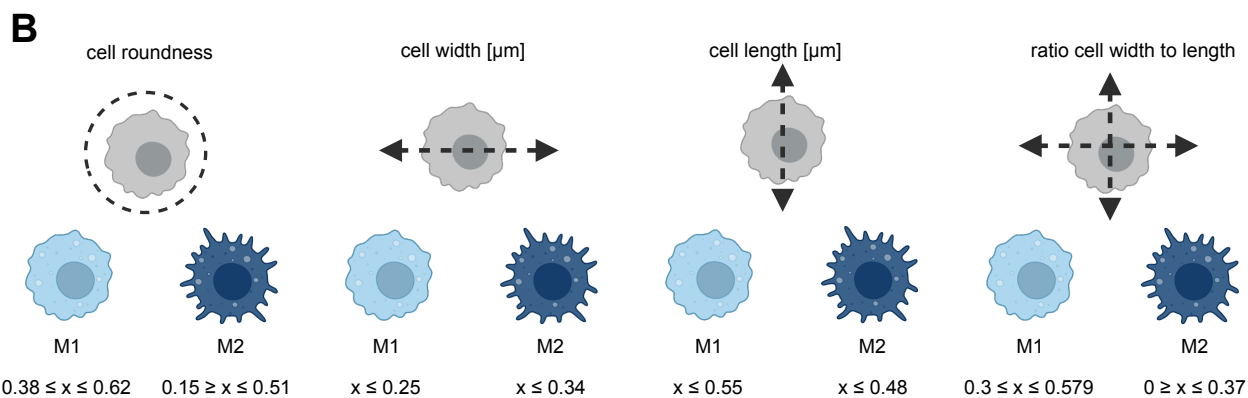
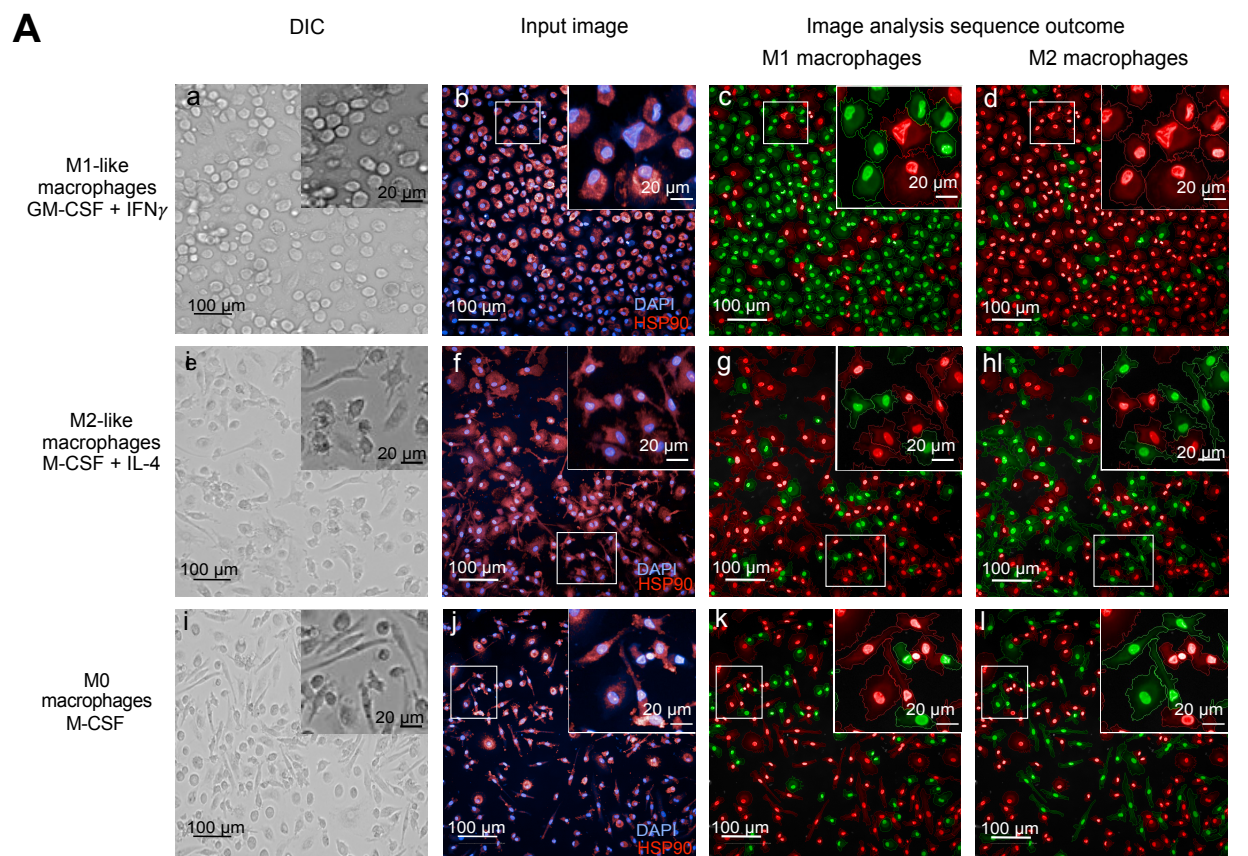


Figure 10: Morphology-based distinction of M1- and M2-like polarised macrophages using confocal HCS.

Monocytes were differentiated into macrophages using either M-CSF or GM-CSF. On day 7 post isolation, cells were either cultivated further under M-CSF to obtain M0 population or polarised into M1-like macrophages using GM-CSF and IFN- γ or M2-like macrophages using M-CSF and IL-4. Macrophages were fixed at day 11. (A) Representative images of differently polarised macrophages. (a,e,i) DIC pictures were acquired with EVOS® FL Auto Fluorescence microscope. (b,f,j) Immunofluorescent pictures acquired with Opera Phenix® confocal microscope. DAPI nuclear staining (blue) and cytoplasm with α -LHSP90 coupled to AF647 (red). Images were analysed with customised image analysis sequence (Harmony® software) and the outcome for detection of (c,g,k) M1-like macrophages and (d,h,l) M2-like macrophages (green = positiv, red = negativ) is depicted. For panels (a-d) M1 macrophages, (e-h) M2-like macrophages and (i-l) M0-like macrophages were used. Scale bar = 100 μ M and scale bar = 20 μ M in close-up images. (B) Parameters established within image analysis sequence for morphological distinction between M1-like and M2-like macrophages. (C) Quantification of polarised macrophages detected within different analysis sequences. Data shown as boxplot, n=5. P-values were calculated using two-tailed unpaired Student's t-test. (*=p<0.05, **=p<0.01, ***=p<0.001, ****=p<0.0001). DIC= differential interference contrast. Parts adapted from (99).

3.1.2.2 Phenotypic characterisation of polarised macrophages

Immunofluorescent staining of polarised macrophages was also used to discriminate between macrophage polarisation states by the expression of various cell surface markers and to confirm the morphology-based distinction. *In vitro* polarised M1- and M2-like macrophages were stained against M1- and M2 macrophage-related antigens. The median fluorescent intensity (MFI) of various cell surface markers was determined according to the gating scheme (Fig.11A). The M1-related markers used included CD86 and CD68 (42) as an activation marker of macrophages, immunoglobulin receptor CD64 (Fc γ I receptor) (104) and HLA-DR as indicator for antigen presentation. For characterisation of M2-like macrophages, the scavenger receptor CD163 (104), myeloid cell inhibitory receptor CD200R (105) and mannose receptor CD206 (104) were used. As macrophages have a high degree of plasticity and the expression of polarisation-related surface markers is not mutually exclusive for one polarisation state, the MFI was depicted, quantifying the expression level of the markers rather than the percentage of marker expressing cells (40, 105). The highest MFI for both subpopulations was observed for HLA-DR. Analysis of the MFI for M1-related surface markers CD86, CD64, CD68 and HLA-DR showed a significantly higher MFI of CD64 (**=p<0.01) and HLA-DR (**=p<0.01) for M1-like versus M2-like macrophages. A significantly higher MFI for M2-like macrophages compared to M1-like macrophages of all investigated M2-related surface markers, CD163 (*=p<0.05), CD200R (**=p<0.01) and CD206 (*=p<0.05), was observed (Fig. 11B). Additionally, a T-distributed stochastic neighbour embedding (tSNE) analysis, which clusters cells according to their overall similarity of various parameters (106), was performed with M0, M1-like and M2-like macrophages (Fig. 11C). A separation between the three clusters was observed which could be clearly assigned to the three different samples used. The cluster allocated to M1-like macrophages showed the highest expression of all M1-related surface markers examined, while the expression of CD200R and CD206 was clearly the highest in the M2-like macrophage cluster. Unpolarised macrophages showed intermediate expression for most of the investigated cell surface markers, except for CD163 for which the M0 cluster showed the highest expression.

In conclusion, the selected morphological and phenotypic parameters allowed a reliable distinction between M1-polarised and M2-polarised macrophages based on cell shape and expression of cell surface markers,

which will be useful for the determination of hMDM polarisation state during *L. infantum* infection.

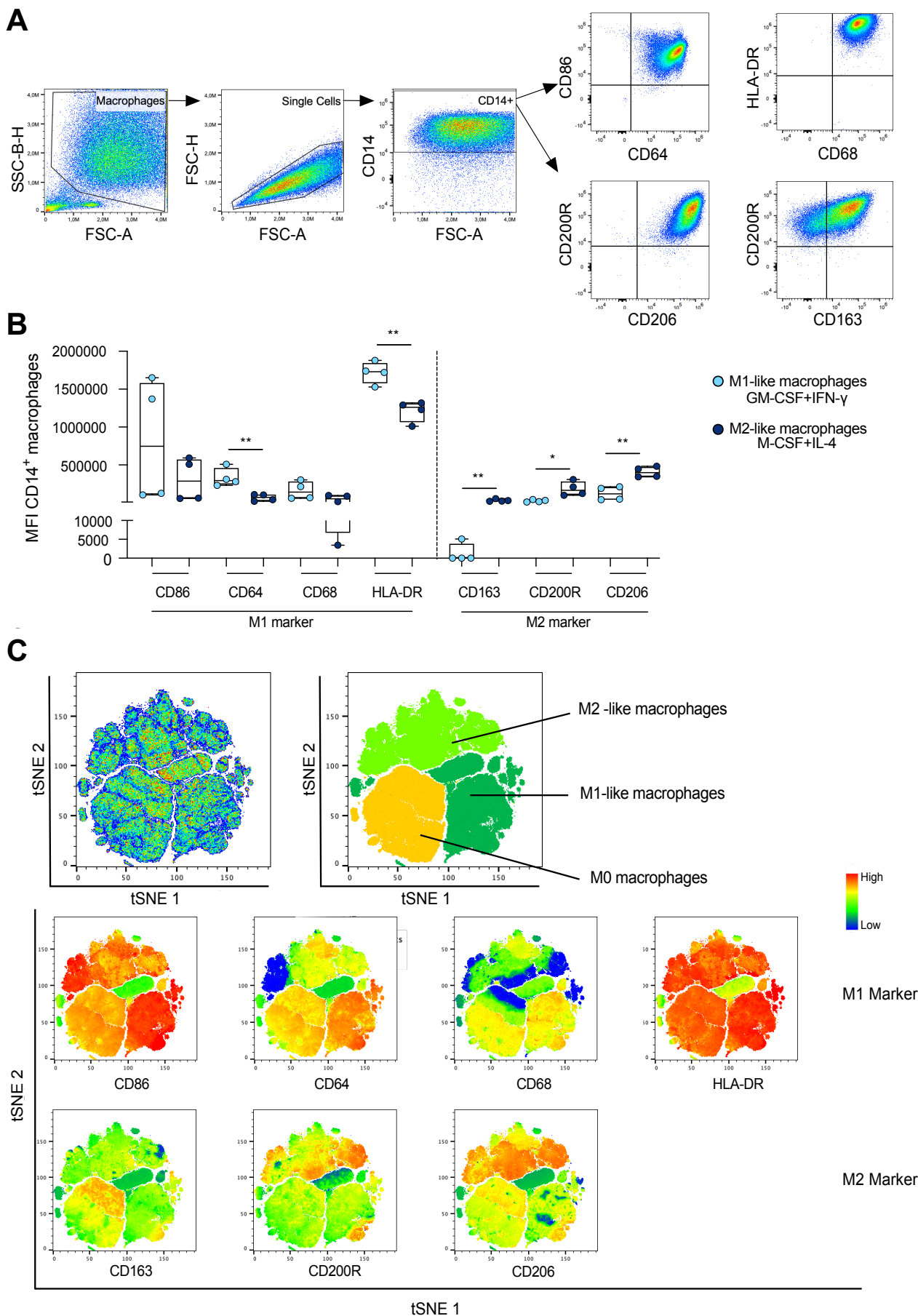


Figure 11: Phenotypic characterisation of M1- and M2-like polarised macrophages using flow cytometry and tSNE analysis.

Monocytes were differentiated into macrophages using either M-CSF or GM-CSF. On day 7 post isolation, cells were either cultivated further under M-CSF to obtain M0 population or polarised into M1-like macrophages (GM-CSF and IFN- γ) or M2-like macrophages (M-CSF and IL-4). Polarised macrophages were immunofluorescently stained at day 11 and analysed by flow cytometry (Cytex® Aurora) (A) Gating strategy to analyse surface marker expression on polarised macrophages on day 11. (B) MFI of M1- or M2- related surface markers on CD14⁺ M1-like or M2-like polarised macrophages. Data shown as boxplot, n=4. p-values were calculated using two-tailed unpaired Student's t-test (C) tSNE analysis of expression of M1- or M2-related surface markers on differently polarised macrophages. Exemplary experiment shown. (*=p<0.05, **=p<0.01, ***=p<0.001, ****=p<0.0001).

3.2 Sex-specific differences during infection with viscerotropic *L. infantum*

Sex-specific differences in the incidence and morbidity of leishmaniasis are described in human epidemiological studies and differences in the infection rate and parasite burden were observed *in vivo* animal experiments and *in vitro* infections of murine bone-marrow derived macrophages (87). To investigate the transferability to *in vitro* infection experiments of primary human macrophages, the sex-specific differences in the course of infection of female and male macrophages with *L. infantum* were investigated in this chapter using image-based quantification of infection parameters and polarisation, as well as cytokine profiling and RNA sequencing of infected cells.

3.2.1 Course of *L. infantum* infection in macrophages from male and female donors

To investigate putative differences in the infection rates or parasite burdens in macrophages from men and women, the infection parameters were quantified at various time points after *in vitro* infection of macrophages with viscerotropic *L. infantum*. The first parameter, viability of hMdMs, was defined as the number of cells per well and assessed as the percentage of control (POC) in relation to uninfected cells. With the exception of 6 hpi for both sexes and 100 hpi for male macrophages, a significant increase in the viability of 80% on average was observed in infected cells compared to uninfected macrophages at each time point (*=p<0.05: **=p<0.01, ***=p<0.001; ****=p<0.0001). However, the viability of infected cells did not differ significantly between sexes (Fig. 12A).

Determination of infected macrophages revealed a high initial infection rate of 90% of cells at 4 hpi, which significantly declined from 28 hpi onwards in both sexes to 30% at 100 hpi. (significances not shown). Although, high inter-experimental variability was observed due to multiple factors including immunological differences of donors, parasite virulence and experimental procedure, a tendency for less infected cells in female donors became apparent for the later time points of infection (28 hpi p=0.0802) (Fig. 12B). For a more conclusive comparison of the results, the values from female and male macrophages that were infected simultaneously were normalised against female MdMs (POC=100). This showed no difference at the initial time points and the last time point evaluated, whereas a significantly increased infection rate in male cells at 28, 52 and 76 hpi (*=p<0.05: **=p<0.01) was observed. The greatest difference was detected at 72 hpi, when the mean infection rate in male cells was twice as high as in female cells (Fig. 12B).

Infected cells from female and male donors contained an average of 10 parasites at the time extracellular parasites were removed (4 hpi), but the number was significantly reduced from 28 hpi

onwards until only 2-3 parasites were detected per cell at 100 hpi (significances not shown). Although the mean parasite number of female macrophages tended to be lower, no statistical significant difference was observed between sexes. This might also be due to the high inter-experimental variability (Fig. 12D). Normalisation of results to female values showed a clear increase of parasite load in male macrophages from 52 hpi to 100 hpi, with almost twice as many parasites in male MdMs compared to female MdMs. But this was only significant at 76 hpi (*=p<0.05) (Fig. 12E).

In conclusion, infection with *L. infantum* triggered increased viability of macrophages in both sexes, and higher infection rates and parasite loads could be observed in male-derived macrophages in comparison to female macrophages, when accounting for inter-experimental variability.

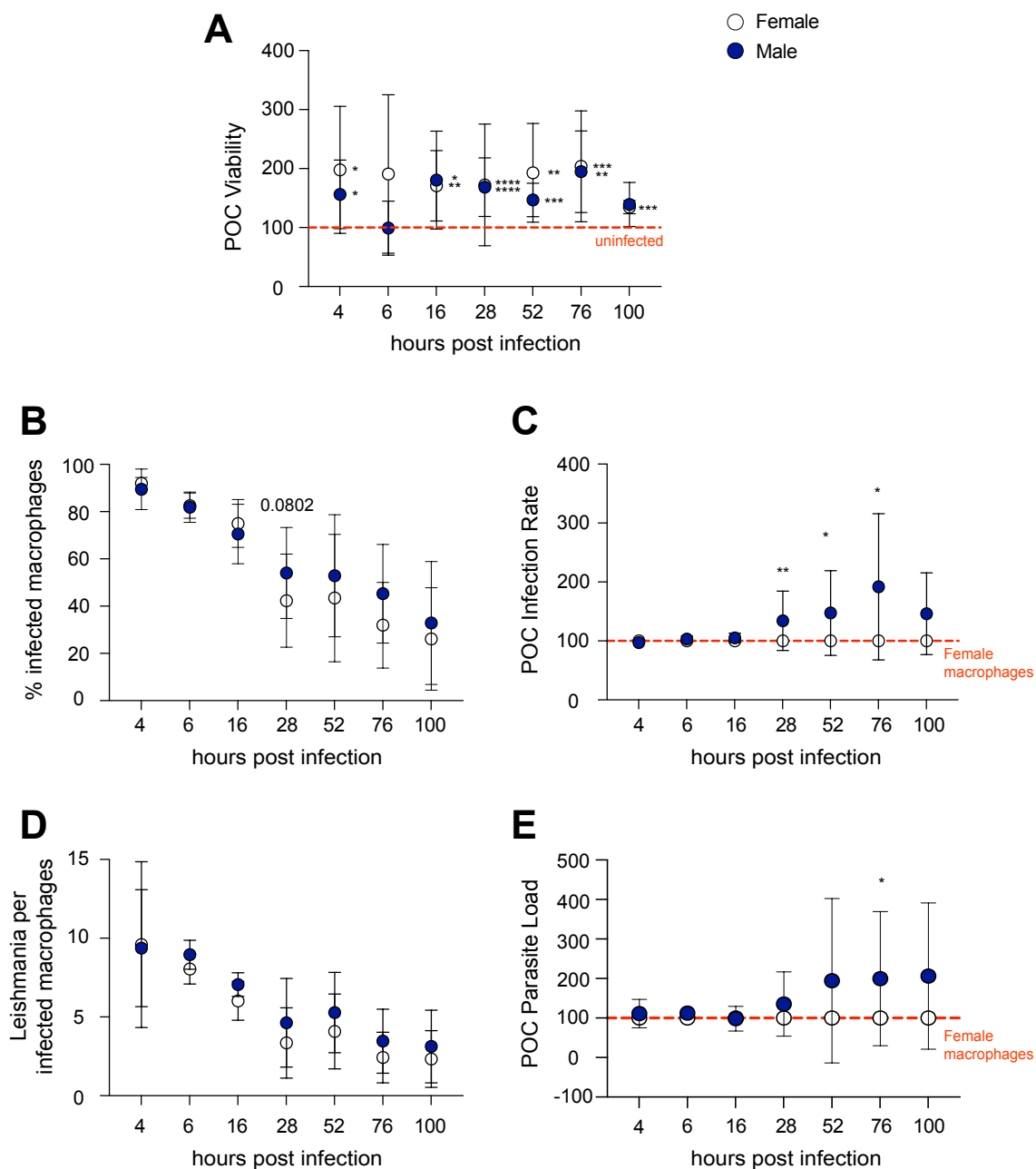


Figure 12: Quantification of infection parameters in female and male *L. infantum*-infected macrophages over time using confocal high content screening.

Mature macrophages from female and male donors were infected with *L. infantum* metacyclic promastigotes at a MOI of 15:1 and incubated for 4-100 hpi. Infection parameters were quantified using Opera Phenix® confocal microscope and customised image analysis sequence (Harmony® software). Depicted are (A) viability, normalised within sex against uninfected control (red dotted line), level of infection as (B) % infected macrophages or (C) normalised to female values (POC infection rate=100) and number of parasites as (D) *Leishmania* per infected macrophage or (E) normalised to female values (POC parasites burden=100). The data represents the mean \pm SD. $n_{F/M\ 4hpi} = 6/6$, $n_{F/M\ 6hpi} = 4/4$, $n_{F/M\ 16hpi} = 10/8$, $n_{F/M\ 28hpi} = 19/17$, $n_{F/M\ 52hpi} = 11/11$, $n_{F/M\ 76hpi} = 10/10$, $n_{F/M\ 100hpi} = 6/6$. P-values were calculated using two-tailed unpaired Students t-test (*= $p < 0.05$; **= $p < 0.01$, ***= $p < 0.001$; ****= $p < 0.0001$). POC = percentage of control.

3.2.2 Characterisation of *L. infantum* infected human macrophages

To further characterise *L. infantum*-infected macrophages, the polarisation of infected macrophages in comparison to uninfected cells was investigated based on phenotypical and morphological properties. To monitor the expression of surface markers associated with polarisation, macrophages were immunofluorescently stained with established M1- and M2-related surface markers and analysed using flow cytometry. Gating was performed as already depicted (Fig. 11A) and the percentage of CD14⁺ macrophages positive for respective surface marker was assessed (Fig. 13A). All surface markers were expressed by a high percentage of cells, M1-related markers on almost 100% of the cells and M2-related markers on at least 90% of cells. Slight differences could be observed in the M2-related surface markers. For example, less male macrophages expressed CD163 than female macrophages in the naïve state. Similar tendencies could be observed in infected cells for CD163 and for expression of CD200R in uninfected cells. All observations were non-significant, which was probably due to the lack of statistical power caused by a low sample size. Additionally, the MFI for the surface markers were analysed. Once again, the highest overall MFI was observed for HLA-DR followed by CD86. No statistically significant differences could be observed when comparing naïve and infected cells, although female macrophages tended to have a lower MFI for CD64 and CD163 under infection. Comparing the MFI between the sexes, a slightly higher expression of HLA-DR on male macrophages was observed (Fig. 13B).

Using the automated image analysis sequence, cells were also examined for their polarisation based on cell morphology as the infection progressed. Analysis of the polarisation of uninfected cells over the course of cultivation showed that M1-like macrophages made up around 35% of the cells in both sexes over the whole time period studied (Fig. 13C). In infected macrophages, an increase of approximately 10% in M1-like macrophage proportion was observed in both female and male macrophages at 4 hpi (Fig 13D). This effect subsided by 28 hpi and the percentage of M1-like macrophages remained at a level similar to uninfected cells. For M2-like macrophages, a mean proportion of 20-30% was observed in uninfected cells throughout the cultivation time period with the lowest proportion at 28 hpi (Fig 13E). Upon infection, a significant reduction of approximately 20% in M2-like macrophages was observed at 4 hpi (*= $p < 0.05$, not shown in graph) followed by a gradual increase as the infection progressed. For male macrophages, the percentage returned to the level of uninfected cells by 28 hpi, whereas it was reduced until 76 hpi in female macrophages. Over the whole course of infection, a clear tendency for higher numbers of M2-like macrophages within male cells was observed, except for 100 hpi (P-values above the graph for comparison

between sexes within infected cells) (Fig. 13F). In addition, the area under the curve (AUC) was calculated using graphs of uninfected and infected cells (Fig 13G). This analysis showed a higher proportion of M1-like macrophages in female (*= $p < 0.05$) and male cells ($p = 0.0649$) in infected cells compared to M2-like macrophages. A significant reduction of M2-like macrophages during infection was observed in female cells (*= $p < 0.05$) compared to uninfected cells.

In summary, infection with *L. infantum* led to a shift in macrophage polarisation, with a reduction in M2-like macrophages and an increase in M1-like macrophages, based on morphological discrimination. This tendency was similar in either sex, however, a trend towards lower levels of M2-like macrophages was observed over time.

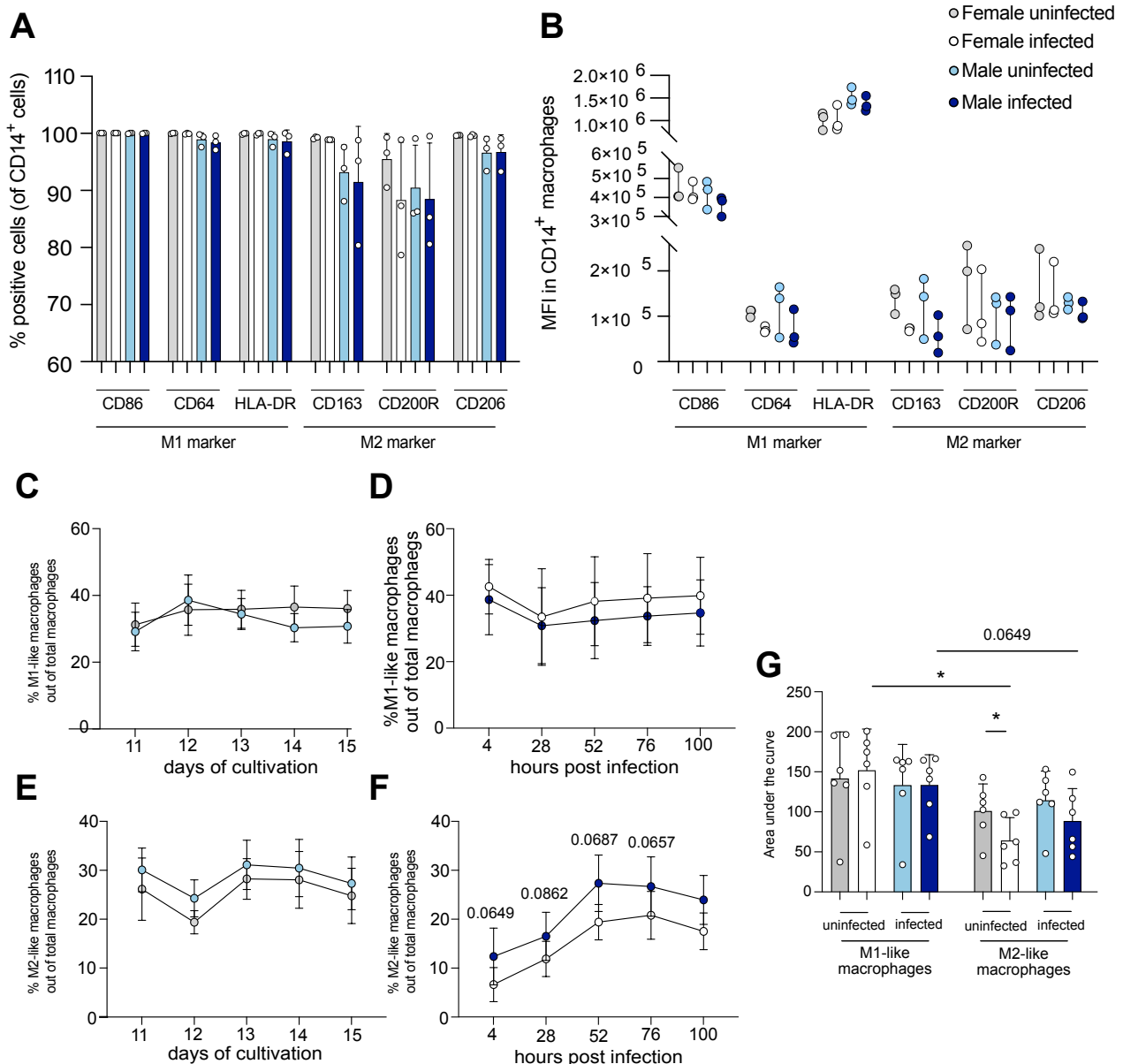


Figure 13: Phenotypical and morphological M1/M2 characterisation of female and male macrophages following *L. infantum* infection.

Mature macrophages from female and male donors were infected with *L. infantum* metacyclic promastigotes at a MOI of 15:1 and incubated for required time period. (A) At 28 hpi, cells from female donors and male donors were stained with antibodies against polarisation-related surface markers. Percentage of CD14⁺ macrophages positive for respective surface marker represented as mean + SD and (B) MFI of M1- and M2 related surface markers on CD14⁺ macrophages, data is shown as boxplot, $n_{F/M} = 3/3$. The proportion of (C, D)

M1-like and (E, F) M2-like macrophages as determined by their morphology using customised image analysis (Harmony® software) in (C, E) uninfected and (D, F) infected macrophages. The data represents mean \pm SD, $n_{F/M}=6/6$. P-values were calculated using two-way ANOVA analysis (G) Display of the area under curve of graphs (C-F). The data represents mean \pm SD. P-values were calculated using two-tailed paired Student's t-test for comparison of different conditions within one sex or two-tailed unpaired Student's t-test for comparison between sexes. (*= $p < 0.05$).

3.2.3 Cytokine profiling of *L. infantum*-infected human macrophages

The supernatant of *L. infantum*-infected macrophages and respective controls was utilised for cytokine profiling using a cytometric bead assay (LEGENDplex™). The customised panel for cytokine profiling included antibodies against pro-inflammatory cytokines that were previously associated to induce parasite killing and host protection in VL, precisely TNF- α , IL-1 β , CCL-2, IP-10 (C-X-C Motif Chemokine Ligand (CXCL) 10), IL-12p70 and IL-18 (107). As the concentration of some of the cytokines tested was outside the detection range, results are presented as the MFI, which directly correlates with the amount of cytokine measured, but no statistical significances could be calculated due to the small sample number. To capture differences as the infection progressed, cytokine levels were assessed at different time points during infection. Additionally, data were visualised as AUC to quantify cytokine levels over time.

An enhanced secretion of TNF- α was observed in infected female and male macrophages compared to uninfected cells at 6 hpi. In both sexes, the amount gradually decreased over the investigated time frame until it was indistinguishable from uninfected cells at 52 hpi. Analysis of the AUC presented a clear induction of TNF- α secretion under infection with the tendency of higher TNF- α levels in supernatants of female cells (Fig. 14A). For IL-1 β , similar amounts were detected in the supernatants for all tested conditions throughout the time course, except for a minimally reduced level for male uninfected cells at 6 hpi. This resulted in quantifying comparable AUCs for all conditions accordingly (Fig. 14B). A general increase of CCL-2 in the supernatant of both uninfected and infected cells was observed over time, but slightly different trends were seen in uninfected and infected macrophages within the sexes. Based on the AUC, a higher amount of CCL-2 was measured for uninfected cells compared to infected ones for female donors, whereas a reverse trend presented in male macrophages (Fig. 14C). IP-10 and IL-12p70 were both secreted to a higher extent from uninfected cells over the investigated time frame, which is also represented in the AUC quantification. Both cytokines showed a minimal increase over time in all studied conditions (Fig. 14D,E). The highest levels of IL-18 were observed in supernatants collected at 6 hpi for all conditions tested, with a gradual decrease over time. Uninfected cells from both sexes consistently secrete higher amounts IL-18, as also seen in the AUC calculation (Fig. 14F).

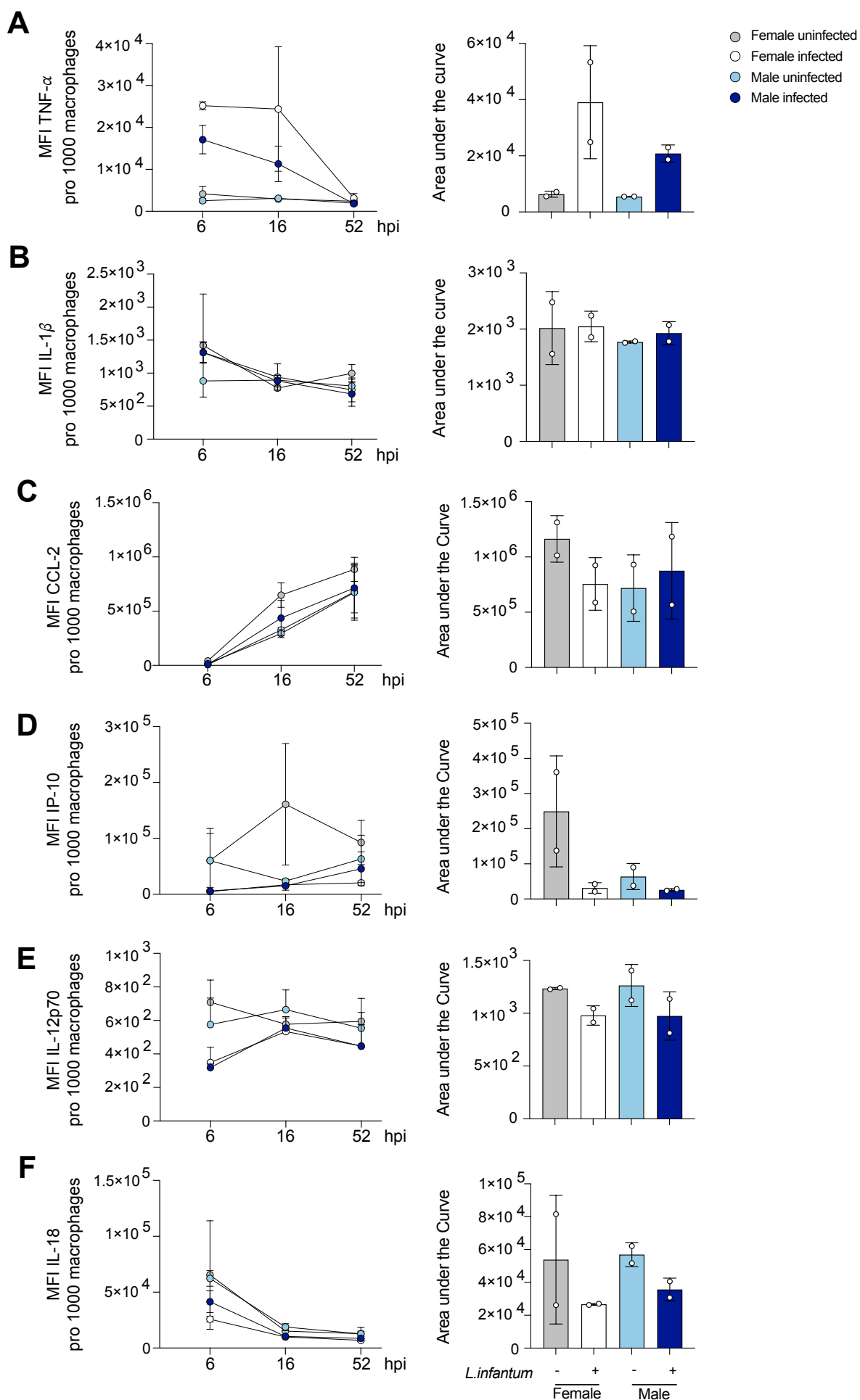


Figure 14: Secretion of cytokines related to parasite elimination by female and male *L. infantum*-infected macrophages using cytometric bead assay.

Mature macrophages from female and male donors were infected with *L. infantum* metacyclic promastigotes at a MOI of 15:1 and incubated for 6-52 hours post infection. At every investigated time point, cytokines related to parasite elimination were measured in the supernatant using cytometric bead assay (LEGENDplex™). MFI of (A) TNF- (B) IL-1 (C) CCL-2 (D) IP-10 (E) IL-12p70 and (F) IL-18 are depicted as progression over time and resulting area under the curve. Data represents mean \pm SD, $n_{F/M\ 6/16\text{hpi}} = 2$ and $n_{F/M\ 52\text{hpi}} = 3$.

The panel also included antibodies against anti-inflammatory cytokines and immune mediators, such as IL-10 and Arginase, which are associated with parasite survival and disease progression. Additionally samples were tested for levels of pro-inflammatory cytokines that have been reported to exacerbate VL, precisely CCL-17, IL-23 and IL-8 (107).

No difference in IL-10 levels could be observed over time in supernatants of uninfected cells from both sexes, whereas increased levels were measured in supernatants of infected macrophages at the initial time point of investigation. The levels decreased gradually until 52 hpi, when they were only minimally higher than those in the supernatant of non-infected cells. Quantification of the AUC for the graphs presented a clear induction of IL-10 secretion under infection with the tendency of higher IL-10 levels in supernatants of female cells (Fig. 15A). No difference in Arginase- and IL-23 levels could be determined over time in the studied comparisons of infection states and sexes, except for a slightly increased level of both immune mediators in the supernatant of uninfected female cells at 6 hpi. However, the amount of both proteins were slightly lower for infected cells compared to non-infected cells, as also seen in the calculation of AUCs (Fig. 15B,D). The level of CCL-17 did not change in the supernatant of male uninfected cells over the investigated time frame, whereas an gradual increase is seen in female counterpart. Infected cells displayed higher levels of CCL17 at 52 hpi compared to the respective control. Corresponding AUC quantification revealed increased amounts of CCL17 in the supernatant of female infected cells compared to uninfected cells, whereas the opposite trend was observed for the supernatant of male-derived macrophages. The general trend of IL-8 levels over time is comparable between the supernatant of uninfected and infected cells and showed a strong increase at 16 hpi compared to 6 hpi, which slightly decreased again at 52 hpi. However, the secretion was lower in uninfected cells for both sexes, as seen in the graph and the associated AUC calculation (Fig. 15E).

In summary, *L. infantum* infection induced unique cytokine profiles in the supernatant of infected macrophages over time, characterised by elevated levels of TNF- α , IL-10, and IL-8 in both sexes. Conversely, secretion of IL-18 and IL-12p70 decreased following infection.

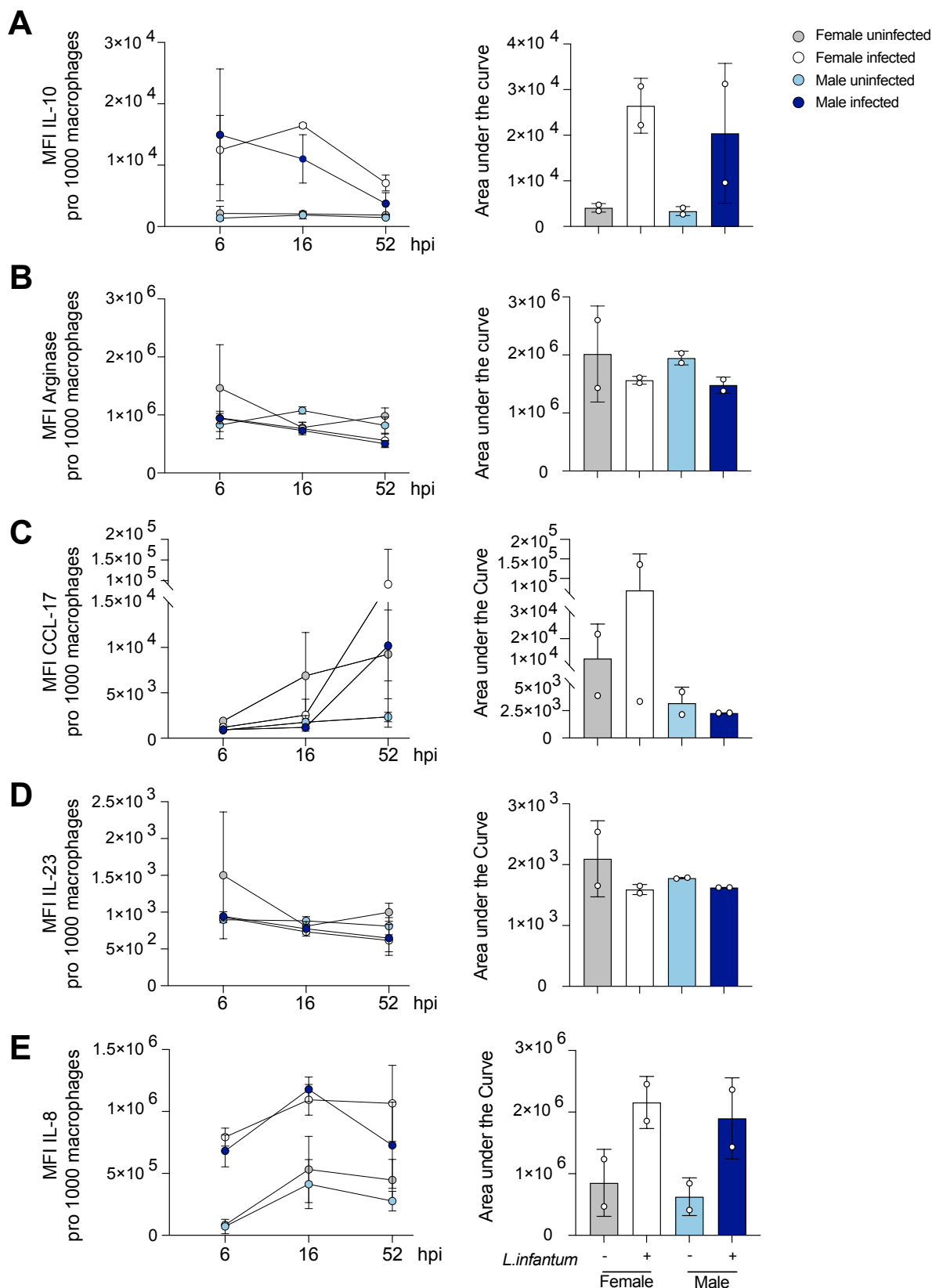


Figure 15: Secretion of cytokines related to parasite survival by female and male *L. infantum*-infected macrophages using cytometric bead assay.

Mature macrophages from female and male donors were infected with *L. infantum* metacyclic promastigotes at a MOI of 15:1 and incubated for 6-52 hours post infection. At every investigated time point, cytokines related to parasite survival and disease progression were measured in the supernatant using cytometric bead assay (LEGENDplex™). MFI of (A) IL-10 (B) Arginase (C) CCL-17 (D) IL-23 and (E) IL-8 are depicted as

progression over time and resulting area under the curve. Data represents mean \pm SD, $n_{F/M\ 6/16\text{hpi}} = 2$ and $n_{F/M\ 52\text{hpi}} = 3$.

3.2.4 Sex-specific transcriptional change in *L. infantum* infected human macrophages

Bulk RNA sequencing was performed to investigate the infection-dependent and sex-specific effects of *L. infantum* infection on the transcriptome of female and male macrophages. For this, RNA was isolated from uninfected and infected macrophages generated from four different female and male donors at different time points during infection. The time points chosen for the analysis were an early time point to monitor the effect of the initial contact between parasites and macrophages on gene regulation (6 hpi), a time point to better unravel the progression to the first significant differences in infection rates seen in preliminary experiments (16 hpi) and a time point in the later infection where the differences are solidified (52 hpi) (Tab S2). Additionally, a phagocytosis control using latex beads was included for each donor and time point.

To investigate sex-specific differences in phagocytosis and to distinguish between parasite-specific effects on gene regulation and effects due to large particle phagocytosis, female and male macrophages were incubated with beads in the same way as with parasites. The beads were red fluorescent (excitation: 575 nm, emission: 610 nm) and, at 2 μm in size, comparable in size to *Leishmania* parasites. This allowed to employ the same automated image analysis sequence to detect the beads and quantify phagocytosis. Macrophages were stained with DAPI for nuclei detection and beads were detected in the AF647 channel (Fig. 16A (a)). Using the customised image analysis sequence, beads were detected as interesting spots (*Select population I*) due to their fluorescence intensity and size (Fig. 16A (b)). Discrimination of macrophages with and without phagocytosed beads was done using the *select population III* building block (Fig 16A (c)). Viability quantification of macrophages during phagocytosis revealed a significantly higher survival of male macrophages compared to cells without phagocytosis beads ($*=p<0.05$) at 16 and 52 hours post phagocytosis, whereas female macrophages only showed increased viability at 52 hours post phagocytosis ($p=0.0531$) (Fig. 16B). The phagocytosis rate, defined as the percentage of macrophages that phagocytosed beads, showed no significant difference between sexes and remained at 80-90% throughout the study (Fig. 16C), with an average of 10-12 internalised beads per macrophage (Fig. 16D). The polarisation of macrophages was examined by morphology-based distinction and showed no significant differences in the proportion of M1-like macrophages upon phagocytosis, ranging from 35-45% of total detected macrophages in all conditions tested, with no sex-specific differences observable (Fig. 16E). At the initial time point of investigation, a 60-75% reduction in the percentage of M2-like macrophages following phagocytosis was observed compared to untreated cells in both sexes, which was almost significant in male macrophages ($p=0.0614$). A significant reduction persisted over time in female and male macrophages ($*=p<0.05$, $**=p<0.01$) with no sex-specific difference in either untreated cells or cells incubated with phagocytosis beads. A comparison of the progression of macrophage polarisation in cells incubated with beads and *L. infantum*-infected cells revealed a similar trend in the proportion of M1-like macrophages for both conditions and sexes over time (Fig. S2A). For M2-like macrophages, a

similar decrease in proportion was observed upon incubation of cells with either beads or parasites at 6 hpi. However, it was observed that while the proportion of M2-like macrophages remained the same in bead-loaded cells throughout the time course, it gradually increased again for *L. infantum*-infected cells until it reached the level of uninfected cells again. Thus, a clear trend towards more M2-like macrophages within macrophages infected with *L. infantum* compared to bead-containing macrophages was seen at 16 hpi which became significant in female cells at 52 hpi ($*=p<0.05$) and almost significant in male cells ($p=0.094$) (Fig. S4B).

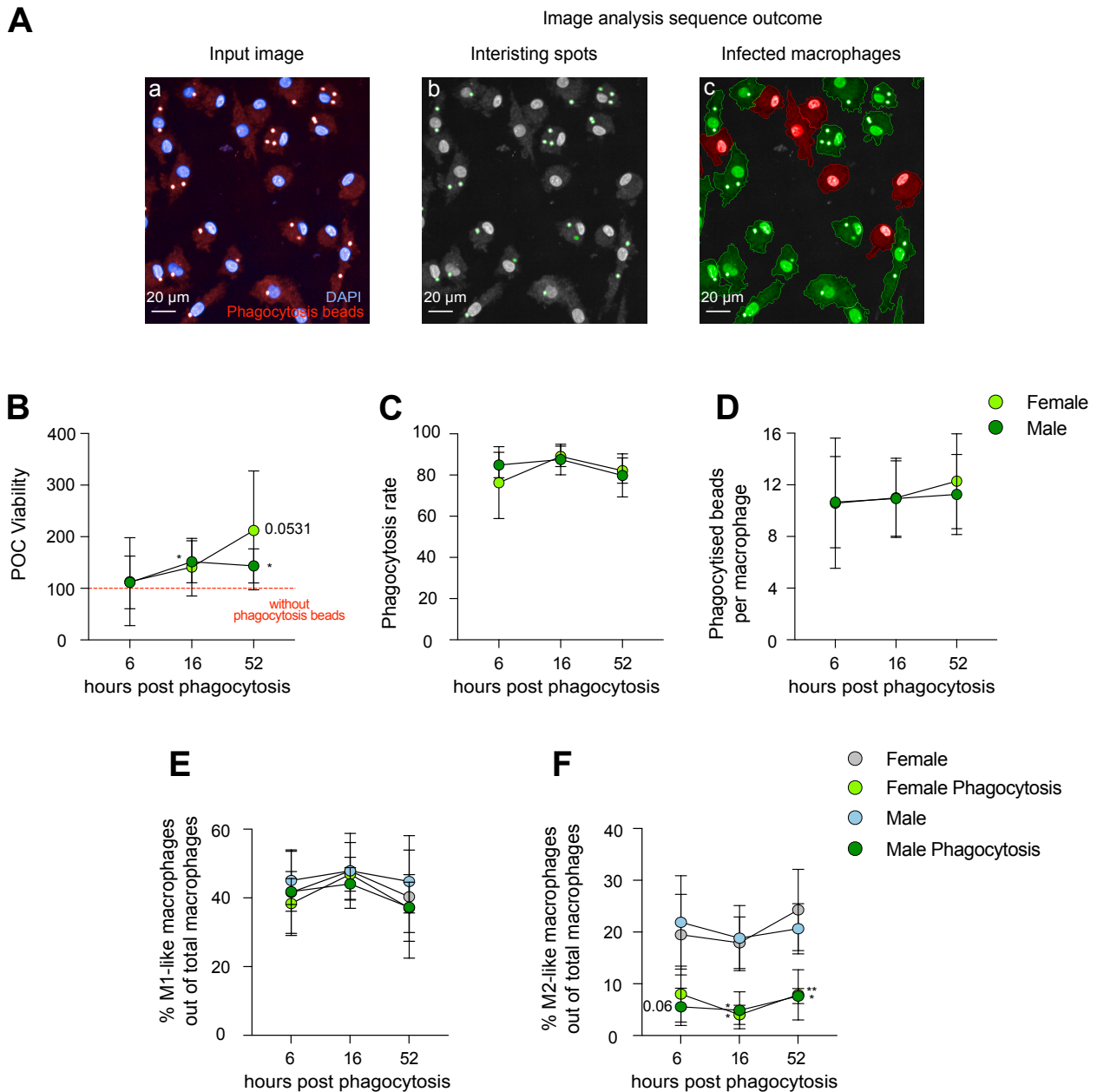


Figure 16: Phagocytosis of carboxylated latex beads by female and male monocyte-derived macrophages.

Mature macrophages were incubated for indicated time periods with carboxylate-modified polystyrene latex beads (red fluorescent, 2 μ m) at a ratio of 15 beads per cell. Macrophages were analysed using Opera Phenix® confocal microscope and analysed using customised image analysis sequence (Harmony software®). (A) Representative confocal image of macrophages at 52 hpi (a) overlay of DAPI channel (nuclei detection, blue) and AF647 channel (fluorescent beads, red), (b) Identification of fluorescent phagocytosis beads as interesting spots indicated by green outline and (c) discrimination of macrophages with phagocytosis as infected cells (positive=green, negative=red). Scale bar=20 μ m. Image analysis was used for

quantification of (B) viability, normalised within sex against control without phagocytosis beads. P-values were calculated using One-sample t-test. Additional quantification of (C) Phagocytosis rate and (D) phagocytised beads per macrophage (E) % M1-like macrophages and (E) M2-like macrophages out of total macrophages. The data represents the mean \pm SD, $n_{F/M} = 4/4$. P-values were calculated using two-way ANOVA analysis. (*= $p < 0.05$; **= $p < 0.01$)

As a first step in the analysis of the transcriptome data, potential differences between female- and male-derived naïve macrophages were investigated. Therefore, the data of uninfected samples was visualised using PCA. This analysis is used to quantify and illustrate the diversity of samples by clustering the ones with a low level of diversity close together and vice versa. In general, a low diversity was observed when conducting PCA for naïve female and male samples, except for a clustering of donor pairs that were isolated simultaneously, indicated by colour (Fig. 16A). Minor differences were also evident in determination of significantly differentially expressed genes (DEGs) between sexes. Pairwise comparison revealed the same top 12 differently regulated genes, based on the average fold change (FC), at each time point, all of which were encoded on the gonosomes. Genes overexpressed in male compared to female macrophages were encoded on the Y-chromosome, such as *ubiquitously transcribed tetra-tricopeptide repeat containing, Y-linked (UTY)*, and genes overexpressed in female cells were encoded on X-chromosome, such as *XIST* (Fig. 16B, Tab. S3-5).

Analysis of samples incubated with phagocytosis beads compared to naïve cells showed the highest regulation on the individual gene level at 6 hpi for both sexes, as defined by the number DEGs ($p < 0.05$), with more than twice as many genes significantly regulated in female macrophages compared to male macrophages ($\text{♀} = 620$, $\text{♂} = 295$). In both sexes, the majority of genes was upregulated compared to respective naïve macrophages ($\text{♀} = 595/620$, $\text{♂} = 218/295$). In both female and male samples, the number of DEGs was drastically reduced at 16 hpi with more DEGs detected again in female samples ($\text{♀} = 287$, $\text{♂} = 53$). At this time point, half of the genes were found to be upregulated and half of the genes were downregulated in both sexes. Except for one significantly downregulated gene between male bead-containing and naïve macrophages, no DEGs were detected at 52 hpi. In general, almost all of the genes exhibited low to medium magnitude of regulation ($\log_2(\text{FC}) < |3|$) (Fig. S3A, Fig. S4A, Tab. S3-S7). The low diversity between bead-containing and naïve macrophages of the same sex especially at later time points of investigation also became apparent by visualisation of data using PCA. Clustering of the samples obtained from the same donor could be observed within female and male samples (node shape) and little to no distance between the different conditions (node colour) was observed at 52 hpi (node size) (Fig. S3B, Fig. S4B). To determine the biological pathways allocated to the DEGs found during phagocytosis, gene orthology (GO) term enrichment for biological processes was performed. In macrophages derived from both sexes, phagocytosis mainly triggered a overexpression of genes associated with cell migration, cell projection organisation and regulation of apoptotic processes at 6 hpi. Additionally, processes such as response to cytokine and biotic stimulus were activated in male macrophages (Fig. S3D, Fig. S4D). On the other hand, genes allocated to processes of immune cell activation and regulation of the immune system were expressed less upon phagocytosis in both sexes at the initial time point (Fig. S3E, Fig. S4E). At 16 hpi, no significant

enrichment could be calculated for male samples due to the low number of DEGs, whereas enrichment of genes involved in the regulation of leukocyte proliferation were upregulated in female macrophages (Fig. S3G). Downregulated genes were mainly linked to TGF- β signaling and chemotaxis (Fig. S3H).

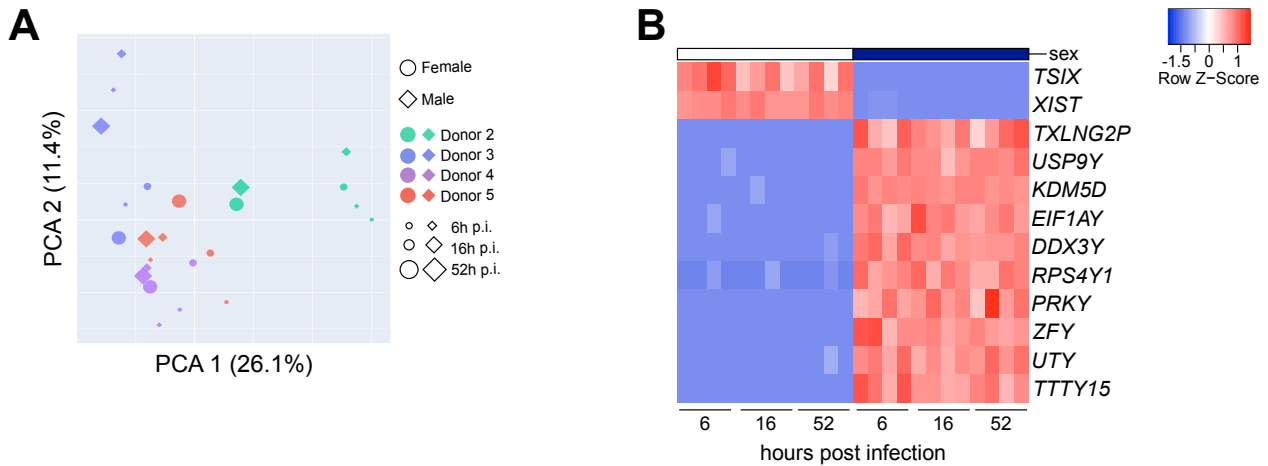


Figure 17: Analysis of differentially expressed genes between naïve female and male macrophages.

(A) PCA of sequenced uninfected macrophages according to biological sex (node shape), donor (node colour) and time of investigation (node size). Variance is indicated for both components as percentage. (B) Heatmap depicting the row z-score of top differentially expressed genes localised on the gonosomes ($p < 0.05$) between uninfected female and male cells over time. Red indicates high expression, blue indicates low expression.

PCA of uninfected and *L. infantum*-infected samples within female and male donors revealed two distinct clusters with regard to PC 1 at 6 hpi, These clusters could be allocated to uninfected (blue) and infected (red) samples in both sexes. Similar distinction was observed for 16 hpi, whereas a clear clustering of donor pairs was observed at 52 hpi in both sexes (black), indicated by node shape (Fig. 17 A,B). When comparing *L. infantum*-infected female and male macrophages with corresponding uninfected controls, the highest number of DEGs ($p < 0.05$) was observed at 6 hpi, with higher number of DEGs presenting in female macrophages ($\text{♀} = 3573$, $\text{♂} = 2609$). Of these DEGs, more genes were upregulated ($\text{♀} = 2145/3573$, $\text{♂} = 1637/2609$) than downregulated ($1428/3573$, $\text{♂} = 972/2609$) while most genes exhibiting a low to medium magnitude of regulation ($\log_2(\text{FC}) < |3|$) and the smallest proportion showing a high regulation ($\log_2(\text{FC}) < |3|$). A decrease in DEGs was observed for either sex at 16 hpi, mounting comparable numbers of DEGs for female and male macrophages ($\text{♀} = 1477$, $\text{♂} = 1373$), with $\sim 50\%$ of the genes up- ($\text{♀} = 730/1477$, $\text{♂} = 669/1373$) and downregulated ($\text{♀} = 747/1477$, $\text{♂} = 704/1373$) and a magnitude of regulation of $\log_2(\text{FC}) < |3|$. Almost no DEGs were examined at 52 hpi in either sex ($\text{♀} = 6$, $\text{♂} = 22$), reinforcing the results of the PCA (Tab. S8-Tab. S13).

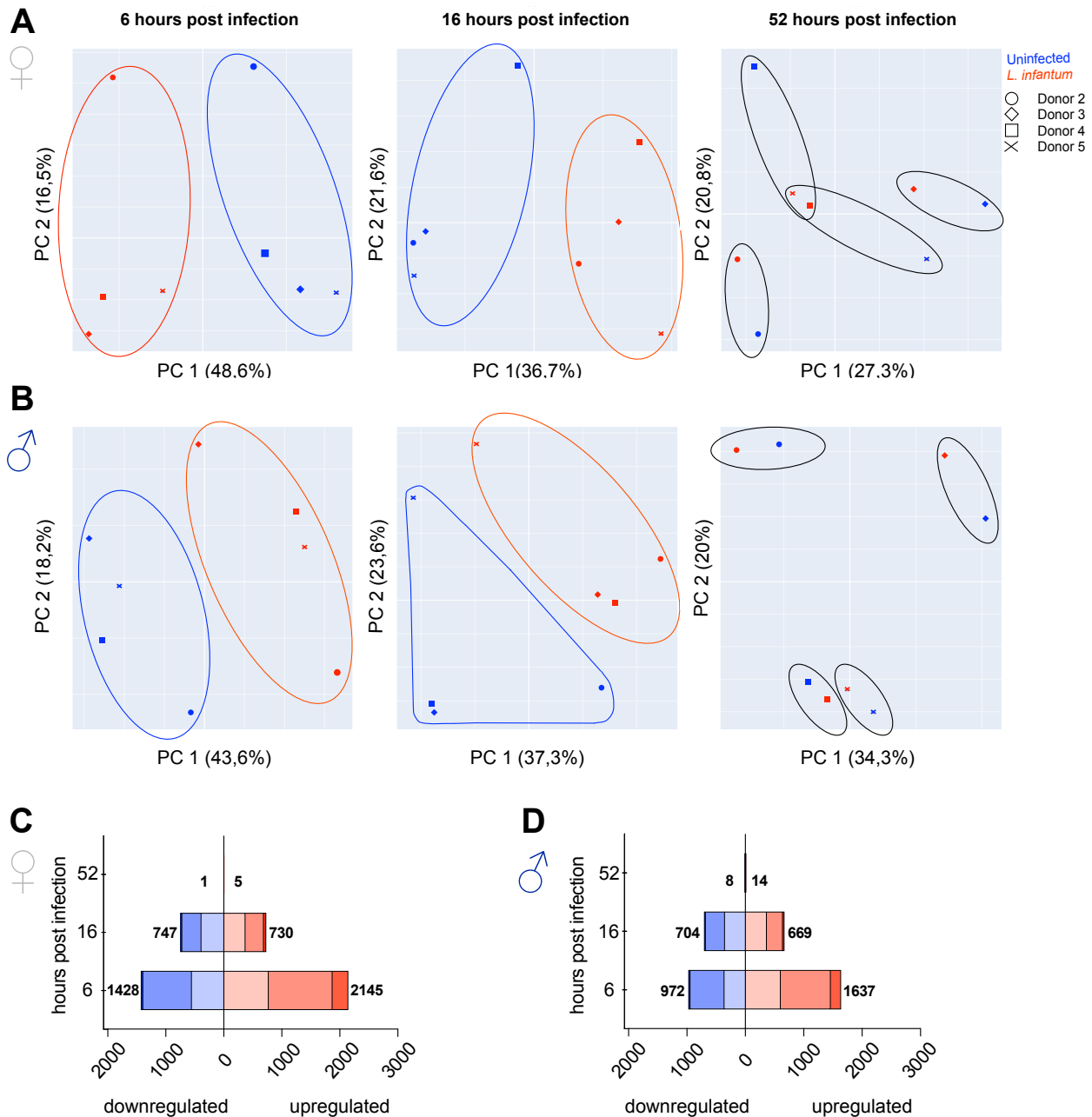


Figure 18: Analysis of differentially expressed genes between uninfected and infected macrophages from female and male donors.

(A) PCA of sequenced uninfected and infected macrophages according to infection status (node colour) and donor (node shape) at 6, 16 and 52 hpi for (A) female and (B) male cells. Variance is depicted for both components as percentage. Clusters of uninfected cells (blue), infected cells (red) and donor pairs (black) are indicated. Number of differentially expressed genes ($p < 0.05$) in *L. infantum*-infected cells in relation to uninfected control for each time point for (C) female and (D) male macrophages. Data shown as horizontal bar plots. Box width correlates with number of differentially expressed genes downregulated (left, blue) and upregulated (right, red). Colour shading correlates with the magnitude of regulation (dark: $\log_2(\text{fold change}) > 3$; medium: $1 < \log_2(\text{fold change}) < 3$, light: $\log_2(\text{fold change}) < 1$).

When directly comparing the DEGs between uninfected and infected macrophages of the same sex at the different time points, most of the genes were exclusively differentially expressed at 6 hpi, as this was the time point where most DEGs were detected. However, there was an overlap of about 30% of the genes differentially regulated at 6 hpi that were also observed at 16 hpi. For the DEGs observed at 16 hpi, this corresponded to a proportion of approximately 40-50% of the downregulated genes and over 70% of the upregulated genes that were also regulated at 6 hpi. In

female samples, no gene was found to be regulated at all investigated time points, whereas one downregulated gene and two upregulated genes were found over the total course of infection in male samples (Fig. 18A,B , Fig. 19A,B).

KEGG pathway analysis of genes upregulated between uninfected and *L. infantum*-infected macrophages within the same sex was performed to identify activated cellular pathways in response to infection at different time points. The top upregulated pathways detected at 6 hpi were similar in both sexes and included, besides ferroptosis as the most strongly induced pathway, mainly immunity-related pathways such as TNF signaling, NF- κ B signaling pathway, hypoxia-inducible factor 1 α (HIF-1 α) signaling pathway, IL-17 signaling and forkhead box O (FoxO) signaling pathway and others (Fig. 18E, Fig. 19E). Genes upregulated at 16 hpi partly allocated to previously described immune pathways in both sexes resulting in their identification among the top-regulated pathways again (e.g. TNF signaling and peroxisome proliferator-activated receptor (PPAR) signaling), although less prominently enriched. In addition, similar metabolic pathways (mineral absorption, chemical carcinogenesis-reactive oxygen species) or individual metabolic pathways, such as cholesterol metabolism in female samples and glutathione metabolism in male samples were affected at 16 hpi (Fig. 18H, Fig. 19H). Biological processes GO term enrichment was performed to determine involved pathways allocated to the downregulated genes between uninfected and infected macrophages of the same sex. At 6 hpi, most of the DEGs were involved in the immune response as well, resulting in an enrichment of immune response-related pathways. For female samples downregulated DEGs were categorised in processes such as inflammatory response, innate immune response, regulation of defence response and cytokine production, whereas male samples showed less expression of genes associated with e.g. macrophage migration, regulation of inflammatory response and B cell activation (Fig. 18D, Fig. 19D). For male samples, the downregulation of genes allocated to B cell activity became even more apparent at 16 hpi, at which many DEGs were defined as part of antibody-dependent cellular cytotoxicity or B cell receptor signaling process. All other top-regulated processes were also connected to immunity and included processes such as cytokine production or regulation of leukocyte proliferation (Fig. 19G). For female samples, most negatively affected processes at 16 hpi were part of the cellular response to stimuli (cellular response to reactive oxygen species or oxidative stress), immune response (inflammatory response, regulation of immune system production) or cytokine production (Fig. 18G). No KEGG pathway or GO term enrichment analysis could be performed for the last time point due to low number of DEGs (Fig. S4).

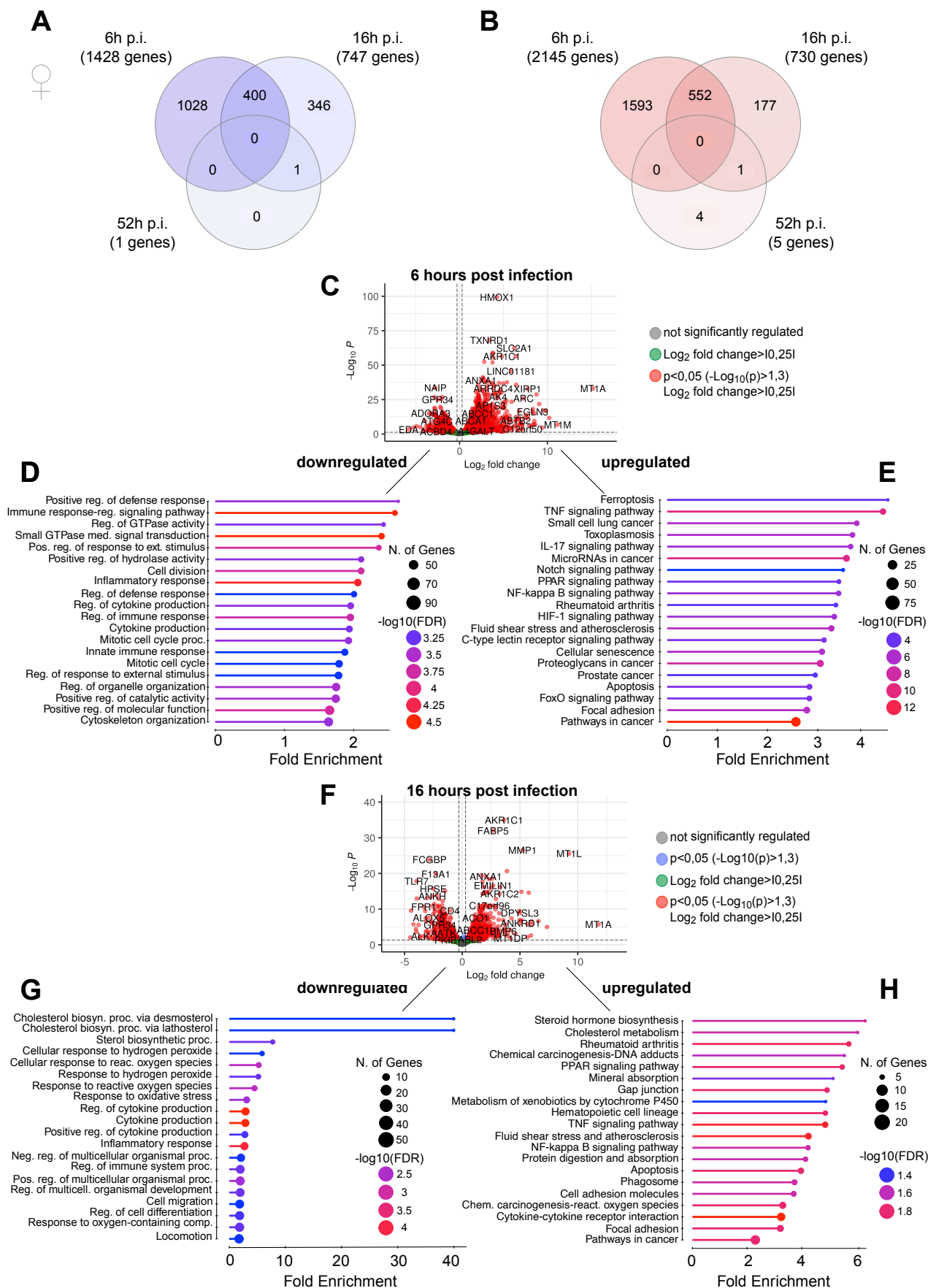


Figure 19: Analysis of differentially expressed genes between uninfected and infected macrophages from female donors.

Venn diagram depicting the number of differentially expressed genes between uninfected and infected samples shared or uniquely expressed between the time points ($p < 0.05$) for (A) down regulated and (B)

upregulated genes. (C, F) Volcano plots depicting relative gene expression according to magnitude of change ($\text{Log}_2(\text{fold change})$) and statistical significance of change ($-\text{Log}_{10}(\text{adjusted p-value})$) between uninfected and infected macrophages. Genes significantly regulated between the conditions ($\text{Log}_2(\text{fold change}) > 10.25$, $p < 0.05$) are marked in red ($\text{Log}_2(\text{fold change}) > 0$ downregulated in infected samples, $\text{Log}_2(\text{fold change}) < 0$ upregulated in infected samples) at (C) 6 hpi and (F) 16 hpi. (E, H) KEGG pathway analysis of significantly upregulated genes in infection ($p < 0.05$, $\text{log}_2(\text{fold change}) > 1$) at (E) 6 hpi and (H) 16 hpi. (D, G) Biological processes GO term enrichment of significantly downregulated genes in infection ($p < 0.05$, $\text{log}_2(\text{fold change}) < -1$) at (E) 6 hpi and (H) 16 hpi. (D, E, G, H) Shown are the top 20 pathways sorted by fold enrichment. Significances of enrichment indicated by colour and number of genes in pathway indicated in node size.

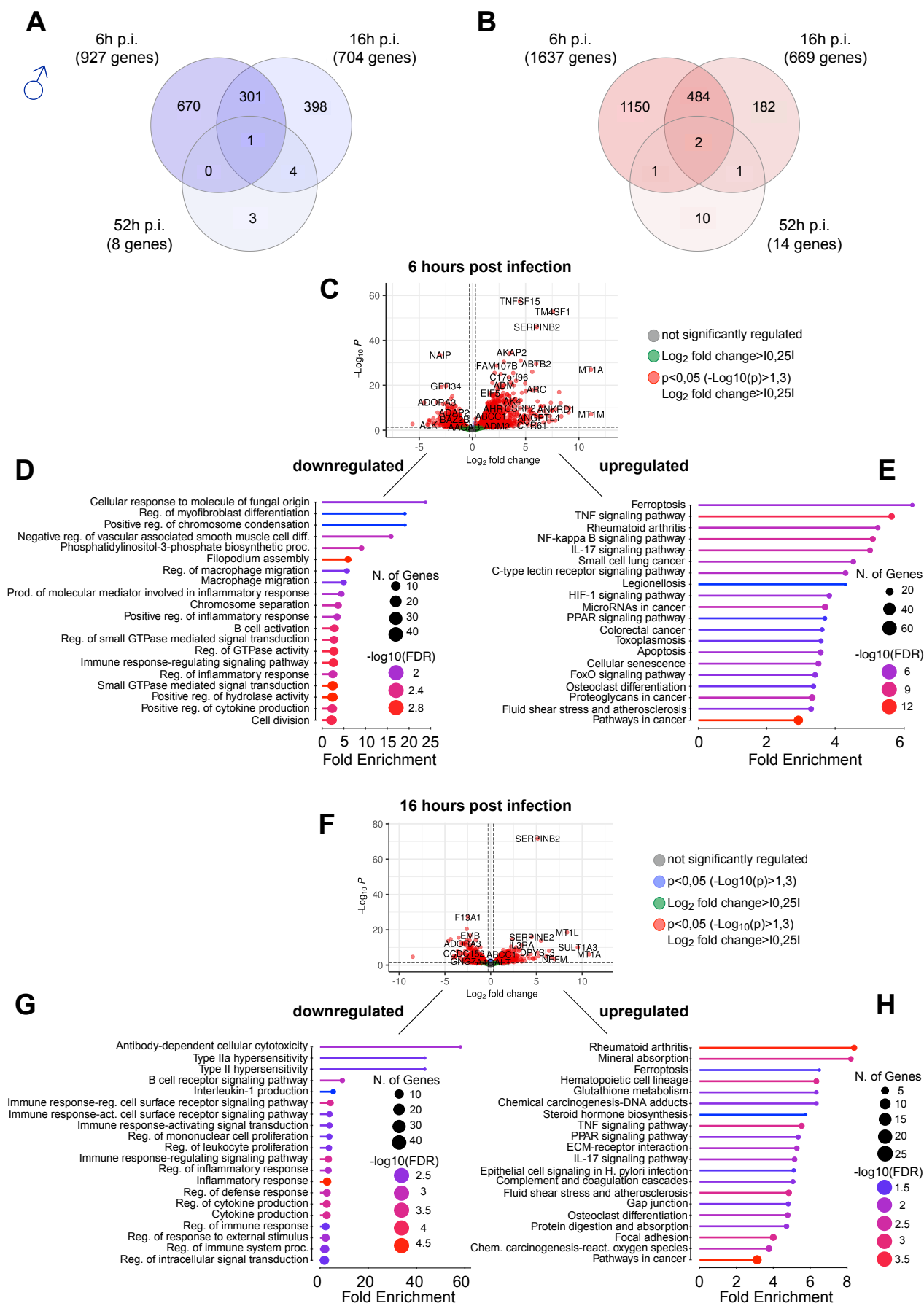


Figure 20: Analysis of differentially expressed genes between uninfected and infected macrophages from male donors.

Venn diagram depicting the number of differentially expressed genes between uninfected and infected samples shared or uniquely expressed between the time points ($p < 0.05$) for (A) down regulated and (B)

upregulated genes. (C, F) Volcano plots depicting relative gene expression according to magnitude of change ($\text{Log}_2(\text{fold change})$) and statistical significance of change ($-\text{Log}_{10}(\text{adjusted } p\text{-value})$) between uninfected and infected macrophages. Genes significantly regulated between the conditions ($\text{Log}_2(\text{fold change}) > 1.025$, $p < 0.05$) are marked in red ($\text{Log}_2(\text{fold change}) > 0$ downregulated in infected samples, $\text{Log}_2(\text{fold change}) < 0$ upregulated in infected samples) at (C) 6 hpi and (F) 16 hpi. (E, H) KEGG pathway analysis of significantly upregulated genes in infection ($p < 0.05$, $\text{log}_2(\text{fold change}) > 1$) at (E) 6 hpi and (H) 16 hpi. (D, G) Biological processes GO term enrichment of significantly downregulated genes in infection ($p < 0.05$, $\text{log}_2(\text{fold change}) < -1$) at (E) 6 hpi and (H) 16 hpi. (D, E, G, H) Shown are the top 20 pathways sorted by fold enrichment, significances of enrichment indicated by colour and number of genes in pathway indicated in node size.

To further investigate the sex differences in gene regulation upon infection more closely, the lists of DEGs between uninfected and *L. infantum*-infected macrophages of the same sex were compared with each other to find regulated genes that were specific for one sex and did not appear in the analysis for the opposite sex. The results were depicted as a Venn diagram separately for up- and downregulated genes and for the different investigation time points. This analysis showed that, except for 52 hpi, the largest proportion of about 60-90% of detected genes were similarly up- and downregulated in both sexes. At 52 hpi, most of the DEGs were exclusively found in male macrophages (Fig. 21A-C, Fig. 22A-C). Each subset of similarly or exclusively expressed genes was used to determine characteristic pathways affected using the Reactome database, which is recommended for smaller gene sets as it provides a more specific mapping of the DEGs especially for human samples (108). The top enriched pathways were depicted in a heatmap with parts of the associated genes.

In accordance with the previously performed KEGG pathway analysis, genes similarly upregulated in female and male macrophages at 6 and 16 hpi were mostly categorised into immunity-related pathways and cytokine response. Associated with these pathways were genes such as *radical SAM domain-containing 2 (RSAD2)*, *Kelch-like ECH-associated protein 1 (KEAP1)*, *CXCL3*, *suppressor of cytokine signaling 3 (SOCS3)*, *interferon regulatory factor 4 (IRF4)* and *interferone-stimulated gene 20 (ISG20)* at both time points and e.g. (*HIF1A*), *heme oxygenase 1 (HMOX1)*, *CXCL2*, *CC motif chemokine ligand 20 (CCL20)*, *IL-10* and *TNF* solely at 6 hpi. Genes encoding proteins of the metallothionein family 1 (MT1) (e.g. *MT1H* and *MT1A*) were detected at both time points with the strongest transcriptional regulation and were associated with mineral absorption. Genes similarly upregulated in a time-dependent manner were allocated to the formation of phagosome (e.g. *tubulin α -4A chain (TUBA4A)*, *procathepsin L (CTSL)* and *auxilin (DNAJ6C)*) at 6 hpi and ROS/RNS catabolism (e.g. *superoxide dismutase 2 (SOD2)* and *neutrophil cytosol factor 2 (NCF2)*) and glycolysis (*α -enolase* and *γ -enolase (ENO1, ENO2)*) at 16 hpi (Fig. 21D,G).

Looking at the genes upregulated in a sex-dependent manner, many genes involved in the interferone signaling could be exclusively found in female macrophages at 6 hpi. Amongst others, *2'-5' oligoadenylate synthetase-like (OASL)*, *Interferon induced protein with tetratricopeptide repeats 2 and 3 (IFIT2, IFIT3)* and *IRF5* were upregulated in female macrophages upon infection. In addition, some cytokine-encoding genes, such as *IL15* and *IL27* were also exclusively upregulated in female samples at the initial time point. At 16 hpi, many genes associated with protein degradation were solely expressed in infected female macrophages. These contained, for example, *proteasomal subunit α type 7 (PSMA7)*, *26S proteasome non-ATPase regulatory subunit 11 (PSMD11)* and *proteasomal ubiquitin receptor (ADMR1)*. Interestingly, genes coding for

chemokines CCL20 and CXCL2, which were upregulated in both sexes at 6hpi, were found upregulated at 16 hpi only in female samples (Fig. 21E, H).

On the other hand, exclusive expression in male macrophages was found for many genes encoding immune mediators and allocated to signaling by interleukins at 6 and 16 hpi, such as *CXCL1*, *IL32*, *CCL1*, *IL1A* and *IL1B*. Additionally, many genes involved in the cellular response to stress, e.g. *TRAF2* and *NCK-interacting protein kinase (TNIK)* and *parafibromin (CDC73)* were also expressed higher in male samples. Specifically regulated at 6 hpi were genes associated with tryptophan metabolism, *indoleamine 2,3-dioxygenase 1 (IDO1)* and *L-amino-acid oxidase (IL4I1)*, and *Leishmania* survival, e.g. *prostaglandin E2 receptor EP4 subtype (PTGER4)* and *guanine nucleotide-binding protein G(I)/G(S)/G(O) subunit γ -5 (GNG5)* that could be detected upon infection in male donors only (Fig. 21F, I).

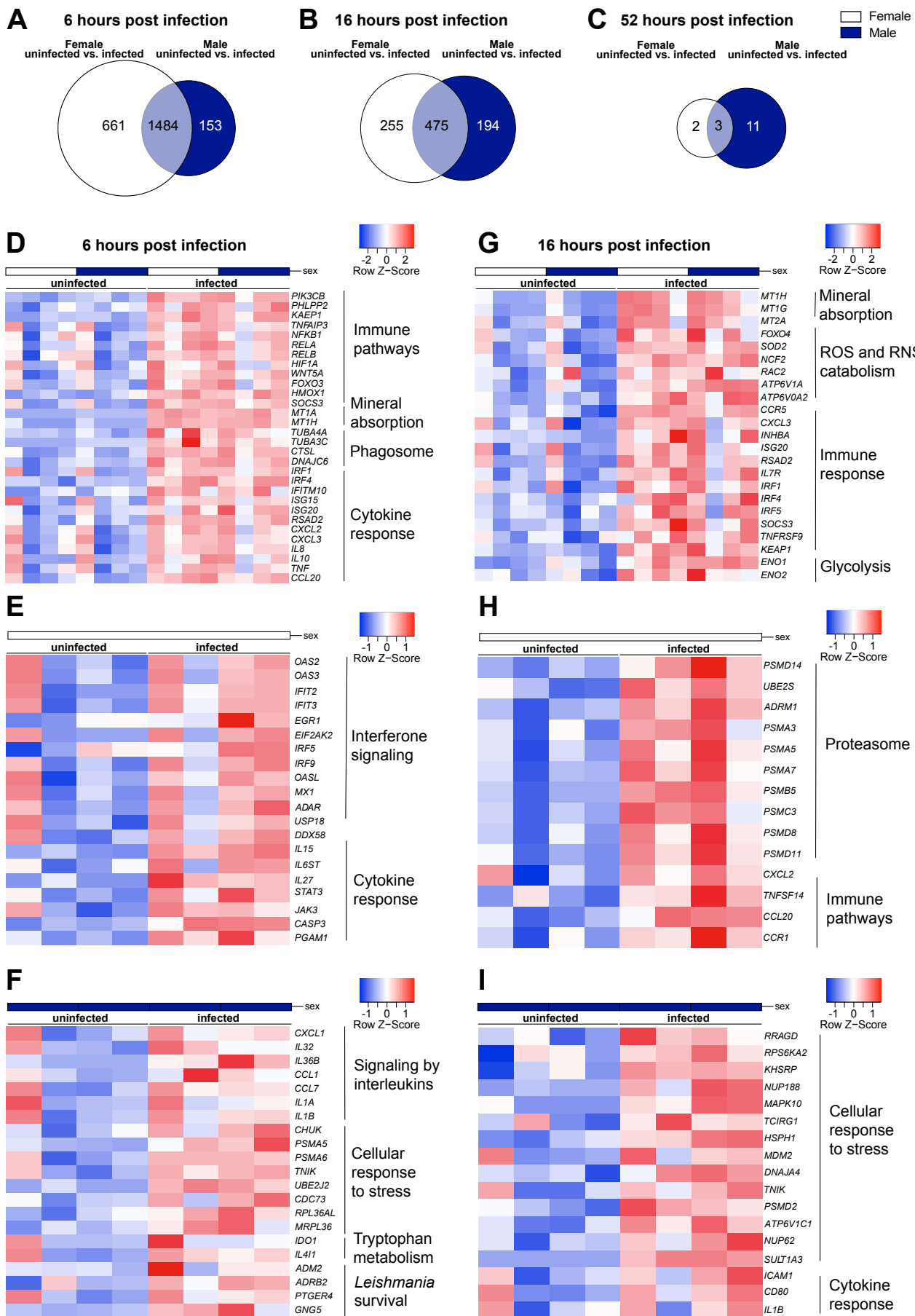


Figure 21: Analysis of differentially upregulated genes between female and male macrophages upon *L. infantum* infection.

Venn diagram depicting the number of differently upregulated genes between female and male donors upon *L. infantum* infection based on the comparison of differentially expressed genes between uninfected and infected samples of same sex ($p < 0.05$) at (A) 6 hpi (B) 16 hpi and (C) 52 hpi. (D-I) Shown are the top pathways identified with Reactome database sorted by fold enrichment and significances of enrichment with corresponding regulated genes as a heatmap for (D, G) similarly expressed genes between female and male donors, (E, H) exclusively upregulated genes in female samples and (F, I) exclusively upregulated genes in male samples at (D-F) 6 hpi and (G-I) 16 hpi. Pathways are indicated at the side of the heatmap. Red indicates high expression, blue indicates low expression.

Analysis of the similarly downregulated genes upon *L. infantum* infection between female and male macrophages revealed many genes coding for mediators of both innate and adaptive immune system at early time points (6 and 16 hpi). At both time points, genes encoding for Toll-like receptors (*TLR7*, *TLR4*) were downregulated in both sexes as well as several surface marker encoding genes (e.g. *CD200R1*, *CD14*). Time-dependent decrease of the expression of genes associated with immune response in both female and male macrophages was observed for genes such as *CD209* and *macrophage mannose receptor 1 (MRC1)*, *caspase 8 and 10 (CASP10, CASP8)* and *cytochrome b-245 heavy chain (CYBB)* at 6 hpi, as well as in endocytosis-related genes (e.g. *sorting nexin-5 (SNX5)* and *exocyst complex component 6 (EXOC6)*). At 16 hpi, less expression of additional genes associated with *Leishmania* infection was observed in both sexes. Amongst others, these genes induced were *IL-18*, *CD163*, *Fcγ receptor-encoding genes (FCGR1A, FCGR3A)* and *NACHT, LRR and PYD domains-containing protein 3 (NLRP3)* (Fig. 22D, G).

Exclusively downregulated genes in female macrophages at 6 hpi were mostly categorised in pathways of DNA replication and cell cycle, with genes such as *DNA polymerase δ subunit 3 (POLD3)* and *DNA replication ATP-dependent helicase/nuclease DNA2 (DNA2)*, or respiratory chain and oxidative phosphorylation pathways (e.g. *Cytochrome c oxidase assembly factor 1 homolog (COA1)* and *mitochondrial inner membrane protein (OXA1L)*). In addition, *CD163*, which was similarly downregulated in both sexes at 16 hpi, already showed significant reduction in expression at 6 hpi in female macrophages. At 16 hpi, exclusively downregulated genes in female infected cells were associated with scavenger receptor binding, as seen by the detection of *macrophage scavenger receptor types I and II (MRS1)* and *SPARC*, as well as with immune response and cell migration, as for example characterised by genes encoding vinculin (*VCL*), caplponin-2 (*CNN2*), *HIF1A (HIF1A)* and *neurogenic locus notch homolog protein 1 (NOTCH1)* (Fig. 22E, H).

No significant enrichment could be performed for the genes only downregulated in male donors at 6 hpi due to the small gene set. However, clustering of DEGs associated with DNA translation and cellular response to stress was observed at 16 hpi, characterised by the downregulated expression of e.g. various genes encoding ribosomal proteins (*RPL*, *RPS*) and translocon-associated protein subunit α (*SSR1*) as well as genes associated with immune response such as *C-type lectin domain family 4 member E (CLEC4A)* or *NLRP1* (Fig. 22F, I).

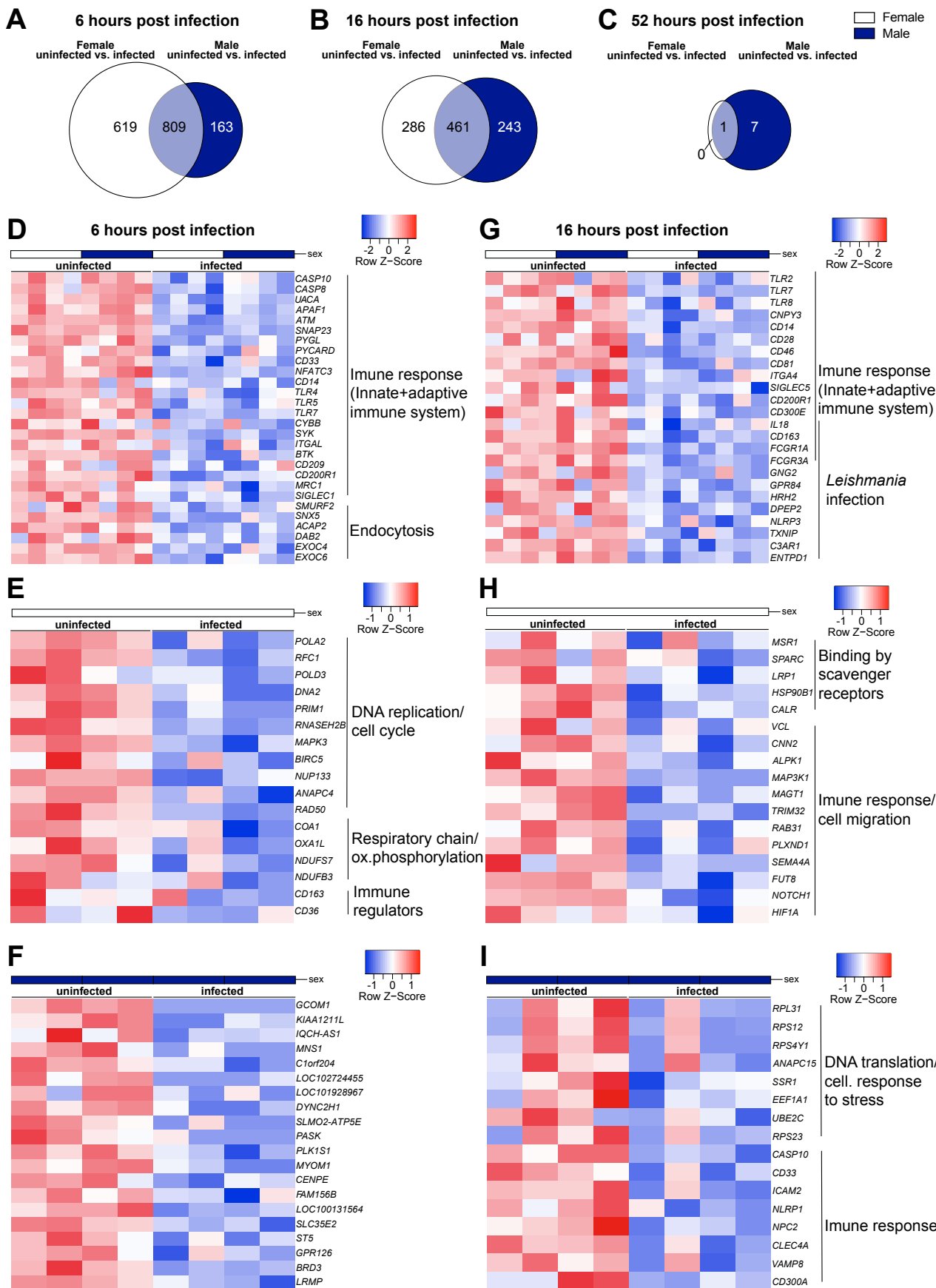


Figure 22: Analysis of differentially downregulated genes between female and male macrophages upon *L. infantum* infection.

Venn diagram depicting the number of differently downregulated genes between female and male donors upon *L. infantum* infection based on the comparison of differentially expressed genes between uninfected and infected samples of same sex ($p < 0.05$) at (A) 6 hpi (B) 16 hpi and (C) 52 hpi. (D-I) Shown are the top pathways identified with Reactome database sorted by fold enrichment and significances of enrichment with corresponding top regulated genes as a heatmap for (D, G) similarly expressed genes between female and male donors, (E, H) exclusively downregulated genes in female samples and (F, I) exclusively downregulated genes in male samples at (D-F) 6 hpi and (G-I) 16 hpi. Pathways are indicated at the side of the heatmap. Red indicates high expression, blue indicates low expression.

As previously discussed, many genes are similarly regulated in female- and male-derived macrophages during infection, but additional analysis was carried out to see if the magnitude of regulation differed between the sexes. Thus, the ratio of $\text{Log}_2(\text{fold change})$ values for genes were calculated and visualised. Although genes were regulated in both sexes, many still showed different levels of induction or suppression, indicated by a quotient smaller than 0.5 (signifying an expression regulation twice the magnitude in male macrophages) or bigger than 2 (at least twofold increase in female macrophages).

Genes that were induced more strongly in female macrophages than in male macrophages at 6 hpi included *matrix metalloproteinase 10 (MMP10)* gene as well as genes coding for metallothionein 1H (*MT1H*), CC motif chemokine ligand 15 (*CCL15*), *IL-8* and CXC motif chemokine receptor 4 (*CXCR4*). In contrast, chemokine encoding genes, such as *CCL20*, *CCL4* and *CXCL3* were more prominently expressed in male macrophages, as well as for example *epiregulin (EREG)* and *TNF- α induced protein 6 (TNFAIP6)* (Fig. 18A).

At 16 hpi, *MMP10* was again the gene with the most pronounced difference in expression regulation with a 50-fold higher induction in female cells compared to male cells. Similar observations, although less pronounced, were made for *Inhibin β -A (INHBA)* and *eukaryotic translation elongation factor 1 α 2 (EEF1A2)*, among others. On the other hand, male cells showed an increased expression of genes coding for TNFAIP3-interactin protein 3 (*TNIP3*), metallothionein 1F (*MT1F*) and glutamine-fructose-6-phosphatase transaminase 2 (*GFPT2*). Differences in the level of gene suppression between female and male cells could be observed for *interacting protein for cytohesin exchange factors 1 (IPCEF1)*, *Ecodyspalin A (EDA)* and G protein-coupled receptor 82 (*GPCR82*), with stronger suppression in female cells at 6 hpi (Fig. 18C). Increased suppression in relation to the opposite sex could for example also be observed for *proteinase-activated receptor 3 (F2LR2)* and *CD300E* in male macrophages and for *Ecto-NOX disulfide-thiol exchanger 1 (ENOX1)* and *Calcium/calmodulin-dependent protein kinase type 1D (CAMK1D)* in female macrophages at 16 hpi (Fig. 18D).

In summary, many common mechanisms were elicited across sexes in their response to infection with *L. infantum*, including vital immunological signaling pathways. However, differences in the magnitude of regulation and also distinct individual adaptations in gene expression were observed for both female- and male-derived macrophages, prompting the need for further exploration into their significance.

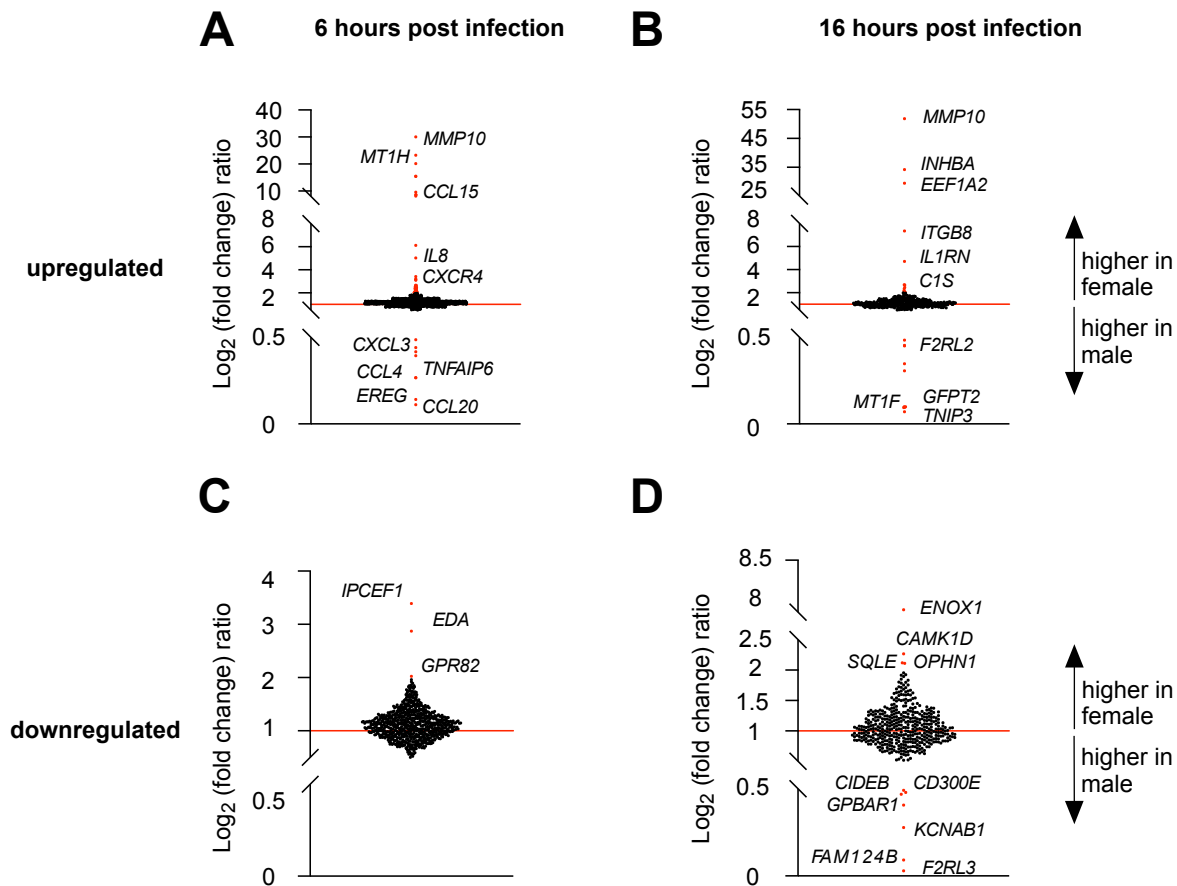


Figure 23: Comparison of the magnitude of gene expression control within similarly regulated genes in female and male macrophages.

The relative magnitude of gene regulation between both sex, assessed by Log₂ (fold change), is depicted for genes that were similarly regulated in female- and male-derived macrophages during infection. Quotient (Log₂ (fold change)_{female} samples/_{male} samples) for upregulated genes at (A) 6 hpi and (B) 16 hpi and for downregulated genes at (C) 6 hpi and (D) 16 hpi. Quotient = 1 (red line) equals similar magnitude of regulation; quotient > 1 equals higher magnitude of regulation in female macrophages; quotient < 1 equals higher magnitude of regulation in male macrophages. Values > 0.5 and < 2 are marked red and individual genes are labeled.

Mapping of the trimmed reads to the *L. infantum* genome revealed the highest alignment of approximately 15-20% at 6 hpi, followed by a gradual decrease over time. The decrease at 16 hpi was almost significant in female macrophages when comparing it to the initial collection time ($p=0.0735$) and became significant after 52 hpi ($*=p<0.05$). In male macrophages, a significant reduction was observed for both time points ($*=p<0.05$). No sex-specific difference was observed in the proportion of aligned reads at any investigated time point. Additionally, the decrease in alignment correlated with the reduction of infected macrophages and parasites per cell (Fig. 19A,B). To investigate the change of gene-specific RNA abundance in *L. infantum* parasites across collection time, samples from both sexes were pooled for each time point and compared to the samples of subsequent collection times after statistically removing the sex-difference. A total of 1149 genes showed altered RNA abundance over time (p -value < 0.05), but none of them showed a Log₂(fold change) > 0.25, indicating a very low level of transcriptional regulation (Fig. 19C).

Analysis of the 448 genes with higher RNA abundance across collection time showed a strong association to the amastin protein family, whereas for the 701 genes with decreased RNA abundance, most of the genes were members of the histone protein family (Tab. S17).

No genes with significantly altered RNA amounts could be identified by pairwise comparison of female and male samples at 16 and 52 hpi (Fig. S6). However, at 6 hpi, sex-specific differences in RNA quantity for 3 genes was observed. *LINF_310028200*, a gene encoding peptidase m20/m25/m40 family-like protein, and *LINF_350005400*, coding for a pyruvate kinase, showed increased RNA levels in female samples compared to male samples. On the other hand, the level of *LINF_310026700*, another gene encoding a peptidase m20/m25/m40 family-like protein, was increased in male samples (Fig. 19D, Tab S18).

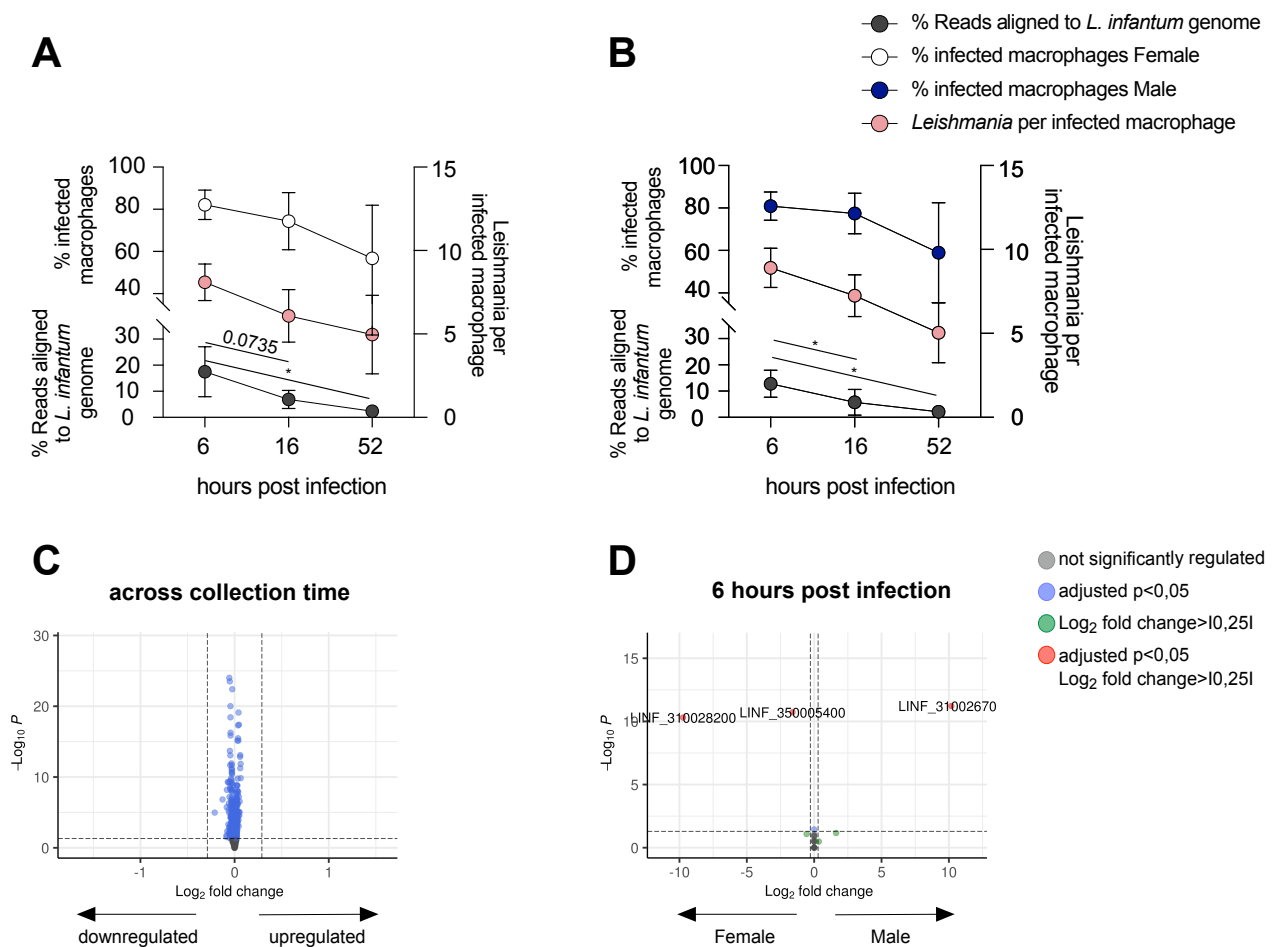


Figure 24: Analysis of differentially expressed genes in *L. infantum* parasites during infection.

Mature macrophages from female and male donors were infected with *L. infantum* metacyclic promastigotes at a MOI of 15:1 and subjected to transcriptional profiling by Next Generation Sequencing. Data was aligned to *L. infantum* genome and infection parameters were quantified microscopically using customised image analysis (Harmony® software). Infection dynamics are depicted in relation to transcriptional activity of parasites for (A) female macrophages and (B) male macrophages. Data represented as mean \pm SD, $n_{F/M}=4$. P-values were calculated using ordinary One-way ANOVA ($*=p < 0.05$). Volcano plots depicting relative gene expression according to magnitude of change ($\text{Log}_2(\text{fold change})$) and statistical significance of change ($-\text{Log}_{10}(\text{adjusted } p\text{-value})$) between (C) samples across collection time (samples pooled for collection time point and sex-difference statistically removed) and between (D) female and male samples at 6 hpi. Individual genes are labeled.

3.3 Influence of steroid hormones on *L. infantum* infection

Macrophages express both estrogen (109) and testosterone receptors (110, 111) on their surface making them susceptible to immune regulation by steroid hormone binding. Therefore, a putative influence of hormone treatment on the infection with *L. infantum* was investigated.

To this end, mature macrophages were treated with the female (17- β -estradiol (E2)) or male (5- α -Dihydrotestosterone (DHT)) steroid hormone of various concentrations for 30 min. After the incubation, *L. infantum* parasites were added for 4 hrs following removal of extracellular parasites and steroid hormones by washing. Cells were further incubated until 28 hpi (Fig. 20 A). Subsequent characterisation of cells was done by confocal microscopy (3.3.1, 3.3.2) and cytokine profiling by cytometric beads assay (3.3.2.2) (Fig. 20 B).

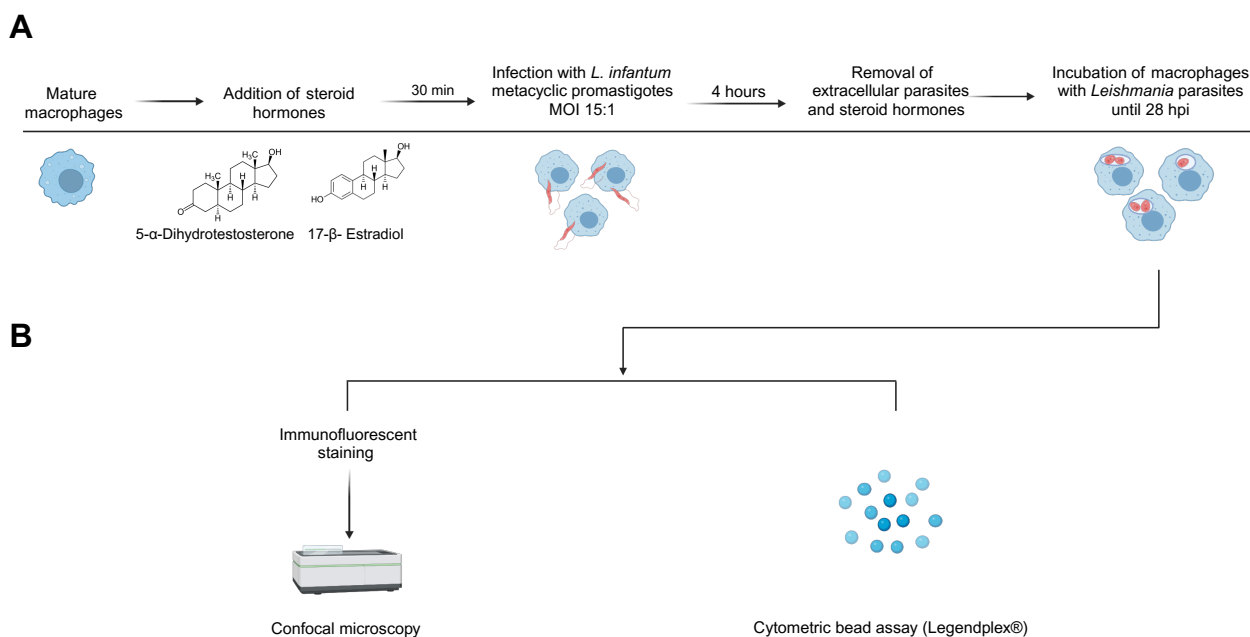


Figure 25: Schematic depiction of the workflow for the treatment of monocyte derived macrophages with steroid hormones before infection with *L. infantum*.

(A) Mature macrophages were treated with steroid hormones (5- α -Dihydrotestosterone or 17- β -Estradiol) in various concentrations (0.01-5 μ M) for 30 minutes before infection with *L. infantum* at an MOI of 15:1. Extracellular parasites were removed after 4 hrs by washing and cells were further incubated until 28 hpi. Subsequently, the cells were fixed and immunofluorescently stained for characterisation by confocal microscopy. The supernatant was used for cytokine profiling by cytometric beads assay (Legendplex™). Figure created with BioRender.com

3.3.1 Influence of androgens on the infection with *L. infantum*

DHT is obtained by the conversion of testosterone by 5 α -reductase and was used for the treatment of mature macrophages with male steroid hormone, as it is the more potent form of testosterone and cannot be metabolised to estradiol by aromatases (112). This way, putative influences are clearly attributable to treatment with androgen. Treatment and infection of macrophages was according to Fig. 20 and cells were stained with DAPI and α -LHSP90-AF647 followed by confocal high content microscopy. Images were analysed with customised image analysis sequence and data are shown as POC of the negative control (infected untreated, POC=100) separately for each sex. To investigate toxic effects due to the treatment with DHT, viability of macrophages was

evaluated by treating uninfected cells with the lowest (0.01 μM) and highest (5 μM) DHT concentration used in the assay. Due to the small number of samples per condition and the high scattering of biological replicates for both sexes, no difference was observed, except significantly reduced viability for female cells after treatment with 2 μM (**= $p < 0.01$) (Fig. 21A). For the infection rate, a clear separation of uninfected (mean POC >10) and infected macrophages could be performed by the algorithm, but no significant DHT-dependent differences were observed in infected samples at any concentration for both sexes (Fig. 21B). Similar observations were obtained for the quantification of parasite burden under DHT treatment (uninfected samples mean POC >2) (Fig. 21C). Additionally, a non-linear regression analysis was performed with the data to visualise correlations of DHT concentration and infection parameters more clearly. This analysis determines the curve and the associated function that best fits the data. Two variables are fitted: the steepness (slope) and the elevation (Y-intercept) of the curve. In this case, the slope illustrates the correlation between sex hormone concentration and infection parameter, with a large slope indicating a strong dependency between the variables. If the slope equals zero, the elevation can be interpreted as the mean Y-value over the different of X-values. When analysing regression for the infection rate in correlation to DHT concentration, a straight line was fitted for female and male data sets with shared slope and Y-intercept, indicating that no sex-specific difference in the influence of DHT treatment was observed ($R^2=0.0000247$). The deviation of the slope (-0.0253 ± 0.8053) from zero was not significant, underlining the result that the DHT treatment at different concentrations did not correlate with the infection rate. The mean infection rate remained unchanged after DHT treatment compared to the control, as shown by the Y-intercept ($Y=97.63 \pm 1.674$) (Fig. S4A). For correlation analysis between parasite burden and DHT concentration, no shared line could be generated between the sexes ($*=p < 0.05$). Both lines have no significant deviation from zero but the slopes have opposite signs. The line fitted to the female data set had a slope of 2.61 ± 2.13 and a Y-intercept at $Y=87.41 \pm 4.428$ ($R^2=0.073$), whereas for the male data set, the line had a slope of $-3,441 \pm 2,394$ and intercepted the Y-axis at $Y=104.6 \pm 4.977$ ($R^2=0.098$). These differences in the slope and Y-intercept, although not significant, may indicate different tendencies for both sexes (Fig. S4B).

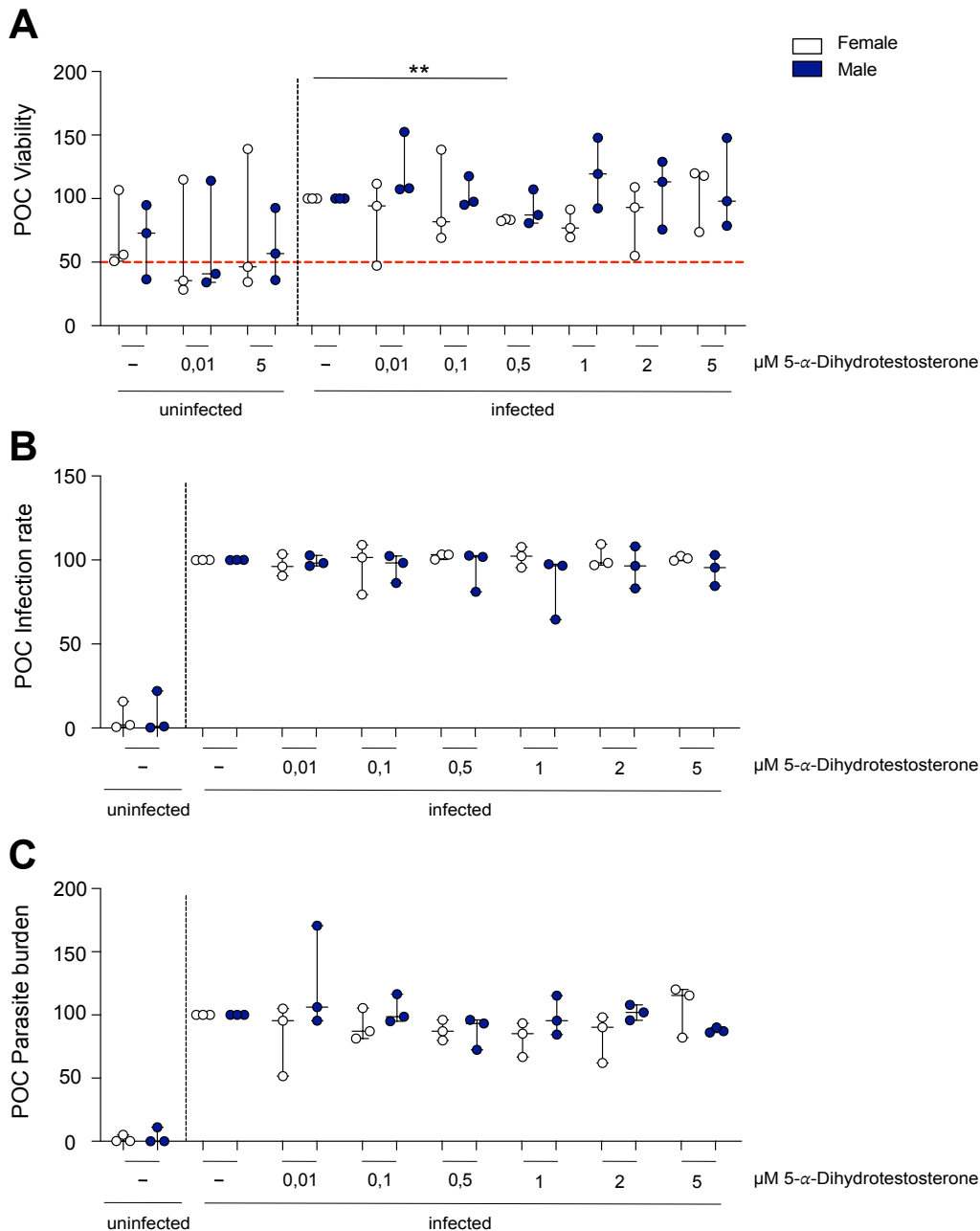


Figure 26: Influence of testosterone treatment on the infection of macrophages with *L. infantum*.

Mature macrophages from female and male donors were treated with 5- α -Dihydrotestosterone in various concentrations (0.01– 5 μM) for 30 minutes before infection with *L. infantum* at an MOI of 15:1. Cells were incubated for 28 hpi. After immunofluorescent staining of the macrophages with DAPI and α -LHSP90 coupled to AF647, (A) viability (below 50% viability possible toxic effect (red dotted line) (B) infection rate and (C) parasite burden were quantified using Opera Phenix® confocal microscope and customised image analysis sequence (Harmony® software). Data is shown as boxplot and is normalised against infected untreated control (POC=100) within each sex. $n_{F/M} = 3/3$ per condition. P-values were calculated using ordinary one-way ANOVA with Dunnett's correction. (**= $p < 0.01$) POC=percentage of control.

3.3.2 Influence of estrogens on the infection with *L. infantum*

As for the analysis of the influence of androgens on the infection with *L. infantum*, estrogen treatment and infection was done according to Fig. 20 and all data is presented as POC. Treatment with E2 had no toxic effect on macrophages, since no significant effect on viability could be observed due to treatment in uninfected or infected samples. However, viability was significantly or nearly significantly reduced in uninfected male macrophages compared to macrophages treated

with E2 at similar concentrations and infected with *L. infantum* ($*=p<0.05$) (Fig. 22A). This result is similar to the increased survival of infected cells observed in the time course of infection (Fig. A). When looking at the infection rate, infected macrophages could be clearly distinguished from uninfected (mean POC>5) macrophages but no significant influence of E2-treatment on the infection rate was observed (Fig. 22B). Analysing the parasite burden under E2-treatment revealed reliable distinction between uninfected (POC>5) and infected cells and a significant reduction of the infection rate in female macrophages when treated with 1 μ M E2 (mean POC=60) ($*=p<0.05$) (Fig. 22C).

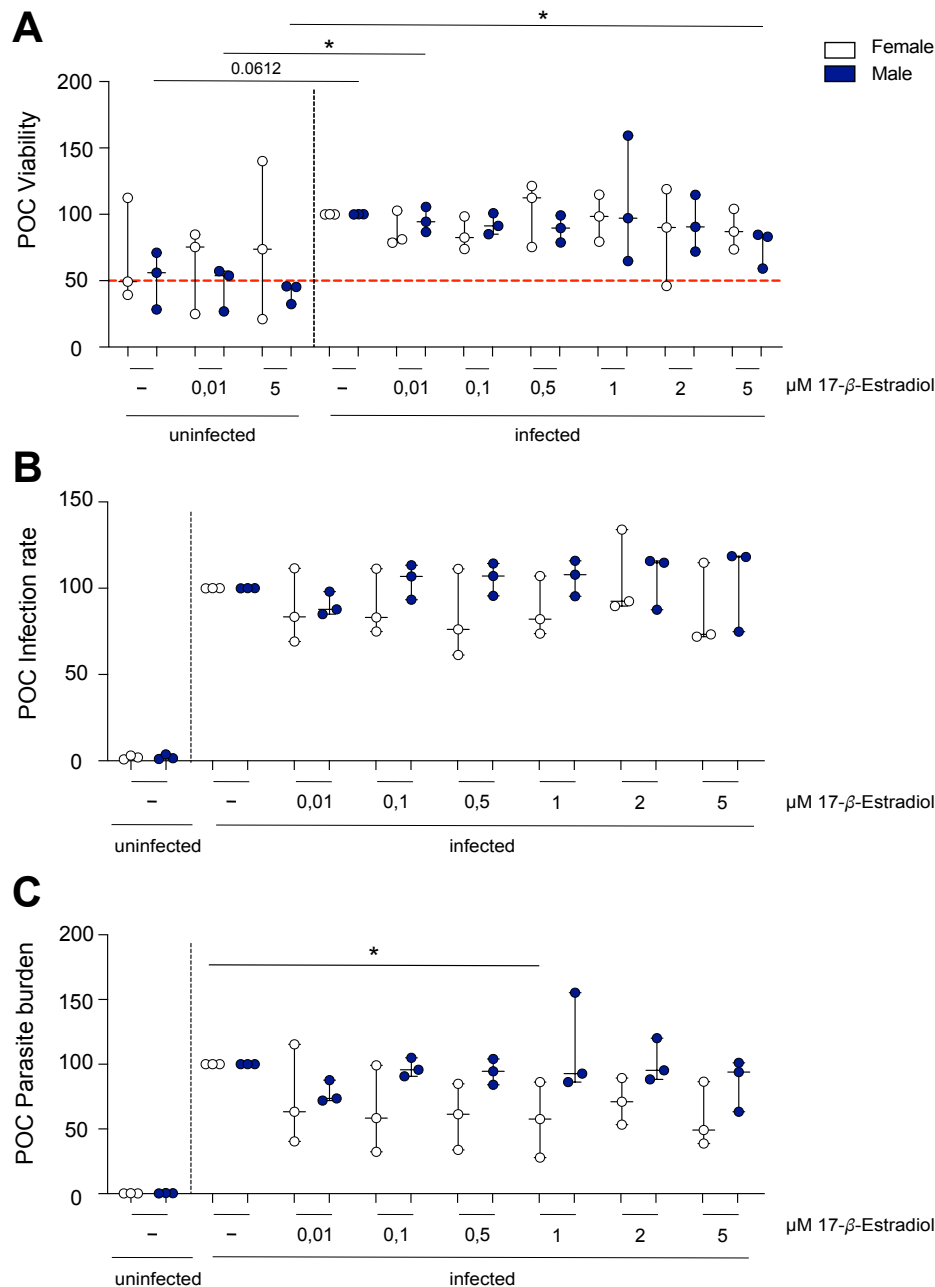


Figure 27: Influence of estradiol treatment on the infection of macrophages with *L. infantum*.

Mature macrophages from female (white) and male (blue) donors were treated with 17- β -Estradiol in various concentrations (0.01– 5 μ M) for 30 minutes before infection with *L. infantum* at an MOI of 15:1. Cells were incubated for 28 hpi. After immunofluorescent staining of the macrophages with DAPI and anti-LHSP90, (A) viability (below 50% viability possible toxic effect (red dotted line) (B) infection rate and (C) parasite burden were quantified using Opera Phenix® confocal microscope and customised image analysis sequence (Harmony® software). Data is shown as boxplot and is normalised against infected untreated control

(POC=100) within each sex. $n_{F/M} = 3/3$ per condition. P-values were calculated using ordinary one-way ANOVA test with appropriate correction. (*= $p < 0.05$) POC=percentage of control.

Non-linear regression analysis to investigate correlation between E2 concentration and infection rate generated a straight line for both sexes with shared Y-intercept ($Y = 96.47 \pm 3.223$) and slope (0.3926 ± 1.55), which was not significantly deviant from zero ($R^2 = 0.0016$), indicating no correlation between infection rate and E2 concentration and no affect on the mean infection rate in either sex (Fig.23 A). When conducting regression analysis for parasite burden data in correlation to E2 concentration, two different lines were calculated for female and male macrophages (**= $p < 0.01$). For male data a straight line was fitted (slope= -0.965 ± 2.453 , Y-intercept at $Y = 96.6 \pm 5.908$, $R^2 = 0.0081$), whereas for female data, the function was described with a slope of -3.318 ± 3.455 and a Y-intercept at $Y = 73.05 \pm 7.182$ ($R^2 = 0.0463$). Although the slopes are not significantly different from each other or significantly deviant from zero, the function for female data has a significantly lower Y-intercept (**= $p < 0.001$), reinforcing the result that female macrophages have a reduced parasite burden upon E2-treatment.

Taken together the results indicated no influence of DHT treatment on the viability, infection rate or parasite burden of *L. infantum*-infected macrophages from either sex. On the other hand, treatment with E2 seemed to reduce parasite burden in female macrophages consistently in all tested concentrations, while the infection rate and viability of macrophages were not affected.

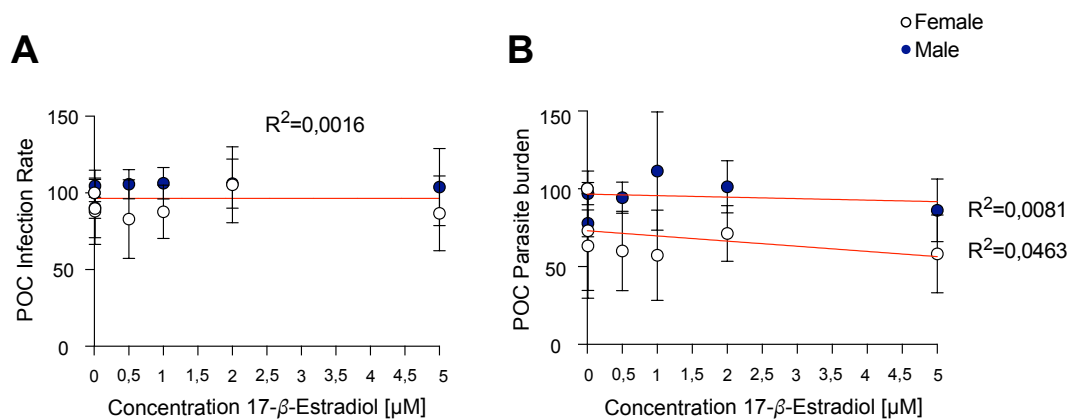


Figure 28: Correlation analysis between estradiol treatment and *L. infantum* infection in female macrophages .

Quantified infection parameters were used for non-linear regression to examine correlation between concentration of hormone treatment and (A) infection rate and (B) parasite burden. Regression line (red) and R^2 are indicated. $R^2 =$ determination coefficient.

3.3.2.1 Cytokine profiling of E2-treated macrophages after *L. infantum* infection

Cytokine profiling of the cell culture supernatant from macrophages pre-treated with 10 μM E2 and infected was performed at 28 hpi by measuring the secreted cytokines using a cytometric bead assay (LEGENDplex™). Respective controls included uninfected, uninfected E2-treated and only infected macrophages. Cytokines associated with parasite elimination are presented in this paragraph, whereas measured anti-inflammatory cytokines will be reviewed in the next paragraph. As the biological replicates show very large deviations in cytokine levels, the results were plotted as a graph for MFI (Fig. 24A) and as heatmaps, in which the different donors were displayed

separately for each sex in order to compare individual trends (Fig. 24B). In female macrophages, varying trends were observed within donors for TNF- α secretion following E2 treatment. Increased secretion was detected in approximately 40% of donors following E2-treatment in uninfected cells and in 60% in infected cells compared to untreated control. However, infection with *L. infantum* triggered reduced TNF- α secretion in untreated cells in 85% of the female donors, but only in 60% of the macrophages treated with E2. In macrophages from male donors, similar influence of the infection was observed as well as a slight E2-dependent increased TNF- α secretion in over 80% of donors in both uninfected and infected condition.

Slightly increased MFI of IL-1 β in the supernatant of uninfected, E2-treated cells compared to untreated samples were detected in both sexes, caused by increased secretion in all male donors and approximately 40% of female donors. The same trend was observed in female infected cells (70% of donors). In general, *L. infantum* infection of macrophages from both sexes led to a decreased secretion of IL-1 β in 70% of female donors and over 80% of male donors, regardless of E2-treatment.

For CCL-2, an estradiol-dependent increase in secretion was observed in 60% of female donors in uninfected macrophages and in 40% in the infected condition compared to the respective untreated control. In male samples, an increased secretion of CCL-2 upon treatment in uninfected cells was observed in over 80% of donors, whereas no unified influence of the treatment could be identified in infected macrophages. The infection with *L. infantum* triggered a reduced CCL-2 secretion from E2-treated macrophages in approximately 70% of donors from either sex and from untreated macrophages in ~ 60% of female and 50% of male donors.

The measurement of IP-10 yielded heterogenous results upon E2 treatment for female macrophages. The infection triggered lower levels of IP-10 in approximately 60% of female donors in both treated and untreated condition, whereas the rest showed increased secretion. A slight E2-dependent increase in the overall MFI of IP-10 was observed in uninfected (50% of donors) and infected (85% of donors) male macrophages as well as a *L. infantum*-dependent decrease of secretion in over 65% of donors in treated and untreated condition.

The secretion of IL-12p70 from uninfected female cells was almost not affected by E2 treatment, whereas an increase in secretion could be observed in all male donors. Infection of untreated female cells led to an almost significant reduction of IL-12p70 levels compared to uninfected cells ($p=0.0624$), whereby the common trend became also clear in the corresponding heatmap. Same tendency was observed in over 80% of treated female cells and untreated and treated male samples upon infection.

No estradiol specific influence on IL-18 levels was observed in either sex or condition, whereas increased levels of IL-18 were observed in uninfected cells compared to infected counterparts in over 70% of donors in both sexes.

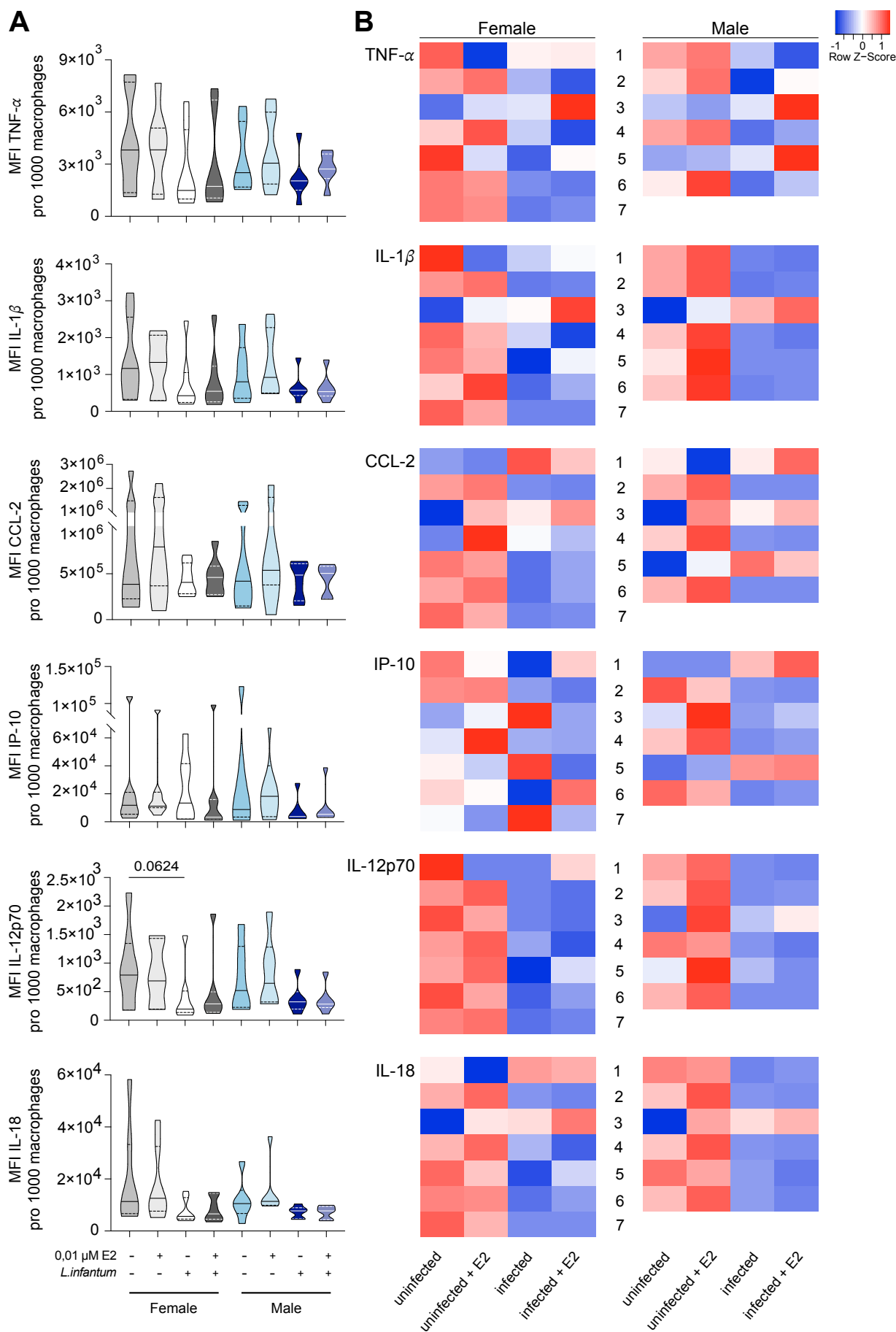


Figure 29: Measurement of cytokines related to parasite elimination in culture supernatants of estradiol-treated female and male macrophages after *L. infantum* infection using cytometric bead assay.

Mature macrophages from female and male donors were treated with 0.01 μ M E2 for 30 min before infection with *L. infantum* metacyclic promastigotes at a MOI of 15:1. Cells were incubated for 28 hpi and cytokines related to parasite elimination were measured in the supernatant using cytometric bead assay (LEGENDplex™). MFI of TNF- α , IL-1 β , CCL-2, IP-10, IL-12p70 and IL-18 are depicted as (A) violin plot with indicated median (solid line) and quartiles (dotted lines) and as (B) heatmap separated by donors. Data represents $n_{F/M} = 7/6$

Almost no E2-dependent influence on IL-10 levels was observed in both sexes. However, a clear induction of IL-10 in the supernatants of over 70% of donors across sex and treatment condition was observed upon infection, whereas the induction tended to be higher in male donors compared to female donors.

The trend in uninfected cells from female donors showed reduced levels of arginase in ~60% of donors following E2 treatment. Interestingly, a E2-dependent increase of arginase could be observed in uninfected cells of all male donors. Opposite trends were additionally observed under *L. infantum* infection, where treatment had no effect on arginase secretion in over 70% of female donors, and decreased secretion was observed in over 80% of male donors. As for most other cytokines, infection with *L. infantum* generally led to a decrease of cytokine secretion in both sexes. In untreated cells, infection triggered reduced arginase secretion in approximately 70% of donors, and in estradiol-treated macrophages in over 80% of donors.

Slight E2-dependent increase in CCL-17 levels were observed for each sex in treated uninfected macrophages compared to respective untreated control. This trend was observed in all female donors and in almost 70% of male donors. However, major donor-specific differences in the effect of E2 treatment were revealed in infected cells. Around 40% of female donors and 30% of male donors showed no effect of treatment, around 30% showed an increased secretion of CCL-17 in each sex, whereas the remaining donors showed decreases levels of CCL-17. Across sexes and treatment status, infection triggered a reduction of CCL-17 levels in 60% and 70% of female donors in untreated and treated samples respectively upon infection. For male donors, reduction was seen in 60% of untreated samples and all treated samples.

Opposite trends could be observed for IL-23 secretion in uninfected female and male macrophages upon treatment. While an estradiol-dependent reduction of IL-23 supernatant levels was measured in almost 60% of female donors, a slight increase was seen in all male donors. IL-23 levels were highly dependent on the infection status of macrophages, since infection with *L. infantum* led to an almost significant reduction in the overall MFI in female treated and untreated cells ($p=0.0624$). The same trend was observed in male macrophages. This is also reflected in the corresponding heatmap, in which a infection dependent decrease in IL-23 levels was observed for over 80% of donors across sex and treatment status.

The levels of IL-8 in the supernatants were highly diverse between donors of either sex. Compared to the corresponding untreated control, E2-treated uninfected samples showed a slightly increased secretion of IL-8 in almost 60% of female donors and over 80% of male donors. However, the pre-treatment and subsequent infection of cells did have a opposite effect on IL-8 secretion for female and male macrophages. In female cells, the pre-treatment triggered a slight increase in almost 60% of donors compared to respective untreated control, whereas in male cells, E2-treatment lead to reduced IL-8 levels after infection in ~80% of donors in comparison to infected cells without E2-

treatment. In general, the infection triggered a decrease in IL-8 secretion in female macrophages regardless of E2-treatment. Almost 60% and over 70% of female donors showed lower IL-8 levels upon infection in untreated and treated condition respectively. For male macrophages, a decrease could be observed in treated cells of over 60% of donors upon infection, whereas an increase of IL-8 in the supernatant was measured for over 80% of donors in untreated macrophages upon infection.

In conclusion, the overall MFI for cytokines in macrophage culture supernatant indicated that *L. infantum* infection tends to decrease the secretion of all measured cytokines at 28 hpi, with the exception of IL-10. These observations were irrespective of estradiol pre-treatment. Generally, E2 treatment exhibited minimal influence on cytokine secretion, with notable variations observed between donors.

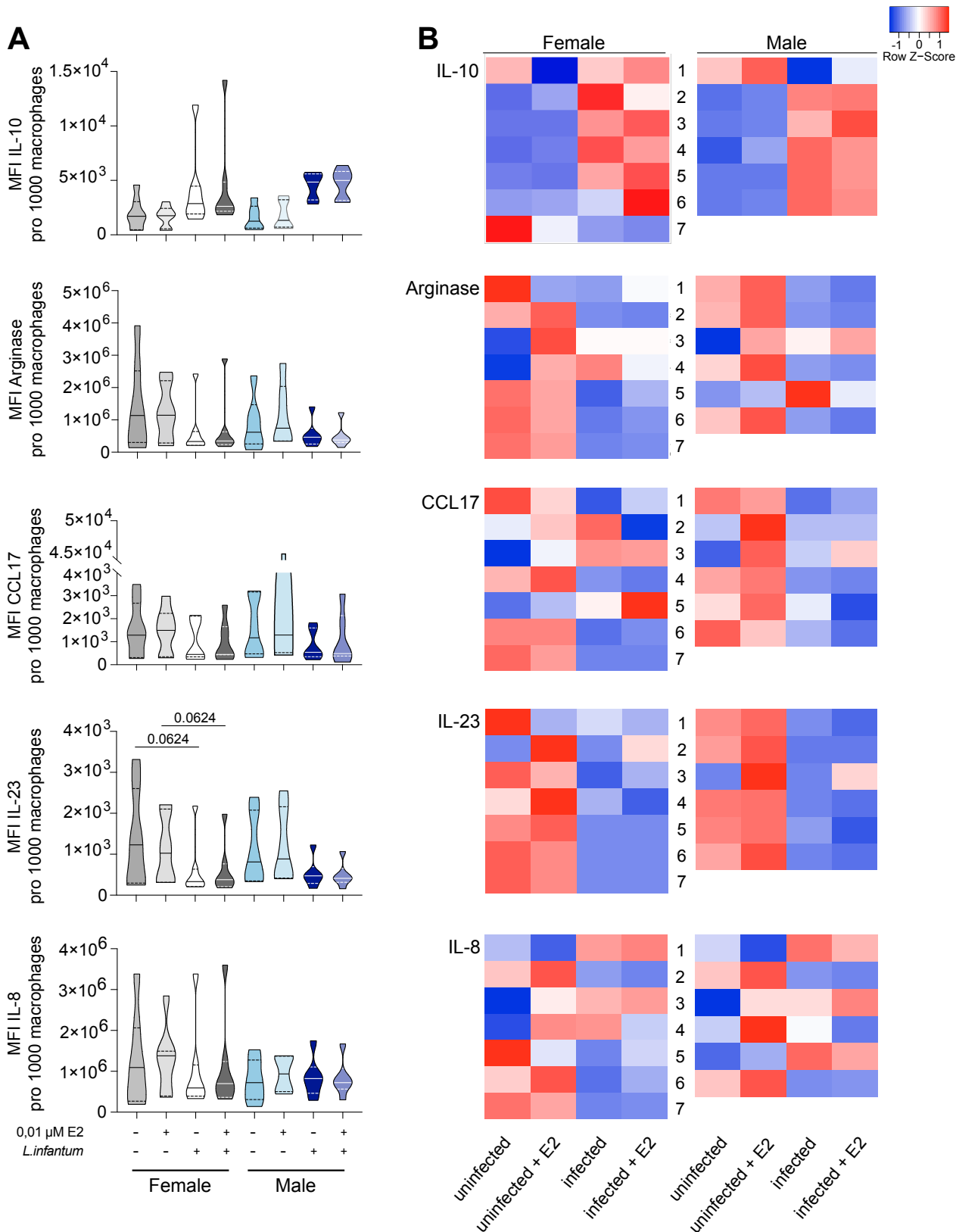


Figure 30: Measurement of cytokines related to parasite survival in culture supernatants of estradiol-treated female and male macrophages after *L. infantum* infection using cytometric bead assay.

Mature macrophages from female and male donors were treated with 0.01 μ M E2 for 30 min before infection with *L. infantum* metacyclic promastigotes at a MOI of 15:1. Cells were incubated for 28 hpi and cytokines related to parasite elimination were measured in the supernatant using cytometric bead assay (LEGENDplex™). MFI of IL-10, Arginase, CCL17, IL-23 and IL-8 are depicted as (A) violin plot with indicated median (solid line) and quartiles (dotted lines) and as (B) heatmap separated by donors. Data represents $n_{F/M} = 7/6$

3.3.3 Influence of steroid hormones on macrophage polarisation

The influence of the treatment with steroid hormones on macrophage polarisation in uninfected and infected cells was evaluated using morphology-based distinction. First, the influence of DHT on polarisation into M1 macrophages was investigated. This analysis showed, that DHT-treatment did not affect M1 polarisation in uninfected cells, regardless of concentration or sex with a proportion of M1-like macrophages of 35-50% in all tested conditions. Compared to similarly treated and infected cells, no significant difference in the proportion could be observed. In general, female donors showed a significantly higher percentage of M1-like macrophages in infected cells compared to male donors in both untreated and treated cells at all concentrations. (*= $p < 0.05$, **= $p < 0.01$, ***= $p < 0.001$). An increased proportion of M1-like macrophages was additionally observed in female infected, untreated cells compared to cells treated with 0.01 μM DHT (***= $p < 0.001$) (Fig. 26A). Quantification of the percentage of M2-like macrophages under DHT-treatment revealed no effect, except for an significant increase of proportion in uninfected female cells treated with 0.01 μM DHT compared to untreated cells (*= $p < 0.05$). M2-like macrophages accounted for around 15-30% in all tested conditions, however, there was a trend towards fewer M2-like macrophages under infection, as evidenced in the reduced median proportions (Fig. 26B). Investigation on the impact of E2-treatment on M1 polarisation of macrophages presented no effect in uninfected cells, whereas a significant decrease in the proportion of M1-like macrophages could be found in infected male cells after treatment with 2 μM E2 (*= $p < 0.05$). Thus, female cells treated with 2 μM E2 tended to have a higher proportion of M1-like macrophages relative to male cells ($p = 0.081$) (Fig. 26C). Apart from a significantly increased proportion of M2-like macrophages in uninfected male cells upon treatment with 2 μM E2, estradiol treatment did not affect polarisation of cells towards M2-like macrophages (Fig. 26D).

In summary, treatment of macrophages with steroid hormones had a minimal effect on macrophage polarisation.

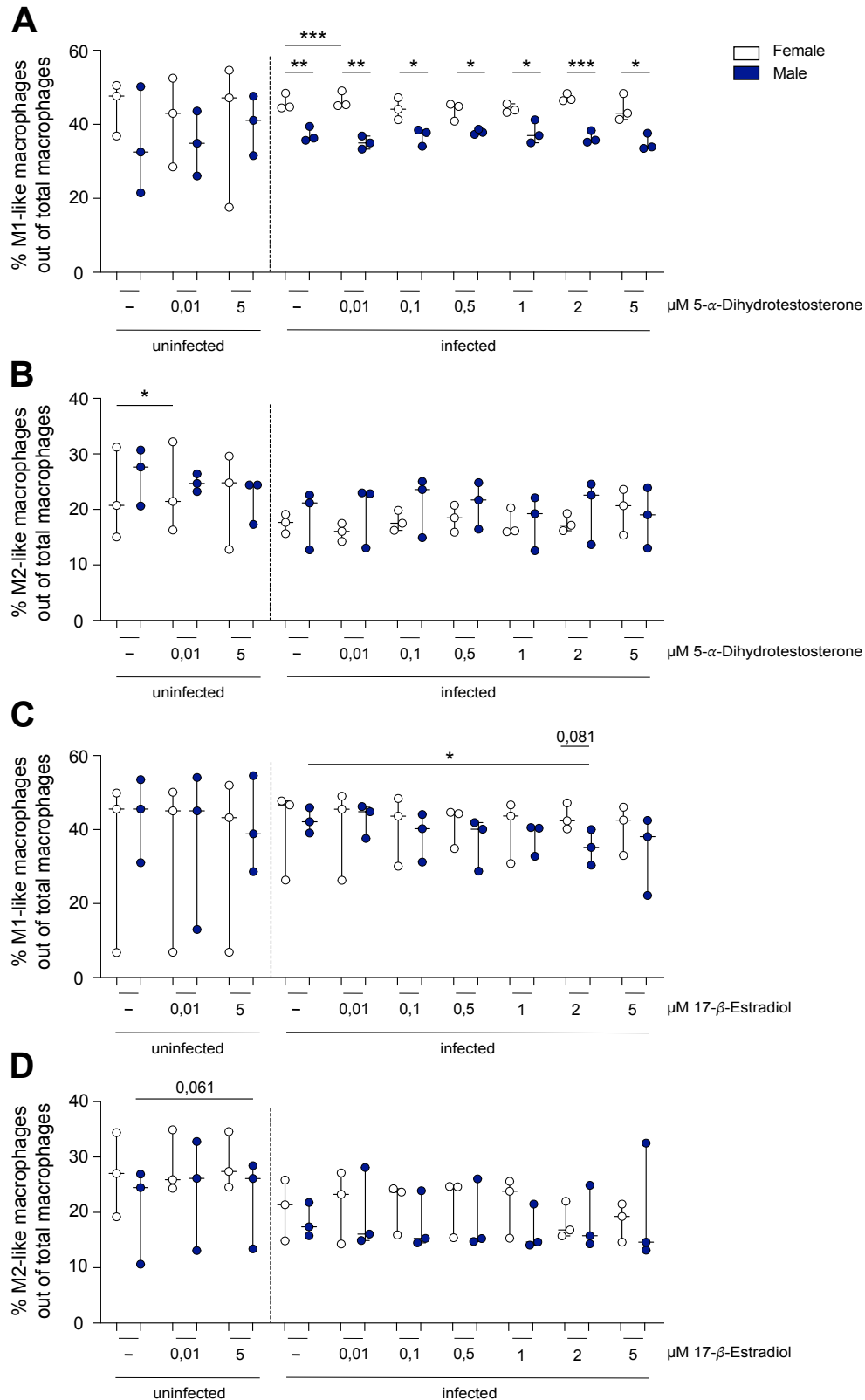


Figure 31: Morphology-based M1/M2 characterisation of steroid hormone-treated female and male macrophages after *L. infantum* infection.

Mature macrophages from female and male donors were treated with various concentrations (0.01 μ M-5 μ M) of steroid hormones (5- α -Dihydrotestosterone or 17- β -Estradiol) for 30 min before infection with *L. infantum* metacyclic promastigotes at a MOI of 15:1. Cells were incubated for 28 hpi. Morphology-based discrimination within macrophages between (A,C) M1-like macrophages and (B,D) M2-like macrophages using customised image analysis (Harmony® software). Data is shown as boxplot, $n_{F/M} = 3/3$. (*= $p < 0.05$, **= $p < 0.01$, ***= $p = 0.001$).

4. Discussion

Transmitted by blood feeding sandflies to mammalian hosts, *Leishmania* spp. parasites are the causative agent of leishmaniasis, an important neglected tropical disease. The manifestations of leishmaniasis vary dependent on the host's immune status and the infecting species and differ in severity. They can range from self-resolving skin ulcerations localised around the inoculation site, CL, to visceral leishmaniasis, VL, which affects organs such as spleen and liver. The fatal outcome commonly observed in untreated cases of the latter form primarily stems from immunosuppression and subsequent susceptibility to secondary infections (8).

There are significant differences in the innate and adaptive immune responses of men and women. While men exhibit a higher susceptibility to parasitic diseases and malignant cancers, autoimmune diseases are more prevalent in women (57, 59, 113). Understanding the underlying biological mechanisms of this sexual dimorphism is crucial for improving individualised treatment regimes.

Epidemiological studies have shown a male predominance of both CL and VL in endemic regions, with higher incidences of both forms and higher mortality for VL. This difference is most likely caused by a complex interaction of various determinants, such as infecting *Leishmania* spp., societal and environmental factors (host gender) as well as biological factors (host sex) (75).

In order to determine the impact of host sex on the immune response as well as on severity and outcome of leishmaniasis, sex-specific characterisation of human primary macrophages as the main host cells for *Leishmania* parasites, was performed on the cellular, immunological and transcriptome level. For this purpose, *in vitro* infection rates and parasite burdens of female- and male-derived primary human macrophages were quantified, the polarisation status of infected macrophages and the cytokine environment were assessed, and a comparative transcriptome study was carried out. In addition, the influence of sex hormones on *L. infantum* infection rates and parasite burden was investigated by *in vitro* treatment of macrophages with either androgens or estrogens prior to infection.

4.1 *In vitro* infection model and HCS assay for human primary macrophages

In recent years, the application of high content screening (HCS) assays has been a major driver of early drug discovery and compound testing (114, 115). During this work, the integration of automated multicolour fluorescence imaging with high-throughput screening analysis enabled simultaneous quantification of multiple readouts, such as viability, infection rates and parasite burdens of infected macrophages, based on the published image analysis sequence by Fehling et al. for murine macrophages (116). Using parasite-specific α -pan-*Leishmania* HSP90 antibody for immunofluorescent staining facilitated the detection of multiple *Leishmania* species without modifying the protocol for each species individually, and circumvented the use of genetically engineered parasite strains, e.g. with fluorescent reporter genes. Although transgenic strains are commonly used due to their more convenient handling, genetic modifications can potentially alter parasite virulence (117) and preclude field isolates from HCS assays. The sequence was adapted for human primary macrophages and additional parameters for the morphology-based distinction of the polarisation states of macrophages were implemented and verified (Tab. S1, Fig. 10, Fig. 11).

The utilisation of primary human macrophages allowed to mimic the *in vivo* stage as close as possible and to consider host factors such as sex, age and medical history.

Using aforementioned staining protocol and image analysis sequence, reliable detection of parasites and infected macrophages was recorded for all utilised *Leishmania* spp., dependent on the used MOI (Fig. 9B-E). Within a macrophage, parasites create a niche known as the parasitophorous vacuole (PV), where they undergo differentiation into the amastigote stage and replicate. These PVs are comprised partly of host endolysosomal components, resulting in an acidic pH environment (100). Using LysoBrite™ Red DND-99 staining, a dye that accumulates in acidic compartments, intracellular localisation of parasites was investigated after 24 hours of infection. Through the specific detection of LysoBrite™ signals surrounding the amastigotes within macrophages upon infection, the intracellular localisation was confirmed (Fig. 8, Fig S1).

Taken together, the infection model based on human primary macrophages and the subsequent high content analysis used and adapted in this study, presents a powerful tool for the investigation of infectivity and intracellular survival across *Leishmania* species and different treatment conditions for macrophages. Additionally, by using cells from male and female donors, this method allows the investigation of sex-specific differences during infection and the validation of identified candidate molecules by specific inhibitors or molecular silencing. However, limitations of the *in vitro* infection assay became apparent, as no parasite replication was observed and infection rates gradually decreased over time, which did not mimic the natural situation completely (Fig. 9B-E, Fig. 12B-E) (118). This phenomenon has been observed by many other researchers and was associated with generally lower division rates of amastigotes, as well as with missing host factors, that are present in *in vivo* experiments or *in vitro* experiments involving multiple cell types (118, 119). Potential factors that could improve the assay include the more advanced preparation of the parasite culture used for infection. Stationary phase promastigote cultures naturally contain up to 50% apoptotic parasites, which are crucial for the infectivity by dampening the immune response and enabling successful infection (120, 121). However, the lower percentage of viable parasites could be another reason for the drastic drop in the percentage of infected macrophages observed after 28 hours of infection. Additionally, by selectively isolating the more infective peanut agglutinin-negative metacyclic promastigotes from a stationary parasite culture, improved infection rates and replication were observed in *L. infantum* infection of human U937 myeloid cell line (122).

4.2 Sex-specific differences during *in vitro* infection of macrophages with *L.*

infantum

To date, sex differences in *Leishmania* infection has primarily been evidenced in experimental rodent models or epidemiological studies. It has been shown that male patients comprise the majority of clinical cases in VL, which was additionally reflected in animal models, where male mice and hamsters exhibited larger lesions and higher parasite loads upon infection with dermatropic *Leishmania* species (75, 76). To this end, this study is the first approach to examine sex differences using human monocyte-derived macrophages derived from both female and male donors. By

monitoring the infection rate and parasite burden over time, pronounced trends towards lower infection rates and fewer parasites per macrophage in female-derived macrophages were noted, starting at 28 hours following initial contact with the parasite. When considering inter-experimental variations, significantly reduced infection rates were consistently observed in female-derived macrophages from 28 hpi to 76 hpi, with the differences peaking at 52 hpi, where the infection rate and parasite burden were reduced by half compared to males (Fig. 12B-E). These observed differences allowed further characterisation of infected macrophages to unravel underlying causes for the differing susceptibilities.

4.2.1 *L. infantum* infection increases viability of human primary macrophages

Over the time course of infection, the viability of macrophages was assessed, based on the detected number of adherent cells. *L. infantum* appears to prolong viability and prevent apoptosis, as almost consistently more macrophages were present in samples infected with *L. infantum* of either sex (Fig. 12A). This phenomenon has been shown for various *Leishmania* spp. with various underlying mechanisms, depending on species and *in vitro* system, summarised in a review from Solano-Gálvez et al. (123). According to the authors, possible mechanism of pathogens inhibiting apoptosis to increase time for replication include modulation of host signaling pathways, expression of anti-apoptotic proteins or induction of host immune responses. Different pathways can lead to the induction of apoptosis, but most commonly the last step is the activation of either Caspase 8 or Caspase 10, starting the execution phase that ultimately leads to the formation of apoptotic bodies (124). Interestingly both caspases showed significantly decreased expression on gene level in both sexes upon infection at 6 hpi (Fig. 22D). Caspase-dependent inhibition of apoptosis is also employed by *L. donovani* in bone marrow-derived macrophages and by *L. major* in neutrophils and hMdMs, respectively (125-127). Additionally, increased expression of *PIK3CB* and *AKT3* as part of the PI3K/Akt signaling pathway in macrophages from either sex at 6 hpi can have regulatory effects on apoptosis, mainly by inactivation of pro-apoptotic proteins, described for other *Leishmania* spp. but not yet for *L. infantum* (123, 128).

4.2.2 *L. infantum* infection affects macrophage polarisation

The high plasticity of macrophages allows them to react to external stimuli with different polarisation states, broadly characterised as pro-inflammatory M1 and anti-inflammatory M2-macrophages, which are crucially involved in the outcome of infection. The different polarisation states can be distinguished by morphology and surface marker expression (102). This way, the macrophage polarisation during infection was analysed in this study.

At the earliest time point of investigation (4 hpi), an increase of M1-like macrophages was observed among infected macrophages of both sexes. However, after 28 hpi, no difference was observed compared to uninfected cells (Fig. 13C,D). The opposite trend was observed for M2-like macrophages, showing an initial decrease, followed by a gradual increase to levels comparable to uninfected macrophages. Interestingly, female macrophages demonstrated a tendency towards fewer M2-like macrophages throughout the observation period (Fig. 13E,F). In general, a strong

trend towards more M1-like macrophages during infection was observed in both sexes (Fig. G). Examining polarisation-related surface marker expression was challenging due to the small sample number, yet it revealed a decreasing trend for the majority of the markers investigated, supporting the reduction of M2-like macrophages, but not reflecting the increased M1-like population (Fig. 13B).

Similar results were obtained in the transcriptome profiling, where significantly downregulated M2-macrophage-related surface marker mRNAs were found. Genes encoding CD200R1, MRC1 (CD206) CD209, previously described markers for M2-polarisation (129), were equally downregulated in both sexes at 6 hpi. Additionally, lower expression of *CD163* was observed in female samples (Fig. 22), largely mirroring the results seen in morphology-based distinction.

This pro-inflammatory polarisation upon infection *in vitro* indicates successful clearance of parasites, since parasite survival is normally found in M2 macrophages (130, 131), as also observed for other infective agents, such as *Chlamydia pneumoniae* (132) and *Cryptococcus neoformans* (40). This initial M1 polarisation was also observed by Ontario et al. when monitoring polarisation in *L. infantum*-infected spleen cells of BALB/c mice (133), whereas in natural infection, VL is normally correlated with high M2 polarisation, characterised by increased arginase levels in the blood (134) and soluble CD163 in human (135, 136) and canine VL (137). This contradiction of polarisation *in vitro/in vivo* compared to natural infections could be partly explained by missing factors of the natural infection, such as sandfly saliva, which was shown to induce M2 polarisation (138).

In particular, the morphology-based investigations of the polarisation states during infection yielded interesting results. In order to investigate the interplay of activation states of macrophages and functional differences triggered by the infection or sex-specific differences further, experiments such as the measurement of NO could give additional insights.

4.2.3 *L. infantum* infection triggers distinct cytokine release in the supernatant of female and male primary human macrophages

Apart from a few cytokines with a defined role in leishmaniasis, such as the protective role of IFN- γ and the exacerbating role of IL-10, most other cytokines can have dual effects during infection. This is highly dependent on the host as well as the infecting *Leishmania spp.* and resulting disease manifestation (107).

In this study, the progression of cytokine secretion over time was measured in the supernatants of *L. infantum*-infected macrophage cultures. Due to the small sample size, comprising a maximum of three donors per sex, and often considerable variations, these results should be interpreted with caution, and additional repetition experiments are necessary.

However, several cytokines showed clear tendencies of a *L. infantum*-triggered secretion. Firstly, TNF- α showed infection-dependent induction, with strong secretion at early time points, and gradually decreasing concentrations over time, seen at the protein (Fig. 14A) and RNA level by increased expression of *TNF* (Fig. 21). Additionally, slightly higher levels of TNF- α were observed in

supernatants of female infected macrophages, however contrasting results were measured at RNA levels ($\text{♀FC}= 1.23$; $\text{♂FC}=2.1$) (Fig. 14A), suggesting putative post-transcriptional events. TNF- α is associated with host protection and parasite elimination by inducing a pro-inflammatory immune response and parasite granuloma formation and maintenance. Parasites are encapsulated by the formation of microbicidal granuloma and thereby the infection is controlled (139-142). Elevated levels were shown in VL patients (141, 143), as well as in *in vivo* rodent models of infection with *L. donovani* (139). Conversely to the results of this study, sex-specific secretion of TNF- α has been shown with a male predominance in murine *L. mexicana* infection (144), and Sellau et al. demonstrated TNF- α secretion to correlate with testosterone levels in human samples and mice (59).

The secretion of IL-18 and expression of *IL18* mRNA were reduced at 6 h of infection compared to uninfected cells in either sex, but no differences could be observed at later time points (Fig. 14F, Fig. 22). IL-18 is another pro-inflammatory cytokine conferring resistance against infections with e.g. *L. donovani*, as IL-18 deficient mice showed overall higher parasite burden (145). However, no epidemiological studies have reported on IL-18 levels and this cytokine has not been studied in the context of sex difference.

Early induction of IL-10 was also observed at the protein level in the supernatants of *L. infantum*-infected macrophages of either sex and at the RNA level (Fig. 15A, Fig. 21). IL-10 promotes the anti-inflammatory, T_H2-associated response that is beneficial for parasite survival and disease progression (146). In animal models, increased IL-10 levels have been shown to be induced upon *Leishmania* infections, with higher levels reported in the lesions of male hamsters (88) and *in vitro*, in murine male-derived macrophages *in vitro* (147).

Lastly, higher protein levels of IL-8 were detected in *L. infantum*-infected macrophages compared to uninfected macrophages over the total course of infection, with comparable levels in both sexes (Fig. 15E), whereas increased expression of *IL8* was only observed at 6 hpi in the transcriptome study (Fig. 21). IL-8 is a pro-inflammatory cytokine, produced by leukocytes as well as many types of tissues upon inflammatory conditions, specifically activating and recruiting neutrophils. Elevated levels of IL-8 have been observed in the serum of VL patients, which subsequently return to normal levels upon resolution of the disease, suggesting its potential as a circulating disease biomarker (148, 149).

In summary, the obtained results at the protein and RNA level generally correlate with the expected cytokine profile for VL, but apart from a tendency towards higher TNF- α secretion in females, no sex-difference was observed in terms of cytokine production. Additional experimentation is needed to substantiate these preliminary findings and give further insights into the sex-dependent cytokine secretion, which has been discussed as a driver for sex difference in parasitic diseases (150).

4.3 Transcriptome profiling of *L. infantum*-infected macrophages

For this transcriptome profiling, samples obtained yielded a mean total read count of 5 million reads total per sample (Tab. S2), which is lower than the recommended sequencing depth for mammalian

cells according to the manufacturer (151). As a result, subtle differences in RNA levels might not be readily detected, particularly in infected cells where reads are additionally shared between both human and parasite genome. This should be taken into account when interpreting the results.

When comparing naïve female- and male-derived macrophages, close to no DEGs were detected except the ones encoded on gonosomes, such as *XIST* and *TSIX*, that are associated with X-chromosome inactivation, and *EIF1AY* or *DDX3Y*, that are encoded on the Y-chromosome (Fig. 17, Tab. S3-5). That was in keeping with other transcriptome studies showing similar expression profiles in male- and female-derived human monocytes (152) or in various murine immune cell types (153).

4.3.1 Transcriptional changes in response to *L. infantum* infection

The strongest transcriptional response, based on the number of DEGs, was seen at early time points of infection and diminished over time (Fig. 18). A phenomenon also observed by other researcher and partly due to the limitations of the applied *in vitro* infection assay and the clearance of the parasite (154). Nevertheless, the results indicated an early transcriptional regulation and prompts the investigation of earlier time points for future *in vitro* studies or transcriptome profilings, as already applied in other publications (155, 156). Interestingly, female macrophages exhibited twice the number of DEGs as males at 6 hpi, a fact also observed in most comparisons of DEGs in neutrophils after infection with *Entamoeba histolytica* (67).

In the comparison of infected and uninfected macrophages of the same sex, KEGG pathway analysis revealed the induction of many immunity-related signaling pathways in both sexes at 6 and 16 hpi, including TNF-signaling and NF- κ B signaling (Fig. 19E,H ; 20E,H).

Most strongly regulated genes at 6 and 16 hpi coded for isoforms of the metallothionein family (Fig. 16A,D ; Fig. 17A,D ; Tab. S11-16). The same tendencies were observed in the transcriptional profiling of macrophages infected with *L. major*, *L. amazoninensis* and *L. chagasi* (154, 157), and also in multiple other infections as reviewed by Dai et al. (158). Genes encoding methallothionein family proteins are induced by a variety of metals or pro-inflammatory mediators, such as TNF- α or glucocorticoids and are involved in metal detoxification and protection against oxidative damage (159). Although the role of this protein family is not yet clear in the context of leishmaniasis, the expression is often associated with transmission of resistance through the regulation of cellular oxidative burst (160).

As had to be expected, a differential transcription of genes associated with *Leishmania* infection and parasite survival was observed. As with many other infections, such as in murine infection with *Plasmodium* spp. or bacterial infections (161, 162), *HMOX1* was induced by the infection with *L. infantum* in both sexes (Fig. 16A, Fig. 17A, Tab. S11-16) and is associated with pathogen survival within the macrophage. It has been shown that the expression of *HMOX1* via the nuclear factor erythroid 2-related factor (NRF2) transcription factor, as for example shown in *L. donovani*, can be induced solely by surface molecules of the parasite. The survival of the parasite is conferred by the

protection from oxidative burst and reduced TNF- α levels and ROS production, as shown in HMOX1^{-/-} mice, that presented lower *L. chagasi* burdens (155, 163, 164).

Another gene involved in *Leishmania* infection, is *NLRP3*, which was downregulated at 16 hpi in female- and male-derived macrophages (Fig. 22). The activation of *NLRP3* inflammasome can have dual effects on *Leishmania* infection, as reviewed by Harrington and Gurung (165). The activation of *NLRP3* inflammasome leads to the increased secretion of IL-18 and IL-1 β , which can have protective roles against leishmaniasis, but different mechanisms for the pathogenic role of *NLRP3* activation and subsequent IL-1 β production were also proposed. Pathogenic mechanisms include increased neutrophil influx and T_H2 biased T-cell response, supporting the growth of *Leishmania* spp. e.g. *L. major* (166).

When comparing the magnification of gene regulation in genes, that were similarly regulated in female- and male-derived macrophages, various differences could be observed between sexes (Fig. 23). Most pronounced was the different regulation for *MMP10*, a gene that was more highly upregulated in female macrophages at 6 and 16 hpi as in male (Fig. 23A,B). Several members of matrix metal proteases are known to impact acute infection by pro-inflammatory cytokine secretion and regulating TLR7 tolerance (167). *MMP10* was shown to increase survival in mice upon *Pseudomonas aeruginosa* infection in comparison to *MMP10*^{-/-} mice. In the *MMP10* deficient mice macrophage numbers were strongly increased in lung tissue and a polarisation towards M1 macrophages was observed (168). Increases *MMP-10* levels were also shown in the lesions of CL patients, but the exact implication in leishmaniasis is still unclear (169, 170).

Additional cytokine-encoding genes to those already described in chapter 4.2.3, were differently expressed during the course of infection, such as *CXCL2*, *CXCL3* and *CCL20* (Fig. 21D,E). These transcripts were also found in transcriptome analyses of spleen macrophages from *L. donovani*-infected hamsters (171) and can be correlated with either parasite killing or persistence through the attraction of other host cells (172, 173). Some interferon stimulated genes, such as *ISG15*, *ISG20* or *RSAD2*, were also upregulated in infection (Fig. 21 D,E). For *RSAD2*, an interferon-inducible antiviral protein, the upregulation was shown in various intracellular infections (174) and sex-specific differences in the magnitude of regulation ($\text{FC}_{\text{f}}=5.6$; $\text{FC}_{\text{m}}=4.24$), were in accordance with the testosterone-dependent expression observed in naïve murine neutrophils, as well as in activated lung epithelium (67, 175).

Another protective mechanism induced upon *L. infantum* infection in either sex was the generation of microbicidal agents in the form of reactive nitrogen and oxygen species (ROS/RNS) in order to combat infection. This was seen in the upregulation of genes, such as *NCF2* and *Ras-related C3 botulinum toxin substrate 2 (RAC2)* (Fig. 21 E), that are involved in the mitochondrial electron transport chain and are crucial for the production of ROS (176, 177). On the other hand, protection against damage of cellular oxidative stress induced by radicals was conferred by *SOD2* linked to the neutralisation of oxidative stress (178).

4.3.2 Sex-specific transcriptional changes in response to *L. infantum* infection

Sex-specific expression was observed for several genes associated with interferon signaling with higher expression in female macrophages at 6 hpi, such as *OASL2* and *OASL3* and several genes encoding interferon-inducible proteins (*IFIT2*, *IFIT3*, *IRF5*, *IRF9*) (Fig. 21F). Interferon signaling was shown to be crucial for the defence against *Leishmania* infection and many other infectious diseases (179, 180). However, expression of genes involved in interferon signaling have been described to act antagonistically to testosterone levels in naïve neutrophils and under infection (67, 181). Also, sex-specific differences in the interferon signaling were proposed as one factor underlying the higher susceptibility of males towards infections, such as hepatic amebiasis or HIV (67, 182).

Differences in the expression of cytokine-encoding genes between *L. infantum* infected male and female macrophages were also observed (Fig. 21 F-I). This was especially apparent for *IL15*, which was specifically expressed in female macrophages upon infection. This interleukin is associated with the suppression of IL-4 and induction of IL-12 secretion in human VL and therefore supports the elimination of the parasite (183, 184). Sex difference in the expression of *IL-15* was also observed in hippocampal tissue after stimulation with LPS (185). *IL27*, also shown to be specifically upregulated upon *L. infantum* infection in female macrophages (Fig. 21F), has a dual role in leishmaniasis. The increased secretion of IL-27 has also been observed in rodent models using different *Leishmania* species, where it was shown that it confers protection towards infection with *L. major* by increased T_H1 polarisation of T-cells, but the opposite is observed for infections with, e.g. *L. donovani* and *L. infantum* infection, where IL-27 deficiency was associated with resistance due to increased IL-17 production and neutrophil influx (186, 187). This sexual dimorphism was also described in the animal model for arthritis, where higher levels of IL-27 led to increased T follicular helper cell (T_{fh}) generation and greater severity in female rats (188).

Genes associated with antibody response and B-cell activation were more strongly downregulated in male macrophages, as seen by the GO term enrichment for biological processes (Fig. 20G, Tab. S11-16). These processes comprised genes, such as *high affinity immunoglobulin γ receptor 1B* (*FCGR1A*) ($\text{♀FC} = -2.39$; $\text{♂FC} = -3.6$), *low affinity immunoglobulin γ Fc region receptor 2B and 3A* (*FCGR2B, FCGR3A*) ($\text{♀FC} = -0.8$; $\text{♂FC} = -1.62$) ($\text{♀FC} = -1.6$; $\text{♂FC} = -1.88$). The role of B-cells has not been studied in detail, but the presence and activation of polyclonal B-cells has been associated with disease exacerbation, as B-cell deficient mice showed later onset of symptoms less pronounced lesions (189, 190) and were able to avert splenomegaly (191). On the other hand, in *L. major*-infected mice it was shown that IgG antibodies specifically increased antigen uptake by DCs via FCGR3 binding, leading to increased T_H1 response by increased antigen presentation (192).

CXCL1, *IL32*, *IL-1 α* and *IL-1 β* , which were higher expressed in male macrophages than in females (Fig. 21). In a prior investigation, increased levels of CXCL1 were observed in classical monocytes from male mice, both under steady-state conditions and on day 3 of hepatic amebiasis, which led to an increased immunopathology by the recruitment of further immune cells. This male bias was similarly observed in human monocytes, with CXCL1 concentration positively correlating with testosterone levels (59). *IL-1 β* levels were also associated with disease progression due to

immunopathology in patients with cutaneous leishmaniasis caused by *L. braziliensis* but did not affect phagocytosis or parasite killing (193). Additionally, mice deficient for IL-1 α or IL-1 β , respectively, were less susceptible to *L. major* infections and showed delayed and milder disease formation and increased T_H1 polarisation (194).

Amongst other genes linked to *Leishmania* survival, such as *PTGER4*, a prostaglandin that is recognised for increasing survival of various *Leishmania* spp. in a only partially understood manner (195), two genes that were specifically expressed in male macrophages, *IDO1* and *IL4I1* (Fig. 21H), are involved in the tryptophan catabolism. These enzymes deplete tryptophan by conversion to kynurenines or indole-3-pyruvate (I3P) respectively, thereby affecting cell function. In cancer, increased conversion of tryptophan by these enzymes has been shown to promote tumor progression by various mechanisms, such as dampening the immune responses (196). Also, *L. major* centrin gene deletion strain (LmCen^{-/-}), in which the conversion of tryptophan was restricted, shown increased pro-inflammatory response in mice by directly affecting cytokine production (197, 198).

For the first time, lower infection rates and parasite burdens were described in the *in vitro* infection of monocyte-derived macrophages from female donors with *L. infantum* compared to macrophages from male donors and sex-specific mechanics underlying this dichotomy were investigated on the transcriptome level. To summarise, shared mechanisms were activated across sexes in their reaction to *L. infantum* infection, including key immunological signaling pathways. Nevertheless, variations in regulatory magnitude and unique individual adjustments in gene expression were detected in macrophages derived from both females and males. This underlines the need for deeper investigations into the implications by, e.g silencing of specific immune pathways or modulation of cytokine production.

4.3.3 Gene-specific RNA abundance of *L. infantum* during infection

The RNA extracted from infected cells was additionally mapped against the genome of *L. infantum* in order to explore alterations in RNA abundance of genes associated with exposure to host protection mechanisms, with pathogenicity markers induced during host cell colonisation, or specific to host sex. The proportion of reads aligned to the parasite genome was the highest at 6 hpi, with a mean of 15-20% of total reads in female- and male-derived macrophages, and gradually decreased over time. At 52 hpi, only 3% of the total reads from macrophages of either sex could be aligned to the *L. infantum* genome of total reads from macrophages of either sex. Thus, as the infection rate and the number of parasites decreased in a similar pattern over time, the decreased proportion of reads is probably not due to reduced transcriptional activity of parasites or increased transcriptional activity of macrophages, but merely to the lower number of parasites present (Fig. 24A,B). By incorporating the *L. infantum* reads obtained from infected male and female macrophages derived from both females and males, more accurate assessment of RNA quantity for specific genes during the infection was possible (Fig. 24C). Simultaneously, separate analyses

were conducted to examine sex-specific changes in RNA abundance at each time point (Fig. 24D, Fig. S6 A,B).

However, *Leishmania* parasites, like all other trypanosomatids, are characterised by the absence of regulatory promoter sequences and enhancer elements on their genome. This absence results in a predominantly unregulated transcription of polycistronic gene clusters, comprising functionally unrelated genes. Regulation takes place at the translation level, with mechanisms such as mRNA stability, mRNA splicing or post-translational modifications also discussed (199-201) Hence, gene expression cannot directly be correlated to translation rates and protein levels, rendering RNA sequencing an unsuitable method for investigating gene expression and protein abundance in *Leishmania* parasites. Alternative approaches, such as ribosome-profiling, in which only the ribosome-bound mRNA is sequenced, or proteomics, are suitable methods for answering these questions (200, 202) but need optimisation for the small amounts of cells in *in vitro* infection systems (Grünebast, J, Bea, A., unpublished observations).

Nevertheless, it is worth mentioning, that the categories of proteins encoded by genes with varying RNA abundance over the course of infection are in accordance with protein categories observed by Bifeld et al. by ribosome-profiling of *L.donovani* promastigotes treated with radicicol, a HSP90-specific inhibitor inducing chemically induced stage differentiation, partially mimicking infection (Tab. S17) (200, 203). Categories with increased abundance include genes coding for amastin-like proteins and proteins, such as A2, which are amastigote-specific and are associated with promastigote to amastigote differentiation (204). Histone-encoding genes exhibited the most pronounced reduction in RNA levels over time (Tab. S17). However, this reduction does not necessarily imply a decrease in protein abundance, as reduced RNA-levels but still increased translation, as measured by ribosome-profiling, were reported by Bifeld et al (200). These changes in histone protein levels detected in amastigotes indicate a change in chromatin structure, which, however, was not shown to affect transcription (200, 202, 205). The exact implications of these findings for the host cell have yet to be fully elucidated.

At 6 hpi, two genes encoding different peptidase m20/m25/m40 family-like proteins exhibited higher RNA amounts in parasites from female or male macrophages, respectively (Tab. S18). These proteins are described as potential virulence factors and have been detected in the secretome of *L. donovani* promastigotes, potentially affecting the host proteome (206, 207). The gene coding for pyruvate kinase, another virulence factor, also presented increased RNA abundance in parasites derived from female macrophage (Tab. S18). This protein is part of the glycolysis cycle and is considered a potential drug target (208, 209). Overall, definite implications for elevated levels of the three proteins encoded by genes with observed sex-specific RNA abundance are missing and the putative influence on infection needs to be investigated further.

4.4 Influence of sex hormones on infection with *L. infantum*

To evaluate the impact of sex hormones on *L. infantum* infection, macrophages were treated with different concentrations (0.01 μ M-5 μ M) of either sex hormone for 30 minutes before subsequent infection. At 28 hpi, macrophages were examined for treatment-related effects on infection

parameters and polarisation state, as well as cytokine secretion. Due to the low sample size of three donors per sex with often significant variations, almost no significant differences were observed upon treatment. Although individual reports indicated an influence of hormones on the viability or polarisation of murine bone-marrow derived macrophages or cell line macrophages (96, 210, 211), both sex hormones did not alter the viability of human primary macrophages in our assay (Fig. 26A, Fig. 27A, Fig. 31). In contrast to other reports showing either increased infection rates and parasite burdens in murine female and male macrophages infected with *L. donovani* or *L. amazonensis*, respectively, upon testosterone treatment and decreased levels in macrophages from male mice for *L. mexicana* (96, 147, 212), supplementation of DHT did not alter the infection rate or parasite burden in either sex (Fig. 26B,C). For E2 treatment, no treatment-specific differences were observed in either sex assessing the infection rate (Fig. 27B), although a linear regression calculated a possible influence of E2 on the parasite burden in female-derived macrophages (Fig. 28B), reflecting results from *L. mexicana* macrophage infection and infection with HIV (147, 182).

Lastly, in contrast to publications reporting increased secretion of pro-inflammatory immune mediators, such as IL-12p7 or NO, or reduced secretion of TNF- α and IL-1 β upon E2-treatment of female cells (147, 211), E2 treatment exhibited minimal influence on cytokine secretion in our studies for either sex (Fig. 29, Fig. 30).

Although most of the cited papers employed comparable *in vitro* infection assays for *Leishmania* parasites and used similar concentrations of sex hormones (0.1 μ M-1 μ M), the treatment regimens for macrophages with androgens or estrogens and time points of analyses varied intensely. Sex hormone application ranged from the use of macrophages from treated mice, *in vitro* treatment of macrophages for 72-24 hours prior to infection, to treatment for 72 hours following infection. These differences may lead to differences in the observed results. Since the treatment regimen presented here is the shortest treatment period, different treatment regimes should be explored to enhance possible treatment-dependent effects. One example would be the continuous supplementation of sex steroids during macrophage differentiation in addition to a treatment boost before infection, since the differentiation of macrophages without endogenous hormones seems to affect cell activation (211).

In summary, the influence of sex hormone treatment varies highly with the infective agent, the infection model and treatment regimen and implies the need for further experimental investigation.

Supplementary data

Table S1: Parameters for customised automated image analysis sequence established in Harmony software®

Analysis building block	Parameters	Objective
Define input		
Input image	Channel: DAPI, AF647 / AF488, AF568 (depending on experimental set-up and staining) Flatfield correction: None Stack processing: Maximum projection	Merging of images from various fluorescence channels and stacks
Find objects		
Find Nuclei	Channel: DAPI ROI: None Method: B Common threshold: 0.02 Area: > 40 μm^2 Splitting coefficient: 19.9 Individual threshold: 0.14 Contrast: > -0.71 Output population: Macrophages	Image segmentation: Determination of nuclei in host cells
Find Cytoplasm	Channel: AF647 / AF488 Nuclei: Macrophages Method: A Individual threshold: 0.06 Output region: Cell, Cytoplasm, Membrane	Image segmentation: Defining single cells by determination of host cell cytoplasm
Find Spots	Channel: AF647 / AF488 ROI: Macrophages Cell Method: B Detection Sensitivity: 0.11 Splitting Sensitivity: 0.844 Output population: Spots	Identification of intracellular spots within defined macrophages
Calculate Object properties		
Calculate Intensity properties	Channel: DAPI Population: Macrophages Region: Nucleus Method: Standard Calculate: Mean Property Prefix: Intensity Nucleus DAPI Output Property: Intensity Nucleus DAPI Mean	Quantification of properties inside defined regions. Removal of border objects
	Channel: AF647 / AF488 Population: Macrophages Region: Cytoplasm Method: Standard Calculate: Mean Property Prefix: Intensity Cytoplasm AF647 / AF488 Output Property: Intensity Cytoplasm AF647 / AF488 Mean	
	Channel: DAPI Population: Spots Region: Spot Method: Standard Calculate: Mean Property Prefix: Intensity Spot DAPI Output Property: Intensity Spot DAPI Mean	

Analysis building block	Parameters	Objective
	Channel: AF647 / AF488 Population: Spots Region: Spot Method: Standard Calculate: Mean Property Prefix: Intensity Spot AF647 / AF488 Output Property: Intensity Spot AF647 / AF488 Mean	
Calculate morphology properties	Channel: AF647 / AF488 Population: Macrophages Region: Cytoplasm Method: Standard Calculate: Area[μ m], Roundness, Width[μ m], Length[μ m], Ration wWidth to Length Property prefix: M1 Cytoplasm Output Property: Standard Channel: AF647 / AF488 Population: Macrophages Region: Cytoplasm Method: Standard (deprecated) Calculate: Area[μ m], Roundness, Width[μ m], Length[μ m], Ration wWidth to Length Property prefix: M2 Cytoplasm Output Property: Standard Channel: AF647 / AF488 Population: Spots Region: Spot Method: Standard (deprecated) Calculate: Area[μ m], Roundness Property prefix: Spot Output Property: Standard	Quantification of properties inside defined regions. Removal of border objects
Calculate properties	Population: Spots Method: By Formula Formula: A/B Variable A: Intensity Spot AF647 / AF488 Mean Variable B: Intensity Spot DAPI Mean Output Property: AF / DAPI Ratio	Calculation of properties of intracellular parasites
Select a Population of Objects		
Select population I (interesting spots)	Population: Spots Method: Filter By Properties Parameter: Spot Roundness ≤ 1.2 Spot Area [μ m ²] $15 \leq X \leq 900$ Spot Roundness > 0.25 Relative Spot intensity > 0.4 Spot Contrast > 0.1 Region intensity > 150 Corrected Spot intensity = Staining-dependent, must be adapted Output Population: interesting spots	Identification of population: Discrimination of interesting spots from total spots

Analysis building block	Parameters	Objective
Select population II (<i>Leishmania</i> parasites)	Population: interesting spots Method: Linear classifier Number of classes = 2 Parameter: Spot Roundness Spot Area [px ²] Spot Contrast Relative Spot intensity Region intensity Spot to Region intensity Spot Background intensity Corrected Spot intensity Uncorrected Spot intensity Intensity Spot AF647 / AF488 Mean Intensity Spot DAPI Mean Output Population A: <i>Leishmania</i> selected Output Population B: false-positive Population: interesting spots Method: Filter by property Parameter: Regression A-B < -3 Output Population: <i>Leishmania</i>	Identification of population: Discrimination of parasites from unspecific intracellular spots
Calculate properties	Population: Macrophages Method: By related population Related population: <i>Leishmania</i> Parameter: Number of <i>Leishmania</i> Mean of Spot Area [px ²] Mean of Spot Roundness Mean of Spot Contrast Mean of Relative Spot intensity Mean of Region intensity Mean of Spot to Region intensity Mean of Spot Background intensity Mean of Corrected Spot intensity Mean of Uncorrected Spot intensity Mean of Intensity Spot AF647 / AF488 Mean Mean of Intensity Spot DAPI Mean Mean of AF/DAPI Ratio Mean of Regression A-B Mean of <i>Leishmania</i> selected Mean of false-positive Property Suffix: per Cell Output Properties: By related Population	
Select population III (infected macrophages)	Population: Macrophages Method: Filter by Property Parameter: Number of <i>Leishmania</i> per cell > 0 Output Population: infected macrophages Population: Macrophages Method: Filter by Property Parameter: Number of <i>Leishmania</i> per cell > 2 Output Population: double infected macrophages Population: Macrophages Method: Filter by Property Parameter: Number of <i>Leishmania</i> per cell > 3 Output Population: double infected macrophages	Identification of population: Discrimination of infected from uninfected macrophages
Select population IV (M1-like polarised macrophages)	Population: Macrophages Method: Filter by Property Parameter: M1 Cytoplasm Roundness $0.38 \leq X \leq 0.62$ M1 Cytoplasm Length ≤ 55 M1 Cytoplasm Width ≤ 25 M1 Cytoplasm Ratio Width to Length $0.3 \leq X \leq 0.579$ Output Population: M1 macrophages	

Analysis building block	Parameters	Objective
	Population: M1 macrophages Method: Filter by Property Parameter: Number of <i>Leishmania</i> per cell > 0 Output Population: infected M1 macrophages	
Select population V (M2-like polarised macrophages)	Population: Macrophages Method: Filter by Property Parameter: M2 Cytoplasm Roundness $0.15 \leq X \leq 0.51$ M2 Cytoplasm Length ≥ 48 M2 Cytoplasm Width ≤ 40 M2 Cytoplasm Ratio Width to Length $0.0 \geq X \leq 0.37$ Output Population: M2 macrophages	
	Population: M2 macrophages Method: Filter by Property Parameter: Number of <i>Leishmania</i> per cell > 0 Output Population: infected M2 macrophages	
Calculate Collated Readout Values		
Define Results	Method: List of Outputs Populations: Macrophages M1 macrophages M2 macrophages Total <i>Leishmania</i> Mean of <i>Leishmania</i> per cell infected macrophages double infected macrophages massive infected macrophages infected M1 macrophages Infected M2 macrophages Method: Formula Output: a/b Variable a: <i>Leishmania</i> Variable b: macrophages Output Name: <i>Leishmania</i> per macrophages Method: Formula Output: a/b Variable a: <i>Leishmania</i> Variable b: infected macrophages Output Name: <i>Leishmania</i> per infected macrophages Method: Formula Output: a/b*100 Variable a: infected macrophages Variable b: macrophages Output Name: percent infected macrophages	

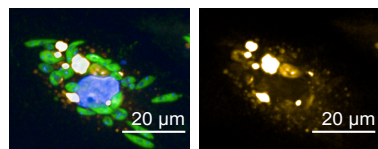
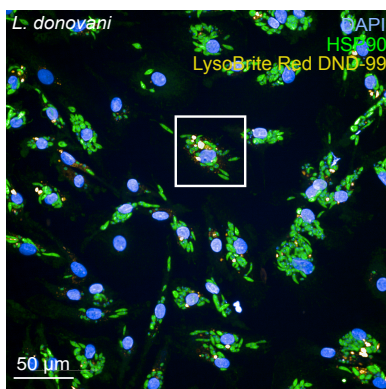
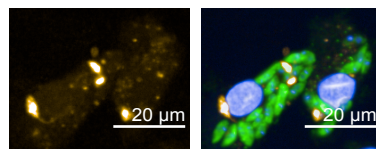
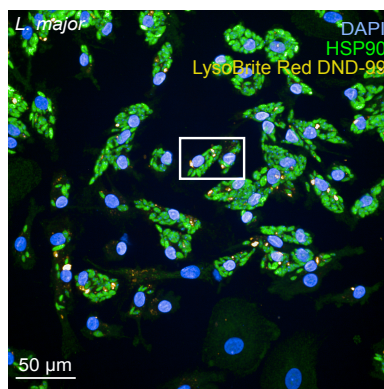
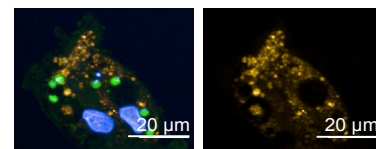
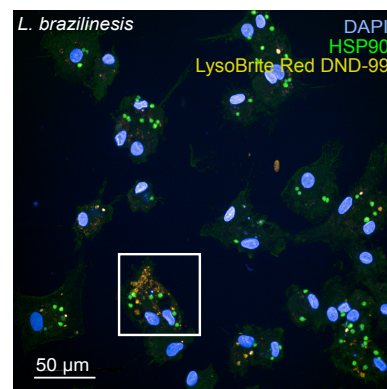
A**B****C**

Figure S1: Determination of intracellular localisation of *Leishmania* spp. amastigotes within human monocyte derived macrophages by labelling of parasitophorous vacuoles.

Mature macrophages were infected with *Leishmania* metacyclic promastigotes (*L. donovani*, *L. major* and *L. braziliensis*,) at 20:1 and incubated for 28 hpi. Before fixation, the cells were incubated with LysoBrite™ Red DND-99 for 2 h at 37°C and 5% CO₂. Images were acquired using the Opera Phenix® confocal microscope. Shown is the nucleus stained with DAPI (blue), *Leishmania* parasites stained with α -LHSP90 in AF488 (green) channel and PVs labelled with LysoBrite® detected in AF568 channel (yellow). Scale bar = 50 μ m and scale bar=20 μ m in close-up pictures. Image acquisition and quantification of fluorescence intensity was carried out by Fahten Habib.

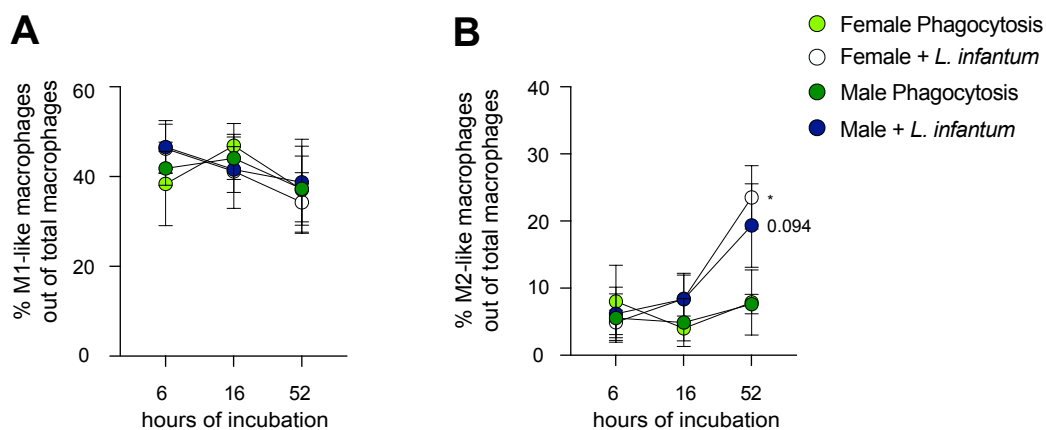


Figure S2: Morphology-based M1/M2 characterisation of female and male macrophages after phagocytosis and *L. infantum* infection.

Mature macrophages from female and male donors were infected with *L. infantum* metacyclic promastigotes at a MOI of 15:1 or incubated with phagocytosis beads at the same ratio for 6-52 hours. Morphology-based discrimination within macrophages between (A) M1-like macrophages and (B) M2-like macrophages using customised image analysis (Harmony® software). Data is shown as mean \pm SD, $n_{F/M} = 4/4$. P-values were calculated using two-way ANOVA analysis. (*= $p < 0.05$)

Table S2: Summary of donor dataset used for transcriptomical analysis and sequencing parameters.

		Female		Male			
Number of donors		4		4			
Donor age [median (IQR)]		32 (30,5-42)		26,5 (23,5-30,5)			
		6 hours post infection		16 hours post infection		52 hours post infection	
	Condition	Female	Male	Female	Male	Female	Male
Total reads mapped on human genome [median (IQR)]	Uninfected	5,75 (5,25-6,3)	5,75 (4,4-6,5)	5,65 (5,4-6,05)	5,1 (4,3-6)	5,55 (4,75-6,6)	4,55 (4,2-5,7)
	Infected	3,25 (2,7-3,9)	3,45 (2,5-4,1)	4,25 (3,2-5,05)	4,45 (4,1-10,6)	5,15 (5-5,4)	5,55 (5,3-5,8)
	Phagocytic control	5,65 (5,1-6,1)	5,25 (4,8-6,5)	5,7 (5,15-6,25)	4,9 (4,7-5,5)	5,05 (4,6-6,25)	5,6 (4,9-6,6)
% infected macrophages in infected samples [median (IQR)]		83,94 (78,7-86,3)	82,1 (76,6-87,13)	75,5 (66,9-84,4)	76,76 (74,5-80,4)	62 (36,6-84,6)	63,12 (40-84,2)
Parasites per infected cell in infected samples		7,74 (7,4-8,63)	9,4 (8,46-9,4)	6,04 (5,07-7)	7 (6,43-7,7)	5,06 (3,5-6,5)	5,32 (3,8-6,5)
Fraction of reads mapped on <i>Leishmania</i> genome in infected samples [median (IQR)]		14,8 (10,9-24)	12,36 (9,6-16)	6,65 (4,66-9,15)	3,9 (2,64-8,91)	2 (0,9-3,84)	1,7 (0,5-3,7)

Table S3: Differentially expressed genes between female and male naïve macrophages at 6 hpi, sorted by log₂(fold change).

Gene ID	Log ₂ (fold change)	p-value	Female naïve 2 VST	Female naïve 3 VST	Female naïve 4 VST	Female naïve 5 VST	Male naïve 2 VST	Male naïve 3 VST	Male naïve 4 VST	Male naïve 5 VST
XIST	-11,399	3,270E-27	10,269	10,472	10,595	10,996	3,493	3,508	3,012	3,012
TSIX	-8,868	2,650E-08	5,581	5,708	6,102	5,822	3,012	3,012	3,012	3,012
HSPA7	-2,074	2,140E-09	8,508	8,443	9,357	7,253	6,332	5,754	7,795	5,922
CCL20	-1,806	5,045E-03	9,568	3,534	4,304	6,798	8,157	3,499	3,603	4,668
CXCL3	-1,394	1,796E-03	13,501	5,773	7,367	10,101	13,083	4,746	5,861	7,689
S100A8	-0,998	6,372E-05	13,037	8,385	8,980	7,023	12,189	7,535	7,845	5,792
CDA	-0,874	4,121E-02	8,120	7,820	7,468	7,650	7,042	6,905	7,070	6,300
S100A9	-0,871	2,515E-03	13,697	11,357	11,368	11,145	12,813	9,921	10,895	10,089
ZFX	-0,745	2,619E-02	9,498	7,313	7,447	7,722	8,857	6,513	6,619	6,811
PNRC1	-0,704	2,872E-02	12,364	9,208	9,485	10,346	12,064	8,384	8,434	9,257
ATOX1	-0,703	1,179E-02	10,656	9,190	9,162	8,837	9,903	8,696	8,222	7,902
ARSD	-0,000	1,179E-02	7,957	8,186	8,558	8,474	7,361	7,337	7,638	7,527
GPR35	-0,000	3,226E-03	6,522	5,581	7,044	7,990	5,601	4,957	5,143	6,271
PLTP	0,000	1,489E-02	10,454	9,288	8,613	9,004	10,946	10,371	9,630	9,632
RCAN1	0,793	5,045E-03	9,437	7,997	7,543	8,011	10,567	8,932	8,021	8,872
HLA-DQB1	0,878	3,071E-03	9,366	10,374	9,803	10,992	9,895	11,195	11,339	12,022
APOC1	1,012	2,704E-02	7,932	9,589	7,899	8,569	8,711	11,030	8,195	10,712
NCAPH	1,137	1,945E-03	5,188	7,448	6,175	7,015	6,397	8,975	6,924	7,888
OXCT1	1,192	2,209E-02	5,997	6,484	4,742	5,988	6,538	8,424	5,591	7,119
FAIM3	1,212	1,690E-03	4,632	6,977	5,493	6,737	5,540	8,390	6,183	7,994
AKAP6	1,227	2,214E-02	4,751	6,075	5,467	5,563	6,164	7,449	6,142	6,475
DPP4	1,511	4,253E-03	5,648	6,742	4,031	6,870	6,312	9,257	5,236	7,915
SLC9B2	1,831	7,678E-07	4,895	7,045	4,307	6,487	6,544	9,194	5,230	7,720
GPAT2	1,935	4,815E-02	4,001	5,053	4,504	3,531	4,618	7,295	5,087	5,273
GREM1	2,328	1,039E-03	4,297	5,467	3,529	4,192	6,362	6,875	4,202	5,860
SPON2	2,383	2,282E-04	3,864	4,821	3,728	4,946	4,951	7,067	4,630	6,573
TACSTD2	3,508	2,704E-02	3,012	3,734	3,522	3,501	4,595	6,098	4,633	4,065
USP9Y	8,547	3,030E-12	3,012	3,012	3,012	3,499	7,131	6,802	7,294	7,211
PRKY	8,878	2,579E-08	3,012	3,012	3,012	3,012	5,697	6,226	5,700	5,491
TTY15	9,042	1,194E-08	3,012	3,012	3,012	3,012	5,910	5,265	6,116	6,121
EIF1AY	9,105	3,713E-14	3,012	3,012	3,532	3,012	8,148	7,097	7,288	7,765
UTY	9,248	2,146E-09	3,012	3,012	3,012	3,012	6,124	5,627	6,307	5,952
ZFY	9,901	4,089E-11	3,012	3,012	3,012	3,012	6,826	5,689	6,136	6,799
TXLNG2P	10,288	3,030E-12	3,012	3,012	3,012	3,012	6,139	5,787	7,182	7,307
RPS4Y1	10,713	3,041E-20	3,012	3,012	3,522	3,012	8,453	8,714	9,149	9,701
KDM5D	11,682	4,614E-18	3,012	3,012	3,012	3,012	7,568	7,935	7,727	8,035
DDX3Y	13,308	5,695E-24	3,012	3,012	3,012	3,012	9,565	8,161	9,474	9,182

Gonosome-specific genes are coloured.

Table S4: Differentially expressed genes between female and male naïve macrophages at 16 hpi, sorted by $\log_2(\text{fold change})$.

Gene ID	Log ₂ (fold change)	p-value	Female naïve 2 VST	Female naïve 3 VST	Female naïve 4 VST	Female naïve 5 VST	Male naïve 2 VST	Male naïve 3 VST	Male naïve 4 VST	Male naïve 5 VST
XIST	-14,750	2,040E-30	10,486	10,947	10,332	10,426	3,815	3,815	3,815	3,815
TSIX	-7,869	3,487E-05	5,377	5,612	5,997	5,273	3,815	3,815	3,815	3,815
HSPA7	-1,671	5,589E-04	8,778	8,300	8,828	7,486	6,412	6,126	8,064	6,536
SGPP2	-1,144	4,039E-02	9,638	9,087	9,714	10,111	9,622	6,776	8,401	8,605
CCL4	-1,069	2,513E-02	10,818	8,920	10,454	10,580	10,650	7,318	8,445	9,572
NCF1	-0,992	8,813E-03	12,298	7,698	9,324	10,326	11,384	7,410	7,814	8,807
ARSD	-0,904	2,097E-03	8,081	8,172	8,182	8,445	7,176	7,279	7,441	7,448
FAM129A	-0,780	2,424E-02	8,930	7,975	7,992	7,969	8,052	7,306	6,932	7,383
IER3	-0,680	1,612E-02	10,669	9,235	11,063	10,673	10,225	8,328	10,296	9,746
TFRC	0,694	1,926E-02	9,535	10,588	7,597	8,878	10,172	11,114	8,592	9,786
HLA-DQA1	0,862	2,424E-02	10,156	10,331	11,008	12,041	11,379	11,912	11,941	12,285
SLC9B2	1,069	2,000E-02	5,388	8,923	5,099	6,065	6,373	9,731	6,174	6,679
DCSTAMP	1,074	1,963E-02	6,339	8,038	5,224	6,118	6,683	9,363	6,318	7,080
TM4SF19	1,0881	1,325E-03	6,303	9,093	6,981	7,416	7,364	10,545	7,371	8,695
MMP7	1,1157	8,183E-04	7,282	9,118	5,609	6,126	8,684	10,047	6,079	7,268
HLA-DQB1	1,1967	1,315E-07	8,600	9,740	10,121	10,883	9,691	11,321	11,453	11,793
ITGA3	1,2190	3,344E-02	4,613	7,712	5,132	5,791	5,306	8,451	6,315	6,747
GAL	1,3614	3,969E-02	4,816	6,943	4,924	5,708	5,776	8,144	6,392	6,073
CD52	1,3919	4,802E-03	6,618	9,424	7,781	7,740	7,829	12,041	7,960	9,520
FAIM3	1,4049	9,275E-03	4,562	7,606	5,042	5,704	5,197	8,364	6,173	7,034
MYL9	1,417	6,063E-04	5,098	7,703	5,224	5,198	5,831	9,146	5,891	6,304
CRABP2	1,631	2,998E-04	4,8229	7,7722	4,9833	5,7969	6,3070	9,3527	5,7708	6,5642
SPON2	2,060	3,034E-02	4,5851	5,7247	3,8146	5,2546	5,6458	7,1717	5,6224	5,8924
TACSTD2	2,443	1,386E-02	4,1607	4,7182	4,9088	4,4695	4,2444	6,6520	6,1634	5,4799
GPAT2	2,500	2,185E-02	4,1784	5,3954	4,2207	4,2137	4,2664	7,1347	5,3605	5,2269
TTY15	8,403	8,447E-07	3,8146	3,8146	3,8146	3,8146	5,8167	5,6326	5,6714	5,8555
UTY	9,151	5,503E-09	3,8146	3,8146	3,8146	3,8146	6,3016	5,8867	6,3065	5,9380
KDM5D	9,220	9,126E-15	3,8146	4,1961	3,8146	3,8146	7,6663	7,6092	7,9062	7,9103
PRKY	9,423	8,924E-10	3,8146	3,8146	3,8146	3,8146	6,5855	6,0284	6,2893	6,0807
ZFY	9,476	5,196E-10	3,8146	3,8146	3,8146	3,8146	6,4427	6,0773	6,2921	6,3668
RPS4Y1	10,110	9,562E-11	3,8146	3,8146	4,3736	3,8146	8,1940	9,3562	8,8992	9,6322
TXLNG2P	10,588	7,743E-14	3,8146	3,8146	3,8146	3,8146	6,9543	6,6351	7,2474	7,1958
USP9Y	10,597	8,173E-14	3,8146	3,8146	3,8146	3,8146	7,1822	6,4944	7,0780	7,2187
EIF1AY	12,232	1,183E-19	3,8146	3,8146	3,8146	3,8146	8,0258	8,1472	7,5494	8,9257
DDX3Y	12,884	1,420E-22	3,8146	3,8146	3,8146	3,8146	8,9720	8,3618	8,7732	8,9349

Gonosome-specific genes are coloured.

Table S5: Differentially expressed genes between female and male naïve macrophages at 52 hpi, sorted by $\log_2(\text{fold change})$.

Gene ID	Log ₂ (fold change)	p-value	Female naïve 2 VST	Female naïve 3 VST	Female naïve 4 VST	Female naïve 5 VST	Male naïve 2 VST	Male naïve 3 VST	Male naïve 4 VST	Male naïve 5 VST
XIST	-14,974	2,816E-31	10,248	11,104	10,674	10,775	4,061	4,061	4,061	4,061
TSIX	-7,934	1,370E-05	5,650	6,042	5,295	6,079	4,061	4,061	4,061	4,061
HSPA7	-2,276	1,051E-09	9,204	9,177	9,452	7,061	6,840	6,788	8,313	5,299
FGL2	-0,674	1,973E-02	10,180	10,361	11,314	9,946	9,145	9,620	10,867	9,202
FABP4	1,497	2,596E-07	5,243	9,196	7,206	7,914	6,226	11,119	8,053	9,328
DYSF	2,428	1,736E-03	5,138	4,709	4,925	5,039	7,276	5,093	5,609	6,907
UTY	7,391	3,254E-08	4,061	4,061	4,387	4,061	6,629	6,200	6,512	6,263
TTY15	8,712	1,238E-07	4,061	4,061	4,061	4,061	6,186	5,696	6,030	6,103
ZFY	9,348	1,653E-09	4,061	4,061	4,061	4,061	6,225	6,179	6,300	6,515
PRKY	9,559	8,700E-10	4,061	4,061	4,061	4,061	7,139	6,145	6,498	5,698
DDX3Y	10,422	2,510E-19	4,061	4,061	4,392	4,061	8,707	8,647	9,047	8,579
RPS4Y1	10,698	8,582E-21	4,061	4,061	4,392	4,061	8,336	9,562	9,165	8,198
USP9Y	11,013	2,456E-15	4,061	4,061	4,061	4,061	7,283	7,244	7,501	7,308
TXLNG2P	11,135	1,956E-14	4,061	4,061	4,061	4,061	7,031	7,748	7,886	6,221
KDM5D	11,682	8,717E-18	4,061	4,061	4,061	4,061	7,679	7,821	7,780	7,987
EIF1AY	11,738	8,717E-18	4,061	4,061	4,061	4,061	7,909	8,190	7,670	7,473

Gonosome-specific genes are coloured.

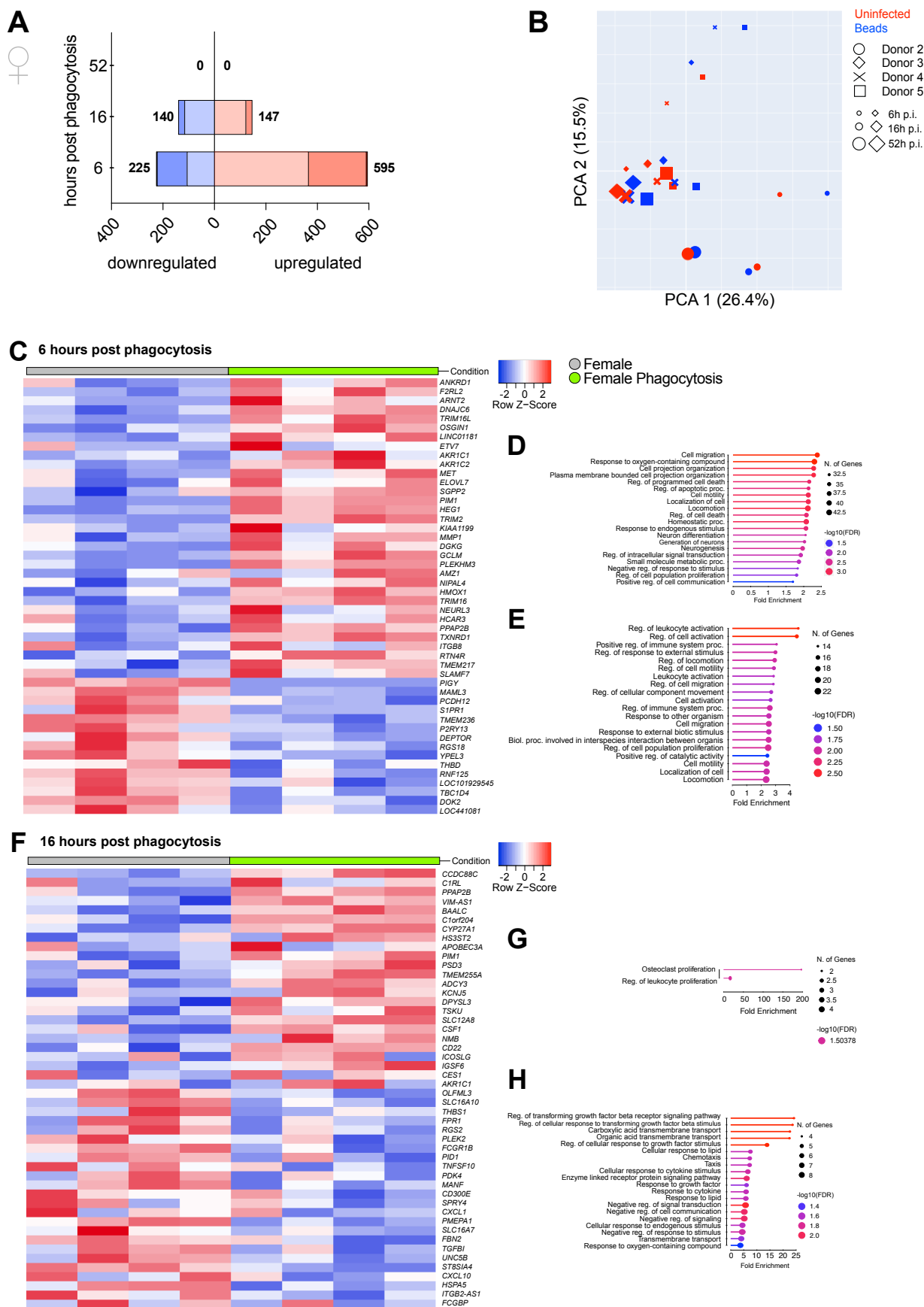
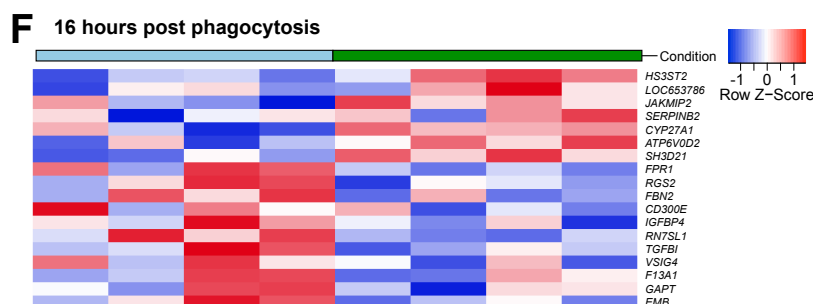
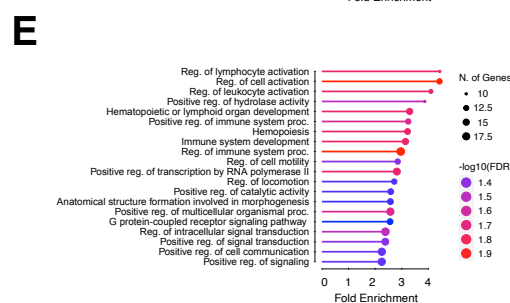
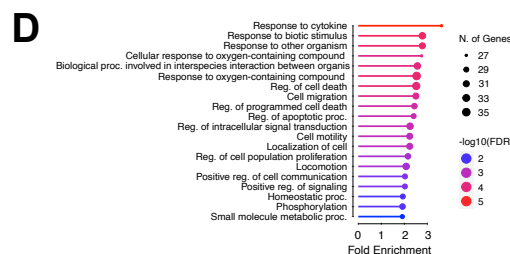
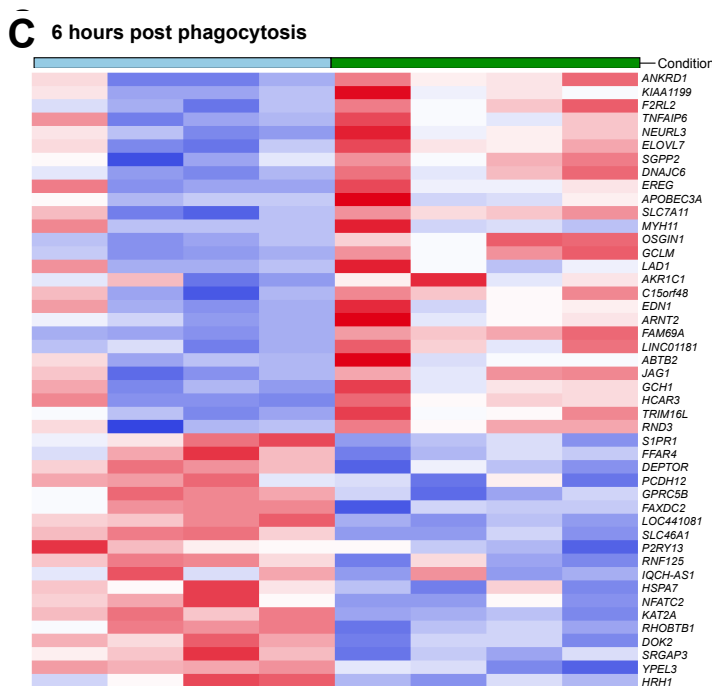
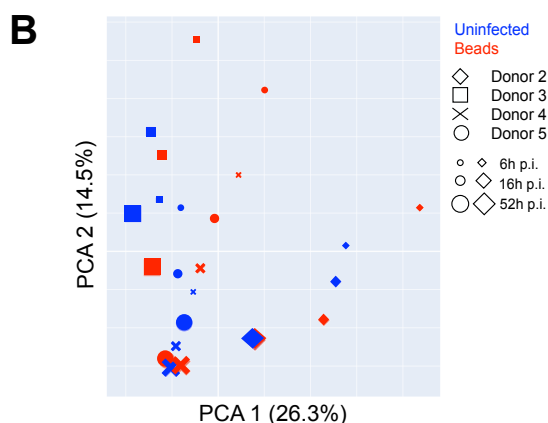
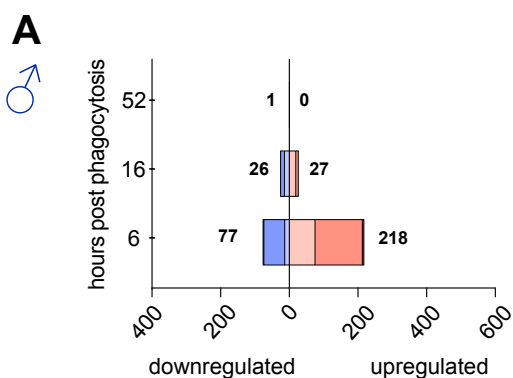


Figure S3: Analysis of differentially expressed genes between naïve and bead-containing macrophages from female donors.

(A) Number of differentially expressed genes ($p < 0.05$) in bead-containing cells in relation to naïve control for each time point. Data shown as horizontal bar plots. Box width correlates with number of differentially expressed genes downregulated (left, blue) and upregulated (right, red). Colour shading correlates with the magnitude of regulation (dark: $\log_2(\text{fold change}) > 3$; medium: $1 < \log_2(\text{fold change}) < 3$, light: $\log_2(\text{fold change}) < 1$). (B) PCA of sequenced naïve macrophages and macrophages incubated with phagocytosis beads according to treatment (node colour), donor (node shape) and time point (node size). Variance is in depicted for both components as percentage. (C, F) Heatmap depicting the row z-score of top differently expressed genes ($-1 > \log_2(\text{fold change}) > 2$, $p < 0.05$) between naïve and bead-containing cells at (C) 6 hours post infection and (F) 16 hours post infection. Red indicates high expression, blue indicates low expression. (D, G) Biological processes GO term enrichment of significantly upregulated genes in phagocytosis ($\log_2(\text{fold change}) > 1$, $p < 0.05$) compared to naïve control at (D) 6 hours post infection and (G) 16 hours post infection. Shown are the top processes sorted by fold enrichment. Significances of enrichment indicated by colour and number of genes allocated to pathway indicated in node size. (E, H) Biological processes GO term enrichment of significantly downregulated genes in phagocytosis ($\log_2(\text{fold change}) < -1$, $p < 0.05$) compared to naïve control at (E) 6 hours post infection and (H) 16 hours post infection.



GAPT	-0,897	7,439E-04	7,680	8,014	9,867	7,656	7,031	7,696	8,598	6,718
RGS1	-0,883	4,289E-02	5,828	7,424	7,231	6,956	5,640	6,822	5,820	6,419
SNHG6	-0,871	2,440E-03	7,564	7,849	9,210	8,463	7,126	7,537	7,902	7,294
CD28	-0,856	2,058E-02	6,274	8,674	6,474	8,320	6,068	8,306	5,857	6,680
FILIP1L	-0,835	2,280E-04	9,395	8,651	8,075	8,090	8,529	7,872	7,183	7,570
RPS27	-0,821	1,131E-03	11,220	11,667	13,313	12,132	10,772	11,364	11,527	11,054
COL23A1	-0,816	8,773E-03	7,949	8,099	8,180	8,036	7,765	7,488	7,265	6,717
EMB	-0,811	1,012E-03	7,948	8,800	9,310	8,426	7,492	8,305	8,207	7,419
TLR7	-0,802	1,516E-02	6,218	8,057	8,630	7,989	6,140	7,547	7,687	6,667
GPR34	-0,798	2,915E-03	8,891	9,996	9,970	10,035	8,558	9,746	8,548	8,650
PON2	-0,797	2,673E-03	7,359	8,499	8,373	8,006	6,794	7,958	7,684	6,967
LINC01094	-0,796	2,222E-03	8,496	8,293	7,608	8,134	7,894	7,788	6,791	7,203
CLEC5A	-0,789	2,280E-04	11,320	11,311	11,748	10,913	10,063	11,039	10,582	10,247
RSAD2	0,800	2,478E-03	10,657	6,417	6,555	7,052	11,319	6,542	7,810	7,753
GGT1	0,809	1,704E-02	8,057	6,550	5,919	6,611	8,429	7,054	6,875	7,409
P2RX7	0,838	1,891E-03	7,610	7,921	7,239	7,617	7,963	8,588	8,519	8,458
TMEM38B	0,854	6,321E-03	7,337	6,387	6,765	6,798	7,812	7,319	7,514	7,444
CD274	0,858	2,707E-03	9,407	7,053	7,987	8,238	9,358	8,078	9,017	9,585
LOC653786	0,865	3,497E-02	5,220	6,706	6,667	6,449	5,603	8,088	7,293	6,678
UCHL1	0,870	3,697E-02	6,024	6,957	6,826	5,823	5,984	7,332	8,264	7,058
SOAT1	0,872	5,447E-05	9,911	9,033	8,716	8,867	10,346	9,756	9,998	9,952
HTRA4	0,873	2,772E-02	7,140	6,918	5,950	6,452	7,927	7,137	7,571	6,892
NOTCH3	0,873	4,476E-03	7,350	6,973	6,859	7,030	7,579	7,754	7,846	8,071
WARS	0,876	1,674E-04	10,477	9,214	8,585	9,306	11,396	9,391	9,858	10,544
RAB42	0,878	2,673E-03	6,668	6,941	6,837	7,087	7,392	7,554	7,682	7,787
TBC1D2	0,891	1,674E-04	8,749	8,310	8,133	8,619	9,540	9,163	9,567	9,055
JAKMIP2	0,901	1,029E-03	7,484	7,990	7,244	7,802	7,820	8,847	8,649	8,564
SVIL	0,902	1,913E-02	6,217	6,121	6,576	6,505	6,462	7,066	7,131	7,601
GM2A	0,933	9,634E-06	13,327	12,749	12,069	12,538	14,063	13,235	13,720	13,677
SEMA6B	0,940	4,336E-04	8,470	7,218	7,897	8,436	9,056	8,793	8,749	9,024
DFNA5	0,941	2,624E-04	8,728	7,917	7,735	7,997	9,062	9,073	9,134	8,730
CD300LF	0,948	1,261E-03	8,354	6,352	7,033	7,076	8,879	7,331	7,519	8,297
HSD3B7	0,951	1,037E-03	7,085	8,417	7,043	7,227	8,098	8,633	8,116	8,305
VAT1	0,952	5,907E-09	10,065	10,470	10,510	10,562	11,067	11,388	11,720	11,296
SLAMF7	0,953	8,138E-05	12,671	10,047	10,240	10,844	12,854	10,972	11,883	12,132
IFITM10	0,960	7,812E-04	6,777	7,235	6,885	7,109	7,661	8,024	7,875	7,631
FAM213B	0,962	1,102E-04	8,427	8,059	7,817	8,550	9,455	8,690	9,338	9,086
ATP6V0D2	0,962	1,037E-03	8,351	8,616	6,616	8,899	9,085	9,313	8,313	9,497
COL8A2	0,996	3,042E-02	6,158	7,110	5,987	5,954	6,661	6,936	7,447	7,368
AKR1C1	1,009	1,577E-03	7,065	8,072	8,529	5,915	6,975	9,317	9,925	6,886
CES1	1,011	4,984E-03	9,280	5,547	6,865	6,333	9,272	6,112	8,075	7,641
IGSF6	1,021	4,520E-06	9,553	8,965	9,465	9,841	9,868	10,218	10,719	11,147
ICOSLG	1,025	1,697E-02	6,246	6,021	7,334	5,223	7,236	7,080	7,663	5,574
CD22	1,028	9,439E-03	6,256	6,898	5,977	6,699	7,290	7,182	7,290	7,244
NMB	1,085	2,505E-02	5,954	6,027	5,771	5,982	5,983	7,297	6,550	6,872
CSF1	1,095	1,037E-03	7,489	8,081	6,701	6,627	8,210	8,372	7,869	8,239
SLC12A8	1,096	1,718E-02	6,007	5,749	6,019	5,935	6,409	6,480	6,804	6,801
TSKU	1,129	1,276E-02	6,622	5,965	5,436	6,268	7,176	6,262	6,490	7,412
DPYSL3	1,131	2,685E-02	6,566	6,557	5,924	5,274	7,300	6,523	6,911	6,893
KCNJ5	1,146	1,929E-03	5,802	7,047	6,386	6,441	6,361	7,720	7,825	7,085
ADCY3	1,155	5,447E-05	7,234	8,081	7,005	7,331	8,187	8,696	8,671	8,160
TMEM255A	1,161	2,280E-04	6,811	6,519	6,863	6,871	7,204	7,559	8,005	7,947
PSD3	1,162	8,068E-03	6,324	7,108	5,769	6,537	6,766	7,239	7,338	8,023
PIM1	1,186	3,208E-06	8,071	6,876	7,079	7,657	8,725	7,932	8,214	8,876
APOBEC3A	1,189	2,799E-02	7,091	4,883	5,247	5,494	8,341	4,935	5,490	6,238
HS3ST2	1,222	2,724E-04	5,958	6,941	6,757	7,510	6,496	8,487	8,059	7,945
CYP27A1	1,237	5,907E-09	10,653	9,905	9,874	10,402	11,248	11,165	11,712	11,732
C1orf204	1,346	3,991E-03	6,489	6,221	5,713	5,629	6,907	6,905	6,802	6,857
BAALC	1,445	5,099E-04	6,475	5,887	6,020	6,484	6,942	6,972	7,631	7,272
VIM-AS1	1,445	1,828E-05	7,472	7,515	6,940	6,155	8,188	8,576	7,955	8,126
PPAP2B	1,522	7,147E-06	7,916	6,954	6,664	6,671	8,484	7,828	8,339	8,594
C1RL	1,584	2,476E-02	6,891	4,877	5,036	5,018	7,469	5,297	5,522	6,129
CCDC88C	1,952	2,228E-05	5,937	5,883	5,569	6,021	6,729	6,562	7,293	7,439

RSAD2	3,632	1,943E-04	10,508	5,226	5,561	4,929	11,945	7,787	10,508	10,255
CACNA1G	3,746	4,845E-03	3,528	4,403	3,528	3,528	5,318	4,991	5,283	4,807
AKR1C1	4,059	9,520E-06	6,784	8,979	4,075	4,283	9,695	11,913	8,076	7,405
ANKRD1	4,244	1,860E-04	6,138	4,025	4,076	3,966	8,765	5,173	6,443	9,064
TM4SF1	4,378	5,691E-07	4,991	4,228	3,917	3,528	8,953	4,623	5,382	5,928
SERPINE2	4,480	1,383E-16	4,333	4,753	4,350	4,772	7,645	6,853	7,664	7,390
COL5A3	4,605	1,184E-04	4,013	4,226	3,528	3,528	5,379	5,230	6,284	5,611
LAMA5	4,687	4,014E-04	3,528	3,528	4,076	3,528	6,158	4,380	5,381	4,695
SLC24A3	4,885	7,083E-05	4,012	4,024	3,528	3,528	6,026	4,620	5,173	5,955
DPYSL3	5,105	7,782E-08	5,582	5,783	4,467	4,734	11,087	7,506	9,082	9,232
SERPINB2	5,138	2,149E-72	7,061	4,025	6,516	6,915	11,363	6,489	11,488	12,178
MT1M	5,252	8,948E-06	5,449	3,528	3,528	3,980	9,262	7,087	6,557	4,625
MMP1	5,487	1,585E-14	4,762	4,412	3,528	4,389	8,029	6,403	7,102	8,795
TFPI2	6,085	1,126E-05	3,528	3,528	3,528	3,966	4,988	4,733	5,972	6,097
MT1G	6,386	6,920E-09	7,837	5,079	3,918	4,303	11,744	11,101	10,298	8,374
MT1H	6,671	3,041E-05	8,028	4,410	3,528	3,528	10,942	10,342	9,270	6,746
NEFM	6,984	4,645E-04	3,528	3,528	3,528	3,528	4,286	5,161	6,131	4,324
MT1L	8,349	2,907E-19	4,158	4,041	3,528	3,528	9,199	8,679	7,673	6,834
SULT1A3	9,518	8,971E-11	3,528	3,528	3,528	3,528	5,860	6,697	6,675	6,392
MT1A	10,750	8,340E-07	3,528	3,528	3,528	3,528	8,863	7,452	7,348	4,972

Table S16: Top differentially expressed genes between male naïve and *L. infantum*-infected macrophages at 52 hpi, sorted by log₂(fold change).

Gene ID	Log ₂ (fold change)	p-value	Male naïve 2 VST	Male naïve 3 VST	Male naïve 4 VST	Male naïve 5 VST	Male <i>L. inf</i> 2 VST	Male <i>L. inf</i> 3 VST	Male <i>L. inf</i> 4 VST	Male <i>L. inf</i> 5 VST
FABP4	-1,593	3,324E-04	6,299	11,149	8,095	9,364	5,649	9,600	7,327	6,626
SERPINF1	-1,338	1,309E-05	7,936	8,164	8,800	7,951	6,827	6,592	7,534	7,208
PID1	-1,279	3,565E-03	5,771	7,137	8,206	7,487	5,362	5,790	7,350	6,327
NR1D2	-1,069	7,438E-05	8,175	8,540	8,765	8,259	7,065	7,697	7,529	7,512
STMN1	-0,928	1,221E-03	7,243	9,045	8,948	7,511	6,314	7,986	8,165	6,911
ZNF704	-0,921	1,432E-02	7,069	7,561	8,016	7,587	6,613	6,713	7,081	6,604
ARL4C	-0,000	1,973E-03	9,007	9,734	10,655	10,292	8,619	8,885	9,553	8,920
FAM156A	-0,000	4,729E-02	6,157	5,312	5,387	5,145	5,197	4,206	4,206	4,206
HK3	0,614	3,670E-02	9,046	9,334	9,046	9,792	9,922	10,263	9,650	10,126
PCK2	0,704	2,451E-02	7,374	7,443	7,701	8,581	7,988	8,156	8,676	9,110
SAMD9L	0,748	2,043E-02	8,754	8,073	7,902	8,048	9,224	8,660	8,777	9,232
ADAMTSL4	0,829	2,451E-02	8,137	7,066	8,346	7,801	8,822	7,890	8,795	9,227
STAT1	0,907	5,748E-04	10,914	9,500	9,471	9,450	11,983	9,870	10,713	10,586
LOC101928429	0,963	2,749E-02	6,637	6,993	6,280	6,248	7,116	8,026	6,934	7,374
FBP1	0,991	1,525E-04	7,635	9,357	7,238	7,749	8,776	10,069	8,435	8,514
COL6A2	1,070	2,325E-03	7,234	8,815	6,736	6,874	8,170	10,068	8,207	7,190
TYMP	1,076	1,221E-03	8,764	8,516	8,605	9,910	10,500	8,963	10,106	10,726
GBP1	1,164	1,525E-04	7,476	6,070	6,498	6,752	8,446	7,030	7,330	7,824
EMILIN1	1,340	1,088E-02	6,561	5,516	5,353	5,654	7,896	5,953	6,075	6,683
ACE	1,347	1,249E-09	8,839	8,439	8,349	8,487	9,808	9,664	9,721	10,158
IL7R	1,469	4,000E-06	9,028	5,216	5,872	7,241	10,758	5,789	7,167	8,062
HSD11B1	2,332	3,541E-06	7,416	4,862	5,295	5,576	8,560	5,834	6,980	7,612

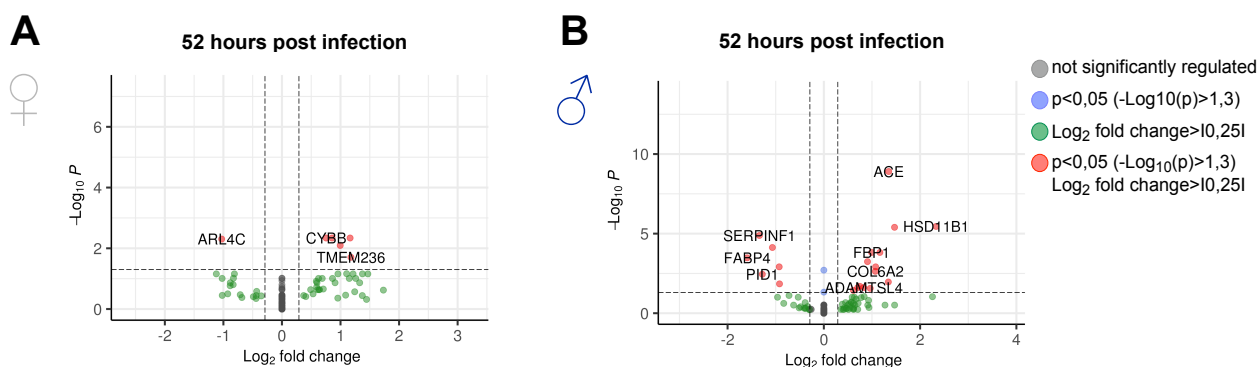


Figure S5: Analysis of differentially expressed genes between naïve and *L. infantum*-infected macrophages at 52 hpi.

Vulcano plots depicting relative gene expression according to magnitude of change (Log₂(fold change)) and statistical significance of change (-Log₁₀(adjusted p-value)) between uninfected and infected macrophages of same sex at 52 hpi. Genes significantly regulated between the conditions (Log₂(fold change) > 10.251, p < 0.05) are marked in red (Log₂(fold change) > 0 downregulated in infected samples, Log₂(fold change) < 0 upregulated in infected samples) from (A) female and (B) male donors.

Table S17: Top 50 differentially expressed genes in infected samples over time pooled from female and male donors.

Gene ID	Protein description	Log ₂ (fold change)	p-value
LINF_160020300	paraflagellar rod protein 1D - putative	-0.21162744	1,0579E-05
LINF_210016800	Histone H2A putative	-0.12796326	1,49598E-07
LINF_340022500	p25- α putative	-0.08648154	0,018016313
LINF_360076000	tartrate-sensitive acid phosphatase acp-3.2 - putative	-0.08616702	0,029625661
EF2-1	elongation factor 2	-0.08382917	1,85215E-06
LINF_290024100	Histone H2A putative	-0.08204346	6,45621E-09
LINF_360050400	Amastin surface glycoprotein putative	-0.07829083	0,004545687
MPC1	Uncharacterised protein family (UPF0041)- putative	-0.07749191	0,0041928
ATG8A.1	ATG8/AUT7/APG8/PAZ2 - putative	-0.07265379	5,17528E-10
LINF_290024000	Histone H2A putative	-0.06605993	0,000478036
LINF_050017500	Surface antigen-like protein	-0.06422872	4,60664E-06
LINF_150005000	Histone H4	-0.06355645	5,30759E-10
LINF_320018300	CRAL/TRIO domain containing protein - putative	-0.06150699	5,55916E-07
LINF_150020000	nucleoside transporter 1 - putative	-0.0605938	0,001388563
LINF_190005200	Histone H2B	-0.05831159	0,007905011
LINF_100016800	Histone H3 putative	-0.05700907	1,12887E-05
LINF_360005100	Histone H4	-0.05632111	9,74195E-25
LINF_140011900	fatty acid elongase	-0.05612934	0,005404693
LINF_300005000	hypothetical protein conserved	-0.05417067	6,44454E-08
LINF_350005100	Histone H4	-0.05340197	4,11898E-10
LINF_310014800	hypothetical protein, conserved	-0.05186492	0,042805221
LINF_090020900	Histone H2B	-0.0511423	3,10397E-24
LINF_200016900	cysteine peptidase - Clan CA - family C2 - putative	-0.05086861	0,016099611
LINF_270018800	Histone H1 - putative	-0.050554	2,01404E-14
LINF_090007200	ATG8/AUT7/APG8/PAZ2 - putative	-0.04939597	0,001829968
LINF_280032000	hypothetical protein, conserved	0,03265599	2,9166E-08
LINF_350020600	hypothetical protein, conserved	0,0328486	1,6374E-10
LINF_340024000	Amastin surface glycoprotein putative	0,0329349	4,7408E-07
LINF_290019400	Amastin surface glycoprotein putative	0,03324119	0,00025536
LINF_330028400	hypothetical protein, conserved	0,03351503	7,9586E-07
LINF_090006400	kinesin, putative	0,0367127	3,3658E-16
LINF_290014200	hypothetical protein	0,03704047	4,9971E-18
ABCG1	ATB-binding cassette protein subfamily G-member 1 - putative	0,03826213	1,2536E-08
LINF_360035700	hypothetical protein, conserved	0,03959799	8,1023E-06
LINF_170017200	hydrolase α/β fold family-like protein	0,03998853	7,192E-16
LINF_270006400	hypothetical protein, conserved	0,04034114	2,9559E-05
LINF_120010000	hypothetical protein, conserved	0,04133721	0,00011706
LINF_130006900	Lipase (class3), putative	0,04175131	7,7359E-20
H1A-2	P-type H ⁺ -ATPase - putative	0,04316441	0,00092223
LINF_290019500	Amastin surface glycoprotein putative	0,04349721	8,1023E-06
LINF_080012000	amastin-like protein	0,04455196	6,3537E-08
AQP1	Aquaglyceroporin 1	0,04617051	4,051E-18
LINF_290019600	Amastin surface glycoprotein putative	0,04985921	2,6665E-05
LINF_080012400	amastin-like protein	0,05370286	9,0618E-06
LINF_220012600	hypothetical protein, conserved	0,05378846	2,7209E-07
LINF_340043900	hypothetical protein, conserved	0,05759735	1,3979E-13
LINF_220012800	A2 protein	0,05974208	5,749E-12
LINF_080011900	amastin-like protein	0,06025268	8,0402E-14
LINF_220012400	hypothetical protein, conserved	0,06418191	1,3794E-12
LINF_220014400	hypothetical protein, conserved	0,06483781	1,4378E-10

Table S18: Differentially expressed genes between infected female and male samples at 6 hpi.

Gene ID	Protein description	Log ₂ (fold change)	p-value
LINF_310026700	peptidase m20/m25/m40 family-like protein	10.180016813373	6.04950044112178E-12
LINF_350005400	pyruvate kinase	-1.6107277734384	1.89074330118092E-11
LINF_310028200	peptidase m20/m25/m40 family-like protein	-9.73278897582303	4.92475140170242E-11

Figure S6: Analysis of differentially expressed genes between naïve and *L. infantum*-infected macrophages at 52 hpi.

Vulcano plots depicting relative gene expression according to magnitude of change ($\text{Log}_2(\text{fold change})$) and statistical significance of change ($-\text{Log}_{10}(\text{adjusted p-value})$) between female and male samples at (A) 16 hpi and (B) 52 hpi.

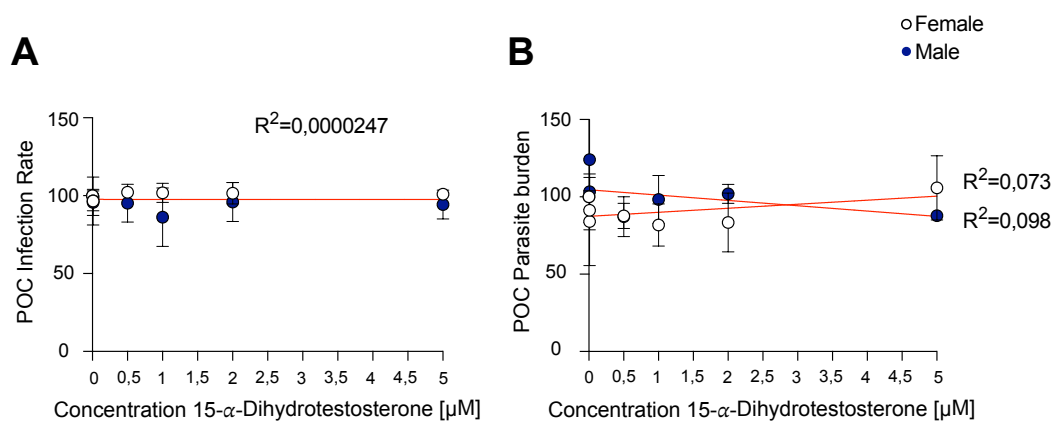


Figure S7: Correlation analysis between testosterone treatment and *L. infantum* infection in female macrophages.

Quantified infection parameters were used for non-linear regression to examine correlation between concentration of hormone treatment and (A) infection rate and (B) parasite burden. Regression line (red) and R^2 are indicated. R^2 = determination coefficient.

Publications

Fehling, H., Niss, H., **Bea, A.**, Kottmayr, N., Brinker, C., Hoenow, S., Sellau, J., Gilberger, T-W., Ting, F., Landschulze, D., Meier, C., Clos, J. & Lotter, H. (2021). High Content Analysis of Macrophage-Targeting *Eh*PIB-Compounds against Cutaneous and Visceral Leishmania Species.

Er-Lukowiak, M., Haenzelmann, S., Rothe, M., Moamenpour, D., Hausmann, F., Khatri, R., Boldt, J., Bärreiter, V., Honecker, B., **Bea, A.**, Groneberg, M., Hansen, C., Fehling, H., Marggraff, C., Cadar, D., Bonn, S., Sellau, J. & Lotter, H. (2023). Testosterone affects type I/type II interferon response of neutrophils during hepatic amebiasis.

Bibliography

1. PAHO. Leishmaniasis [Available from: <https://www.paho.org/en/topics/leishmaniasis>].
2. Alvar J, et al. Leishmaniasis worldwide and global estimates of its incidence. *PLoS One*. 2012;7(5):e35671.
3. WHO. Leishmaniasis 2023 [Available from: <https://www.who.int/news-room/fact-sheets/detail/leishmaniasis#:~:text=Leishmaniasis%20is%20caused%20by%20protozoan,and%20lack%20of%20financial%20resources>].
4. Kholoud K, et al. Management of Leishmaniasis in the Era of Climate Change in Morocco. *Int J Environ Res Public Health*. 2018;15(7).
5. Trájer AJ, Grmasha RA. The potential effects of climate change on the climatic suitability patterns of the Western Asian vectors and parasites of cutaneous leishmaniasis in the mid- and late twenty-first century. *Theoretical and Applied Climatology*. 2023.
6. Steverding D. The history of leishmaniasis. *Parasit Vectors*. 2017;10(1):82-.
7. Mann S, et al. A Review of Leishmaniasis: Current Knowledge and Future Directions. *Curr Trop Med Rep*. 2021;8(2):121-32.
8. Murray HW, et al. Advances in leishmaniasis. *The Lancet*. 2005;366(9496):1561-77.
9. WHO. Leishmaniasis 2023 [Available from: <https://www.who.int/data/gho/data/themes/topics/gho-ntd-leishmaniasis>].
10. Callahan HL, et al. Leishmaniasis: Temperature Sensitivity of Promastigotes in Vitro as a Model for Tropism in Vivo. *Experimental Parasitology*. 1996;84(3):400-9.
11. Torres-Guerrero E, et al. Leishmaniasis: a review. *F1000Res*. 2017;6:750-.
12. Piscopo TV, Mallia Azzopardi C. Leishmaniasis. *Postgrad Med J*. 2007;83(976):649-57.
13. Gossage SM, et al. Two separate growth phases during the development of *Leishmania* in sand flies: implications for understanding the life cycle. *Int J Parasitol*. 2003;33(10):1027-34.
14. Bates PA. Transmission of *Leishmania* metacyclic promastigotes by phlebotomine sand flies. *Int J Parasitol*. 2007;37(10):1097-106.
15. Bates PA. Revising *Leishmania*'s life cycle. *Nature Microbiology*. 2018;3(5):529-30.
16. Laskay T, et al. Neutrophil granulocytes -Trojan horses for *Leishmania major* and other intracellular microbes? *Trends in Microbiology*. 2003;11(5):210-4.
17. Kaye P, Scott P. Leishmaniasis: complexity at the host-pathogen interface. *Nature Reviews Microbiology*. 2011;9(8):604-15.
18. Scarpini S, et al. Visceral Leishmaniasis: Epidemiology, Diagnosis, and Treatment Regimens in Different Geographical Areas with a Focus on Pediatrics. *Microorganisms*. 2022;10(10):1887.
19. Avila-García M, et al. Transplacental transmission of cutaneous *Leishmania mexicana* strain in BALB/c mice. *Am J Trop Med Hyg*. 2013;89(2):354-8.
20. Esch KJ, Petersen CA. Transmission and epidemiology of zoonotic protozoal diseases of companion animals. *Clin Microbiol Rev*. 2013;26(1):58-85.

21. Kushwaha AK, et al. Domestic mammals as reservoirs for *Leishmania donovani* on the Indian subcontinent: Possibility and consequences on elimination. *Transboundary and Emerging Diseases*. 2022;69(2):268-77.
22. Gradoni L, Gramiccia M. *Leishmania infantum* Tropism: Strain genotype or host immune status? *Parasitology Today*. 1994;10(7):264-7.
23. Guerbouj S, et al. Genomic polymorphism of *Leishmania infantum*: a relationship with clinical pleomorphism? *Infection, Genetics and Evolution*. 2001;1(1):49-59.
24. El Hamouchi A, et al. Genetic polymorphism in *Leishmania infantum* isolates from human and animals determined by nagt PCR-RFLP. *Infect Dis Poverty*. 2018;7(1):54.
25. Gramiccia M, et al. Two syntopic zymodemes of *Leishmania infantum* cause human and canine visceral leishmaniasis in the Naples area, Italy. *Acta Tropica*. 1992;50(4):357-9.
26. Pratlong F, et al. Isoenzymatic analysis of 712 strains of *Leishmania infantum* in the south of France and relationship of enzymatic polymorphism to clinical and epidemiological features. *J Clin Microbiol*. 2004;42(9):4077-82.
27. Aronson NE, Magill AJ. 104 - Leishmaniasis. In: Ryan ET, Hill DR, Solomon T, Aronson NE, Endy TP, editors. *Hunter's Tropical Medicine and Emerging Infectious Diseases (Tenth Edition)*. London: Elsevier; 2020. p. 776-98.
28. Reimão JQ, et al. Laboratory Diagnosis of Cutaneous and Visceral Leishmaniasis: Current and Future Methods. *Microorganisms*. 2020;8(11).
29. Guerin PJ, et al. Visceral leishmaniasis: current status of control, diagnosis, and treatment, and a proposed research and development agenda. *The Lancet Infectious Diseases*. 2002;2(8):494-501.
30. Dalton JE, Kaye PM. Immunomodulators: use in combined therapy against leishmaniasis. *Expert Review of Anti-infective Therapy*. 2010;8(7):739-42.
31. Buates S, Matlashewski G. Treatment of Experimental Leishmaniasis with the Immunomodulators Imiquimod and S-28463: Efficacy and Mode of Action. *The Journal of Infectious Diseases*. 1999;179(6):1485-94.
32. Alberts B JA, Lewis J, et al. *Molecular Biology of the Cell-Innate Immunity* [Book]. Garland Science; 2002 [4th edition:[Available from: <https://www.ncbi.nlm.nih.gov/books/NBK26846/#>].
33. Marshall JS, et al. An introduction to immunology and immunopathology. *Allergy, Asthma & Clinical Immunology*. 2018;14(2):49.
34. Riera Romo M, et al. Innate immunity in vertebrates: an overview. *Immunology*. 2016;148(2):125-39.
35. Lazarov T, et al. Physiology and diseases of tissue-resident macrophages. *Nature*. 2023;618(7966):698-707.
36. Mass E, et al. Tissue-specific macrophages: how they develop and choreograph tissue biology. *Nature Reviews Immunology*. 2023;23(9):563-79.
37. Gordon S, Taylor PR. Monocyte and macrophage heterogeneity. *Nature Reviews Immunology*. 2005;5(12):953-64.
38. Cedric Auffray, et al. Blood Monocytes: Development, Heterogeneity, and Relationship with Dendritic Cells. *Annual Review of Immunology*. 2009;27(1):669-92.

39. El Kasmi KC, et al. Toll-like receptor-induced arginase 1 in macrophages thwarts effective immunity against intracellular pathogens. *Nat Immunol.* 2008;9(12):1399-406.
40. Davis MJ, et al. Macrophage M1/M2 Polarization Dynamically Adapts to Changes in Cytokine Microenvironments in *Cryptococcus neoformans* Infection. *mBio.* 2013;4(3):10.1128/mbio.00264-13.
41. Raggi F, et al. Regulation of Human Macrophage M1-M2 Polarization Balance by Hypoxia and the Triggering Receptor Expressed on Myeloid Cells-1. *Front Immunol.* 2017;8:1097.
42. Zhang J, et al. Role of CD68 in tumor immunity and prognosis prediction in pan-cancer. *Sci Rep.* 2022;12(1):7844.
43. Biswas SK, et al. Macrophage polarization and plasticity in health and disease. *Immunol Res.* 2012;53(1-3):11-24.
44. Ambarus CA, et al. Systematic validation of specific phenotypic markers for in vitro polarized human macrophages. *Journal of Immunological Methods.* 2012;375(1):196-206.
45. Sica A, Mantovani A. Macrophage plasticity and polarization: in vivo veritas. *J Clin Invest.* 2012;122(3):787-95.
46. Martinez FO, Gordon S. The M1 and M2 paradigm of macrophage activation: time for reassessment. *F1000Prime Rep.* 2014;6:13.
47. Orliaguet L, et al. Mechanisms of Macrophage Polarization in Insulin Signaling and Sensitivity. *Front Endocrinol (Lausanne).* 2020;11:62.
48. Wang Q, et al. Targeting M2 Macrophages Alleviates Airway Inflammation and Remodeling in Asthmatic Mice via miR-378a-3p/GRB2 Pathway. *Frontiers in Molecular Biosciences.* 2021;8.
49. Yang S, et al. Macrophage: Key player in the pathogenesis of autoimmune diseases. *Front Immunol.* 2023;14:1080310.
50. dos Santos Meira C, Gedamu L. Protective or Detrimental? Understanding the Role of Host Immunity in Leishmaniasis. *Microorganisms.* 2019;7(12):695.
51. Elmahallawy EK, et al. Host immune response against leishmaniasis and parasite persistence strategies: A review and assessment of recent research. *Biomed Pharmacother.* 2021;139:111671.
52. Costa-da-Silva AC, et al. Immune Responses in Leishmaniasis: An Overview. *Trop Med Infect Dis.* 2022;7(4).
53. Liu D, UZONNA J. The early interaction of *Leishmania* with macrophages and dendritic cells and its influence on the host immune response. *Frontiers in Cellular and Infection Microbiology.* 2012;2.
54. Tripathi P, et al. Immune response to leishmania: paradox rather than paradigm. *FEMS Immunology & Medical Microbiology.* 2007;51(2):229-42.
55. Alexander J, Brombacher F. T helper1/t helper2 cells and resistance/susceptibility to leishmania infection: is this paradigm still relevant? *Front Immunol.* 2012;3:80.
56. Martínez-López M, et al. *Leishmania* Hijacks Myeloid Cells for Immune Escape. *Front Microbiol.* 2018;9.
57. Klein SL, Flanagan KL. Sex differences in immune responses. *Nat Rev Immunol.* 2016;16(10):626-38.
58. Sellau J, et al. Androgen-dependent immune modulation in parasitic infection. *Semin Immunopathol.* 2019;41(2):213-24.

59. Sellau J, et al. Androgens predispose males to monocyte-mediated immunopathology by inducing the expression of leukocyte recruitment factor CXCL1. *Nature Communications*. 2020;11(1):3459.
60. Miga KH, et al. Telomere-to-telomere assembly of a complete human X chromosome. *Nature*. 2020;585(7823):79-84.
61. Migeon BR. Why females are mosaics, X-chromosome inactivation, and sex differences in disease. *Gend Med*. 2007;4(2):97-105.
62. Mousavi MJ, et al. Escape from X chromosome inactivation and female bias of autoimmune diseases. *Molecular Medicine*. 2020;26(1):127.
63. Snider H, et al. Sex Hormones and Modulation of Immunity against Leishmaniasis. *Neuroimmunomodulation*. 2009;16:106-13.
64. Gubbels Bupp MR, Jorgensen TN. Androgen-Induced Immunosuppression. *Front Immunol*. 2018;9:794.
65. Marchetti PM, Barth JH. Clinical biochemistry of dihydrotestosterone. *Annals of Clinical Biochemistry*. 2013;50(2):95-107.
66. Fuentes N, Silveyra P. Estrogen receptor signaling mechanisms. *Adv Protein Chem Struct Biol*. 2019;116:135-70.
67. Er-Lukowiak M, et al. Testosterone affects type I/type II interferon response of neutrophils during hepatic amebiasis. *Frontiers in Immunology*. 2023;14.
68. Viselli SM, et al. Castration alters peripheral immune function in normal male mice. *Immunology*. 1995;84(2):337-42.
69. Roden AC, et al. Augmentation of T cell levels and responses induced by androgen deprivation. *J Immunol*. 2004;173(10):6098-108.
70. Rettew JA, et al. Testosterone Reduces Macrophage Expression in the Mouse of Toll-Like Receptor 4, a Trigger for Inflammation and Innate Immunity. *Biology of Reproduction*. 2008;78(3):432-7.
71. Miller L, Hunt JS. Sex steroid hormones and macrophage function. *Life Sci*. 1996;59(1):1-14.
72. Maret A, et al. Estradiol enhances primary antigen-specific CD4 T cell responses and Th1 development in vivo. Essential role of estrogen receptor alpha expression in hematopoietic cells. *Eur J Immunol*. 2003;33(2):512-21.
73. Owens IPF. Sex Differences in Mortality Rate. *Science*. 2002;297(5589):2008-9.
74. Guerra-Silveira F, Abad-Franch F. Sex bias in infectious disease epidemiology: patterns and processes. *PLoS One*. 2013;8(4):e62390.
75. Lockard RD, et al. Sex-Related Differences in Immune Response and Symptomatic Manifestations to Infection with *Leishmania* Species. *Journal of Immunology Research*. 2019;2019:4103819.
76. Cloots K, et al. Male predominance in reported Visceral Leishmaniasis cases: Nature or nurture? A comparison of population-based with health facility-reported data. *PLoS Negl Trop Dis*. 2020;14(1):e0007995.
77. Davies CR, et al. The epidemiology and control of leishmaniasis in Andean countries. *Cad Saude Publica*. 2000;16(4):925-50.
78. Solomon M, et al. Gender and Cutaneous Leishmaniasis in Israel. *Tropical Medicine and Infectious Disease*. 2022;7(8):179.

79. Jeronimo SM, et al. An emerging peri-urban pattern of infection with *Leishmania chagasi*, the protozoan causing visceral leishmaniasis in northeast Brazil. *Scand J Infect Dis*. 2004;36(6-7):443-9.
80. Harhay MO, et al. Who is a typical patient with visceral leishmaniasis? Characterizing the demographic and nutritional profile of patients in Brazil, East Africa, and South Asia. *Am J Trop Med Hyg*. 2011;84(4):543-50.
81. Lima Á LM, et al. Changing epidemiology of visceral leishmaniasis in northeastern Brazil: a 25-year follow-up of an urban outbreak. *Trans R Soc Trop Med Hyg*. 2017;111(10):440-7.
82. Muñoz G, Davies CR. *Leishmania panamensis* transmission in the domestic environment: the results of a prospective epidemiological survey in Santander, Colombia. *Biomedica*. 2006;26 Suppl 1:131-44.
83. Lezama-Davila CM, et al. Sex-associated Susceptibility in Humans with Chiclero's Ulcer: Resistance in Females is Associated with Increased Serum-levels of GM-CSF. *Scandinavian Journal of Immunology*. 2007;65(2):210-1.
84. Gosch CS, et al. American tegumentary leishmaniasis: epidemiological and molecular characterization of prevalent *Leishmania* species in the State of Tocantins, Brazil, 2011-2015. *Rev Inst Med Trop Sao Paulo*. 2017;59:e91.
85. Soares L, et al. Epidemiology of cutaneous leishmaniasis in central Amazonia: a comparison of sex-biased incidence among rural settlers and field biologists. *Tropical Medicine & International Health*. 2014;19(8):988-95.
86. Rodríguez NE, et al. Epidemiological and Experimental Evidence for Sex-Dependent Differences in the Outcome of *Leishmania infantum* Infection. *Am J Trop Med Hyg*. 2018;98(1):142-5.
87. Bernin H, Lotter H. Sex Bias in the Outcome of Human Tropical Infectious Diseases: Influence of Steroid Hormones. *The Journal of Infectious Diseases*. 2014;209(suppl_3):S107-S13.
88. Travi BL, et al. Gender is a major determinant of the clinical evolution and immune response in hamsters infected with *Leishmania* spp. *Infect Immun*. 2002;70(5):2288-96.
89. Lezama-Dávila CM, et al. 17Beta-estradiol increases *Leishmania mexicana* killing in macrophages from DBA/2 mice by enhancing production of nitric oxide but not pro-inflammatory cytokines. *Am J Trop Med Hyg*. 2007;76(6):1125-7.
90. Bryson KJ, et al. BALB/c mice deficient in CD4 T cell IL-4R α expression control *Leishmania mexicana* Load although female but not male mice develop a healer phenotype. *PLoS Negl Trop Dis*. 2011;5(1):e930.
91. Slapničková M, et al. Gene-specific sex effects on eosinophil infiltration in leishmaniasis. *Biol Sex Differ*. 2016;7:59.
92. Mock BA, Nacy CA. Hormonal modulation of sex differences in resistance to *Leishmania* major systemic infections. *Infect Immun*. 1988;56(12):3316-9.
93. Anuradha, et al. Sex-influenced population kinetics of *Leishmania donovani* in hamsters. *Indian J Exp Biol*. 1990;28(9):876-9.
94. Lezama-Dávila CM, et al. Role of phosphatidylinositol-3-kinase- γ (PI3K γ)-mediated pathway in 17 β -estradiol-induced killing of *L. mexicana* in macrophages from C57BL/6 mice. *Immunology & Cell Biology*. 2008;86(6):539-43.

95. Yin G, et al. Effect of testosterone on *Leishmania donovani* infection levels of murine bone marrow derived-macrophages. *Zhongguo Ji Sheng Chong Xue Yu Ji Sheng Chong Bing Za Zhi*. 1998;16(4):251-5.
96. Liu L, et al. Modulation of *Leishmania donovani* infection and cell viability by testosterone in bone marrow-derived macrophages: signaling via surface binding sites. *Steroids*. 2005;70(9):604-14.
97. Niss HE. Etablierung von Verfahren zur fluoreszenzmikroskopischen Hochdurchsatzanalyse eines in vitro Infektionsmodells mit *Leishmania major* in der Erforschung immunstimulierender Moleküle. University of Lübeck2020.
98. Fernandes MC, et al. Dual Transcriptome Profiling of *Leishmania*-Infected Human Macrophages Reveals Distinct Reprogramming Signatures. *mBio*. 2016;7(3):10.1128/mbio.00027-16.
99. Habib F. Characterization of the immune response elicited in *Leishmania*-infected human macrophages by treatment with immunostimulatory compounds. Hamburg University of Applied Sciences (HAW)2021.
100. Batista MF, et al. The Parasitic Intracellular Lifestyle of Trypanosomatids: Parasitophorous Vacuole Development and Survival. *Frontiers in Cell and Developmental Biology*. 2020;8.
101. Adai V, et al. Application of CRISPR/Cas9-Based Reverse Genetics in *Leishmania braziliensis*: Conserved Roles for HSP100 and HSP23. *Genes (Basel)*. 2020;11(10).
102. Rostam HM, et al. Image based Machine Learning for identification of macrophage subsets. *Sci Rep*. 2017;7(1):3521.
103. Porcheray F, et al. Macrophage activation switching: an asset for the resolution of inflammation. *Clin Exp Immunol*. 2005;142(3):481-9.
104. Goerdts S, Orfanos CE. Other functions, other genes: alternative activation of antigen-presenting cells. *Immunity*. 1999;10(2):137-42.
105. Minas K, Liversidge J. Is the CD200/CD200 receptor interaction more than just a myeloid cell inhibitory signal? *Crit Rev Immunol*. 2006;26(3):213-30.
106. Van der Maaten L, Hinton G. Visualizing data using t-SNE. *Journal of machine learning research*. 2008;9(11).
107. Osero BO, et al. Unravelling the unsolved paradoxes of cytokine families in host resistance and susceptibility to *Leishmania* infection. *Cytokine: X*. 2020;2(4):100043.
108. Gable AL, et al. Systematic assessment of pathway databases, based on a diverse collection of user-submitted experiments. *Briefings in Bioinformatics*. 2022;23(5).
109. Murphy AJ, et al. Estradiol regulates expression of estrogen receptor ERalpha46 in human macrophages. *PLoS One*. 2009;4(5):e5539.
110. Benten WP, et al. Testosterone signaling through internalizable surface receptors in androgen receptor-free macrophages. *Mol Biol Cell*. 1999;10(10):3113-23.
111. Mantalaris A, et al. Localization of androgen receptor expression in human bone marrow. *The Journal of Pathology*. 2001;193(3):361-6.
112. Kasarinaite A, et al. The Influence of Sex Hormones in Liver Function and Disease. *Cells*. 2023;12:1604.
113. Cai JJ, et al. Androgen actions on endothelium functions and cardiovascular diseases. *J Geriatr Cardiol*. 2016;13(2):183-96.

114. Fraietta I, Gasparri F. The development of high-content screening (HCS) technology and its importance to drug discovery. *Expert Opin Drug Discov.* 2016;11(5):501-14.
115. Asehli H, et al. The emerging importance of High Content Screening for future therapeutics. *Journal of Microscopy and Ultrastructure.* 2017.
116. Fehling H, et al. High Content Analysis of Macrophage-Targeting EhP1b-Compounds against Cutaneous and Visceral Leishmania Species. *Microorganisms.* 2021;9(2):422.
117. Singh N, Dube A. Reporter Genes in Parasites. 2016. p. 2325-33.
118. Vanaerschot M, et al. Linking In Vitro and In Vivo Survival of Clinical Leishmania donovani Strains. *PLoS One.* 2010;5(8):e12211.
119. Gupta S. Visceral leishmaniasis: experimental models for drug discovery. *Indian J Med Res.* 2011;133(1):27-39.
120. Lee N, et al. Programmed cell death in the unicellular protozoan parasite Leishmania. *Cell Death & Differentiation.* 2002;9(1):53-64.
121. van Zandbergen G, et al. Leishmania disease development depends on the presence of apoptotic promastigotes in the virulent inoculum. *Proceedings of the National Academy of Sciences.* 2006;103(37):13837-42.
122. Alcolea PJ, et al. In vitro infectivity and differential gene expression of Leishmania infantum metacyclic promastigotes: negative selection with peanut agglutinin in culture versus isolation from the stomodeal valve of Phlebotomus perniciosus. *BMC Genomics.* 2016;17(1):375.
123. Solano-Gálvez S-G, et al. Leishmania: manipulation of signaling pathways to inhibit host cell apoptosis. *Therapeutic Advances in Infectious Disease.* 2021;8:20499361211014977.
124. Elmore S. Apoptosis: a review of programmed cell death. *Toxicol Pathol.* 2007;35(4):495-516.
125. Privé C, Descoteaux A. Leishmania donovani promastigotes evade the activation of mitogen-activated protein kinases p38, c-Jun N-terminal kinase, and extracellular signal-regulated kinase-1/2 during infection of naive macrophages. *Eur J Immunol.* 2000;30(8):2235-44.
126. Guerfali FZ, et al. Simultaneous gene expression profiling in human macrophages infected with Leishmania major parasites using SAGE. *BMC Genomics.* 2008;9:238.
127. Sarkar A, et al. Infection of neutrophil granulocytes with Leishmania major activates ERK 1/2 and modulates multiple apoptotic pathways to inhibit apoptosis. *Med Microbiol Immunol.* 2013;202(1):25-35.
128. Ruhland A, et al. Leishmania promastigotes activate PI3K/Akt signalling to confer host cell resistance to apoptosis. *Cellular Microbiology.* 2007;9(1):84-96.
129. Martinez FO, et al. Transcriptional Profiling of the Human Monocyte-to-Macrophage Differentiation and Polarization: New Molecules and Patterns of Gene Expression1. *The Journal of Immunology.* 2006;177(10):7303-11.
130. Atri C, et al. Role of Human Macrophage Polarization in Inflammation during Infectious Diseases. *Int J Mol Sci.* 2018;19(6).
131. Tomiotto-Pellissier F, et al. Macrophage Polarization in Leishmaniasis: Broadening Horizons. *Front Immunol.* 2018;9:2529.
132. Buchacher T, et al. M2 Polarization of Human Macrophages Favors Survival of the Intracellular Pathogen Chlamydia pneumoniae. *PLoS One.* 2015;10(11):e0143593.

133. Ontoria E, et al. Transcriptional Profiling of Immune-Related Genes in *Leishmania infantum*-Infected Mice: Identification of Potential Biomarkers of Infection and Progression of Disease. *Front Cell Infect Microbiol.* 2018;8:197.
134. Abebe T, et al. Arginase activity - a marker of disease status in patients with visceral leishmaniasis in ethiopia. *PLoS Negl Trop Dis.* 2013;7(3):e2134.
135. Silva RL, et al. sCD163 levels as a biomarker of disease severity in leprosy and visceral leishmaniasis. *PLoS Negl Trop Dis.* 2017;11(3):e0005486.
136. Roy S, et al. An IL-10 dominant polarization of monocytes is a feature of Indian Visceral Leishmaniasis. *Parasite Immunol.* 2018;40(7):e12535.
137. Moreira PR, et al. Polarized M2 macrophages in dogs with visceral leishmaniasis. *Vet Parasitol.* 2016;226:69-73.
138. Carregaro V, et al. Nucleosides present on phlebotomine saliva induce immunosuppression and promote the infection establishment. *PLoS Negl Trop Dis.* 2015;9(4):e0003600.
139. Tumang MC, et al. Role and effect of TNF-alpha in experimental visceral leishmaniasis. *J Immunol.* 1994;153(2):768-75.
140. Murray HW. Tissue granuloma structure-function in experimental visceral leishmaniasis. *Int J Exp Pathol.* 2001;82(5):249-67.
141. Araújo-Santos T, et al. Anti-parasite therapy drives changes in human visceral leishmaniasis-associated inflammatory balance. *Sci Rep.* 2017;7(1):4334.
142. Bosch-Nicolau P, et al. Leishmaniasis and tumor necrosis factor alpha antagonists in the Mediterranean basin. A switch in clinical expression. *PLoS Negl Trop Dis.* 2019;13(8):e0007708.
143. Barral-Netto M, et al. Tumor Necrosis Factor (Cachectin) in Human Visceral Leishmaniasis. *The Journal of Infectious Diseases.* 1991;163(4):853-7.
144. Satoskar A, Alexander J. Sex-determined susceptibility and differential IFN-gamma and TNF-alpha mRNA expression in DBA/2 mice infected with *Leishmania mexicana*. *Immunology.* 1995;84(1):1-4.
145. Mullen AB, et al. Endogenous interleukin-18 is involved in immunity to *Leishmania donovani* but its absence does not adversely influence the therapeutic activity of sodium stibogluconate. *Immunology.* 2006;119(3):348-54.
146. Kane MM, Mosser DM. The role of IL-10 in promoting disease progression in leishmaniasis. *J Immunol.* 2001;166(2):1141-7.
147. Isaac-Márquez AP, Lezama-Dávila CM. Cytokine regulation of female-macrophage resistance to *Leishmania mexicana* parasites. Role of IL-12p70. *Parasite Immunology.* 2020;42(2):e12685.
148. Ahmadi A, et al. Evaluation of interleukin 8 +2767 A/T polymorphism in visceral leishmaniasis. *Asian Pacific Journal of Tropical Medicine.* 2016;9(11):1075-7.
149. Muhammed Hassan G, et al. Evaluation of IL-8, nitric oxide and macrophage inhibitory factor as clinical circulatory markers in patients with cutaneous leishmaniasis, before and during sodium stibogluconate treatment. *Cytokine.* 2024;173:156450.
150. Klein SL. Hormonal and immunological mechanisms mediating sex differences in parasite infection. *Parasite Immunology.* 2004;26(6-7):247-64.

151. Illumina. [Available from: https://knowledge.illumina.com/library-preparation/rna-library-prep/library-preparation-rna-library-prep-reference_material-list/000001243].
152. So J, et al. Sexual dimorphism of monocyte transcriptome in individuals with chronic low-grade inflammation. *Biology of Sex Differences*. 2021;12(1):43.
153. Gal-Oz ST, et al. ImmGen report: sexual dimorphism in the immune system transcriptome. *Nature Communications*. 2019;10(1):4295.
154. Fernandes MC, et al. Dual Transcriptome Profiling of Leishmania-Infected Human Macrophages Reveals Distinct Reprogramming Signatures. *mBio*. 2016;7(3):e00027-16.
155. Saha S, et al. Leishmania donovani Targets Host Transcription Factor NRF2 To Activate Antioxidant Enzyme HO-1 and Transcriptional Repressor ATF3 for Establishing Infection. *Infect Immun*. 2021;89(7):e0076420.
156. Chaparro V, et al. Transcriptional profiling of macrophages reveals distinct parasite stage-driven signatures during early infection by Leishmania donovani. *Sci Rep*. 2022;12(1):6369.
157. Ettinger NA, Wilson ME. Macrophage and T-Cell Gene Expression in a Model of Early Infection with the Protozoan Leishmania chagasi. *PLOS Neglected Tropical Diseases*. 2008;2(6):e252.
158. Dai H, et al. Metallothionein 1: A New Spotlight on Inflammatory Diseases. *Front Immunol*. 2021;12:739918.
159. Coyle P, et al. Metallothionein: the multipurpose protein. *Cellular and Molecular Life Sciences CMLS*. 2002;59(4):627-47.
160. Subramanian Vignesh K, Deepe GS, Jr. Metallothioneins: Emerging Modulators in Immunity and Infection. *Int J Mol Sci*. 2017;18(10).
161. Chung SW, et al. Heme oxygenase-1-derived carbon monoxide enhances the host defense response to microbial sepsis in mice. *J Clin Invest*. 2008;118(1):239-47.
162. Epiphanio S, et al. Heme oxygenase-1 is an anti-inflammatory host factor that promotes murine plasmodium liver infection. *Cell Host Microbe*. 2008;3(5):331-8.
163. Luz NF, et al. Heme oxygenase-1 promotes the persistence of Leishmania chagasi infection. *J Immunol*. 2012;188(9):4460-7.
164. Bichiou H, et al. Leishmania Parasites Differently Regulate Antioxidant Genes in Macrophages Derived From Resistant and Susceptible Mice. *Frontiers in Cellular and Infection Microbiology*. 2021;11.
165. Harrington V, Gurung P. Reconciling protective and pathogenic roles of the NLRP3 inflammasome in leishmaniasis. *Immunol Rev*. 2020;297(1):53-66.
166. Charmoy M, et al. The Nlrp3 inflammasome, IL-1 β , and neutrophil recruitment are required for susceptibility to a nonhealing strain of Leishmania major in C57BL/6 mice. *Eur J Immunol*. 2016;46(4):897-911.
167. Rohani MG, et al. Macrophage MMP10 Regulates TLR7-Mediated Tolerance. *Frontiers in Immunology*. 2018;9.
168. McMahan RS, et al. Stromelysin-2 (MMP10) Moderates Inflammation by Controlling Macrophage Activation. *J Immunol*. 2016;197(3):899-909.

169. Taslimi Y, et al. Profiling inflammatory response in lesions of cutaneous leishmaniasis patients using a non-invasive sampling method combined with a high-throughput protein detection assay. *Cytokine*. 2020;130:155056.
170. Fantecelle CH, et al. Transcriptomic landscape of skin lesions in cutaneous leishmaniasis reveals a strong CD8(+) T cell immunosenescence signature linked to immunopathology. *Immunology*. 2021;164(4):754-65.
171. Kong F, et al. Transcriptional Profiling in Experimental Visceral Leishmaniasis Reveals a Broad Splenic Inflammatory Environment that Conditions Macrophages toward a Disease-Promoting Phenotype. *PLOS Pathogens*. 2017;13(1):e1006165.
172. D. Rousseau SD, F. Anjuère, B. Ferrua, K. Fragaki, Y. Le Fichoux, J. Kubar. Sustained parasite burden in the spleen of *Leishmania infantum*-infected BALB/c mice is accompanied by expression of monocyte chemotactic protein-1 (MCP-1) transcripts and lack of protection against challenge.. 2001. *European Cytokine Network*. 2001;12(2):340-7.
173. Gupta G, et al. CXC Chemokine–Mediated Protection against Visceral Leishmaniasis: Involvement of the Proinflammatory Response. *The Journal of Infectious Diseases*. 2009;200(8):1300-10.
174. Zhang S, et al. Delineation of diverse macrophage activation programs in response to intracellular parasites and cytokines. *PLoS Negl Trop Dis*. 2010;4(3):e648.
175. Yang CX, et al. Widespread Sexual Dimorphism in the Transcriptome of Human Airway Epithelium in Response to Smoking. *Sci Rep*. 2019;9(1):17600.
176. Diebold BA, Bokoch GM. Molecular basis for Rac2 regulation of phagocyte NADPH oxidase. *Nat Immunol*. 2001;2(3):211-5.
177. Li J, et al. ROS Regulate NCF2, Key Metabolic Enzymes and MDA Levels to Affect the Growth of *Fusarium solani*. *Agriculture*. 2022;12(11):1840.
178. Lara S, et al. The Human Monocyte-A Circulating Sensor of Infection and a Potent and Rapid Inducer of Inflammation. *Int J Mol Sci*. 2022;23(7).
179. McNab F, et al. Type I interferons in infectious disease. *Nature Reviews Immunology*. 2015;15(2):87-103.
180. Lukhele S, et al. Type I interferon signaling, regulation and gene stimulation in chronic virus infection. *Semin Immunol*. 2019;43:101277.
181. Gupta S, et al. Sex differences in neutrophil biology modulate response to type I interferons and immunometabolism. *Proc Natl Acad Sci U S A*. 2020;117(28):16481-91.
182. Tasker C, et al. 17 β -Estradiol Protects Primary Macrophages Against HIV Infection Through Induction of Interferon-Alpha. *Viral Immunology*. 2014;27(4):140-50.
183. Milano S, et al. IL-15 in human visceral leishmaniasis caused by *Leishmania infantum*. *Clin Exp Immunol*. 2002;127(2):360-5.
184. Silva LLL, et al. IL-15 enhances the capacity of primary human macrophages to control *Leishmania braziliensis* infection by IL-32/vitamin D dependent and independent pathways. *Parasitol Int*. 2020;76:102097.
185. Speirs I, Tronson N. Sex differences in hippocampal cytokines after systemic immune challenge2018.
186. Quirino GFS, et al. Interleukin-27 (IL-27) Mediates Susceptibility to Visceral Leishmaniasis by Suppressing the IL-17-Neutrophil Response. *Infect Immun*. 2016;84(8):2289-98.

187. Jafarzadeh A, et al. Interleukin-27 Functional Duality Balances Leishmania Infectivity and Pathogenesis. *Front Immunol.* 2020;11:1573.
188. Dimitrijević M, et al. Sex differences in Tfh cell help to B cells contribute to sexual dimorphism in severity of rat collagen-induced arthritis. *Sci Rep.* 2020;10(1):1214.
189. Smelt SC, et al. B cell-deficient mice are highly resistant to *Leishmania donovani* infection, but develop neutrophil-mediated tissue pathology. *J Immunol.* 2000;164(7):3681-8.
190. Wanasen N, et al. Pathogenic role of B cells and antibodies in murine *Leishmania amazonensis* infection. *Int J Parasitol.* 2008;38(3-4):417-29.
191. Omachi S, et al. B-cell activating factor deficiency suppresses splenomegaly during *Leishmania donovani* infection. *Biochem Biophys Res Commun.* 2017;489(4):528-33.
192. Ikeogu NM, et al. *Leishmania* Immunity: Advancing Immunotherapy and Vaccine Development. *Microorganisms.* 2020;8(8).
193. Santos D, et al. IL-1 β Production by Intermediate Monocytes Is Associated with Immunopathology in Cutaneous Leishmaniasis. *J Invest Dermatol.* 2018;138(5):1107-15.
194. Voronov E, et al. IL-1-induced inflammation promotes development of leishmaniasis in susceptible BALB/c mice. *International Immunology.* 2010;22(4):245-57.
195. Nascimento MT, et al. Prostaglandin E2 contributes to *L. braziliensis* survival and therapeutic failure in cutaneous leishmaniasis. *Emerg Microbes Infect.* 2023;12(2):2261565.
196. Zeitler L, Murray PJ. IL4i1 and IDO1: Oxidases that control a tryptophan metabolic nexus in cancer. *Journal of Biological Chemistry.* 2023;299(6).
197. Fiore A, Murray PJ. Tryptophan and indole metabolism in immune regulation. *Current Opinion in Immunology.* 2021;70:7-14.
198. Oljuskina T, et al. *Leishmania* major centrin knock-out parasites reprogram tryptophan metabolism to induce a pro-inflammatory response. *iScience.* 2023;26(9):107593.
199. Myler PJ, et al. The *Leishmania* genome project: new insights into gene organization and function. *Medical Microbiology and Immunology.* 2001;190(1):9-12.
200. Bifeld E, et al. Ribosome Profiling Reveals HSP90 Inhibitor Effects on Stage-Specific Protein Synthesis in *Leishmania donovani*. *mSystems.* 2018;3(6).
201. Grünebast J, Clos J. *Leishmania*: Responding to environmental signals and challenges without regulated transcription. *Computational and Structural Biotechnology Journal.* 2020;18:4016-23.
202. Grünebast J, et al. Life Cycle Stage-Specific Accessibility of *Leishmania donovani* Chromatin at Transcription Start Regions. *mSystems.* 2021;6(4):e0062821.
203. Wiesgigl M, Clos J. Heat shock protein 90 homeostasis controls stage differentiation in *Leishmania donovani*. *Mol Biol Cell.* 2001;12(11):3307-16.
204. Rochette A, et al. Characterization and developmental gene regulation of a large gene family encoding amastin surface proteins in *Leishmania* spp. *Molecular and Biochemical Parasitology.* 2005;140(2):205-20.
205. Rosenzweig D, et al. Retooling *Leishmania* metabolism: from sand fly gut to human macrophage. *Faseb j.* 2008;22(2):590-602.

206. Silverman JM, et al. Proteomic analysis of the secretome of *Leishmania donovani*. *Genome Biol.* 2008;9(2):R35.
207. Magalhães RD, et al. Identification of differentially expressed proteins from *Leishmania amazonensis* associated with the loss of virulence of the parasites. *PLoS Negl Trop Dis.* 2014;8(4):e2764.
208. Chawla B, Madhubala R. Drug targets in *Leishmania*. *J Parasit Dis.* 2010;34(1):1-13.
209. Amiri-Dashatan N, et al. Discovery of Novel Pyruvate Kinase Inhibitors Against *Leishmania major* Among FDA Approved Drugs Through System Biology and Molecular Docking Approach. *Turk J Pharm Sci.* 2021;18(6):710-7.
210. Yang L, et al. 17 β -estradiol modulates the viability, phenotype, endocytosis, and inflammatory cytokine expression of RAW264.7 macrophages. *European Journal of Inflammation.* 2016;14(1):10-7.
211. Enright S, Werstuck GH. Investigating the Effects of Sex Hormones on Macrophage Polarization. *International Journal of Molecular Sciences.* 2024;25(2):951.
212. de Oliveira Rekowsky LL, et al. Influence of Testosterone in Neglected Tropical Diseases: Clinical Aspects in Leprosy and In Vitro Experiments in Leishmaniasis. *Trop Med Infect Dis.* 2023;8(7).

Schematic figures were created with a licensed version of BioRender (<https://www.biorender.com/>).

Acknowledgments

First and foremost, I would like to thank Prof. Dr. Hanna Lotter and PD Dr. Joachim Clos for providing and supervising this doctoral project. The fruitful discussions and constructive recommendations helped making this project such an interesting, educational and stimulating experience. Thank you for all your support during this special time.

Thank you, Prof. Dr. Tim-Wolf Gilberger, for also being an evaluator of this thesis.

Thank you, Dr. Nicole Gilberger and Ralf Krumkamp, for co-supervising this thesis and especially thank you, Ralf, for your input and expertise on my statistical issues and questions.

Dear, Dr. Helena Fehling, without your scientific guidance and input, this project would not have been the same. Thank you for your patience, support, your encouraging words, your open ears on every U-Bahn ride back from work, long talks about work-related and non work-related subjects and bringing such a positive energy everywhere. And of course, thank you and Momo for enduring sleepless nights and making our holidays possible by cat-sitting our Lotte, which hopefully was also a bit enjoyable.

A huge thank you to the Transfusionsmedizin und Blutspendezentrum, UKE, for the reliable provision of donor samples and the easy and uncomplicated cooperation.

For the many analyses of my transcriptome data and fruitful and uncomplicated cooperation, I want to thank Dr. Sonja Hänzelmann and especially Fabian Hausmann from AG Bonn (ZMNH), for always being available for my questions, long e-mails and open for every of my new suggestions, if possible.

Along this line, I want to thank Dr. Anna Bachmann for the assessment of my transcriptome data and giving honest and helpful advices, when I could not see the forest through all the trees.

A very warm thank you goes out to all the current and former group members of AG Clos and AG Lotter for all the open conversations, fun times and laboratory support. My dearest Leishmaniacs, Dr. Janne Grünebast, Dr. Constanze Kröber-Boncardo, Christine Brinker, Anne MacDonald, Dorothea Zander-Dinse and all the master and bachelor students during this time, thank you for the wonderful times I got to spend with you in last almost 5 years. For all the constructive discussions about unexpected data, lunch and coffee breaks, long days in the lab or celebratory drinks in the evening. You made coming to work so much more enjoyable and something to look forward to and keep me sane, especially during COVID-times. I hope, we stay in contact and can follow our journeys much longer! Thank you to Dr. Marco Er-Lukowiak, Dr. Helena Fehling, Claudia Marggraff (the angel and heart of lab 6), Barbara Honecker, Melanie Lütkemeyer, Charlotte Hansen, Nils Grothe and Stefanie Tewes for sharing the good, the bad and the ugly sides of a PhD, your

unbiased scientific opinions and helpful comments and for being able to forget about work together while having a blast on the Hedi, on game or carnival nights or at the strawberry field! I will always cherish these memories and happily look back at them! At lunch, the borders get blurry between working groups, so I want to include Pilar Martínez, Julieta Anders and Yasmin Schmitz, because you accompanied my way and without the motivational words and good laughs we had together, that whole experience would not have been the same! Same applies to my dearest Herzis, Barbara Honecker, Johanna Steffens, Cari Lehmann, András Bencsik and Lennart Heepmann. I enjoyed our time together so much and think we made a wonderful group! From coating 30 ELISA plates over tanning and swimming in the sea in Travemünde to being able to celebrate your PhDs with you, it was very special to have such a cool group around for the entire PhD-time!

Last, but by no means least, I want to thank my family and BNITM-external friends, that supported me in every way possible, by sending packages with supportive sweets, long phone calls, or the opportunity to write parts of my thesis whilst everything else has been taken care of by my parents. Special thanks to Julian for your love, patience, never-ending words of motivation and reality checks for calming me down. I could not have done it without either of you!